UAB

The Role of the TiO$_2$ Surface in Heterogeneous Photocatalytic Reactions: Mechanistic and Kinetic Implications

Juan Felipe Montoya Arango

PhD Thesis

Program of PhD in Chemistry

Advisors:

José Peral Perez
Pedro Salvador Salvador

Department of Chemistry
Sciences Faculty
2013

UNIVERSITAT AUTÒNOMA DE BARCELONA

DEPARTAMENT DE QUÍMICA

UNITAT DE QUÍMICA FÍSICA

JOSÉ PERAL PEREZ, Profesor Titular de Química Física del Departamento de Química de la Universitat Autònoma de Barcelona, y PEDRO SALVADOR SALVADOR, Profesor de Investigación del Consejo Superior de Investigaciones Científicas

Certificamos:

Que **Juan Felipe Montoya Arango** ha realizado bajo nuestra dirección en el Departamento de Química de la Universitat Autònoma de Barcelona el trabajo que lleva por título:

The Role of the TiO₂ Surface in Heterogeneous Photocatalytic Reactions: Mechanistic and Kinetic Implications

Que se presenta en esta memoria para optar al grado de Doctor en Química.

José Peral Perez   Pedro Salvador Salvador

Foreword

TiO$_2$ photocatalysis has been extensively studied over the last three decades. The output of this research effort is an increasing fundamental understanding of the phenomena involved in the process and the successful application of photocatalytic technological devices in different areas such as environmental purification, renewable energy production, and design of materials with "self cleaning" properties. However, the scientific community in the field of photocatalysis recognizes that several fundamentals issues still remain unclear.

In the 80 and 90's decades several reaction mechanisms and kinetic models were proposed for the interpretation of the large body of experimental data concerning TiO$_2$-assisted photooxidation reactions. Despite the huge advance in the fundamental knowledge of these topics that was achieved, several assumptions taken as truths by the scientific community were challenged by the findings of surface science studies on TiO$_2$ crystals reported in the first decade of this century. These findings brought new insights into the surface chemistry of TiO$_2$. It was demonstrated that the TiO$_2$ catalyst can not be considered just as particles devoid of surface structure. Conversely, the chemical structure of the catalyst surface and its interaction with molecules in the reaction media is a determinant factor to understand the events triggered by TiO$_2$ excitation.

This PhD thesis is aimed at elucidating some alternative interpretations of kinetics and mechanisms of photocatalytic oxidation reactions taking into account the aforementioned novel insights. This task has been addressed by a comprehensive analysis of the scientific literature on the topic of surface chemistry of TiO$_2$ and by an experimental study comprising TiO$_2$-surface/substrate interactions, their relationship with kinetics of photooxidation reactions, and mechanistic issues related to photocatalytic oxidation of several model compounds.

The above issues are discussed in detail in four published articles and three manuscripts to be submitted for publication in the near future. Therefore, this thesis is a compendium of such articles organized in the following chapters:

(1) **General introduction**. Because each article has its particular introduction and reference sections the objective of this chapter was not to make an exhaustive review of all the topics covered along this thesis. Instead of that, this section is aimed at showing to the reader a brief context of the social and scientific problems that this research pretends to address. Additionally, a brief overview of the basic concepts behind TiO_2 photocatalysis is included in this section. This overview also includes a contextualization about some "hot topics" that are matter of current controversy in this field. The most relevant scientific literature on these topics, especially review articles and books, is reviewed in this section. Special emphasis was done in the comparison between old reviews (especially from the 90's decade) and the newest reviews (some of them published this year) to contrast old interpretations of photocatalysis phenomena and the current state of the controversy about some "hot topics" in this field.

(2) **Goals and Scope**. The aims and objectives of this research work are presented in this section.

(3) **Results and Discussion.** This chapter is presented as a compendium of four published articles grouped by issues in two main sections:

A. *Kinetic analysis of photocatalytic reactions*. This section include the following article:

- Montoya, J. F.; Salvador, P. "The Influence of Surface Fluorination in the Photocatalytic Behavior of TiO_2 Aqueous Dispersions: An Analysis in the Light of the Direct-Indirect Kinetic Model". *Applied Catalysis B: Environmental* **2010,** *94* (1-2), 97-107.

B. *Mechanisms of photocatalytic reactions.* This section include the following articles:

"Effects of Hydroxyl Radicals and Oxygen Species on the 4-Chlorophenol Degradation by Photoeletrocatalytic Reactions with TiO_2-Film Electrodes by J. Yang, J. Dai, Ch. Chen, J. Zhao; J. Photochem. Photobiol. A: Chem. 208 (2009) 66-77". *Journal of Photochemistry and Photobiology A: Chemistry* **2010,** *210* (2-3), 215-216.

- Montoya, J. F.; Peral, J.; Salvador, P. "Surface Chemistry and Interfacial Charge-Transfer Mechanisms in Photoinduced Oxygen Exchange at O_2-TiO_2 Interfaces". *ChemPhysChem* **2011,** *12* (5), 901-907.

- Montoya, J. F.; Ivanova, I.; Dillert, R.; Bahnemann, D. W.; Salvador, P.; Peral, J. "Catalytic Role of Surface Oxygens in TiO_2 Photooxidation Reactions: Aqueous Benzene Photooxidation with $Ti^{18}O_2$ under Anaerobic Conditions". *J. Phys. Chem. Lett.* **2013,** *4* (9), 1415-1422.

(4) Conclusions and Outlook. General conclusions and perspectives of the conducted research are reviewed in this section.

(5) Annexes. This chapter contains additional research results reported in three manuscripts that will be submitted for publication in the near future. These manuscripts are complementary to the articles reported in chapter 3 and are also grouped by issues in the same sections of chapter 3.

A. *Kinetic analysis of photocatalytic reactions.* This section include the following manuscripts:

- Montoya, J. F.; Peral, J.; Salvador, P. "Comprehensive Analysis of Kinetics and Mechanisms of TiO_2 Photocatalytic Reactions. I) Theoretical approach through the D-I model".

- Montoya, J. F.; Atitar, M.F.; Bahnemann, D.W.; Peral, J.; Salvador, P. "Comprehensive Analysis of Kinetics and Mechanisms of TiO_2 Photocatalytic Reactions. II) Experimental validation of the D-I model**".**

B. *Mechanisms of photocatalytic reactions.* This section include the following manuscript:

- Montoya, J. F.; Peral, J.; Bahnemann, D.W.; Salvador, P. "About the Capital Role of TiO_2 Surface Lattice Oxygens in Liquid Phase Photocatalytic Reactions".

Chapter 5 is an extension of the results reported in chapter 3. It was not explicitly included in the "Results and Discussion" chapter because these manuscripts may be subjected to modifications after the evaluation process at the scientific journals.

Acknowledgements

I am grateful to my PhD advisors for their support, comprehension, fruitful discussions and their skilled supervision of this research work. Thank you to introduce me in the winding but exciting road of scientific research.

I also would like to express my gratitude to Professor Detlef Bahnemann for giving me the opportunity to develop part of the experimental work of this thesis at the Leibniz Universität. There I received the priceless technical assistance of Irina Ivanova and Mohamed Atitar. Moreover, I thank the help of Johannes Melcher with Raman measurements. Besides, I collected a lot of ideas from discussions with Dr. Amer Hakki, Dr. Ralf Dillert and Jenny Schneider. Further, in Hannover the friendship of colleagues such as Pilar Esteban, Ana Blanco, Mathias Strauss, Matic Krivec and Ayad Alkaim was a fundamental factor to have a good performance in the research work.

In Barcelona I received the support and wise hints of Dr. Ulises Matias Garcia and the help of Ashley Black Serra. I enjoy a very good working environment with my colleague Katherine Villa. I got inspiration from my former group members Anna Serra and Marc Estruga. I made several friends such as Francisco Zarur, Jorge Ali, Irene Reiche, Linay Santacruz, Isaias Lans and Hansel Gomez. In general, I enjoyed a lot the camaraderie at the physical chemistry unit. I have spent a great time working there.

I have special memories of my friends from Colombia: Edwin Jurado, Jorge Velasquez, Eliana Cardona, Fernando Castaño, Juan David Peña, among others. I feel grateful because I know I can count on your support at difficult times. It always helps me to succeed at any task including this thesis.

My wife Astrid Cuervo deserves a special mention because she has been the essential partner of this adventure. Without her love, company and support it would be impossible to finish this task. My father, mother, brother and sisters are always in my heart and are one of my main reasons to succeed achieving different goals along my life.

<div align="right">

Thanks to everyone

Juan Felipe

</div>

Glossary of Acronyms and Symbols

adb	adiabatic
AFM	Atomic Force Microscopy
Bz	Benzene
CB	Conduction Band
CO_2	Carbon Dioxide
D-I	Direct Indirect
DT	Direct Transfer
e_f^-	Free Electron
E_g	Band Gap
EPA	Environmental Protection Agency
EPS	Electron Photoemission Spectra
FA	Formic Acid
F-TiO_2	Fluorinated Titania
h_f^+	Free Hole
h_s^+	Surface Trapped Hole
H_2O	Water
$H_2^{18}O$	Oxygen-Isotope-Labeled Water
ICT	Interfacial Charge Transfer
ins	inelastic
IT	Indirect Transfer
λ	Wavelength
L-H	Langmuir Hinshewoold
NHE	Normal Hydrogen Electrode
O_2	Molecular Oxygen
$^{18}O_2$	Oxygen-Isotope-Labeled Molecular Oxygen
O_s	TiO_2 Surface Lattice Oxygen
$^\bullet OH$	Hydroxyl Radicals

PhO	Phenol
POIE	Photo-induced Oxygen Isotope Exchange
$(RH_2)_{aq}$	Dissolved Organic Compound
$(RH_2)_s$	Chemisorbed Organic Compound
SCS	Surface Science Studies
TiO_2	Titanium Dioxide
$Ti^{18}O_2$	Oxygen-Isotope-Labeled Titania
UHV	Ultra High Vacuum
VB	Valence Band

CONTENTS

CHAPTER 1

GENERAL INTRODUCTION

1.1 Sustainable Development and Chemistry

The global energy demand is expected to experiment a huge increase in the next decades as a result of the high economic growth in some developing countries and the increase of the population.[1] If the energy consumption continues growing at the current rate (around 1.6% per year), the global energy production must be increased around 100% in about 40 years. Actually, only in developing countries, just the electricity demand is expected to increase by 150% in the next two decades.[1] The preferred option up to date to cover this huge energy demand is to burn fossil fuels. As a result, a higher rate of consumption of this non-renewable resources and the consequent increase in the CO_2 concentration at the atmosphere would be expected in the future if most of the energy supply continue to be fulfilled by fossil fuel sources. An alternative to this non-sustainable perspective is the production of renewable energy and a more efficient energy usage.

Besides the energy demand, another big challenge associated to the economic growth is the intensive use of planet resources and the consequent pollution of the environment. Multiple natural resources have been affected by human activities, being water contamination one of the most critical problems due to the vital role of hydrosphere for the sustainability of the life on the planet. Indeed, one of the most pervasive problems afflicting people throughout the world is the inadequate access to sanitation and clean water.[2] Problems related to safe water supply are expected to grow worse in the near future. Thus, intensive research on new methods for water remediation is required. It is critical to find new water treatment methods at lower cost and less energy consumption, while at the same time minimizing the use of chemicals and the impact on the environment. [2]

Chemistry has played a role as one of the causes of the aforementioned problems. Chemical waste dumping and the intensive use of energy for industrial activities that require chemical transformations have contributed to the current pollution problems. Therefore, chemistry has been part of the problem. However, this scientific discipline has also a huge potential to become part of the solution. In fact, the United

States Environmental Protection Agency (EPA) has recognized this potential proposing the concept of Green Chemistry.[3] A brief definition of this concept is: *"the design of chemical products and processes that reduce or eliminate the use or generation of hazardous substances. Green chemistry applies across the life cycle of a chemical product, including its design, manufacture, and use".[3]* The achievement of a chemistry of lower environmental impact requires to follow, as much as possible, the green chemistry principles[4] in the design and implementation of any chemical process.

The application of green chemistry guidelines to water treatment and energy production processes can help to overcome some environmental problems associated to the application of traditional technologies to those activities. In particular, from a green chemistry perspective energy production must move from the current technologies that deal with fossil fuels oxidation to others based on renewable resources. On the other hand, new processes of water purification with fewer expenses associated to chemical products would be desirable. Thus, chemistry research oriented to achieve these objectives has a great potential to provide solutions for these problems. If research finally succeeds in the development of new technologies for the above mentioned issues, chemistry will become an important part of the solution to the negative impact that human activities have caused on the planet.

1.2 A Brief Overview of TiO_2 Photocatalysis

Electron transfer reactions on irradiated metal oxides surfaces have been intensively studied as one attractive alternative for the remediation of polluted water[2,5] and the renewable production of energy.[1] Among several materials used for this purpose, titanium dioxide (TiO_2) has shown to be one of the most promising material used because it is highly photoreactive, cheap, non-toxic, chemically and biologically inert, and photostable.[5] However, further work is required to improve the photonic efficiency of this material in order to achieve cost competitiveness with respect to the traditional technologies and thereby, its application to large scale renewable energy production and/or wastewater treatment.

An intensive research effort on solar energy conversion using semiconductor catalysts has been made since the 70's decade. The publication of the hallmark article by Fujishima and Honda[6] about water splitting at a TiO_2/Pt photoelectrochemical cell triggered continuous attempts to apply semiconductors catalysts to the production of renewable energy. [7-21] Besides, a parallel endeavor has been focused on the application of TiO_2 to the degradation of water and gas phase pollutants.[5,10,15,22-38] Despite the huge potential of photocatalysis to become a widely applied technology for these issues, research has yet to succeed in developing a sound and comprehensive description and understanding of all the involved phenomena at molecular scale. [39]

The optical and electronic properties of the semiconductor materials used in the aforementioned applications are described by the band model according to the principles of semiconductor physics. [40-43] The band model can be conveniently approached as an extension of the molecular orbital theory, where molecular orbitals are formed by linear combination of the corresponding atomic orbitals. Because a solid is formed by a huge number of atoms ($6x10^{23}$ atoms/mol), the overlapping of their corresponding atomic orbitals leads to continuous bands of energy levels. The highest energy band which is occupied with electrons is called the valence band (VB) and the lowest unoccupied energy band is known as the conduction band (CB). For semiconductor solids there is a forbidden region of energy called the "bandgap" (E_g) which is located amid the VB and CB. [40-43]

It is widely accepted among the scientific community that the first step of any photocatalytic reaction is the excitation of the semiconductor with a photon of energy equal or greater than E_g. [15,27,29,31,33,34,37,39] After excitation, an electron $\left(e_f^-\right)$ is promoted from the VB into the CB leaving a hole $\left(h_f^+\right)$ behind. The amount of energy necessary to achieve the generation of these charge carriers depends on the electronic and optical properties of each semiconductor material. The E_g of anatase TiO_2 is 3.2 eV while that of rutile TiO_2 is 3.0 eV.[39] This mean that generation of electron-hole pairs at TiO_2 require excitation by light with a wavelength $\left(\lambda\right)$ shorter than 400 nm $\left(\lambda \leq 400nm\right)$, namely in the ultraviolet (UV) region of the electromagnetic spectra.

Once the charge carriers have been generated, they can follow several pathways: bulk recombination, migration to the semiconductor surface, surface recombination, and trapping by (adsorbed) substrate molecules.[31,39] When the charge carriers are recombined their energy is dissipated. If a suitable scavenger or a surface defect is available to trap the electron or hole, recombination is prevented and redox reactions may occur. [31] The photogenerated h_f^+ are powerful oxidizing agents (+1.0 to 3.5 V vs. NHE depending on the semiconductor and pH), while the e_f^- are good reductants (+0.5 to -1.5 V vs. NHE). [31] The oxidizing power of the h_f^+ is commonly applied to the photodegradation of organic substrates, one of the most studied applications of TiO_2 photocatalysis for environmental remediation. [38]

The organic substrates can react with h_f^+ through two different types of charge transfer mechanisms. A chemisorbed organic compound $(RH_2)_s$ can directly trap a h_f^+, or a dissolved organic compound $(RH_2)_{aq}$ reacts with holes previously trapped at intrinsic surface states, known as surface trapped holes $\left(h_s^+\right)$. [44] The former process occurs via a direct transfer (DT) mechanism while the later via an indirect transfer (IT) mechanism. Both processes can be correlated with the well known outer sphere (IT) and inner sphere (DT) electron transfer mechanisms.[44] Several possible pathways of hole transfer processes at the semiconductor/electrolyte interface are depicted in Figure 1.
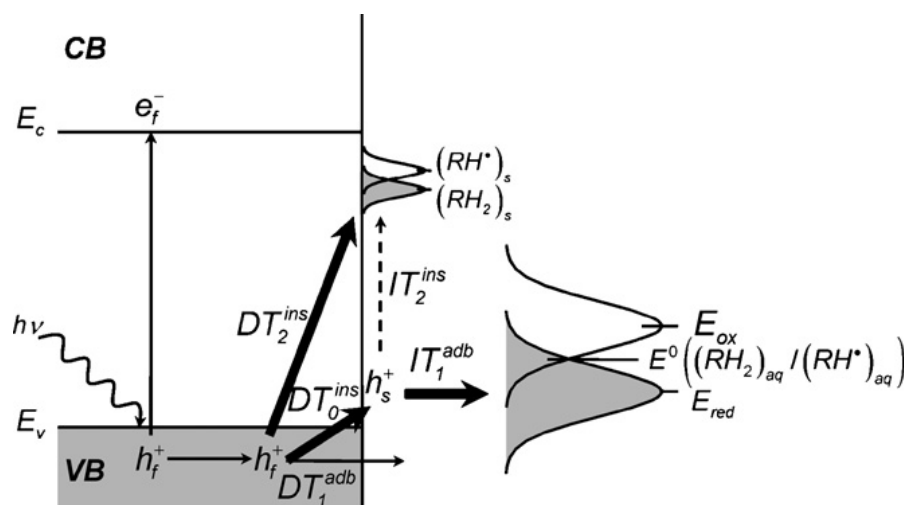
Figure 1. Energy diagram showing interfacial hole transfer reactions. Direct hole transfers (DT) of h_f^+ to filled energy levels of intrinsic bandgap surface states, $(RH_2)_{aq}$ dissolved species or extrinsic bandgap states associated with $(RH_2)_s$ surface-bound species, are represented by $DT_{ins}{}^0$, $DT_1{}^{adb}$ and $DT_2{}^{ins}$, respectively. Indirect transfer of h_s^+ holes to filled energy levels of either $(RH_2)_s$ surface bound species or $(RH_2)_{aq}$ dissolved species is represented by their respective rates $IT_2{}^{ins}$ and $IT_1{}^{adb}$. $IT_2{}^{ins}$ mechanism is depicted by means of a dotted vertical arrow indicating that, in general, its rate can be considered to be negligible. Adopted from reference 44 (copyright 2007, Elsevier).

The pathways $IT_2{}^{ins}$ and $DT_1{}^{adb}$ are depicted with thin or dotted arrows in Figure 1 because their rate can be considered negligible with respect to the others. [44] $DT_1{}^{adb}$ is an adiabatic hole transfer, hence its rate equation has an exponential reorganization energy term. As a result, its rate is very small compared with the pathways of inelastic hole transfers ($DT_0{}^{ins}$ or $DT_2{}^{ins}$). On the other hand, $IT_2{}^{ins}$ implies a reaction of h_s^+ with $(RH_2)_s$ which is very improbable because both species are immobile on the semiconductor surface. Thus, the rate of $IT_2{}^{ins}$ is negligible with respect to $IT_1{}^{adb}$ that represent the reaction of a h_s^+ with a mobile molecule, i.e. a dissolved organic substrate $(RH_2)_{aq}$.

Therefore, the $IT_2{}^{ins}$ and $DT_1{}^{adb}$ pathways will not be discussed here. Hence, according to Figure 1 once a h_f^+ is generated, it can follows two possible routes, being trapped at the semiconductor surface by either intrinsic surface states ($DT_0{}^{ins}$) or by a
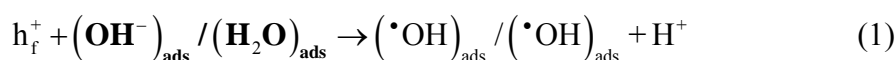
chemisorbed organic molecule (DT_2^{ins}). These hole transfer processes are inelastic (ins). It is worth noting that the DT_2^{ins} transfer imply the direct oxidation of an organic molecule. In contrast, the DT_0^{ins} transfer imply just the production of an h_s^+ at the semiconductor surface. The oxidation of an organic substrate requires an additional step (IT_1^{adb}) where the h_s^+ is adibatically (adb) transferred to a dissolved organic molecule. Thus, two main oxidation mechanisms of organic substrates by holes can be distinguished: one known as DT where a chemisorbed organic molecule is oxidized in a one step process and other known as IT that requires the generation of a h_s^+ and its subsequent reaction with a dissolved organic molecule. [44]

Because DT and IT mechanisms can simultaneously coexist and both lead to a similar distribution of photooxidized products their distinction is difficult. In fact, such distinction is the matter of an old but still not closed controversy. [44-51] The lack of consensus among the scientific community around this and other related topics demonstrate that detailed mechanisms of the photocatalytic processes are far to be clear.

Some critical issues that must be addressed to gain a deeper understanding of photocatalysis phenomena are those related to the charge carrier transfer at the solid/liquid interface[39,44,50,51,52] and also those related to the surface chemistry of metal oxides. [53] During the last decade, the surface science field has paid considerable attention to the study of chemistry at well-defined single crystal TiO_2 surfaces.[53-62] As a result, molecular level insights into photon initiated events occurring at TiO_2 surfaces has been achieved[60]. Details of the mechanisms of adsorption, interfacial charge transfer, and chemical reactions of several adsorbates at the TiO_2 surface have been disclosed at atomic scale. [54-62] However, the instrumentation used in surface science studies (SCS) requires ultra high vacuum conditions (UHV) and therefore, this body of knowledge must be used with care for the interpretation of photocatalytic phenomena of particles in contact with pollutants in gas or liquid phase.[5] For this reason, the important findings of these SCS have rarely been applied to the elucidation of reaction mechanisms of the most typical photocatalytic systems, i.e those in which the TiO_2 is in contact with a fluid phase. Notwithstanding, it is a necessity to take into account some

relevant findings achieved by SCS of TiO_2 for the elucidation of some kinetic and mechanistic issues of photocatalytic reactions that still remain unclear.

For instance, new insights into the water photooxidation reaction on TiO_2 have been attained by a detailed interpretation of electron photoemission spectra (EPS) of water adsorbed at rutile TiO_2 surfaces[63-66]. In particular, the commonly assumed reaction of direct oxidation of water, either dissociatively or molecularly adsorbed, by holes (eq 1) has been called into question. [63-66]

$$h_f^+ + \left(\mathbf{OH^-}\right)_{\mathbf{ads}} / \left(\mathbf{H_2O}\right)_{\mathbf{ads}} \rightarrow \left(\mathbf{^{\bullet}OH}\right)_{\mathbf{ads}} / \left(\mathbf{^{\bullet}OH}\right)_{\mathbf{ads}} + H^+ \qquad (1)$$

Almost forty years later that water splitting at a TiO_2 electrode was reported,[6] the SCS on TiO_2 provide information that challenge the commonly assumed production of hydroxyl radicals $\left(^{\bullet}OH\right)$ through reaction 1. This has important implications for the fundamental understanding of photocatalysis because reaction 1 has been long (and it is still) assumed as a fundamental step not only of water photooxidation reaction[8] but also of photocatalytic oxidation of organic substrates. [10,24-38] Even the most recent reviews[15, 36-38] on the topic of applications of TiO_2 for environmental purification still assign a crucial role to the $^{\bullet}OH$ species generated from reaction 1 as primary oxidizing agents of organic pollutants. A graphical example of this is depicted in Figure 2 which shows a typical scheme used to explain the basic mechanisms of TiO_2 photocatalysis.
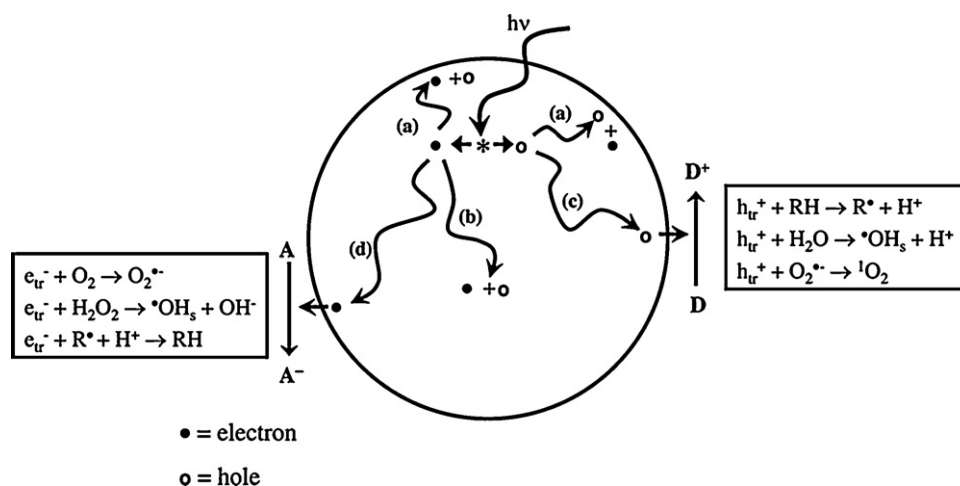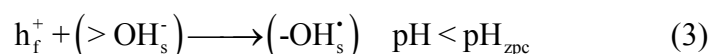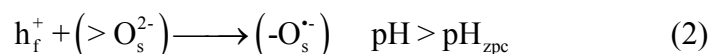

Figure 2. Processes that are supposed to occur on a bare TiO_2 particle after UV excitation. Adapted from reference 38 (copyright 2012, Elsevier).

As can be seen in Figure 2 the direct oxidation of water (eq 1) is still invoked as a primary event triggered by TiO_2 excitation despite the recent reported evidence about the thermodynamic and kinetic constraints that make such reaction unlikely. [63-66] Moreover, in Figure 2 the charge carriers generated within the catalyst particle react with acceptors or donors that belong to the reaction media (extrinsic surface states), namely water (H_2O), molecular oxygen (O_2) or organic substrates. These set of reactions would produce several types of reactive radicals $\left(O_2^{\cdot-}, {}^{\cdot}OH, R^{\cdot}, {}^1O_2\right)$ that further oxidize the organic substrates. Although the schematic view of Figure 2 seems a compendium of all the possible elementary steps of the photocatalytic process, it disregards the participation of the semiconductor lattice itself into the sequence of elemental reactions. This is an important handicap of traditional photocatalysis reaction mechanisms because the SCS on TiO_2 surfaces of the last decade have demonstrated that the surface lattice of a semiconductor is "dynamic". [53-62] This means that during the course of a photocatalytic reaction the surface lattice atoms can be incorporated into the reaction products, oxygen vacancies at the catalyst surface can be produced, and subsequently healed if there is suitable species to fill such vacancies in the reaction media. [53-62]

The above mentioned discoveries yielded by the SCS on TiO_2 surfaces open the possibility to envisage new mechanistic pathways for photocatalytic reactions. For instance, the possibility of generation of reactive species by hole trapping at the TiO_2 surface lattice oxygens (intrinsic surface states) and their subsequent participation in photooxidation reactions must be considered. Since long time ago, several authors have reported electron paramagnetic resonance (EPR) evidence showing that holes are trapped at the TiO_2 lattice oxygens (eqs 2 or 3). [67-69]

$$h_f^+ + \left(> O_s^{2-}\right) \longrightarrow \left(-O_s^{\cdot-}\right) \quad pH > pH_{zpc} \qquad (2)$$

$$h_f^+ + \left(> OH_s^-\right) \longrightarrow \left(-OH_s^{\cdot}\right) \quad pH < pH_{zpc} \qquad (3)$$

The products of reactions 2 or 3 are TiO_2 lattice radical species $\left(\left(-OH_s^{\cdot}\right)/\left(-O_s^{\cdot-}\right)\right)$ which can further react with organic substrates. However, this

possible reaction pathway is commonly overlooked in the traditional mechanistic proposals of photooxidation reactions[27] as can be seen in scheme 2. The omission of $\left(\text{-OH}_s^{\bullet}\right)/\left(\text{-O}_s^{\bullet-}\right)$ radicals as reactive species in photocatalysis leaves without any plausible explanation some relevant experimental facts: (1) The photoinduced oxygen isotope exchange (POIE) between TiO_2 surface lattice oxygen atoms (O_s) and those from gas-phase molecular oxygen ($^{18}O_2$ (g)). [70-75] It is evident that POIE phenomena imply the removal of oxygen atoms from the TiO_2 lattice. This removal necessarily implies that the Ti-O bonds at the lattice are weakened during the illumination of the catalyst. Hole trapping according to eqs 2 or 3 leads to Ti-O bond weakening because one electron from the Ti-O covalent bond is removed. Therefore, plausible mechanisms for the POIE phenomena can be formulated invoking the participation of $\left(\text{-OH}_s^{\bullet}\right)/\left(\text{-O}_s^{\bullet-}\right)$ radical species. In contrast, none of the reactions depicted in scheme 2 can explain why the oxygen lattice is removed from a TiO_2 sample under UV irradiation. (2) During the water photooxidation reaction the TiO_2 surface lattice is distorted as was recently demonstrated by atomic force microscopy (AFM) images of TiO_2 crystals taken before and after water photooxidation experiments. [64] Such atomic surface roughening implies that in the course of water photooxidation at TiO_2 some chemical bonds at the semiconductor lattice are lengthened. This fact can be readily explained by a reaction mechanism which involve $\left(\text{-OH}_s^{\bullet}\right)/\left(\text{-O}_s^{\bullet-}\right)$ as reaction intermediates. [66] In contrast, the direct oxidation of water (eq 1) must produce no distortion at the semiconductor lattice.

The above two examples reflects that reaction mechanisms in photocatalysis must take into account the generation of $\left(\text{-OH}_s^{\bullet}\right)/\left(\text{-O}_s^{\bullet-}\right)$ radicals, and their subsequent reactions with organic substrates, in order to give a comprehensive explanation to the phenomena involved in the photocatalytic process. If a new mechanistic pathway with $\left(\text{-OH}_s^{\bullet}\right)/\left(\text{-O}_s^{\bullet-}\right)$ radical species is formulated new kinetic expressions must be deduced from it.

It is worth noting that the $\left(\text{-OH}_s^{\cdot}\right)/\left(\text{-O}_s^{\cdot\cdot}\right)$ radicals are surface trapped holes $\left(h_s^+\right)$ that can be adibatically transferred to a dissolved organic molecule (pathway IT_1^{adb} in Figure 1). Because $\left(\text{-OH}_s^{\cdot}\right)/\left(\text{-O}_s^{\cdot\cdot}\right)$ radicals are overlooked in the traditional reactions mechanisms, the IT_1^{adb} route for hole transfer which involves these species is also neglected by the kinetic models proposed for photocatalytic reactions. Indeed, the most widely used kinetic model in photocatalysis, the Langmuir-Hinshewoold (L-H) kinetic model, do not consider oxidation reactions with $\left(\text{-OH}_s^{\cdot}\right)/\left(\text{-O}_s^{\cdot\cdot}\right)$ and neglect the IT_1^{adb} route of hole transfer. [27,29,31] Although a wide range of photocatalytic kinetic data can be fitted to a L-H type kinetic expression, this model has serious weak points that have been extensively reviewed by several research groups. [5,44,45,50,76-80] As a consequence, an alternative kinetic approach based on the degree of electronic interaction between the organic substrate and the semiconductor surface has been recently proposed. [44, 47-49] This approach, known as the direct-indirect (D-I) kinetic model considers all the possible routes for hole transfer depicted in Figure 1. This leads to several kinetic expressions that can be applied for each mechanisms of hole transfer showed in Figure 1. In a specific photocatalytic oxidation, one of the hole transfer routes would prevail depending on the degree of interaction of the organic molecule with the TiO_2 surface. Specifically, in the absence of chemisorption of the organic substrate this is oxidized by h_s^+ via a IT mechanisms, while a chemisorbed organic compound is directly oxidized by h_f^+ via a DT mechanism. Therefore, unless the L-H model which proposes a unique kinetic expression for all the organic substrates, the D-I model proposes different kinetic equations for DT and IT photooxidation mechanisms.

The above discussed items are only few examples of "hot topics" under debate in the field of photocatalysis. This debate demonstrates that there is still space for interpretation and that, so far, the discussion is not closed. Although there are a lot of additional items that are matter of current controversy in the photocatalysis field, the above discussion was just centered in kinetic and mechanisms of photooxidation reactions because this PhD thesis will address these topics in detail.

References to Chapter 1

(1) Kamat, P. V. Energy Outlook for Planet Earth. *J. Phys. Chem. Lett.* **2013,** *4* (10), 1727-1729.

(2) Shannon, M. A.; Bohn, P. W.; Elimelech, M.; Georgiadis, J. G.; Marinas, B. J.; Mayes, A. M. Science and technology for water purification in the coming decades. *Nature* **2008,** *452* (7185), 301-310.

(3) United States Environmental Protection Agency (EPA). *Green Chemistry [online]* http://www.epa.gov/greenchemistry (consulted on June 14th, 2013).

(4) Anastas, P.T.; Warner, J.C. *Green Chemistry: theory and practice*. 11th ed.; Oxford University Press: Oxford, 2000.

(5) Friedmann, D.; Mendive, C.; Bahnemann, D. TiO$_2$ for Water Treatment: Parameters Affecting the Kinetics and Mechanisms of Photocatalysis. *Applied Catalysis B: Environmental* **2010,** *99* (3–4), 398-406.

(6) Fujishima, A.; Honda, K. Electrochemical Photolysis of Water at a Semiconductor Electrode. *Nature* **1972,** *238* (5358), 37-38.

(7) Van Damme, H.; Hall, W. K. Photoassisted Decomposition of Water at the Gas-Solid Interface on Titanium Dioxide. *Journal of the American Chemical Society* **1979,** *101* (15), 4373-4374.

(8) Nishimoto, S. I.; Ohtani, B.; Kajiwara, H.; Kagiya, T. Photoinduced Oxygen Formation and Silver-Metal Deposition in Aqueous Solutions Of Various Silver Salts By Suspended Titanium Dioxide Powder. *J. Chem. Soc. , Faraday Trans. 1* **1983,** *79* (11), 2685-2694.

(9) O'Regan, B.; Gratzel, M. A Low-Cost, High-Efficiency Solar Cell Based On Dye-Sensitized Colloidal TiO$_2$ Films. *Nature* **1991,** *353* (6346), 737-740.

(10) Fujishima, A.; Rao, T. N.; Tryk, D. A. Titanium Dioxide Photocatalysis. *Journal of Photochemistry and Photobiology C: Photochemistry Reviews* **2000,** *1* (1), 1-21.

(11) Asahi, R.; Morikawa, T.; Ohwaki, T.; Aoki, K.; Taga, Y. Visible-Light Photocatalysis in Nitrogen-Doped Titanium Oxides. *Science* **2001,** *293* (5528), 269-271.

(12) Grätzel, M. Dye-sensitized Solar Cells. *Journal of Photochemistry and Photobiology C: Photochemistry Reviews* **2003,** *4* (2), 145-153.

(13) Beranek, R.; Kisch, H. Surface-Modified Anodic TiO$_2$ Films for Visible Light Photocurrent Response. *Electrochemistry Communications* **2007,** *9* (4), 761-766.

(14) Rajeshwar, K. Hydrogen Generation at Irradiated Oxide Semiconductor Solution Interfaces. *Journal of Applied Electrochemistry* **2007,** *37* (7), 765-787.

(15) Fujishima, A.; Zhang, X.; Tryk, D. A. TiO$_2$ Photocatalysis and Related Surface Phenomena. *Surface Science Reports* **2008,** *63* (12), 515-582.

(16) Smith, A. M.; Nie, S. Semiconductor Nanocrystals: Structure, Properties, and Band Gap Engineering. *Accounts of Chemical Research* **2009,** *43* (2), 190-200

(17) Bard, A. J. Inner-Sphere Heterogeneous Electrode Reactions. Electrocatalysis and Photocatalysis: The Challenge. *Journal of the American Chemical Society* **2010,** *132* (22), 7559-7567.

(18) Chen, X.; Liu, L.; Yu, P. Y.; Mao, S. S. Increasing Solar Absorption for Photocatalysis with Black Hydrogenated Titanium Dioxide Nanocrystals. *Science* **2011,** *331* (6018), 746-750.

(19) Nakata, K.; Fujishima, A. TiO_2 photocatalysis: Design and Applications. *Journal of Photochemistry and Photobiology C: Photochemistry Reviews* **2012,** *13* (3), 169-189.

(20) Serpone, N.; Emeline, A. V. Semiconductor Photocatalysis: Past, Present, and Future Outlook. *J. Phys. Chem. Lett.* **2012,** *3* (5), 673-677.

(21) Yang, J.; Wang, D.; Han, H.; Li, C. Roles of Cocatalysts in Photocatalysis and Photoelectrocatalysis. *Accounts of Chemical Research* **2013**. In Press, **DOI:** 10.1021/ar300227e

(22) Frank, S. N.; Bard, A. J. Heterogeneous Photocatalytic Oxidation of Cyanide Ion in Aqueous Solutions At Titanium Dioxide Powder. *Journal of the American Chemical Society* **1977,** *99* (1), 303-304.

(23) Frank, S. N.; Bard, A. J. Heterogeneous Photocatalytic Oxidation of Cyanide and Sulfite in Aqueous Solutions at Semiconductor Powders. *J. Phys. Chem.* **1977,** *81* (15), 1484-1488.

(24) Okamoto, K. i.; Yamamoto, Y.; Tanaka, H.; Tanaka, M.; Itaya, A. Heterogeneous Photocatalytic Decomposition of Phenol over TiO_2 Powder. *Bulletin of the Chemical Society of Japan* **1985,** *58* (7), 2015-2022.

(25) Matthews, R. W. Photooxidation of Organic Impurities in Water Using Thin Films of Titanium Dioxide. *J. Phys. Chem.* **1987,** *91* (12), 3328-3333.

(26) Al-Ekabi, H.; Serpone, N.; Pelizzetti, E.; Minero, C.; Fox, M. A.; Draper, R. B. Kinetic Studies In Heterogeneous Photocatalysis. 2. Titania-Mediated Degradation Of 4-Chlorophenol Alone And In A Three-Component Mixture Of 4-Chlorophenol, 2,4-Dichlorophenol, And 2,4,5-Trichlorophenol In Air-Equilibrated Aqueous Media. *Langmuir* **1989,** *5* (1), 250-255.

(27) Turchi, C. S.; Ollis, D. F. Photocatalytic Degradation of Organic Water Contaminants: Mechanisms Involving Hydroxyl Radical Attack. *Journal of Catalysis* **1990,** *122* (1), 178-192.

(28) Kormann, C.; Bahnemann, D. W.; Hoffmann, M. R. Photolysis of Chloroform and Other Organic Molecules in Aqueous Titanium Dioxide Suspensions. *Environmental Science & Technology* **1991,** *25* (3), 494-500.

(29) Fox, M. A.; Dulay, M. T. Heterogeneous Photocatalysis. *Chemical Reviews* **1993,** *93* (1), 341-357.

(30) Mills, A.; Morris, S.; Davies, R. Photomineralisation Of 4-Chlorophenol Sensitised By Titanium Dioxide: A Study of The Intermediates. *Journal of Photochemistry and Photobiology A: Chemistry* **1993,** *70* (2), 183-191.

(31) Hoffmann, M. R.; Martin, S. T.; Choi, W.; Bahnemann, D. W. Environmental Applications of Semiconductor Photocatalysis. *Chemical Reviews* **1995,** *95* (1), 69-96.

(32) Theurich, J.; Lindner, M.; Bahnemann, D. W. Photocatalytic Degradation of 4-Chlorophenol in Aerated Aqueous Titanium Dioxide Suspensions: A Kinetic and Mechanistic Study. *Langmuir* **1996,** *12* (26), 6368-6376.

(33) Mills, A.; Le Hunte, S. An Overview of Semiconductor Photocatalysis. *Journal of Photochemistry and Photobiology A: Chemistry* **1997,** *108* (1), 1-35.

(34) Alfano, O. M.; Bahnemann, D.; Cassano, A. E.; Dillert, R.; Goslich, R. Photocatalysis In Water Environments Using Artificial and Solar Light. *Catalysis Today* **2000,** *58* (2-3), 199-230.

(35) Peiro, A. M.; Ayllon, J. A.; Peral, J.; Domenech, X. TiO$_2$-photocatalyzed Degradation Of Phenol And Ortho-Substituted Phenolic Compounds. *Applied Catalysis B: Environmental* **2001,** *30* (3-4), 359-373.

(36) Gaya, U. I.; Abdullah, A. H. Heterogeneous Photocatalytic Degradation of Organic Contaminants Over Titanium Dioxide: A Review Of Fundamentals, Progress And Problems. *Journal of Photochemistry and Photobiology C: Photochemistry Reviews* **2008,** *9* (1), 1-12.

(37) Malato, S.; Fernandez-Ibañez, P.; Maldonado, M. I.; Blanco, J.; Gernjak, W. Decontamination and Disinfection Of Water By Solar Photocatalysis: Recent Overview And Trends. *Catalysis Today* **2009,** *147* (1), 1-59.

(38) Ochiai, T.; Fujishima, A. Photoelectrochemical Properties of TiO$_2$ Photocatalyst and Its Applications for Environmental Purification. *Journal of Photochemistry and Photobiology C: Photochemistry Reviews* **2012,** *13* (4), 247-262.

(39) Zhang, L.; Mohamed, H. H.; Dillert, R.; Bahnemann, D. Kinetics and Mechanisms of Charge Transfer Processes in Photocatalytic Systems: A Review. *Journal of Photochemistry and Photobiology C: Photochemistry Reviews* **2012,** *13* (4), 263-276.

(40) Morrison, S.R. *Electrochemistry at Semiconductor and Oxidized Metal Electrodes*. Plenum Press. New York, **1980**.

(41) Cox, P.A. *The Electronic Structure and Chemistry of Solids*, Oxford University Press, Oxford, **1987**.

(42) Memming, R. *Semiconductor Electrochemistry*, first ed., Wiley-VCH, Weinheim, **2001**.

(43) Kasap, S.O. *Principles of Electronic Materials and Devices*, McGraw-Hill, New York, **2006**.

(44) Monllor-Satoca, D.; Gomez, R.; Gonzalez-Hidalgo, M.; Salvador, P. The "Direct-Indirect" Model: An Alternative Kinetic Approach in Heterogeneous Photocatalysis Based on The Degree Of Interaction Of Dissolved Pollutant Species with The Semiconductor Surface. *Catalysis Today* **2007,** *129* (1-2), 247-255.

(45) Minero, C. Kinetic Analysis of Photoinduced Reactions at the Water Semiconductor Interface. *Catalysis Today* **1999,** *54* (2-3), 205-216.

(46) Minero, C.; Mariella, G.; Maurino, V.; Pelizzetti, E. Photocatalytic Transformation of Organic Compounds in the Presence of Inorganic Anions. 1. Hydroxyl-Mediated and Direct Electron-Transfer Reactions of Phenol on a Titanium Dioxide-Fluoride System. *Langmuir* **2000,** *16* (6), 2632-2641.

(47) Villarreal, T. L.; Gomez, R.; Gonzalez, M.; Salvador, P. A Kinetic Model for Distinguishing between Direct and Indirect Interfacial Hole Transfer in the Heterogeneous Photooxidation of Dissolved Organics on TiO_2 Nanoparticle Suspensions. *J. Phys. Chem. B* **2004,** *108* (52), 20278-20290.

(48) Montoya, J. F.; Velasquez, J. A.; Salvador, P. The Direct-Indirect Kinetic Model in Photocatalysis: A Reanalysis of Phenol and Formic Acid Degradation Rate Dependence on Photon Flow and Concentration in TiO_2 Aqueous Dispersions. *Applied Catalysis B: Environmental* **2009,** *88* (1-2), 50-58.

(49) Montoya, J. F.; Salvador, P. The Influence of Surface Fluorination in the Photocatalytic Behaviour of TiO_2 Aqueous Dispersions: An Analysis In The Light of the Direct-Indirect Kinetic Model. *Applied Catalysis B: Environmental* **2010,** *94* (1-2), 97-107.

(50) Minero, C.; Bedini, A.; Maurino, V. Glycerol as a Probe Molecule to Uncover Oxidation Mechanism in Photocatalysis. *Applied Catalysis B: Environmental* **2012,** *128*, 135-143.

(51) Montoya, J. F.; Peral, J.; Salvador, P. Commentary on the article: "A New Kinetic Model For Heterogeneous Photocatalysis With Titanium Dioxide: Case Of Non-Specific Adsorption Considering Back Reaction, by S. Valencia, F. Cataño, L. Rios, G. Restrepo and J. Marín, published in Applied Catalysis B: Environmental, 104 (2011) 300-304". *Applied Catalysis B: Environmental* **2012,** *111-112*, 649-650.

(52) Akimov, A. V.; Neukirch, A. J.; Prezhdo, O. V. Theoretical Insights into Photoinduced Charge Transfer and Catalysis at Oxide Interfaces. *Chemical Reviews* **2013,** *113* (6), 4496-4565.

(53) Campbell, C. T.; Sauer, J. Introduction: Surface Chemistry of Oxides. *Chemical Reviews* **2013,** *113* (6), 3859-3862.

(54) Henderson, M. A. The Interaction of Water With Solid Surfaces: Fundamental Aspects Revisited. *Surface Science Reports* **2002,** *46* (1-8), 1-308.

(55) Diebold, U. The Surface Science of Titanium Dioxide. *Surface Science Reports* **2003,** *48* (5-8), 53-229.

(56) Liu, L. M.; Crawford, P.; Hu, P. The Interaction Between Adsorbed OH And O_2 On TiO_2 Surfaces. *Progress in Surface Science* **2005,** *84* (5-6), 155-176.

(57) Thompson, T. L.; Yates, J. T. Surface Science Studies of The Photoactivation Of TiO_2 new Photochemical Processes. *Chemical Reviews* **2006,** *106* (10), 4428-4453.

(58) Pang, C. L.; Lindsay, R.; Thornton, G. Chemical Reactions On Rutile TiO_2(110). *Chemical Society Reviews* **2008,** *37* (10), 2328-2353.

(59) Besenbacher, F.; Lauritsen, J. V.; Linderoth, T. R.; Laegsgaard, E.; Vang, R. T.; Wendt, S. Atomic-Scale Surface Science Phenomena Studied By Scanning Tunneling Microscopy. *Surface Science* **2009,** *603* (10-12), 1315-1327.

(60) Henderson, M. A. A Surface Science Perspective on Photocatalysis. *Surface Science Reports* **2011,** *66* (6-7), 185-297.

(61) Henderson, M. A.; Lyubinetsky, I. Molecular-Level Insights Into Photocatalysis From Scanning Probe Microscopy Studies On TiO_2 (110). *Chemical Reviews* **2013,** *113* (6), 4428-4455.

(62) Pang, C. L.; Lindsay, R.; Thornton, G. Structure of Clean and Adsorbate-Covered Single-Crystal Rutile TiO_2 Surfaces. *Chemical Reviews* **2013,** *113* (6), 3887-3948.

(63) Nakamura, R.; Nakato, Y. Primary Intermediates of Oxygen Photoevolution Reaction on TiO_2 (Rutile) Particles, Revealed By In Situ FTIR Absorption and Photoluminescence Measurements. *Journal of the American Chemical Society* **2004,** *126* (4), 1290-1298.

(64) Imanishi, A.; Okamura, T.; Ohashi, N.; Nakamura, R.; Nakato, Y. Mechanism of Water Photooxidation Reaction at Atomically Flat TiO_2 (Rutile) (110) and (100) Surfaces: Dependence on Solution pH. *Journal of the American Chemical Society* **2007,** *129* (37), 11569-11578.

(65) Salvador, P. On the Nature of Photogenerated Radical Species Active in the Oxidative Degradation of Dissolved Pollutants with TiO_2 Aqueous Suspensions: A Revision in the Light of the Electronic Structure of Adsorbed Water. *J. Phys. Chem. C* **2007,** *111* (45), 17038-17043.

(66) Salvador, P. Mechanisms of Water Photooxidation At n-TiO_2 Rutile Single Crystal Oriented Electrodes Under UV Illumination in Competition With Photocorrosion. *Progress in Surface Science* **2011,** *86* (1-2), 41-58.

(67) Howe, R. F.; Gratzel, M. EPR Study of Hydrated Anatase Under UV Irradiation. *J. Phys. Chem.* **1987,** *91* (14), 3906-3909.

(68) Micic, O. I.; Zhang, Y.; Cromack, K. R.; Trifunac, A. D.; Thurnauer, M. C. Trapped Holes On Titania Colloids Studied By Electron Paramagnetic Resonance. *J. Phys. Chem.* **1993,** *97* (28), 7277-7283.

(69) Dimitrijevic, N. M.; Saponjic, Z. V.; Rabatic, B. M.; Poluektov, O. G.; Rajh, T. Effect of Size and Shape of Nanocrystalline TiO_2 on Photogenerated Charges. An EPR Study. *J. Phys. Chem. C* **2007,** *111* (40), 14597-14601.

(70) Courbon, H.; Formenti, M.; Pichat, P. Study of Oxygen Isotopic Exchange Over Uv Irradiated Anatase Samples and Comparison with Photooxidation of Isobutane Into Acetone. *Journal of Physical Chemistry* **1977,** *81* (6), 550-554.

(71) Sato, S. Hydrogen and oxygen isotope exchange reactions over illuminated and nonilluminated titania. *J. Phys. Chem.* **1987,** *91* (11), 2895-2897.

(72) Sato, S.; Kadowaki, T.; Yamaguti, K. Photocatalytic oxygen isotopic exchange between oxygen molecule and the lattice oxygen of titanium dioxide prepared from titanium hydroxide. *J. Phys. Chem.* **1984,** *88* (14), 2930-2931.

(73) Pichat, P.; Courbon, H.; Enriquez, R.; Tan, T. T. Y.; Amal, R. Light-Induced Isotopic Exchange Between O_2 and Semiconductor Oxides, A Characterization Method That Deserves not to be Overlooked. *Research on Chemical Intermediates* **2007,** *33* (3-5), 239-250.

(74) Montoya, J. F.; Peral, J.; Salvador, P. Surface Chemistry and Interfacial Charge-Transfer Mechanisms in Photoinduced Oxygen Exchange at O_2-TiO_2 Interfaces. *ChemPhysChem* **2011,** *12* (5), 901-907.

(75) Mikhaylov, R. V.; Lisachenko, A. A.; Titov, V. V. Investigation of Photostimulated Oxygen Isotope Exchange on TiO_2 Degussa P25 Surface upon UV-Vis Irradiation. *J. Phys. Chem. C* **2012,** *116* (44), 23332-23341

(76) Emeline, A. V.; Ryabchuk, V.; Serpone, N. Factors Affecting The Efficiency Of A Photocatalyzed Process In Aqueous Metal-Oxide Dispersions: Prospect Of Distinguishing Between Two Kinetic Models. *Journal of Photochemistry and Photobiology A: Chemistry* **2000,** *133* (1-2), 89-97.

(77) Emeline, A. V.; Ryabchuk, V. K.; Serpone, N. Dogmas and Misconceptions in Heterogeneous Photocatalysis. Some Enlightened Reflections. *J. Phys. Chem. B* **2005,** *109* (39), 18515-18521.

(78) Ollis, D. F. Kinetics of Liquid Phase Photocatalyzed Reactions: An Illuminating Approach. *The Journal of Physical Chemistry B* **2005,** *109* (6), 2439-2444.

(79) Ollis, D. Kinetic Disguises in Heterogeneous Photocatalysis. *Topics in Catalysis* **2005,** *35* (3), 217-223.

(80) Mills, A.; Wang, J.; Ollis, D. F. Kinetics of Liquid Phase Semiconductor Photoassisted Reactions: Supporting Observations for a Pseudo-Steady-State Model. *The Journal of Physical Chemistry B* **2006,** *110* (29), 14386-14390.

(81) Mills, A.; Wang, J.; Ollis, D. F. Dependence of the kinetics of liquid-phase photocatalyzed reactions on oxygen concentration and light intensity. *Journal of Catalysis* **2006,** *243* (1), 1-6.

(82) Ohtani, B. Preparing Articles on Photocatalysis-Beyond the Illusions, Misconceptions, and Speculation. *Chemistry Letters* **2008,** *37* (3), 216-229.

CHAPTER 2

GOALS AND SCOPE

This PhD thesis is aimed at elucidating some relevant features of the mechanisms of interfacial charge transfer (ICT) processes at the semiconductor/fluid-phase interface and at disclosing new mechanistic pathways for photocatalytic oxidation reactions that can satisfactorily account for the large body of experimental data reported within the field of photocatalysis.

Although the aforementioned phenomena can be studied at any semiconductor/fluid-phase interface, it is desirable to select a widely studied system in order to take advantage of the considerable body of knowledge available in the scientific literature. Since the most common systems employed in mechanistic and kinetic studies of photocatalytic oxidation reactions consist of TiO_2 nanoparticles suspended in liquid phase, most of the experimental work reported in this thesis is devoted to the study of photooxidation reactions at TiO_2/liquid interfaces. Nevertheless, relevant findings reported in the literature about the surface chemistry at the gas-phase/TiO_2 interfaces or even at TiO_2 surfaces exposed to UHV have been also analyzed in detail. This set of experimental and theoretical information has been collected to achieve the following specific aims:

1. **To establish in detail how the degree of electronic interaction between the semiconductor surface and the organic substrate influences the ICT processes**. This aim can be focused on three objectives: (1) To analyze the degree of interaction of several model organic substrates with bare TiO_2 or fluorinated TiO_2 surfaces by mean of spectroscopy techniques. (2) To assess the kinetic behavior of TiO_2-assisted photooxidation reactions of each model compound. (3) To formulate a mathematical correlation able to describe the relationship between the kinetic behavior of a specific organic substrate and its interaction with the TiO_2 surface.

2. **To elucidate the role played by the TiO_2 surface lattice oxygens (O_s) in photocatalytic oxidation reactions**. This aim can be focused on two objectives: (1) To overhaul in detail the scientific literature about POIE phenomena and relevant findings of SCS on TiO_2 in order to gain a better

understanding of the chemical reactivity of the O_s and also to envisage plausible photocatalytic reaction mechanisms which consider the participation of O_s into the sequence of elementary steps. (2) To develop a comprehensive experimental study of TiO_2 photooxidation reactions under carefully controlled amounts of O_2 and/or H_2O in the reaction media or using oxygen-isotope-labeled titania ($Ti^{18}O_2$) as catalysts in order to acquire experimental evidence that allow to distinguish whether the O_s are actually involved into the elementary steps of the TiO_2-assisted oxidation reactions or not.

The above mentioned issues have been studied at TiO_2/fluid-phase interfaces. However, some mechanistic and kinetic features explored in this work have implications beyond this particular reaction system because some basic principles of ICT processes and surface chemistry at metal oxides discussed here are applicable to a wide range of semiconductor materials. Notwithstanding, the interpretations of photocatalysis phenomena achieved from studies with TiO_2 can not be directly extrapolated and must be used with care for the interpretation of phenomena at different semiconductor catalysts.

CHAPTER 3

RESULTS AND DISCUSSION

SECTION A

Kinetic Analysis of

Photocatalytic Reactions

The interpretation of kinetic data of photocatalytic oxidation reactions has largely relied on the L-H kinetic model. This model yields a kinetic expression for photocatalytic reactions based on some assumptions about the reaction mechanisms. Some relevant assumptions are: (1) The chemical nature of the semiconductor surface does not change in the course of photooxidation reactions. (2) The dark adsorption-desorption equilibrium is not perturbed under illumination (3) The charge transfer mechanisms do not depend on the degree of electronic interaction between the semiconductor surface and the organic substrate to be photooxidized. (4) The nature of the primary oxidizing species has no influence on the kinetic behavior. Thus, there is a unique L-H rate equation applicable to any type of organic substrate, no matters if it is mainly oxidized by holes, surface lattice radicals or free hydroxyl radicals in the bulk of the solution.

The above assumptions have been called into question in the last decade by several research groups. Therefore, an alternative approach to interpret the kinetics of photocatalytic reactions is required. Our research group has proposed the D-I model as an alternative. The research work presented in this section (Publication 1), and the respective complementary results of the annexes chapter (Manuscripts 1 and 2), were carried out in order to develop suitable kinetic expressions able to predict the dependence of the reaction rate on photon flow and the initial concentration of the substrate to be photooxidized. On the other hand, one important objective was to formulate rate equations that include kinetic constants with a well defined physical meaning. Indeed, the lack of physical meaning of the L-H rate constants is one of the main drawbacks that must be overcome by any alternative kinetic model. Because the scientific literature concerning the aforementioned items is extensively reviewed in the publication 1 and the manuscripts 1 and 2, this brief introduction does not cite any reference. The objective here is just summarizing the main issues of kinetics of photocatalytic reactions addressed by this research. Details can be found in the respective publications.

The development of suitable kinetic expressions for photocatalytic reactions requires the formulation of a plausible reaction mechanism. As discussed above, some

assumptions, made to deduce the L-H rate equation, have been challenged. Thus, the formulation of an alternative kinetic model must start proposing an alternative reaction mechanism. As discussed in the introduction the main assumption made by the D-I model is that there are two types of charge transfer mechanisms, direct transfer (DT) and indirect transfer (IT). The prevalence of each mechanism is determined by the degree of electronic interaction between the organic substrate and the semiconductor surface. When there is strong electronic interaction (chemisorption) the DT mechanisms prevails. In the absence of chemisorption IT is the only working mechanism of charge transfer. If both types of adsorption modes (chemisorption and physisorption) coexist both DT and IT mechanisms coexists. In this situation, the prevalence of one charge transfer mechanisms depend on the proportion of organic molecules that are able to be chemisorbed at the semiconductor surface and the relative reaction rate of each reaction pathway.

The research work presented in the publication 1 and the manuscripts 1 and 2 is devoted to test if the D-I model is able not only to yield mathematical expressions to predict the kinetic behavior of several reaction systems but also to test if the main assumptions made by the D-I model are correct or not. This test of the D-I model requires, as starting point, to study in detail the degree of interaction between several model organic substrates and the semiconductor surface. Throughout this work, the interactions of three organic compounds were studied by spectroscopy techniques: formic acid (FA), phenol (PhO) and benzene (Bz). It was found that these three organic substrates represent three paradigmatic cases: the main adsorption mode of FA is chemisorption even in aqueous solution where a competition between the FA and water molecules for the adsorption sites at the TiO_2 surface is expected. This means that FA is able to displace the adsorbed water molecules from the TiO_2 surface and become chemisorbed. Bz is only physisorbed at the TiO_2 surface. Finally, both adsorption modes (physisorption and chemisorption) coexist in the case of phenol. By analyzing adsorption isotherms of phenol at the TiO_2 surface in the presence of water and acetonitrile it could be established that the proportion of phenol molecules that are able to be chemisorbed depend on the solvent. In the presence of water, a low amount of phenol molecules are able to be chemisorbed due to the competition of water for the

adsorption sites. In contrast, in the presence of acetonitrile, phenol molecules are readily chemisorbed at the TiO_2 surface. According to our working hypothesis, reaction rate of phenol oxidation in acetonitrile turned out to be clearly faster than in water in spite of the important source of hydroxyl radicals posed by this solvent.

Besides the observed differences in the adsorption modes attributable to the chemical nature of the organic substrate, important modifications in such adsorption modes ascribable to the chemical structure of the TiO_2 surface were also found. This aspect was explored in detail in publication 1 by using a well known method to modify the TiO_2 surface structure, i.e TiO_2 surface fluorination. It was found that fluorinated TiO_2 (F-TiO_2) interacts with the organic substrates in a way that is clearly different to the interaction of bare TiO_2. Chemisorption of FA is hindered on F-TiO_2 because fluoride ions occupy the adsorption sites at the TiO_2 surface. As a result, fluorination had a detrimental effect on the FA photooxidation rate. Because phenol in aqueous solution weakly interacts with the TiO_2 surface, fluorination does not produce a significant change in its adsorption mode. However, the energy levels of F-TiO_2 are modified with respect to bare TiO_2. Indeed, it was demonstrated by electrochemical measurements that there is a higher degree of overlapping between the energy levels of F-TiO_2 and PhO molecules than that between bare TiO_2 and PhO. As a consequence, the photooxidation rate of PhO was enhanced by TiO_2 surface fluorination. In general, the effect of the TiO_2 surface fluorination in the kinetic behavior was found to be dependent on the prevalent charge transfer mechanism. If an organic substrate is mainly photooxidized by a DT mechanism, fluorination caused a decrease in the photooxidation rate due to the blocking of adsorption sites at the TiO_2 surface by fluoride ions. In contrast, if an organic substrate is mainly photooxidized by an IT mechanism, fluorination cause an increase in the photooxidation rate due to the enhanced overlapping between the energy levels of the semiconductor and the organic substrate.

Once the interaction modes of the different organic substrates with TiO_2 or F-TiO_2 were elucidated by spectroscopy techniques and the analysis of adsorption isotherms, a comparative kinetic study was carried out. It was found that the kinetic

behavior of each model compound is directly related with the interaction mode of the organic substrate with the TiO_2 or the $F-TiO_2$ surfaces. When chemisorption prevails the kinetic behavior can be described by a mathematical equation deduced for DT mechanism. In contrast, in the absence of chemisorption the kinetics can only be described by a mathematical equation deduced for IT mechanism. When both adsorption modes coexist the kinetic behavior is modeled by an expression that combines both the DT and the IT equations. In general, the set of kinetic data collected in this work could be adjusted to the equations proposed by the D-I model for different cases of interaction modes of the model compounds with the semiconductor surface. Moreover, it was shown that the experimental data collected in this work can not be explained in the frame of the assumptions and the rate equation yield by the L-H kinetic model.

Publication 1

"The Influence of Surface Fluorination in the Photocatalytic Behavior of TiO$_2$
Aqueous Dispersions: An Analysis in the Light of the Direct-Indirect Kinetic Model".

Applied Catalysis B: Environmental **2010,** *94* (1-2), 97-107

Contents lists available at ScienceDirect

Applied Catalysis B: Environmental

The influence of surface fluorination in the photocatalytic behaviour of TiO$_2$ aqueous dispersions: An analysis in the light of the direct–indirect kinetic model

J.F. Montoya [a], P. Salvador [b,c,*]

[a] Departamento de Química, Universidad Autónoma de Barcelona, Spain
[b] Departament de Ciències Matemàtiques i Informàtica, Universitat de les Illes Balears, Palma de Mallorca, E-07071, Spain
[c] Instituto de Catálisis y Petroleoquímica, CSIC, Spain

A B S T R A C T

TiO$_2$ surface fluorination is known to produce an enhancement of the photocatalytic oxidation rate of some organic compounds such as phenol, acid orange, azo dye Acid Red 1 and benzoic acid, while leads to a clear decrease of the photooxidation quantum yield of other compounds like formic acid, and dichloroacetate. Here we show that these differences in behaviour cannot be explained in the framework of the classical "Langmuir–Hinshelwood" (L–H) kinetic model, although they are compatible with the predictions of the alternative, recently developed "Direct–Indirect"(D–I) model [19]. For weak electronic interaction of the TiO$_2$ surface with dissolved substrate species, as it is for instance the case for phenol, the D–I model predicts that photooxidation takes place mainly via an interfacial, indirect transfer (IT) mechanism involving inelastic trapping of valence band free holes by terminal, twofold coordinated oxygen ions, and further adiabatic transfer to dissolved substrate species. On the basis of open-circuit voltage measurements, the origin of the photooxidation quantum yield increase observed in these cases when the TiO$_2$ surface becomes fluorinated is attributed to the partial substitution of water molecules adsorbed on terminal Ti sites by fluoride ions, leading to: (1) an interfacial decrease of the electron-hole recombination rate as the surface concentration of recombination centres associated with terminal Ti sites diminishes; (2) an increase of the IT rate of surface trapped holes to reduced dissolved species, because of the upward shift experimented by the semiconductor energy levels with respect to filled electrolyte energy levels. In contrast, for strong electronic interaction of substrate species with the naked TiO$_2$ surface, as it is for instance the case of formate ions at low enough pH, photooxidation mainly take place via an interfacial, direct transfer (DT) mechanism, involving inelastic trapping of valence band free holes by specifically adsorbed substrate species. The photooxidation quantum yield decrease observed in this case is explained to be due to a diminution of the density of TiO$_2$ surface sites active for adsorption of formate ions. The enhanced photogeneration of free OH$_S^\bullet$ radicals and/or photooxidation rate of water molecules in the liquid phase with free VB holes, assumed by some authors as the origin of the observed photooxidation quantum yield increase at the fluorinated TiO$_2$ surface, should be disregarded as far as both processes appears to be thermodynamically and kinetically hindered.

© 2009 Elsevier B.V. All rights reserved.

1. Introduction

The photocatalytic properties of semiconductors are greatly influenced by their surface composition and structure, as far as the efficiency of photoinduced charge transfer process taking place at the semiconductor-aqueous electrolyte interface is affected [1]. For instance, the presence of dissolved inorganic anions is known to affect the mineralization processes of organic compounds under photocatalytic conditions [2]. In particular, surface fluorination (i.e., specific adsorption of fluoride ions on terminal Ti atoms), which is different than F$^-$ doping (i.e., substitution of F$^-$ for O^{2-} lattice ions), strongly modifies the TiO$_2$ surface properties. The specific adsorption of fluoride anions on the semiconductor surface at acidic pH leads to the formation of Ti$_S$–F$^{1/3-}$ surface states with displacement of water molecules single bonded to terminal Ti cations, according to the surface exchange reaction (1) [3], written according to the Multisite Complexation (MUSIC) model introduced by Hiemstra et al. [4,5]

$$Ti_S - OH_2^{2/3+} + F_{aq}^- \Leftrightarrow Ti_S - F^{1/3-} + H_2O \tag{1}$$
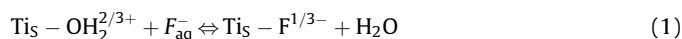
where super index indicates formal charge of ions specifically adsorbed on terminal Ti atoms.

* Corresponding author at: Departament de Ciències Matemàtiques i Informàtica, Universitat de les Illes Balears, Palma de Mallorca, E-07071, Spain.
E-mail address: dmipss9@uib.es (P. Salvador).

Nomenclature

ϕ	incident photon flux ($cm^{-2} s^{-1}$)
V_{fb}	semiconductor flat band potential (V)
C_{sc}	layer capacitance (F)
$[F_S^-]$	surface concentration of adsorbed fluoride ions (cm^{-2})
E_{st}^*	steady-state open-circuit potential under illumination (V)
$[e_f^-]$	concentration of conduction band free electrons (cm^{-3})
$[h_f^+]$	concentration of valence band free holes (cm^{-3})
$[h_S^+]$	concentration of surface trapped holes (cm^{-3})
$[Ti_S^{III}]$	concentration of Titanium surface states with oxidation degree III (cm^{-3})
$[Ti_S^{IV}]$	concentration of Titanium surface states with oxidation degree IV (cm^{-3})
$[RH_2]_{aq}$	aqueous concentration of organic species (cm^{-3})
$[RH_2]_S$	TiO_2 surface density of chemisorbed organic species (cm^{-2})
$[PhO]_{aq}$	aqueous concentration of phenol species (cm^{-3})
$[PhO]_S$	TiO_2 surface density of chemisorbed phenol species (cm^{-2})
$[FA]_{aq}$	aqueous concentration of formic acid species (cm^{-3})
$[O_S^{2-}]$	TiO_2 surface density of terminal oxygen ions (cm^{-2})
A	Langmuir adsorption constant (cm^3)
B	density of surface sites available for adsorption of dissolved substrate species (cm^{-2})
V_0	photogeneration rate of free electron-hole pairs ($cm^{-3} s^{-1}$)
V_1	trapping rate of valence band free holes by terminal oxygen ions ($cm^{-3} s^{-1}$)
V_{-1}	detrapping rate of valence band free holes by terminal oxygen ions ($cm^{-3} s^{-1}$)
V_2	trapping rate of conduction band free electrons by Ti_S^{IV} surface states ($cm^{-3} s^{-1}$)
V_{-2}	detrapping rate of trapped electrons at Ti_S^{III} surface states ($cm^{-3} s^{-1}$)
V_{r1}	recombination rate of free electrons with surface trapped holes ($cm^{-3} s^{-1}$)
V_{r2}	recombination rate of electrons trapped at Ti_S^{III} surface states with surface trapped holes ($cm^{-3} s^{-1}$)
V_{r3}	recombination rate of electrons trapped at Ti_S^{III} surface states with valence band free holes ($cm^{-3} s^{-1}$)
V_{red}	electroreduction rate of dissolved oxygen species ($cm^{-3} s^{-1}$)
QY	quantum yield

Subscripts

st	steady-state conditions
nak	naked electrode
F^-	fluorinated electrode
S	surface
f	free
O_2	oxygen saturated electrolyte
N_2	nitrogen saturated electrolyte
ox	oxidation

Superscripts

*	illumination conditions
0	dark conditions
i	indirect interfacial transfer of charge
d	direct interfacial transfer of charge

The displacement of single bonded hydroxyl groups by fluoride ions according to reaction (1')

$$Ti_S - OH^{1/3-} + F_{aq}^- \Leftrightarrow Ti_S - F^{1/3-} + OH_{aq}^- \qquad (1')$$
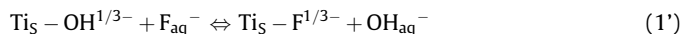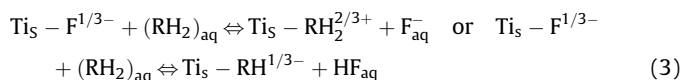
is far less favourable than (1), because: (1) the equilibrium reaction has a pK between 6.5 [6], and 8.0 [1], which means that at the pH = 3.5 employed in experiments reaction (1') is shifted to the left; (2) the adsorption energy of hydroxyl groups exceeds that of water molecules [7]. On the other hand, the displacement of terminal, hydroxyl groups by fluoride ions is highly improbable, as they are twofold coordinated to terminal Ti atoms, while adsorbed water species are only onefold coordinated. Furthermore, according to reaction (1), the TiO_2 surface electric charge becomes less positive under surface fluorination, while according to reaction (1') no net change of the surface electric charge takes place.

The competitive adsorption of $(RH_2)_{aq}$ dissolved substrate species and water molecules on the naked TiO_2 surface is represented by the exchange reaction:

$$Ti_S - OH_2^{2/3+} + (RH_2)_{aq} \Leftrightarrow Ti_S - RH^{1/3-} + H_3O^+ \qquad (2)$$

In contrast, according to the reaction (3), on the fluorinated surface $(RH_2)_{aq}$ adsorption, is hindered to a great extent (shifted to the left), which means modification of TiO_2 photocatalytic properties [3,8–15]

$$Ti_S - F^{1/3-} + (RH_2)_{aq} \Leftrightarrow Ti_S - RH_2^{2/3+} + F_{aq}^- \quad or \quad Ti_s - F^{1/3-}$$
$$+ (RH_2)_{aq} \Leftrightarrow Ti_S - RH^{1/3-} + HF_{aq} \qquad (3)$$

According to photocatalytic studies reported in the last few years, TiO_2 fluorination seems to increase the photooxidation rate of phenol [3,8–10,14,15] azo dye Acid Red 1 [11,12] benzoic acid [12], tetramethyl ammonium at pH 5–7 [13], and acid orange [14], while decreasing the photooxidation rate of formic acid [12], tetramethyl ammonium at pH 3 [13] and dichloroacetate [14]. The negative effect of fluorination on the photooxidation rate has been attributed mainly to the inhibition of the hole transfer mediated oxidation process, because of the hindered adsorption of the organic substrate on fluorinated TiO_2. In contrast, the rate increasing effect has been attributed by some authors not only to decrease of the electron-hole recombination rate, but to the higher availability of photogenerated $OH^{\bullet}$ radicals in the liquid phase when the TiO_2 surface becomes fluorinated [3,8–10,14]. More recently [15], other authors have considered the influence that a negative shift of TiO_2 energy levels due to surface fluorination has on the photoinduced charge transfer rate at the semiconductor-electrolyte interface. All these effects will be analyzed here in detail here.

In order to be able to perform a realistic kinetic analysis of the photocatalytic reactions taking place at the semiconductor (TiO_2)-aqueous electrolyte interface, we have recently developed a kinetic model, the "Direct–Indirect" (D–I) model [16–20], as an alternative to the nearly universal "Langmuir–Hinshelwood" (L–H) model, which has been applied almost robotically since the 1950s [21].

The L–H model is based on the existence of specific adsorption of RH_2 organic substrate species on the semiconductor surface when adsorption is modelled through a Langmuir type isotherm. In contrast, the D–I model, is based on the degree of interaction between $(RH_2)_{aq}$ dissolved species with the semiconductor surface, introducing basic concepts, like direct, indirect, adiabatic and inelastic transfer of charge at the semiconductor–electrolyte interface, as fundamental tools [19]. The prevalence of DT on IT, or vice versa, not only depends on the extent of electronic interaction of TiO_2-substrate and on the volumetric concentration of substrate dissolved molecules, determining the surface density of chemisorbed species according to an specific adsorption isotherm, but on the illumination intensity. While at low enough values of the illumination flux the IT prevails on the DT mechanism, under high enough photon flux DT prevails on IT [17,19], as shown schematically in Fig. 1. Furthermore, the D–I model predicts a photon flux independent quantum yield for the DT mechanism (case of strong substrate-TiO_2 electronic interaction), while for IT, in the absence of specific adsorption of substrate species, an steadily quantum yield decreases as the photon flux increases is predicted, a limiting value of QY = 1 being reached for $\Phi \to 0$. As will be shown in Section 6, a linear dependence of the QY on $\Phi^{-1/2}$ is also predicted for high enough Φ values.

Here some experimental results and hypothesis found in the literature, concerning the effect of surface fluorination on photocatalytic activity of TiO_2, will be critically reviewed in the light of the D–I model.

2. Experimental

All chemicals were used in the experiments as received without further purification. Working solutions were prepared with ultrapure water (Millipore MilliQ, 15 MΩ cm). Sodium perchlorate monohydrate (extra pure) and phenol (extra pure) were supplied by Scharlau. Perchloric acid (p.a., 60%), sodium hydroxide (p.a.), hydrofluoric acid (p.a., 48%) and formic acid (p.a., 99%) were supplied by Merck. The pH of all the solutions was adjusted to 3.5 using 1 M NaOH or 1 M $HClO_4$. Titanium dioxide nanoparticles were supplied by Degussa-Hüls (P25, 20 nm). The oxide slurry for
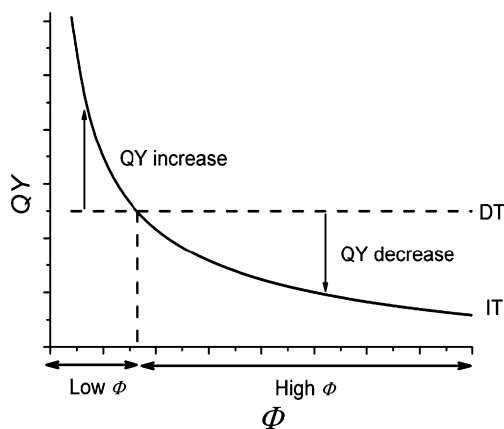

Fig. 1. Schematic representation obtained from Fig. 10 of Ref. [17], of the photooxidation quantum yield (QY) dependence on the photon flux (Φ) predicted by the D–I kinetic model, for both interfacial direct transfer (DT) and indirect transfer (IT) of VB photogenerated holes. Note that for DT a photon flux independent photooxidation quantum yield is predicted, while for IT, in the absence of specific adsorption of substrate species, an steadily quantum yield decreases as the photon flux increases is obtained. For substrates species specifically adsorbed on the TiO_2 surface, the photooxidation quantum yield at low enough Φ values is generally determined by adiabatic IT. In contrast, at high enough Φ values (standard experimental conditions), inelastic DT of free holes to reduced species specifically adsorbed on terminal Ti atoms prevails on IT. In the absence of specific adsorption IT is the only working mechanism.

deposition was made using Triton X-100 and acetylaceton 99% from Aldrich.

The nanostructured P25 thin films used in the photoelectrochemical experiments were prepared as follows: 1 g of Degussa P25 powder was ground with a mixture of 30 μL of acetylacetone and 330 μL of distilled water, until the slurry was homogeneous. Next it was diluted with 1.3 mL of distilled water, and 100 μL of the surfactant Triton X-100 were added. 20 μL of the slurry were spread over a (3×1) cm^2 FTO conducting glass plate (U-type TCO glass, Asahi Glass Co., Japan, with a resistance of 10–15 Ω/square) by means of the so-called "Dr Blade" method. It was let to dry in open air for 5 min and finally it was annealed in air for 1 h at 450 °C, giving rise to a 11 μm-thick film as determined by Scanning Electron Microscopy measurements. n-TiO_2 films used for impedance measurements were prepared by thermal oxidation in air at 500 °C, for 0.5 h, of 99.9% purity Ti sheet (0.1 cm thick) previously polished to a mirror finish. The depletion layer capacitance (C_{sc}) of the n-TiO_2/aqueous electrolyte interface was obtained from measurements of impedance and phase angle [22,23].

The electro- and photoelectrochemical measurements were performed using a standard experimental setup, composed of a computer controlled potentiostat, Wenking-POS 73, and a 150 W Bausch&Lomb Xe arc lamp as illumination source. The electrochemical cell was a conventional three-electrode cell with a 1 mm thick fused silica window, purged with nitrogen (or oxygen). The counter and reference electrodes were a Pt wire and a Ag/AgCl/KCl(sat) electrode, respectively. The working solutions were 0.5 M $NaClO_4$ with 0.01 M (HF + NaF), buffered to pH 3.5. Incident light intensity was measured with an optical power meter (Oriel model 70310) equipped with a thermopile head (Ophir Optronics 71964).

The ATR-FTIR experiments were carried out with a Nicolet Nexus 8700 Spectrometer equipped with a MCT detector. The ATR-FTIR cell was provided with a semi cylindrical ZnSe prism. TiO_2 films were deposited on the prism by applying 1.2 μL mm^{-2} of a 0.4 M TiO_2 P25 suspension. It was dried in air overnight at 60 °C, yielding a 5 μm-thick film. The spectra were obtained by averaging 50 scans at a resolution of 8 cm^{-1}. ATR-IR spectra of the adsorbate species on TiO_2 were recorded with respect to a $NaClO_4$ 0.1 M (pH 3.5) solution as reference. Solution spectra were recorded on the uncoated ZnSe prism.

3. Expected effect of TiO_2 fluorination on the quantum yield of photocatalytic oxidation of formic acid and phenol according to the D–I model

Because of the strong specific adsorption in the presence of water, the photooxidation of formic acid (formate ions) on naked TiO_2, at low enough pH is a paradigm of interfacial DT of charge [20]. The small frequency shift and the general, drastic intensity increase of the HCOOH-related bands in the presence of the TiO_2 film observed in the ATR-IR spectra of Fig. 2a support this thesis. On the other hand, the general signal decrease of formate bands observed when the TiO_2 surface becomes fluorinated (Fig. 2b), indicates that the specific adsorption of formate ions is partially inhibited by adsorbed fluoride ions. In contrast, according to the D–I model, an IT photooxidation mechanism has been found to dominate phenol photooxidation [20], which predicts an scarce specific adsorption of this compound on TiO_2, as in fact indicates the ATR-IR spectra shown in Fig. 2c, where the presence of a thick nanostructured film of TiO_2 does not affect phenol bands intensity. Therefore, phenol photooxidation kinetics should not be affected by TiO_2 surface fluorination, in contradiction with the experimental observation that phenol photooxidation rate increases when the naked TiO_2 surface becomes fluorinated [3,15]. It has been suggested that this behaviour may be due to a decrease in the
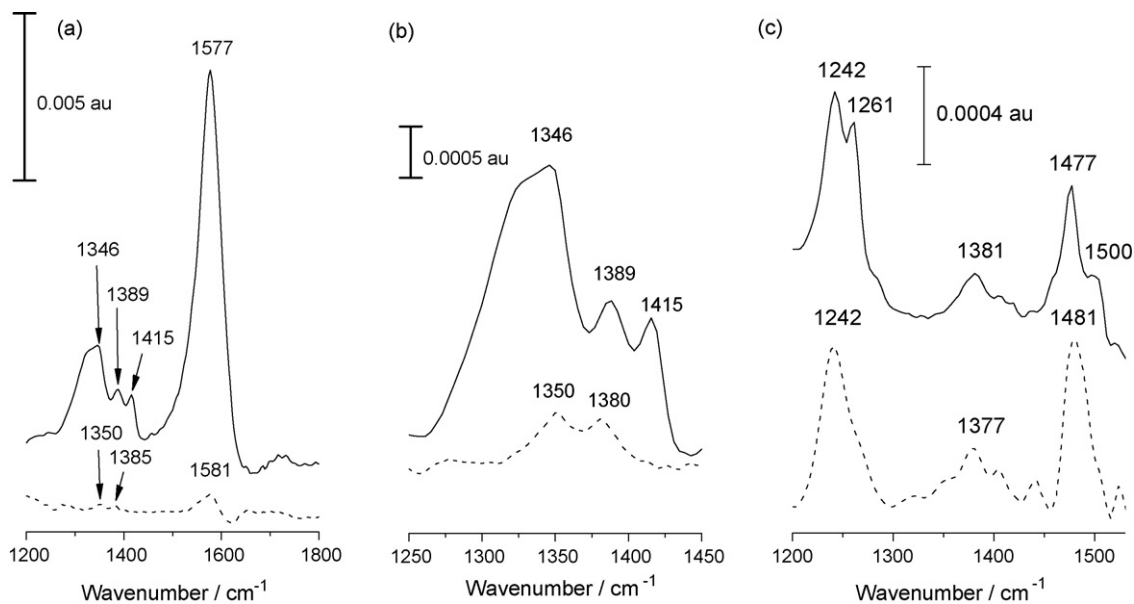
Fig. 2. ATR-IR spectra at room temperature for: (a) 0.01 M formic acid (pH 3.5) in the presence (——) and in the absence (- - - - -) of a 5 μm-thick nanostructured TiO$_2$ (P25) film, the appearing bands being assigned to [35]: 1346 cm^{-1}, symmetric COO group stretching, 1389 cm^{-1}, H–C=O group bending and 1577 cm^{-1} asymmetric COO stretching; (b) 0.01 M formic acid (pH 3.5), without (——) and with 0.01 M (HF + NaF) added (- - - - -). Fluoride was added once the organic was adsorbed at equilibrium. Both spectra were taken in the presence of a 5 nm-thick nanostructured TiO$_2$ (P25) film; (c) 0.01 M phenol (pH 3.5) in the presence (——) and the absence (- - - - -) of a 5 nm-thick nanostructured TiO$_2$ (P25) film. The bands for the solution spectrum can be assigned as follows [36]: 1242 cm^{-1}, C–O stretching, 1381 cm^{-1} in plane C–O–H bending and 1477 and 1500 cm^{-1}, aromatic ring C–C stretching. In all cases the supporting electrolyte was 0.1 M NaClO$_4$.

recombination rate of surface trapped holes with electrons trapped at $Ti_S^{III} - F_S^{4/3-}$ surface states because of the strong electronegativity of fluorine [14,15]. Obviously, a surface recombination rate decrease should induce an increase of the transfer rate of surface trapped holes to $(RH_2)_{aq}$ species. As we will show in Section 5, transient open-circuit photopotential measurements at the TiO$_2$-aqueous electrolyte interface allow to obtain direct information about the influence of surface fluorination on the kinetics of the surface electron-hole recombination process.

4. Influence of surface fluorination on the TiO$_2$ flatband potential

An important parameter defining the concentration of CB electrons and, therefore, affecting electron-hole recombination kinetics, is the semiconductor flatband potential, V_{fb} [22]. It is well known that a change of the semiconductor net surface charge produces a potential drop at the Helmholtz double layer and therefore a V_{fb} shift [22]. According to reaction (1), this should be the behaviour expected under fluorination of the TiO$_2$ surface at pH 3.5, as a decrease of the positive surface electric charge excess is produced, so that a flatband potential shift towards more negative potentials $(-\Delta V_{fb})$ should take place. This hypothesis can be verified form measurements of the depletion layer capacitance (C_{sc}) at the TiO$_2$-electrolyte interface both in the absence and presence of dissolved fluoride ions. In fact, Fig. 3 shows the Mott–Schottky plots obtained for a n-TiO$_2$ polycrystalline thin film in contact with 0.5 M NaClO$_4$ (pH 3.5) without and with addition of 0.01 M (HF + NaF). Since the intercept of the linear plot to the potential axis can be considered as a reliable V_{fb} measurement [22], it is inferred from Fig. 3 that a flatband potential shift between 50 and 60 mV towards negative values is produced under surface fluorination conditions. Similar measurements have been performed recently by Cheng et al. [15], with a TiO$_2$ film prepared by direct thermal oxidation of a Ti sheet in air at 600 °C, and further fluorination by electrode etching in 0.5 M H$_2$SO$_4$ solution containing 0.5% NaF, under anodic polarization. These authors obtained a $V_{fb} \approx -0.21$ V (SCE) for the unetched TiO$_2$, which is shifted

negatively by about 80 mV under fluorination. While these V_{fb} values are slightly more positive than those obtained here, the V_{fb} shift obtained under fluorination is very similar to that obtained by us, as should correspond to a substitution of F$^-$ ions for adsorbed hydroxyl groups.

Since the Helmholtz layer at the TiO$_2$-electrolyte interface behave like a capacitor with a capacitance C_H between 10^{-5} [22] and 4×10^{-5} F cm^{-2} [23], it must be $\Delta V_{fb} = \Delta q / C_H$, where according to (1) Δq represents the increase of surface negative charge due to substitution of specifically adsorbed neutral water molecules by negatively charged fluoride ions $(\Delta q = e[F_s^-]$, $e = 1.6 \times 10^{-19}$ Coul being the elemental electronic charge). Consequently, the following mean value of surface concentration of adsorbed fluoride ions is obtained,

$$[F_s^-] = \frac{\Delta V_{fb} C_H}{e} \approx \frac{0.055 \, V \times 2.5 \times 10^{-5} \, F \, cm^{-2}}{e}$$
$$\approx \frac{1.375 \times 10^{-6} \, Coul \, cm^{-2}}{e} \approx 10^{13} \, ions \, cm^{-2}.$$
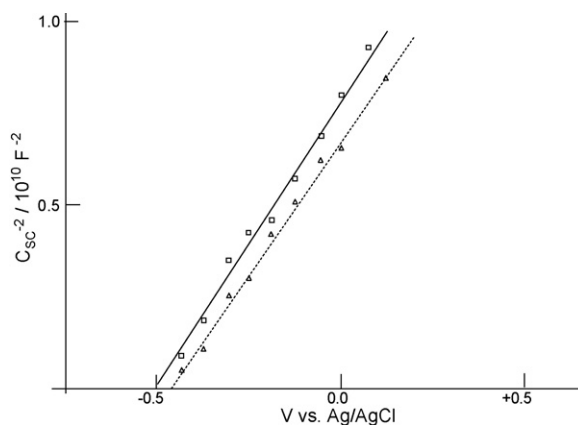

Fig. 3. Mott–Schottky plots of a TiO$_2$ thin film in contact with a 0.5 M NaClO$_4$ aqueous electrolyte (pH 3.5), without (- - - -) and with addition (——) of 0.01 M (HF + NaF). The frequency used was 1 kHz.

This value is in reasonable good agreement with that obtained by Rob van Veen et al. for the surface concentration of fluoride adsorbed on TiO_2 in contact with 0.01 M NaF [24].

5. Influence of surface fluorination on the open-circuit photopotential transients at the TiO_2-aqueous electrolyte interface

5.1. Deoxygenated electrolyte

As pointed out previously [25], the photoelectrochemical behaviour of an illuminated TiO_2 nanostructured electrode in a photoelectrochemical cell under open-circuit conditions is analogous to that of TiO_2 nanoparticles suspended in an electrolyte. In both cases photogenerated electron-hole pairs can either recombine at the semiconductor surface in the absence of suitable electron and hole scavengers in the electrolyte, or be transferred to suitable dissolved electron and/or hole acceptors. The situation of the illuminated nanostructured TiO_2 electrode in contact with a deareated, indifferent aqueous electrolyte (absence of dissolved electron and hole scavengers) under open-circuit conditions is schematized in Fig. 4a. Both photogenerated free holes (h_f^+) and electrons (e_f^-) accumulate at the valence band (VB) and conduction band (CB), respectively at a rate V_0. In a first approximation, it can be assumed that under steady-state illumination conditions the concentrations of CB electrons, $[e_f^-]^*$, VB holes, $[h_f^+]^*$, and Ti_S^{III} species, $[Ti_S^{III}]^*$ satisfy Eqs. (4)–(6)

$$\frac{d[e_f^-]^*}{dt} = V_0 - V_{r1} - V_2 + V_{-2} = 0, \tag{4}$$

$$\frac{d[h_f^+]^*}{dt} = V_0 - V_1 + V_{-1} - V_{r3} = 0 \tag{5}$$

$$\frac{d[Ti_S^{III}]^*}{dt} = V_2 - V_{r2} - V_{r3} - V_{-2} = 0, \tag{6}$$

where V_0 represents the photogeneration rate of $e_f^- - h_f^+$ pairs, V_1 and V_{-1} are the trapping and detrapping rate of VB free holes by surface traps, respectively, ($V_{-1} \ll V_1$ for h_S^+ surface states with an energy kT above E_v), V_2 the trapping rate of free electrons by Ti_S^{IV} intrinsic surface states, V_{-2} the detrapping rate of trapped electrons at Ti_S^{III} surface states ($V_{-2} \ll V_2$ for Ti_S^{III} surface states with an energy about kT below E_c), V_{r1} the $e_f^- - h_S^+$ recombination rate, and V_{r2} and V_{r3} the recombination rate of electrons trapped at

Ti_S^{III} surface states with h_S^+ and h_f^+, respectively. The steady-state open-circuit potential under illumination, (E_{st}^*), is determined by the concentration of conduction band electrons in the dark, $[e_f^-]_{st}^0$ and under illumination, $[e_f^-]_{st}^*$, according to the expression:

$$E_{st}^* = \frac{kT}{q} \ln \frac{[e_f^-]_{st}^*}{[e_f^-]_{st}^0} \tag{7}$$

When illumination is stopped ($V_0 = 0$), the electron-hole recombination process continues in the dark at a rate $V_r = V_{r1} + V_{r2} + V_{r3}$, until a new steady value for the electron concentration in the dark is reached; then an open-circuit voltage E_{st}^0 is measured in the dark. During the relaxation process in the dark, both the CB free electron concentration and the Ti_S^{III} surface states concentration varies with time according to:

$$\frac{d[e_f^-]^0}{dt} = -V_{r1} - V_2 + V_{-2} \tag{8}$$

and

$$\frac{d[Ti_S^{III}]^o}{dt} = V_2 - V_{r2} - V_{r3} - V_{-2}, \tag{9}$$

so that

$$\frac{d[e_f^-]^0}{dt} + \frac{d[Ti_S^{III}]^0}{dt} = -(V_{r1} + V_{r2} + V_{r3}).$$

Since in general $d[T_s^{III}]^0/d[e_f^-]^0 \ll 1$ [26], the electron concentration decay rate in the dark can be approached by:

$$\frac{d[e_f^-]^0}{dt} = -(V_{r1} + V_{r2} + V_{r3}) \tag{10}$$

As generally accepted, Ti_S represent a continuous distribution of bandgap surface states below the CB edge, acting not only as CB electron traps, but as surface centres for both recombination with VB holes and interfacial electron transfer to oxidized electrolyte species [27]. It can be reasonably assumed on the other hand, that because of the strong electronegativity of fluorine, the effectiveness of Ti_S^{IV} sites as electron traps after F^- complexation will be drastically reduced, which implicates that

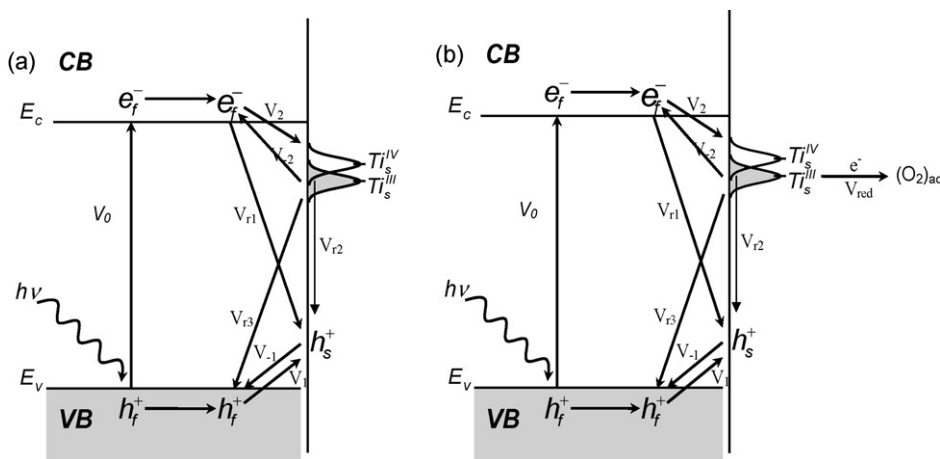$$\left(\frac{d[Ti_S^{III}]^0}{d[e_f^-]^0}\right)_{nak} > \left(\frac{d[Ti_S^{III}]^0}{d[e_f^-]^0}\right)_{F^-}$$

Fig. 4. Schematic energy diagram of the illuminated nanostructured TiO_2 electrode under open-circuit conditions, in contact with: (a) deareated aqueous electrolyte; (b) oxygen saturated electrolyte. V_0 indicates the photogeneration rate of electro-hole pairs, V_1 and V_{-1} the trapping and detrapping rate of free holes by intrinsic surface states, V_2 the trapping rate of free electrons by Ti_S^{IV} intrinsic surface states, V_{-2} the detrapping rate of trapped electrons at Ti_S^{III} surface states, $V_{r,1}$ the recombination rate of conduction band electrons with surface trapped holes, $V_{r,2}$ and $V_{r,3}$ the recombination rate of electrons trapped at Ti_S^{III} surface states with surface trapped holes and free holes, respectively and V_{red} the rate of dissolved oxygen electroreduction.
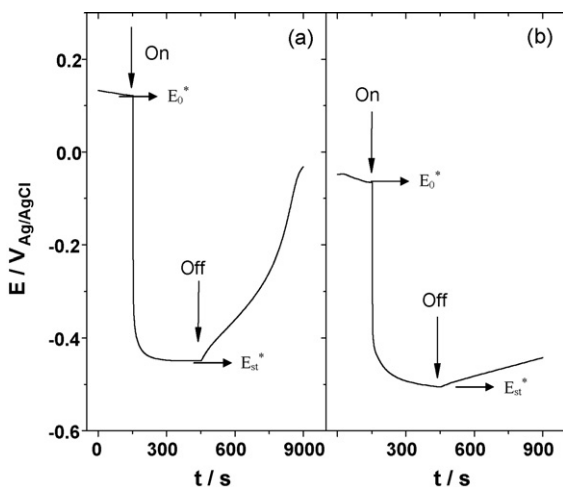
Fig. 5. Time dependence of the open-circuit voltage, at room temperature, in the dark after an illumination period, for a nanostructured TiO_2 (P25) electrode either naked (a) or surface fluorinated (b), in contact with a deoxygenated aqueous electrolyte: (a) 0.5 M $NaClO_4$, pH 3.5, (b) 0.5 M $NaClO_4$, 0.01 M (HF + NaF), pH 3.5. Electrode thickness, 10 μm. Electrolyte-electrode side (EE) illumination with a 150 W Xe lamp (incident light power 0.27 W).
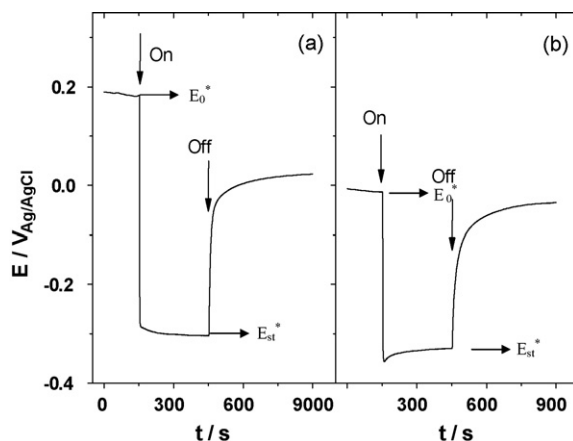

Fig. 6. Time dependence of the open-circuit voltage at room temperature, in the dark after an illumination period, for a nanostructured TiO_2 (P25) electrode, either naked (a) or surface fluorinated (b), in contact with an oxygen saturated aqueous electrolyte: (a) 0.5 M $NaClO_4$, pH 3.5, (b) 0.5 M $NaClO_4$, 0.01 M (HF + NaF), pH 3.5. Electrode thickness, 10 μm. Electrolyte-electrode side (EE) illumination with a 150 W Xe lamp (incident light power 0.27 W).

From the time-dependent open-circuit voltage experimental results shown in Fig. 5 for a TiO_2 (P25) electrode in contact with an indifferent, deoxygenated aqueous electrolyte, in can be inferred that the initial value of dE^0/dt in the dark, just after an illumination period, decreases from ≈ 0.60 to ≈ 0.15 mV s^{-1} (i.e., about a factor of 4) under electrode fluorination. This indicates that the initial electron concentration decay rate, $d[e_f^-]^0/dt$, and according to (10) the recombination rate of electrons trapped at Ti_S^{III} surface states with surface trapped holes ($V_{r2} = k_{r2}[Ti_s^{III}][h_s^+]$) and/or valence band free holes ($V_{r3} = k_{r3}[Ti_s^{III}][h_f^+]$), slows down when the TiO_2 surface becomes fluorinated, an effect mainly due to a decrease of the concentration of Ti surface active centres, $[Ti_S^{III}]$. In fact, a decrease of about one order of magnitude has been estimated recently for the pseudo-first-order surface recombination rate constant of TiO_2 (P25) under surface fluorination [28].

5.2. Oxygenated electrolyte

As schematized in Fig. 4b, in the presence of dissolved oxygen, CB electrons are transferred to the electrolyte via an O_2 electroreduction process taking place in a two-step interfacial electron transfer mechanism [29]. In the first step (limiting step) CB electrons are transferred inelastically to bandgap surface states associated with Ti_S^{IV} ions, at a rate $V_2 = k_2[Ti_S^{IV}][e_f^-]$, while in a second step electrons trapped at Ti_S^{III} ions are transferred adiabatically to dissolved O_2 molecules at a rate $V_{red} = k_{red}[Ti_S^{III}][O_2]_{aq}$, in such a way that

$$V_{red} = V_2 - V_{-2} - V_{r3} - V_{r2} \approx V_2 - V_{r3} - V_{r2}$$
$$= k_2[Ti_s^{IV}][e_f^-] - k_{r2}[Ti_S^{III}][h_S^+] - k_{r3}[Ti_S^{III}][h_f^+]$$

If we compare the time-dependent open-circuit voltage results of Fig. 6 in the oxygenated electrolyte, with those of Fig. 5 for the deoxygenated electrolyte, the following features can be appreciated: (1) During the relaxation process in the dark, dE^0/dt, increases by about a factor of 30 when the electrolyte becomes oxygenated, for the naked electrode, and by about a factor of 100 for the fluorinated electrode. (2) Under electrode fluorination the initial value of dE^0/dt during the relaxation process in the dark diminishes by about a factor of 4 in the N_2 saturated electrolyte, while this diminution only reaches about a factor of 1.5 in the O_2 saturated electrolyte. (3) In both the N_2 and O_2 saturated

electrolyte E_{st}^* shifts by 50–60 mV towards negative potentials under surface fluorination, which is equivalent to an increment in the concentration of CB electrons of about one order of magnitude. (4) In both the naked and fluorinated TiO_2 E_{st}^* shifts towards positive potentials by about 0.14 V when the electrolyte becomes oxygenated, which means a diminution in the concentration of CB electrons of more than two orders of magnitude

$$\left(\frac{([e_f^-]_{st}^*)_{N_2}}{([e_f^-]_{st}^*)_{O_2}} \approx 10^2 \right).$$

In order to correctly interpret these experimental results, it must be taken into account, according to the scheme of Fig. 4b, that the recombination rate in the oxygen saturated electrolyte is $(V_r)_{O_2} = V_{red} + (V_{r1} + V_{r2} + V_{r3})_{O_2}$, while in the nitrogen saturated electrolyte $(V_r)_{N_2} = (V_{r1} + V_{r2} + V_{r3})_{N_2}$. And taking into account that

$$\frac{(dE^0/dt)_{O_2}}{(dE^0/dt)_{N_2}} = \frac{(V_r)_{O_2}}{(V_r)_{N_2}} = \frac{(V_{r1} + V_{r2} + V_{r3})_{O_2} + V_{red}}{(V_{r1} + V_{r2} + V_{r3})_{N_2}}$$

the increase of dE^0/dt during the relaxation process in the dark when the electrolyte becomes oxygenated, at both the naked and fluorinate electrode, should be attributed to an increase of the density Ti_S centres active in interfacial transfer of conduction band electrons to dissolved O_2 molecules and interfacial recombination, in such a way that $(V_{r1} + V_{r2} + V_{r3})_{O_2} + V_{red} > (V_{r1} + V_{r2} + V_{r3})_{N_2}$. On the other hand, the diminution of Ti_s centres under surface fluorination, produces a decrease of the term $(V_{r1} + V_{r2} + V_{r3}) + V_{red}$ in both the oxygen saturated and nitrogen saturated electrolyte, so that dE^0/dt diminishes in both cases. Finally, the observed photovoltage shift between 50 and 60 mV towards negative potentials under surface fluorination ($60 \text{ mV} \geq |E_{nak}^* - E_{F^-}^*| = |\Delta E^*| \geq 50 \text{ mV}$), in both the deoxygenated and the oxygenated electrolyte, must be attributed to a shift of identical magnitude experimented by the flatband potential of TiO_2, as was shown in Section 4.

6. Kinetic analysis of the influence of TiO_2 surface fluorination on the photooxidation of specifically adsorbed and non-adsorbed substrates

In order to study the influence of TiO_2 surface fluorination on the photooxidation rate of adsorbing and non-adsorbing substrates, we have chosen formic acid and phenol as model organic
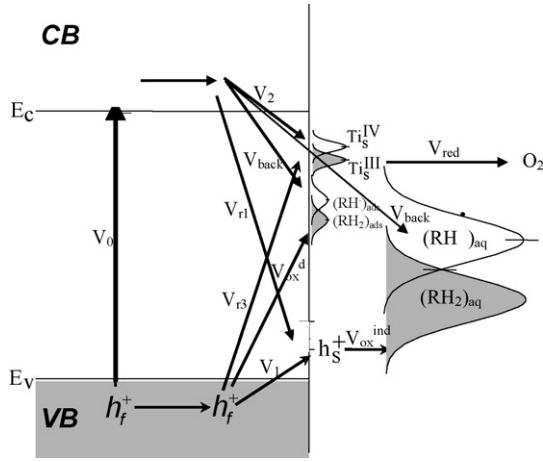
Fig. 7. Energy diagram showing primary reactions of electron-hole generation and recombination, as well as electron and hole transfer to non-adsorbed and specifically adsorbed dissolved species, taking place at the TiO$_2$ electrolyte interface under UV illumination according to the D–I model.

compounds where photooxidation takes place via mechanisms of interfacial DT and IT, respectively [20]. The scheme of Fig. 7 indicates primary recombination and interfacial charge transfer reactions to be considered in the kinetic analysis of photooxidation of specifically adsorbed and non-adsorbed substrate species. The IT photooxidation rate of non-adsorbed species can be written as

$$V_{ox}^{i} = k_{ox}^{i}[h_{s}^{+}][(RH_2)_{aq}],$$ (11)

while the DT photooxidation rate of specifically adsorbed species is

$$V_{ox}^{d} = k_{ox}^{d}[h_{f}^{+}][(RH_2)_{s}],$$ (12)

so that, in general, the quantum yield can be written as:

$$QY = \frac{V_{ox}^{d} + V_{ox}^{i} - V_{back}}{V_0}.$$ (13)

However, when both V_{ox}^{d} and V_{ox}^{i} represent initial photooxidation rates (i.e., $\lim_{t \to 0} \frac{d[RH_2]}{dt}$), as usually considered in photocatalytic experiments, the term V_{back} is negligible with respect to V_{ox}^{d} and V_{ox}^{i}, since for $t \to 0$ [RH$^\bullet$] $\ll$ [(RH$_2$)], so that Eq. (13) becomes:

$$QY \approx QY_{ox}^{d} + QY_{ox}^{i}$$ (13')

With the help of the energy diagram in Fig. 7, the following complex mathematical expression for QY_{ox}^{i} is obtained (see Eq. (A12) of the appendix)

In agreement with a previous analysis of the photooxidation quantum yield for IT, which excluded the participation of bandgap surface states associated to Ti ions in interfacial reactions (see for instance Eq. (18) of Ref. [17]), Eq. (14) indicates that the photooxidation quantum yield of non-adsorbed substrate species depends on the inverse square root of the incident photon flux. Furthermore, Eq. (14) allows to analyze the influence of TiO$_2$ surface fluorination on the quantum yield (QY_{ox}^{i}). In fact, as it was shown in Section 5, surface fluorination produces a diminution of the concentration of Ti$_S$, surface adsorption centres (both [Ti$_S^{III}$] and [Ti$_S^{IV}$]), so that according to (14) a decrease of QY_{ox}^{i} should be expected as the TiO$_2$ surface becomes fluorinated.

On the other hand, the following expression is obtained for QY_{ox}^{d} (see Eq. (A14) of the appendix)

$$QY_{ox}^{d} = \frac{v_{ox}^{d}}{v_0}$$

$$= \frac{k_{ox}^{d}AB[(RH_2)_{aq}]}{(1 + A[(RH_2)_{aq}])(k_1[O_S^{2-}] + k_{r3}[Ti_S^{III}]) + k_{ox}^{d}AB[(RH_2)_{aq}]}$$ (15)

In contrast with Eq. (14), Eq. (15) indicates a photon flux independent quantum yield for the DT mechanism.

6.1. Influence of TiO$_2$ fluorination on the formic acid (FA) photooxidation quantum yield

Since dissolved FA species, mainly present as formate anions at pH 3.5, strongly interact with the TiO$_2$ surface, both DT and IT mechanisms should participate in their photooxidation mechanism (i.e., $QY(FA) = QY_{ox}^{i} + QY_{ox}^{d}$), so that both Eqs. (14) and (15) must be taken into account. However, according to the experimental results by Dijkistra et al., for FA photooxidation on TiO$_2$ (Degussa P-25), in the photon flux range $\rho \leq 10^{-4}$ Einst m^{-2} s^{-1} [30], a photon flux independent quantum yield is observed. The same conclusion has been obtained recently by us [20] from FA photooxidation kinetic experimental data by Davidov and Smirnotis [31], indicating that $Q_{ox}^{i} \ll Q_{ox}^{d}$, so that for [(RH$_2$)]$_{aq} \equiv$ [FA]$_{aq}$, it can be written:

$$QY_{ox}(FA) \approx QY_{ox}^{d}(FA)$$

$$= \frac{k_{ox}^{d}AB[(FA)_{aq}]}{(1 + A[(FA)_{aq}])(k_1[O_S^{2-}] + k_{r3}[Ti_S^{III}]) + k_{ox}^{d}AB[(FA)_{aq}]}$$ (16)

On the other hand, it has been reported that the rate of FA photooxidation decreases by about a 16% when TiO$_2$ becomes fluorinated [11], (i.e., $(QY)_{ox}^{nack}/(QY)_{ox}^{F^-} \approx 1.2$). This result is congruent with Eq. (16), not only due to the decrease of terms B and [Ti$_S^{III}$], but also of the k_{ox}^{d} rate constant, which depends on the electronic interaction between the TiO$_2$ surface and dissolved FA

$$QY_{ox}^{i} = \frac{-k_{ox}^{i}[(RH_2)_{aq}]k_2[Ti_S^{IV}]}{2k_{r1}k_0\phi} - \frac{k_{r3}[Ti_S^{III}]}{2[k_1[O_S^{2-}] + k_{r3}[Ti_S^{III}] + k_{ox}^{d}[(RH_2)_S]]} -$$
$$\frac{k_{ox}^{d}[(RH_2)_S]}{2[k_1[O_S^{2-}] + k_{r3}[Ti_S^{III}] + k_{ox}^{d}[(RH_2)_S]]} +$$
$$\left\{ \left(\frac{\{k_2[Ti_S^{IV}]k_{ox}^{i}[(RH_2)_{aq}][k_1[O_S^{2-}] + k_{r3}[Ti_S^{III}] + k_{ox}^{d}[(RH_2)_S]] + k_0\phi k_{r1}k_{r3}[Ti_S^{III}] + k_0\phi k_{r1}k_{ox}^{d}[(RH_2)_S]\}}{2k_{r1}k_0\phi[k_1[O_S^{2-}] + k_{r3}[Ti_S^{III}] + k_{ox}^{d}[(RH_2)_S]]} \right)^2 \right.$$
$$\left. + \frac{k_{ox}^{i}k_1k_2[O_S^{2-}][Ti_S^{IV}][(RH_2)_{aq}]}{k_{r1}k_0\phi[k_1[O_S^{2-}] + k_{r3}[Ti_S^{III}] + k_{ox}^{d}[(RH_2)_S]]} \right\}^{\frac{1}{2}}$$ (14)

species; indeed, a diminution of residual positive charge of the semiconductor surface under fluorination should produce a weaker electrostatic attraction towards negatively charged formate ions.

6.2. Influence of TiO₂ fluorination on phenol (PhO) photooxidation quantum yield

In the absence of specific adsorption, as was shown to be the case for phenol in Section 3, photooxidation takes place exclusively via an IT mechanism [17,19,20], so that Eq. (16) must be employed to define the phenol photooxidation quantum yield, which becomes:

$$
\begin{aligned}
QY^i_{ox}(PhO) = \; & \frac{-k^i_{ox}[(PhO)_{aq}]k_2[Ti^{IV}_S]}{2k_{r1}k_0\phi} - \frac{k_{r3}[Ti^{III}_S]}{2[k_1[O^{2-}_S] + k_{r3}[Ti^{III}_S] + k^d_{ox}[(PhO)_S]]} - \\
& \frac{k^d_{ox}[(PhO)_S]}{2[k_1[O^{2-}_S] + k_{r3}[Ti^{III}_S] + k^d_{ox}[(PhO)_S]]} + \\
& \left\{ \left(\frac{\{k_2[Ti^{IV}_S]k^i_{ox}[(PhO)_{aq}][k_1[O^{2-}_S] + k_{r3}[Ti^{III}_S] + k^d_{ox}[(PhO)_S]] + k_0\phi k_{r1}k_{r3}[Ti^{III}_S] + k_0\phi k_{r1}k^d_{ox}[(PhO)_S]\}}{2k_{r1}k_0\phi[k_1[O^{2-}_S] + k_{r3}[Ti^{III}_S] + k^d_{ox}[(PhO)_S]]} \right)^2 \right. \\
& \left. + \frac{k^i_{ox}k_1k_2[O^{2-}_S][Ti^{IV}_S][(PhO)_{aq}]}{k_{r1}k_0\phi\left[k_1[O^{2-}_S] + k_{r3}[Ti^{III}_S] + k^d_{ox}[(PhO)_S]\right]} \right\}^{\frac{1}{2}}
\end{aligned}
\tag{17}
$$

Eq. (17) can be simplified by assuming reasonably that $k_1[O^{2-}_S] \gg k_{r3}[Ti^{III}_S] + k^d_{ox}[(PhO)_S]$, $V_1 \gg V_{r3}$ and $[O^{2-}_S] \gg [Ti^{III}_S]$ [17], resulting:

$$
\begin{aligned}
QY^i_{ox}(PhO) \approx \; & -\frac{k^i_{ox}[(PhO)_{aq}]k_2[Ti^{IV}_S]}{2k_{r1}k_0\phi} \\
& + \left\{ \left(\frac{\{k_2[Ti^{IV}_S]k^i_{ox}[(PhO)_{aq}]\}}{2k_{r1}k_0\phi} \right)^2 + \frac{k^i_{ox}k_2[Ti^{IV}_S][(PhO)_{aq}]}{k_{r1}k_0\phi} \right\}^{\frac{1}{2}}
\end{aligned}
\tag{18}
$$

According to Eq. (18), it can be seen that $QY \rightarrow 1$ for $\Phi \rightarrow 0$. Finally, for high enough photon flux Eq. (18) becomes:

$$
QY^i_{ox}(PhO) \approx \left\{ \frac{k^i_{ox}k_2[Ti^{IV}_S][(PhO)_{aq}]}{k_{r1}k_0} \right\}^{\frac{1}{2}} \phi^{-\frac{1}{2}},
\tag{19}
$$

which indicates a linear phenol quantum yield dependence on the square root of the photon flux. The same photon flux dependence was obtained in the absence of Ti_S recombination and interfacial electron transfer centres (see for instance Eq. (19) of Ref. [17]),

On the other hand, it has been reported that the rate of phenol photooxidation increases up to about a factor of 3 when TiO₂ becomes surface fluorinated [8]. This behaviour that has been explained to be due to the increase of photogenerated OH radical species active in phenol photooxidation as the TiO₂ surface becomes fluorinated. Although the photooxidation of surface-bond water species becomes hindered because of the substitution of Ti^{IV}_S bonded water species by F⁻ ions, the photooxidation of dissolved water species with free VB holes, leading to the generation of free $OH^\bullet_{aq}$ radicals, is strengthened, which results in a higher photooxidant potential [3,8,10–14]. However, this explanation is refutable on the basis of the following arguments: (1) The photooxidation of either adsorbed (Ti^{IV}_S bonded) water species or free (solvated) hydroxyl ions appears to be thermodynamically and kinetically hindered [32]. (2) The same argument should apply in general to the photooxidation of any dissolved compound,

independently on whether they are specifically adsorbed or not, which is not the case, for instance, for formic acid, as its photooxidation quantum yield does not increase but decreases under surface fluorination. (3) It was shown in Section 4 that the equilibrium surface concentration of specifically adsorbed fluoride ions on TiO₂ in contact with a 0.01 M NaF + HF aqueous solution at pH 3.5 and room temperature ($[F^-_S] \approx 10^{13}$ cm⁻²), is more than one order of magnitude lower than that of a monolayer of adsorbed water ($[H_2O]_{sv} \approx 5 \times 10^{14}$ cm⁻²), which indicates that $[H_2O]^{F^-}_S = [H_2O]^{nak}_s - [F^-_S] \approx [H_2O]^{nak}_s$) and, therefore, that the photogeneration rate of adsorbed OH_S radicals should not be appreciably affected by surface fluorination.

According to Eq. (19), a diminution of $[Ti^{IV}_S]$ due to surface fluorination should lead to a phenol photooxidation quantum yield decrease, which is in contradiction with the increase by about a factor of 3 observed experimentally. On the other hand the rate constants k_0 and k_{r1} should not be affected by surface fluorination, but k_2 may decrease because of the repulsive effect of F⁻ ions adsorbed on terminal Ti atoms on conduction band electrons. However a decrease of k_2 does not implicate an increase, as observed experimentally, but a diminution of $QY^i_{ox}(PhO)$. A simple and reasonable explanation to this experimental observation can be found in the increase of the IT rate constant k^i_{ox} as the TiO₂ surface becomes fluorinated. Let us demonstrate that this hypothesis is coherent with the flatband potential shift of about 0.06 V towards negative values observed experimentally in Section 4, as recently claimed by Cheng et al. [15]. In fact, according to the Marcus–Gerischer fluctuating energy model for interfacial transfer
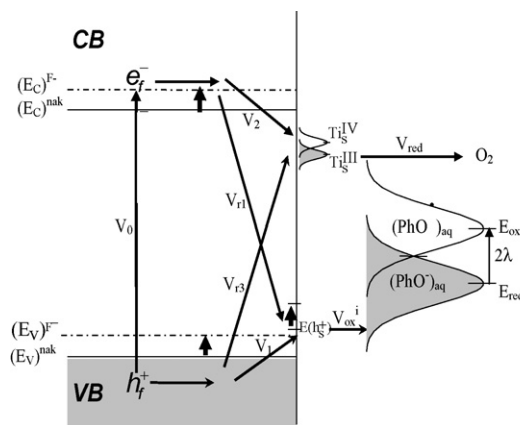

Fig. 8. Energy diagram showing adiabatic, IT of surface trapped holes to non-specifically adsorbed, dissolved phenol species, as well as adiabatic transfer of CB electrons to dissolved oxygen molecules. Note that under surface fluorination TiO₂ energy levels are shifted upward between 0.05 and 0.06 eV, while empty end filled phenol energy levels remain pined, so that according Eqs. (19) and (20) the adiabatic hole transfer rate constant k^i_{ox} increases as shown in Table 1.

Table 1
Estimated effect of TiO$_2$ surface fluorination on the IT rate constant, k_{ox}^i, for phenol photooxidation, according to the D–I model, for different values of $E(h_s^+) - E_V$, λ and ΔV_{fb}.

λ (eV)	$[E(h_s^+) - E_V]$ (eV)	$[E_{red}(PhO) - E(h_s^+)]^{nak}$ (eV)	$[k_{ox}^i]^{nak}$ (cm^3 s^{-1})	$[E_{red}(PhO) - E(h_s^+)]^{F^-}$ (eV)	$[k_{ox}^i]^{F^-}$ (cm^3 s^{-1})	$\left(\frac{[k_{ox}^i]^{F^-}}{[k_{ox}^i]^{nak}}\right)^{1/2}$	ΔV_{fb} (eV)
0.7	0.1	1.2	4.6×10^{-10}	1.15	2.3×10^{-9}	2.2	0.05
0.7	0.2	1.1	1.1×10^{-8}	1.04	6.3×10^{-8}	2.4	0.06
0.6	0.1	1.3	3.1×10^{-13}	1.25	2.4×10^{-12}	2.8	0.05
0.6	0.2	1.2	1.7×10^{-11}	1.14	1.6×10^{-10}	3.1	0.06

k_{ox}^i values were estimated according to the Marcus-Gerischer expression: $k_{ox}^i \propto \exp - \left[\frac{(E_{red}(PhO) - E(h_s^+))^2}{4\lambda kT} \right]$.

of charge under weak semiconductor-electrolyte electronic interaction [33], the photooxidation rate constant for IT can be defined by the expression:

$$k_{ox}^i(PhO) = A' \exp - \left[\frac{(E_{red}(PhO) - E(h_s^+))^2}{4\lambda kT} \right], \qquad (20)$$

where A' is a constant, $E(h_s^+)$ is the energy of holes trapped at O_S^{2-} surface states located just above the VB edge (E_v) [32], E_{red} (PhO) is the most probable value of the Gaussian distribution of filled energy levels corresponding to dissolved phenol species and λ is the reorganization energy of the (PhO/PhO$^\bullet$) redox couple. k_{ox}^i(PhO) can be evaluated from (20), with the help of the energy diagram of Fig. 8, on the basis that $E_{redox}^0(PhO) - E_v(TiO_2)^{nak} \approx 2.0 V$ [34],

$$E_{red}(PhO) - E(h_s^+)^{nak} = \left[E_{redox}^0(PhO) - E_v^{nak} - \lambda \right] - (E(h_s^+) - E_v)^{nak},$$

$$E_{red}(PhO) - E(h_s^+)^{F^-} = \left[E_{redox}^0(PhO) - E_v^{F^-} - \lambda \right]$$
$$- (E(h_s^+) - E_v)^{F^-}, \qquad (E(h_s^+) - E_v)^{nak}$$
$$= (E(h_s^+) - E_v)^{F^-}$$

and

$$E_v^{F^-} - E_v^{nak} = E^{F^-}(h_s^+) - E^{nak}(h_s^+) = \Delta V_{fb} \approx 0.06 V.$$

Table 1 shows interfacial hole transfer rate constant values for PhO photooxidation at the naked $((k_{ox}^i)^{nak})$ and fluorinated surface $((k_{ox}^i)^{F^-})$, estimated from Eq. (20) for reasonable values of the reorganization energy between 0.7 and 0.6 eV [22], and of $E(h_s^+)$ between 0.1 and 0.2 eV above the TiO$_2$ VB edge [32]. According to Eq. (19),

$$\frac{(QY_{ox}^i)^{F^-}}{(QY_{ox}^i)^{nak}} \approx \left(\frac{(k_{ox}^i)^{F^-}}{(k_{ox}^i)^{nak}} \right)^{1/2} \left(\frac{[Ti_s^{IV}]^{F^-}}{[Ti_s^{IV}]^{nak}} \right)^{\frac{1}{2}}$$

and taking into account that

$$[Ti_S]^{F^-} = [Ti_S]^{nak} - [F_s^-] = 5 \times 10^{14} - 10^{13} \text{ cm}^{-2} = 4.9 \times 10^{14} \text{ cm}^{-2},$$

it can be written that

$$\left(\frac{[Ti_s^{IV}]^{F^-}}{[Ti_s^{IV}]^{nak}} \right)^{\frac{1}{2}} \approx \left(\frac{4.9 \times 10^{14} \text{ cm}^{-2}}{5 \times 10^{14} \text{ cm}^{-2}} \right)^{\frac{1}{2}} \approx 0.99$$

so that

$$\frac{(QY_{ox}^i)^{F^-}}{(QY_{ox}^i)^{nak}} \approx \left(\frac{(k_{ox}^i)^{F^-}}{(k_{ox}^i)^{nak}} \right)^{1/2}$$

and, therefore, the value of $((QY_{ox}^i)^{F^-}/(QY_{ox}^i)^{nak}) \approx 3$ found experimentally is in reasonable good agreement with the estimated values reported in Table 1.

7. Conclusions

The analysis of open-circuit potential transients and impedance measurements at the TiO$_2$-electrolyte interface under different experimental conditions indicates that TiO$_2$ surface fluorination in 0.01 M HF + NaF aqueous solution (pH 3.5), is responsible of the following main effects: (1) a net decrease of positive electric charge at the semiconductor surface due to the substitution of water molecules adsorbed at terminal Ti atoms by fluoride ions, resulting in a concentration of specifically adsorbed F$^-$ species of the order of 10^{13} cm^{-2}; (2) a parallel diminution of the concentration of surface sites associated with terminal Ti atoms, active in the specific adsorption of dissolved substrate species; (3) a diminution of surface recombination centres associated with terminal $[Ti_S^{IV}]$ ions; (4) a simultaneous lessening of the surface electron-hole recombination rate and dissolved oxygen electroreduction rate.

According to the D–I kinetic model, the consequence of these effects on the photooxidation kinetics of substrate species can be resumed as follows: under surface fluorination the specific adsorption of dissolved substrates species on terminal Ti atoms becomes inhibited and a diminution of the photooxidation rate is produced when the DT mechanism prevails on the IT mechanism, as experimentally observed for formic acid [20]. In contrast, when the electronic interaction of substrate species with the TiO$_2$ surface is weak, as it is the case for phenol [20], the induced upward flatband potential shift produces an increased overlapping between empty electronic energy levels of surface trapped holes and filled energy levels of reduced, dissolved substrate species, which leads to an increase of the IT photooxidation rate constant.

The photocatalytic mechanism of phenol degradation, invoking the increasing participation of free OH$_{aq}^\bullet$ radicals generated by direct photooxidation of free water species with BV holes should be ruled out as neither free nor surface-bound water species can be photoxidized with VB holes. The only radical species active in oxidative photocatalytic processes should be: (a) VB free holes able to react inelastically with specifically adsorbed substrates; (b) holes trapped at terminal twofold coordinated bridging oxygen ions able to be transferred adiabatically to reduced, dissolved substrates; (c) free OH$^\bullet$ radicals, superoxide radicals and/or H$_2$O$_2$ species generated via interfacial transfer of photogenerated conduction band electrons to dissolved O$_2$.

Appendix A

Under pseudo-steady-state conditions the following equalities can be written with the help of the energy diagram in Fig. 7 [17]:

$$V_0 = k_0 \varphi \tag{A1}$$

where k_0 is a constant parameter and φ is the incident photon flux,

$$\frac{d[e_f^-]}{dt} \approx V_0 - V_{r1} - V_2 = 0, \tag{A2}$$

$$\frac{d[h_f^+]}{dt} \approx V_0 - V_1 - V_{r3} - V_{ox}^d = 0, \tag{A3}$$

$$V_1 = V_{r1} + V_{ox}^i, \tag{A4}$$

so that combining (A3) and (A4) we have

$$V_{r1} = V_0 - V_{ox}^i - V_{r3} - V_{ox}^d \tag{A5}$$

Developing (A2) we obtain that

$$[e_f^-] = \frac{k_0 \phi}{k_{r1}[h_s^+] + k_2[Ti_s^{IV}]}, \tag{A6}$$

while developing (A3) and (A5) it is

$$[h_f^+] = \frac{k_0 \phi}{k[O_s^{2-}] + k_{r3}[Ti_s^{III}] + k_{ox}^d[RH_2]_s} \tag{A7}$$

and

$$[e_f^-] = \frac{k_0 \phi - k_{ox}^i[h_s^+][(RH_2)_{aq}] - k_{r3}[h_f^+][Ti_s^{III}] - k_{ox}^d[h_f^+][(RH_2)_s]}{k_{r1}[h_s^+]}, \tag{A8}$$

where the concentration of specifically adsorbed species, $(RH_2)_S$, can be approached by a Langmuir type adsorption isotherm.

$$[(RH_2)_s] = \frac{AB[(RH_2)_{aq}]}{1 + A[(RH_2)_{aq}]}, \tag{A9}$$

A being the adsorption constant of dissolved substrate species on TiO_2 and B the concentration of TiO_2 surface sites where adsorption takes place ($B \approx [Ti_S]$). On the other hand, by combining (A6), (A7) and (A8) expression (A10) is obtained for the concentration of surface trapped holes.

$$\begin{aligned}
[h_S^+] = & \frac{-k_2[Ti_S^{IV}]}{2k_{r1}} - \frac{k_0\phi k_{r3}[Ti_S^{III}]}{2k_{ox}^i[(RH_2)_{aq}][k_1[O_S^{2-}] + k_{r3}[Ti_S^{III}] + k_{ox}^d[(RH_2)_S]]} - \\
& \frac{k_0\phi k_{ox}^d[(RH_2)_S]}{2k_{ox}^i[(RH_2)_{aq}][k_1[O_S^{2-}] + k_{r3}[Ti_S^{III}] + k_{ox}^d[(RH_2)_S]]} + \\
& \left\{ \left(\frac{k_2[Ti_S^{IV}]k_{ox}^i[(RH_2)_{aq}][k_1[O_S^{2-}] + k_{r3}[Ti_S^{III}] + k_{ox}^d[(RH_2)_S]] + k_0\phi k_{r1}k_{r3}[Ti_S^{III}] + k_0\phi k_{r1}k_{ox}^d[(RH_2)_S]}{2k_{ox}^i k_{r1}[(RH_2)_{aq}][k_1[O_S^{2-}] + k_{r3}[Ti_S^{III}] + k_{ox}^d[(RH_2)_S]]} \right)^2 \right. \\
& \left. + \frac{k_0\phi k_1 k_2[O_S^{2-}][Ti_S^{IV}]}{k_{ox}^i k_{r1}[(RH_2)_{aq}][k_1[O_S^{2-}] + k_{r3}[Ti_S^{III}] + k_{ox}^d[(RH_2)_S]]} \right\}^{\frac{1}{2}}
\end{aligned} \tag{A10}$$

Further, by considering that

$$QY_{ox}^i = \frac{v_{ox}^i}{v_0} = \frac{k_{ox}^i[RH_2]_{aq}}{k_0\varphi}[h_S^+], \tag{A11}$$

the following expression is obtained for the quantum yield for IT by combining (A10) and (A11)

$$QY_{ox}^i = \frac{-k_{ox}^i[(RH_2)_{aq}]k_2[Ti_S^{IV}]}{2k_{r1}k_0\phi} - \frac{k_{r3}[Ti_S^{III}]}{2[k_1[O_S^{2-}] + k_{r3}[Ti_S^{III}] + k_{ox}^d[(RH_2)_S]]} -$$

$$\frac{k_{ox}^d[(RH_2)_S]}{2[k_1[O_S^{2-}] + k_{r3}[Ti_S^{III}] + k_{ox}^d[(RH_2)_S]]} +$$

$$\left\{ \left(\frac{\{k_2[Ti_S^{IV}]k_{ox}^i[(RH_2)_{aq}][k_1[O_S^{2-}] + k_{r3}[Ti_S^{III}] + k_{ox}^d[(RH_2)_S]] + k_0\phi k_{r1}k_{r3}[Ti_S^{III}] + k_0\phi k_{r1}k_{ox}^d[(RH_2)_S]\}}{2k_{r1}k_0\phi[k_1[O_S^{2-}] + k_{r3}[Ti_S^{III}] + k_{ox}^d[(RH_2)_S]]} \right)^2 \right.$$
$$\left. + \frac{k_{ox}^i k_1 k_2[O_S^{2-}]\left[Ti_S^{IV}\right][(RH_2)_{aq}]}{k_{r1}k_0\phi[k_1[O_S^{2-}] + k_{r3}[Ti_S^{III}] + k_{ox}^d[(RH_2)_S]]} \right\}^{\frac{1}{2}}$$

(A12)

On the other hand, taking into account that

$$V_{ox}^d = k_{ox}^d[h_f^+][(RH_2)_S],$$

(A13)

the following expression is obtained for DT quantum yield by combining (A1), (A7), (A8) and (A13):

$$QY_{ox}^d = \frac{v_{ox}^d}{v_0} = \frac{k_{ox}^d AB[(RH_2)_{aq}]}{(1 + A[(RH_2)_{aq}])(k_1[O_S^{2-}] + k_{r3}[Ti_S^{III}]) + k_{ox}^d AB[(RH_2)_{aq}]}$$

(A14)

References

[1] M.R. Hoffmann, S.T. Martin, W. Choi, D. Bahnemann, Chem. Rev. 95 (1995) 69.
[2] M. Abdullah, G.K.C. Low, R.W. Mathews, J. Phys. Chem. 94 (1990) 6820.
[3] C. Minero, G. Mariella, V. Maurino, E. Pelizzetti, Langmuir 16 (2000) 2632.
[4] T. Hiemstra, W.H. van Riemsdijk, G.H. Bolt, J. Colloid Interf. Sci. 179 (1989) 91.
[5] T. Hiemstra, W.H. van Riemsdijk, G.H. Bolt, J. Colloid Interf. Sci. 179 (1989) 105.
[6] C.A. Giacomelli, M.J. Avena, C.P. De Pauli, Langmuir 11 (1998) 3483.
[7] Y. Suda, T. Morimoto, Langmuir 3 (1987) 786.
[8] C. Minero, G. Mariella, V. Maurino, D. Vione, E. Pelizzetti, Langmuir 16 (2000) 8964.
[9] P. Calza, E. Pelizzetti, Pure Appl. Chem. 73 (2001) 1839.
[10] J.S. Park, W. Choi, Langmuir 20 (2004) 11523.
[11] M. Mrowetz, E. Selli, Phys. Chem. Chem. Phys. 7 (2005) 1100.
[12] M. Mrowetz, E. Selli, New J. Chem. 30 (2006) 108.
[13] M.S. Vohra, S. Kim, W. Choi, J. Photochem. Photobiol. A: Chem. 160 (2003) 55.
[14] H. Park, W. Choi, J. Phys. Chem. B 108 (2004) 4086.
[15] X.F. Cheng, W.H. Leng, D.P. Liu, Y.M. Xu, J.Q. Zang, C.N. Cao, J. Phys. Chem. C 112 (2008) 8725.
[16] T. Lana-Villarreal, R. Gómez, M. Neumann-Spallart, N. Alonso-Vante, P. Salvador, J. Phys. Chem. B 108 (2004) 15172.
[17] T. Lana-Villarreal, R. Gómez, M. González, P. Salvador, J. Phys. Chem. B 108 (2004) 20278.
[18] I. Mora-Seró, T. Lana-Villarreal, J. Bisquert, A. Pitarch, R. Gómez, P. Salvador, J. Phys. Chem. B 109 (2005) 3371.
[19] D. Monllor-Satoca, R. Gómez, M. González-Hidalgo, P. Salvador, Catal. Today 129 (1/2) (2007) 247.
[20] J.F. Montoya, J. Velásquez, P. Salvador, Appl. Catal. B: Environ. 88 (2009) 50.
[21] A.V. Emeline, V.K. Ryabchuk, N. Serpone, J. Phys. Chem. B 109 (2005) 18515.
[22] S.R. Morrison, Electrochemistry at Semiconductors and Oxidized Metal Electrodes, Plenum Press, New York, 1980.
[23] M. Tomkiewicz, J. Electrochem. Soc. 126 (1979) 1505.
[24] J.A. Rob van Veen, F.T.G. Veltmaat, G. Jonkers, J. Chem. Soc., Chem. Commun. (1985) 1656.
[25] R. Gómez, P. Salvador, Solar Energy Mat. Solar Cells 88 (2005) 377.
[26] J. Bisquert, V.S. Vikhrenko, J. Phys. Chem. B 108 (2004) 2313.
[27] P. Salvador, M. Gonzalez-Hidalgo, A. Zaban, J. Bisquert, J. Phys. Chem. B. 109 (2005) 15915.
[28] D. Monllor-Satoca, R. Gomez, J. Phys. Chem. C 112 (2008) 139.
[29] D. Tafalla, P. Salvador, Ber. Bunsenges. Phys. Chem. 91 (1987) 475.
[30] M.F.J. Dijkstra, H.J. Pannemann, J.G.M. Winkelman, J.J. Kelly, A.A.C.M. Beenackers, Chem. Eng. Sci. 57 (2002) 4895.
[31] L. Davydov, P.G. Smirnotis, J. Catal. 191 (2000) 105.
[32] P. Salvador, J. Phys. Chem. C 111 (2007) 17038.
[33] H. Gerischer, Surf. Sci. 18 (1969) 97.
[34] E. Pelizzetti, C. Minero, Electrochim. Acta 38 (1993) 47.
[35] F.P. Rotzinger, J.M. Kesselman-Truttmann, S.J. Hug, V. Shklover, M. Grätzel, J. Phys. Chem. B 108 (2004) 5004.
[36] H. Günzler, H.-U. Gremlich, IR Spectroscopy. An Introduction, Wiley-VCH, 2002.

SECTION B

Mechanisms of photocatalytic Reactions

In the last decade the surface science field has brought new insights into the surface chemistry of TiO_2. Some details of the mechanism of photocatalytic reactions have been disclosed at atomic scale. One particular feature revealed by those studies is the active participation of the TiO_2 surface lattice atoms in several processes observed at the TiO_2 surface such as adsorption, dissociation, oxidation of adsorbates, among others. These great achievements open the possibility to envisage new mechanistic pathways for photocatalytic reactions. Especially important is to take into account the TiO_2 surface structure and reactivity.

The research work presented in this section (Publication 2 to 4), and the respective complementary results of the annexes chapter (Manuscript 3), was aimed to ascertain what is the role played by the TiO_2 surface lattice atoms (O_s) in photocatalytic oxidation reactions. In particular, our objective was to investigate the reactivity of the O_s at the TiO_2/fluid-phase interfaces. Notwithstanding, to collect experimental evidence that allow us to inquire what is the participation of O_s in photocatalytic reactions is not straightforward.

The most common systems employed in mechanistic studies of photocatalytic oxidation reactions consist of TiO_2 nanoparticles exposed to liquid or gas phase. The nature of these systems is very different to those employed in the surface science studies of TiO_2, namely well define surfaces exposed to ultra high vacuum. As a result, it is more difficult to elucidate the role played by O_s in this type of systems because by its nature the surface structure of nanoparticles is poorly defined (populated of several surface defects) and the presence of oxygen atoms at the liquid or gas phase makes difficult to distinguish between the O_s atoms and the oxygen atoms from water or molecular oxygen present in the reaction media.

One method to overcome the aforementioned difficulties is to trace the fate of the oxygen atoms during the course of a photocatalytic reaction by isotopic tracing. Two relevant examples of this methodology were found in the scientific literature: (1) Studies of photooxidation of aromatic compounds, in particular 4-chlorophenol, using oxygen-isotope-labeled water ($H_2{}^{18}O$) and/or labeled molecular oxygen ($^{18}O_2$). (2) Studies of photoinduced oxygen isotope exchange (POIE) between oxygen atoms from

$^{18}O_2$ in the gas phase and the TiO_2 lattice oxygens. Because of their relevance, we have decided to make a systematic review of the scientific literature concerning both topics in order to propose plausible mechanisms able to explain the reported experimental data. The publication 2 of this work proposes an alternative mechanistic route which explain how the oxygen atoms from $H_2^{18}O$ are incorporated into the oxidation products of 4-chlorophenol. Our mechanistic proposal invoke the direct participation of the O_s as hole traps, the incorporation of O_s into the products and the generation of oxygen vacancies at the TiO_2 surface that are healed by the oxygen atoms from $H_2^{18}O$. The publication 3 proposes a similar mechanism to explain the POIE phenomena and the competition between POIE and photooxidation reactions.
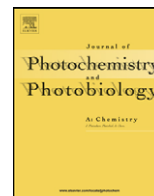
Once we had proposed a theoretical reaction mechanism to explain literature experimental data, we decided to look for direct experimental evidence to support the new mechanism. Because the main feature of the new reaction mechanism is the exchange of the O_s in the course of photocatalytic reactions, we had to look for an experimental methodology able to corroborate this hypothesis. The publication 4 reports a method to in situ trace the fate of the O_s in a photocatalytic reaction. By monitoring the isotopic composition of the carbon dioxide (CO_2) evolved from the photocatalytic mineralization of aqueous benzene with oxygen-isotope-labeled titania ($Ti^{18}O_2$), we were able to discern what is the proportion of O_s that are incorporated into the final oxidation product of the studied photocatalytic reaction. We found in this case that approximately 10^{-3} monolayer of O_s were exchange in this photocatalytic reaction. None of the precedent photocatalytic reaction mechanisms can explain this experimental observation. In contrast, the new mechanism proposed by us in publications 2 and 3 is able to explain this behavior.

In order to collect more experimental evidence to support the new mechanism we used the same experimental methodology to study the photooxidation of other organic substrates (phenol and benzaldehyde). Additionally, we studied the photooxidation of water with $Ti^{18}O_2$. In all cases, we found that O_s are exchanged in the course of the photocatalytic reactions. This set of evidence demonstrated that the new mechanism operates in the photooxidation of several substrates including water. These results are reported in the manuscript 3.

- 49 -

In general, the output of the theoretical analysis (publications 2 and 3) and the isotopic tracing experimental studies (publication 4 and manuscript 3) was a new mechanistic pathway for photocatalytic oxidation reactions. This new pathway explicitly considers the participation of O_s in the photocatalytic reactions and therefore considers that the TiO_2 surface is continuously changing as the reaction proceeds.

Publication 2

Comments on the Published Article "Effects of Hydroxyl Radicals and Oxygen Species on the 4-Chlorophenol Degradation by Photoeletrocatalytic Reactions with TiO_2-Film Electrodes by J. Yang, J. Dai, Ch. Chen, J. Zhao; J. Photochem. Photobiol. A: Chem. 208 (2009) 66-77". *Journal of Photochemistry and Photobiology A: Chemistry* **2010,** *210* (2-3), 215-216.

Contents lists available at ScienceDirect

Journal of Photochemistry and Photobiology A: Chemistry

journal homepage: www.elsevier.com/locate/jphotochem

Comments on the published article "Effects of hydroxyl radicals and oxygen species on the 4-chlorophenol degradation by photoeletrocatalytic reactions with TiO$_2$-film electrodes by J. Yang, J. Dai, Ch. Chen, J. Zhao; J. Photochem. Photobiol. A: Chem. 208 (2009) 66–77"☆,☆☆

J.F. Montoya[a], J. Peral[a], P. Salvador[b],†

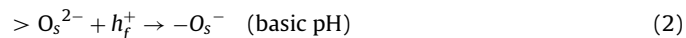[a] Departamento de Química, Universidad Autónoma de Barcelona, 08193, Cerdanyola del Vallés, Spain
[b] Departamento de Matemáticas e Informática, Universidad de las Islas Baleares, 07122, Palma de Mallorca, Spain

On the basis of isotopic tracer experiments with $^{18}OH_2$, Yang et al. [1] have claimed recently that OH radicals appearing in the primary hydroxylated intermediates of the photoeletrocatalytic oxidation of 4-chlorophenol on TiO$_2$-thin film electrodes, are mainly generated via oxidation of water species adsorbed on the semiconductor surface with photogenerated valence band (VB) free holes, h_f^+, according to reaction (1)

$$h_f^+ + (OH_2)_{ads} \rightarrow OH_{ads}^\bullet + H^+ \qquad (1)$$

This claim is in contradiction with the evidence obtained from ultraviolet photoelectron spectra (UPS) that reaction (1) is hindered both thermodynamically and kinetically [2]. In order to avoid this contradiction, the following alternative mechanism for 4-chlorophenol photooxidation is proposed.

As indicated in ref. [2], energy levels of O:2p orbitals associated with 3-fold-coordinate bulk oxygen atoms compose the top of TiO$_2$ VB, while those associated with 2-fold-coordinated bridging oxygen atoms of the TiO$_2$ surface ($> O_s^{2+}$) should be located at the bottom of the bandgap region. Consequently, after thermalization, h_f^+ holes are inelastically trapped by $> O_s^{2-}$ surface oxygen atoms, giving rise to surface trapped holes, h_s^+ associated with either 1-fold coordinated bridging oxygen radicals ($-O_s^-$) or bridging hydroxyl radicals $-OH_s^\bullet$, depending on the electrolyte pH. Therefore, instead of reaction (1), reactions (2) and (3) should be written

$$> O_s^{2-} + h_f^+ \rightarrow -O_s^- \quad \text{(basic pH)} \qquad (2)$$

$$> O_s^{2+} + H_{aq}^+ + h_f^+ \rightarrow -OH_s^\bullet \quad \text{(acidic pH)} \qquad (3)$$

These reactions in fact represent the initial step of the photocatalytic oxidation of organic compounds, in general, [3,4] and phenol in particular [5]. In a second step, a surface trapped hole is transferred adiabatically to a dissolved 4-chlorophenol molecule weakly interacting with the TiO$_2$ surface and a 4-chlorophenoxil radical is generated according to reaction (4) [5]. Simultaneously, 4-chlorophenoxil radicals may be generated via inelastic transfer of VB free holes to specifically adsorbed 4-chlorophenol species, as assumed by Yang et al. (see Eq. (2) of ref. [1]), although this alternative reaction seems to be improbable in aqueous medium [5].

$$(4)$$
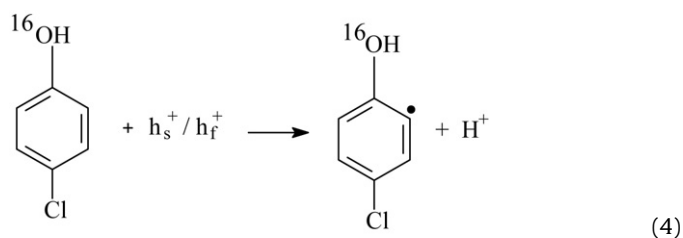
According to reaction (5), hydroquinone and/or chloro-catechol is further produced via trapping of a surface trapped hole (either $-O_s^-$ or $-OH_s^\bullet$) by a chlorophenoxil radical.

$$(5)$$

The bridging oxygen vacancy, $V\left[> O_s^{2+}\right]$, left behind at the TiO$_2$ surface during reaction (5) is rapidly filled with a $^{18}OH^-$ ion, via
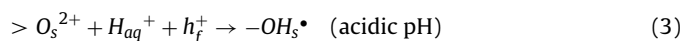

☆ Answer from Dr. J. Yang: We have read carefully the comments proposed by J.F.Montoya et al., concerning our recently published paper "Effects of hydroxyl radicals and oxygen species on the 4-chlorophenol degradation by photoelectrocatalytic reactions with TiO$_2$-film electrodes" (J. Photochem. Photobiol. A: Chem. 208 (2009) 66–77).

☆☆ Based on the related references of the comments, J.F.Montoya et al. explanation of the generation of ^{18}O oxygenated intermediates (detected by our experiments) is reasonable to a certain extent. J.F.Montoya et al. have emphasised the important role of bridging oxygen atom and bridging oxygen vacancies in the photocatalytic mechanism, which are indeed neglected in our recently published paper.
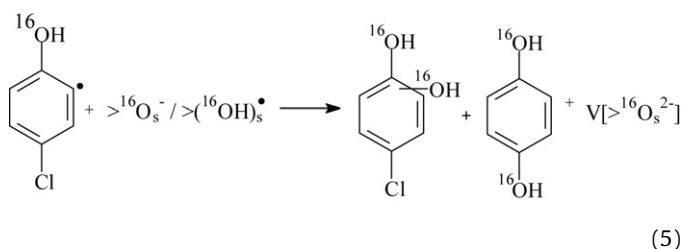
† Corresponding author.
  E-mail address: dmipss9@uib.es (P. Salvador).

dissociative adsorption of a $^{18}H_2O$ molecule from the electrolyte, according to reaction (6). Such a of regeneration of bridging oxygen atoms was first demonstrated via high resolution STM experiments by Schaub et al. [6] and further confirmed by Wendt et al. [7].

$$V\left[>{}^{18}O_s{}^{2+}\right] + {}^{18}OH_2 \to > {}^{18}OH_s{}^{-} + H^{+} \tag{6}$$
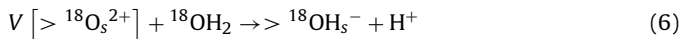
The $> {}^{18}OH_s{}^{-}$ bridging hydroxyl so generated is further oxidized with a valence band free hole and a bridging hydroxyl radical is generated according to reaction (7)

$$> {}^{18}OH_s{}^{-} + h_f{}^{+} \to -{}^{18}OH_s{}^{\bullet} \tag{7}$$

Finally, according to reaction (8), an hydroxilated intermediate is generated via the attack of a 4-chlorophenoxil radical generated in (4) with the bridging hydroxyl radical generated in (7)

$$\tag{8}$$
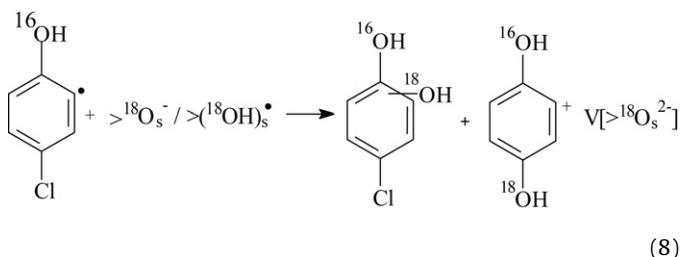
From reaction (8), a new oxidative cycle is initiated with reaction (6).

Summing up, the proposed mechanism of 4-chlorophenol photooxidation reasonably explain the generation of ^{18}O oxygenated intermediates, as detected experimentally by Yang et al., [1] without invoking the participation of $^{18}OH^{\bullet}$ radicals generated from the photooxidation of $^{18}OH_2$ adsorbed molecules with VB free holes. Particularly singular is the role that bridging oxygen atoms and bridging oxygen vacancies play in the proposed mechanism. This has been described with more detail in a recent publication on the photoinduced oxygen exchange reactions taking place at the gas phase-TiO$_2$ interface [8].

References

[1] J. Yang, J. Dai, Ch. Chen, J. Zhao, Effects of hydroxyl radicals and oxygen species on the 4-chlorophenol degradation by photoelectrocatalytic reactions with TiO$_2$-film electrodes, J. Photochem. Photobiol. A: Chem. 208 (2009) 66–77.
[2] P. Salvador, On the nature of photogenerated radical species active in the oxidative degradation of dissolved pollutants with TiO$_2$ aqueous suspensions: a revision in the light of the electronic structure of adsorbed water, J. Phys. Chem. C 111 (2007) 17038.
[3] T. Lana-Villarreal, R. Gómez, M. Neumann-Spallart, N. Alonso-Vante, P. Salvador, Semiconductor photooxidation of pollutants dissolved in water: a kinetic model for distinguishing between direct and indirect interfacial hole transfer, J. Phys. Chem. B 108 (2004) 15172.
[4] D. Monllor-Satoca, R. Gómez, M. González-Hidalgo, P. Salvador, The "direct-indirect" model: an alternative kinetic approach in heterogeneous photocatalysis based on the degree of interaction of dissolved pollutant species with the semiconductor surface, Catal. Today 129 (1–2) (2007) 247.
[5] J.F. Montoya, J. Velásquez, P. Salvador, The "direct-indirect" model in photocatalysis: a reanalysis of phenol and formic acid photodegradation rate dependence on photon flux and concentration in TiO$_2$ aqueous suspensions, Appl. Catal. B: Environ. 88 (2009) 50.
[6] R. Schaub, P. Thostrup, N. Lopez, E. Laegsgaard, I. Stensgaard, J.K. Norskov, F. Besenbacher, Oxygen vacancies as active sites for water dissociation on rutile TiO$_2$ (110), Phys. Rev. Lett. 87 (2001) 266104/1.
[7] S. Wendt, J. Matthiensen, R. Schaub, E.K. Vestergaard, E. Laegsgaard, F. Besenbacher, Formation and splitting of paired hydroxyl groups on rutile TiO$_2$ (110), Phys. Rev. Lett. 96 (2006) 066107/4.
[8] J.F. Montoya, J. Peral, P. Salvador, Surface chemistry and interfacial charge transfer mechanisms in the photoinduced oxygen exchange at the O$_2$ gas-phase interface: competition with the photooxidation of organic species and influence of adsorbed water, submitted for publication.

Publication 3

"Surface Chemistry and Interfacial Charge-Transfer Mechanisms in Photoinduced Oxygen Exchange at O_2-TiO_2 Interfaces". *ChemPhysChem* **2011,** 12 (5), 901-907.

Surface Chemistry and Interfacial Charge-Transfer Mechanisms in Photoinduced Oxygen Exchange at O₂–TiO₂ Interfaces**

Juan Felipe Montoya,[b] José Peral,[b] and Pedro Salvador*[a]

Experimental results obtained over the last three decades on photoinduced oxygen isotopic exchange (POIE) of TiO₂ oxygen atoms with those of adsorbed water molecules and gaseous O₂ are analyzed in the light of recent information from the literature on the interaction of water and O₂ species with the TiO₂ surface (obtained by application of surface spectroscopy techniques in combination with high-resolution scanning tunnelling microscopy). The analysis emphasizes the singular role that bridging oxygen ions and bridging oxygen vacancies play in TiO₂ surface chemistry and interfacial electron transfer at the gas phase–TiO₂ interface in the absence and presence of water. The observed competition between POIE and the photo-oxidation (PO) of organic compounds is analyzed in terms of the recently developed direct-indirect (D-I) kinetic model for heterogeneous photocatalysis (D. Monllor-Satoca et al., *Catal. Today*, **2007**, *129*, 247, and references therein).

1. Introduction

Since 1977, when Frank and Bard proposed the purification of water via the photocatalytic decomposition of pollutants,[1,2] the interest in the application of TiO₂ heterogeneous photocatalysis with a decontamination purpose has grown exponentially (more than 2500 publications appeared on this subject up to 2009). In particular, heterogeneous photocatalysis at the gas phase–TiO₂ interface has emerged as an interesting tool for decontamination, deodorization, and disinfection of air over the last decades.[3–5]

Among the studied reactions in the field of gas phase–TiO₂ heterogeneous photocatalysis, photoinduced oxygen isotopic exchange (POIE) at room temperature between oxygen molecules and the TiO₂ surface has received special attention as a source of valuable information about constituent elementary steps of most photocatalytic reactions where O₂ is involved as an acceptor of photogenerated electrons.[6–18] The interpretation of POIE phenomena allows us to obtain key information about the nature of the active species involved in the photocatalytic reactions, thus evidencing the important role that terminal oxygen atoms can play as active species in photo-oxidation (PO) reactions taking place at the TiO₂–gas phase interface.[18] These findings open new ways of surface chemistry research in liquid-phase photocatalysis. Further, the information obtained from these studies may be useful for the synthesis of semiconducting materials, under control of active surface lattice defects, leading to more efficient photocatalytic systems. For instance, the use of dissolved chemical species able to block TiO₂ bridging oxygen atoms to promote the direct transfer of photogenerated valence-band (VB) free holes to organic molecules chemisorbed at terminal Ti ions—the most efficient interfacial charge-transfer mechanism in the photoinduced oxidation of organics—may lead to an important improvement of the PO efficiency.

In 1977 Pichat et al. found a correlation between the TiO₂ activity for POIE and the photocatalytic oxidation of isobutane.[8]

The observation that POIE does not take place in the presence of isobutane allowed these authors to infer that the same oxygen species of the TiO₂ surface participate in both reactions. More recently, Pichat and co-workers showed that POIE is a very sensitive method for evaluating the mobility of TiO₂ terminal oxygen atoms and understanding their incorporation into gas-phase substrate species during PO interfacial reactions,[18] a subject of primary interest in heterogeneous photocatalysis.

As proposed by Pichat et al.,[18] and represented schematically in Figure 1, the POIE mechanism between gas-phase $^{18}O_2$ and oxygen atoms of $M_x^{16}O_y$ semiconducting metal oxides ($Ti^{16}O_2$ in particular) should involve the simultaneous generation of $^{16}O_s^{\bullet-}$ surface radicals, via trapping of photogenerated VB free holes, h_f^+, by $^{16}O_s^{2-}$ surface ions [Eq. (1)]:

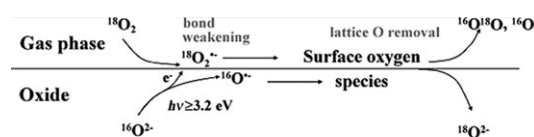$$Ti -^{16}O_s^{2-} + h_f^+ \rightarrow Ti -^{16}O_s^{\bullet-} \tag{1}$$

Figure 1. Scheme of the POIE mechanism proposed by Pichat et al., reproduced with permission from ref. [18]. Copyright (2007) VPS.

[a] Dr. P. Salvador
Departament de Ciències Matemàtiques i Informàtica
Universitat de les Illes Balears, 07071 Palma de Mallorca (Spain)
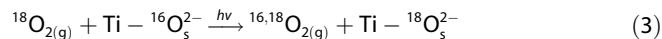Fax: (+34) 971-173003
E-mail: dmipss9@uib.es

[b] J. F. Montoya, Dr. J. Peral
Departamento de Química, Universidad Autónoma de Barcelona
08193 Cerdanyola del Vallés (Spain)

[**] Competition with the Photo-oxidation of Organic Species and Influence of Adsorbed Water

and superoxide radicals, via electroreduction of $^{18}O_2$ molecules in the gas phase with photogenerated conduction band (CB) free electrons, e_f^- [Eq. (2)]:

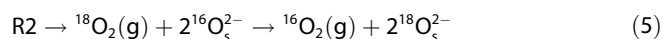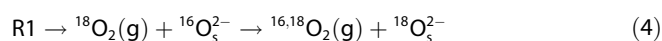$$^{18}O_2(g) + e_f^- \rightarrow {}^{18}O_2^{\bullet-} \tag{2}$$

the POIE global reaction being [Eq. (3)]:

$$^{18}O_{2(g)} + Ti - {}^{16}O_s^{2-} \xrightarrow{h\nu} {}^{16,18}O_{2(g)} + Ti - {}^{18}O_s^{2-} \tag{3}$$

which involves the breaking of the $^{18}O-{}^{18}O$ bond in the $^{18}O_2$ molecule and the $Ti - O_s^{\bullet-}$ bond at the semiconductor surface. Alternatively, Tanaka proposed that the POIE mechanism proceeds via a weakly held $O_3^{\bullet-}$ intermediate formed from the reaction between O_2 and $O^{\bullet-}$. Although instable $O_3^{\bullet-}$ radicals over UV-irradiated MgO have been apparently detected by Tench and Lawson[19] and by Wong and Lundsford,[20] they appeared to be inactive for POIE.

In general, POIE is assumed to occur according to the following reaction pathways [Eqs. (4) and (5)]:[18]

$$R1 \rightarrow {}^{18}O_2(g) + {}^{16}O_s^{2-} \rightarrow {}^{16,18}O_2(g) + {}^{18}O_s^{2-} \tag{4}$$

$$R2 \rightarrow {}^{18}O_2(g) + 2{}^{16}O_s^{2-} \rightarrow {}^{16}O_2(g) + 2{}^{18}O_s^{2-} \tag{5}$$

depending on whether one or two O_s^{2-} ions of the semiconductor surface participate in the reaction. In the case of TiO_2, the R1 pathway seems to prevail over R2, since the experimentally detected amount of $^{16,18}O_2(g)$ is much greater than the amount of $^{16}O_2(g)$.[7,8,12]

Pichat et al. also found that the POIE activity of different TiO_2 samples was very similar to their activity for isobutane[8] and methanol[18] photo-oxidation. An analogous correlation between POIE and PO was observed by Sato et al. for the oxidation of ethane on a home prepared TiO_2 sample calcined at various temperatures,[12] a fact that was attributed by these authors to the participation of photogenerated $O_s^{\bullet-}$ radicals as active surface species in both mechanisms. The same conclusion was reached by Pichat et al. after observing that $^{18}O_2(g)$ does not exchange oxygen atoms with the TiO_2 surface when either isobutane[8] or methanol[18] are present in the gas phase.

On the other hand, Muggli and Falconer[17] studied the POIE mechanism between gas-phase $^{16}O_2$ and $H_2{}^{18}O$ adsorbed onto Degussa P-25, mainly detecting $^{16,18}O_2$ and a small amount of $^{18}O_2$ as reaction products. These authors also investigated the photo-oxidation of ethanol co-adsorbed with $H_2{}^{18}O$, in the presence of $^{16}O_2(g)$. Under these conditions, the authors did not found a significant amount of $^{18}O_2$ or $^{16,18}O_2$, in spite of the fact that a significant amount of $H_2{}^{18}O$ was present at the TiO_2 surface. Interestingly, these results seem to reinforce the thesis formulated by Pichat et al.[18] and Sato et al.[12] that the same oxygen surface species, probably $O_s^{\bullet-}$, are active in POIE and PO mechanisms.

Since Pichat's POIE mechanism, schematized in Figure 1, only defines initial species ($^{16}O_s^{2-}$ and $^{18}O_2(g)$) and final products ($^{18}O_s^{2-}$, $^{16}O_{2(g)}$, and $^{16,18}O_{2(g)}$), a knowledge of the intermediate

reaction steps is necessary to reach a deeper understanding of the POIE processes involved in the presence and absence of adsorbed water. With this purpose in mind, we will develop here an auto-consistent POIE reaction mechanism based on the participation of twofold-coordinated bridging oxygen ions ($> O_{br}^{2-}$), the most abundant oxygen species present at rutile and anatase lower energy crystal faces, as natural hole-trapping species at the naked TiO_2 surface. Further, we will consider the photogeneration of bridging oxygen vacancies as a key to understand the interaction of O_2 and H_2O molecules in the gas phase with the TiO_2 surface at intermediate steps of the POIE mechanism. Two main POIE reactions will be analyzed, exchange of gas-phase O_2 and oxygen atoms of adsorbed water molecules and with $> O_{br}^{2-}$ surface ions. The photo-oxidation of co-adsorbed organic molecules in competition with POIE will also be analyzed.

2. The Role of Twofold-Coordinated Bridging Oxygen Atoms as Natural TiO_2 Surface Traps for Photogenerated VB Free Holes

It is generally accepted that water species adsorbed on fivefold-coordinated terminal Ti atoms (Ti_t) are efficient traps for photogenerated VB free holes (h_f^+) at the TiO_2 surface, thus being the main source of surface $OH^{\bullet}$ radicals active in photocatalytic reactions [Eq. (6)]:

$$Ti_t - OH_2 + h_f^+ \rightarrow Ti - OH^{\bullet} + H^+ \tag{6}$$
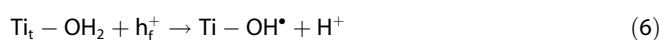
However, based on the interpretation of metastable impact electronic spectra (MIES) and ultraviolet photoelectron spectra (UPS) of hydrated, well-defined TiO_2 surfaces, evidence has been recently obtained that the photo-oxidation of adsorbed water species on TiO_2 is not only kinetically but also thermodynamically hindered.[21, 22]

At the bulk of stoichiometric TiO_2, titanium and oxygen atoms are six- and threefold-coordinated, respectively. In contrast, at the TiO_2 surface (independently of whether the anatase or the rutile crystal face is considered), terminal Ti atoms are fivefold-coordinated, while a large part of oxygen atoms, known as bridging oxygen ions ($> O_{br}^{2-}$), are twofold-coordinated. Since the Ti—O bonding energy is expected to diminish when the coordination of O^{2-} ions decreases from three- to twofold, a lower bonding energy should be expected for $> O_{br}^{2-}$ when compared to threefold-coordinated terminal oxygen ions. This implicates that energy levels of O:2p orbitals associated with terminal, bridging oxygen ions should be above those associated with threefold-coordinated oxygen ions constituting the top of the TiO_2 VB at the bulk. Consequently, after thermalization, photogenerated VB free holes should be trapped at bridging oxygen ions, leading to the generation of bridging oxygen radicals ($-O_{br}^{\bullet-}$) [Eq. (7)]:[21,22]

$$> O_{br}^{2-} + h_f^+ \rightarrow -O_{br}^{\bullet-} \tag{7}$$

Note that the coordination of $-O_{br}^{\bullet-}$ radicals is onefold instead of twofold, as one $Ti-O_{br}^{2-}$ bond is broken under hole

trapping. This means that the bond strength of $-O_{br}^{\bullet-}$ radicals with the TiO₂ surface becomes considerably weakened.

3. Tentative Mechanism for POIE between Oxygen Atoms of Gas-Phase $^{18}O_2$ and $>^{16}O_{br}^{2-}$ Ions

The time dependence of the isotopic composition of gas-phase O₂ during the POIE experiments, first obtained by Pichat et al.,[8] is reproduced in Figure 2. Similar experimental results were later obtained by Sato.[13]

Two well-defined zones can be distinguished in Figure 2: zone 1, for $t \leq 9$ min, and zone 2, for $9 < t < 15$ min. Initially ($t \approx 0$), the only detected photogenerated oxygen species are $^{16,18}O_2(g)$, $^{16}O_2(g)$ being apparently not generated. As the illumination time increases, the concentration of $^{16,18}O_2(g)$ within zone 1 increases, although the $^{16,18}O_2(g)$ generation rate,

$$r_1 = \frac{d[^{16,18}O_2(g)]}{dt},$$ progressively decreases, becoming zero within

zone 2. In contrast, the $^{16}O_2(g)$ generation rate, $r_2 = \frac{d[^{16}O_2(g)]}{dt}$, progressively increases in zone 1 and becomes approximately constant in zone 2. On the other hand, the destruction rate of $^{18}O_2(g)$ in zone 1, at any time, is apparently equal to the generation rate of $^{16}O_2(g) + {}^{16,18}O_2(g)$, while in zone 2 the generation rate of $^{16}O_2(g)$ seems equal to the destruction rate of $^{18}O_2(g)$, the $^{16,18}O_2$ concentration apparently reaching a steady-state value. A tentative explanation of these experimental fea-
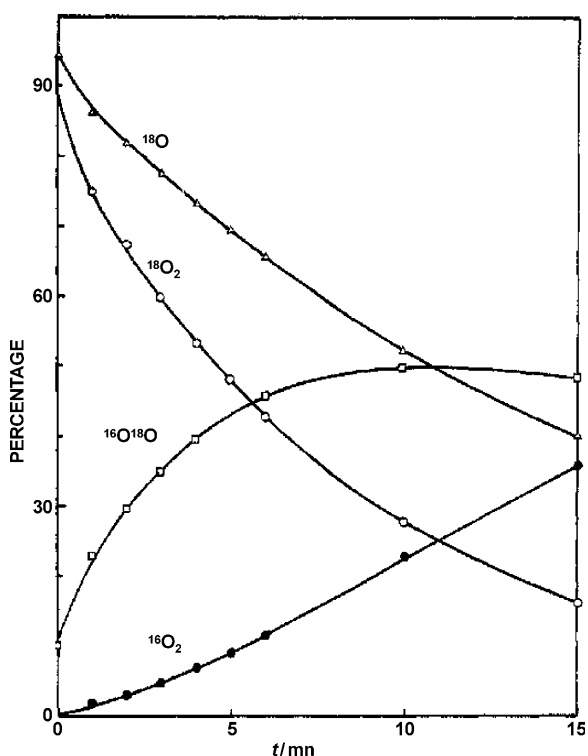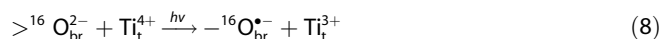
tures is given in the reaction scheme of Figure 3. Reaction step (8) defines the generation of TiO₂-surface-trapped electron–hole pairs under UV illumination [Eq. (8)]:

$$>^{16}O_{br}^{2-} + Ti_t^{4+} \xrightarrow{h\nu} -^{16}O_{br}^{\bullet-} + Ti_t^{3+} \tag{8}$$

that is, VB free holes are trapped by the twofold-coordinated bridging oxygen ions ($>^{16}O_{br}^{2-}$), generating onefold-coordinat-

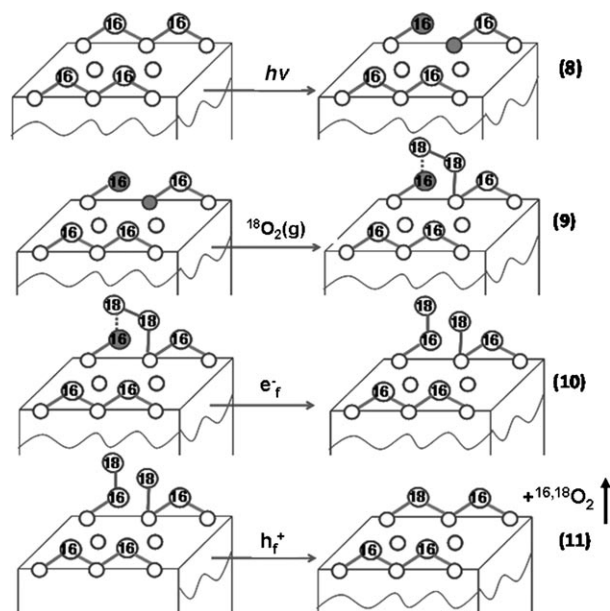**Figure 3.** Mechanistic scheme for POIE between oxygen atoms of $^{18}O_2(g)_{(g)}$ and terminal $>{}^{16}O_{br}^{2-}$ ions at the TiO₂–gas interface under UV illumination in the absence of adsorbed water. Large white circle: bridging oxygen ion; large grey circle: bridging oxygen radical; small white circle: Ti⁴⁺ ion; small grey circle: Ti³⁺ ion.

ed bridging oxygen radicals ($O_{br}^{\bullet-}$), while photogenerated CB free electrons are trapped at neighboring sixfold-coordinated terminal Ti_t^{4+} cations, generating Ti_t^{3+} cations. Since the mobility of surface-trapped electron–hole pairs becomes considerably reduced, their probability of recombination should be rather low even if they occupy neighboring surface sites. Further, as the electron lost by $>^{16}O_{br}^{2-}$ ions belongs to a bonding O:2p orbital, one of its two bonds to terminal Ti_t^{4+} should be broken, the corresponding photogenerated $-^{16}O_{br}^{\bullet-}$ radical becoming onefold-coordinated. In step (9) the electron trapped at a Ti_t^{3+} cation is transferred to a $^{18}O_2(g)$ molecule,[23] the Ti_t^{3+} cation being re-oxidized and a $^{18}O_2^{-} - Ti_t^{4+}$ bond simultaneously generated [Eq. (9)]:

$$-^{16}O_{br}^{-} + Ti_t^{3+} + {}^{18}O_2(g) \rightarrow {}^{16}O_{br}^{-}....^{18}O_2^{-} - Ti_t^{4+} \tag{9}$$
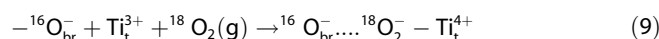
It should be noted that the $^{18}O - {}^{18}O$ bond within the adsorbed superoxide ion is probably weaker than that within the $^{18}O_2(g)$ molecule.[24]

In step (10) a photogenerated CB free electron is transferred to the superoxide ion through the Ti_t^{4+} ion, so that the $^{18}O-^{18}O$ bond within the $^{18}O_2$ molecule becomes broken, one of its

Figure 2. Time evolution of the isotopic gas-phase O₂ composition during POIE between oxygen atoms of $^{18}O_2(g)$ and terminal $>{}^{16}O_{br}^{2-}$ ions, at the TiO₂–gas interface under UV illumination. Reproduced with permission from ref. [8]. Copyright (1977) American Chemical Society.

oxygen atoms remaining attached to the Ti_t^{4+} cation as an $^{18}O^{2-}$ ion, while the remaining ^{18}O ad-atom becomes bonded to the $-{^{16}O_{br}}^{\bullet-}$ radical generated in step (8), giving rise to a one-fold-coordinated $-(^{16}O-^{18}O)_{br}^{\bullet-}$ radical at a bridging site [Eq. (10)]:

$$-{^{16}O_{br}^{\bullet-}} \cdots {^{18}O_2^-} - Ti_t^{4+} \xrightarrow{+e_f^-} -(^{16}O-^{18}O)_{br}^{\bullet-} + Ti_t^{4+} + {^{18}O^{2-}} \qquad (10)$$
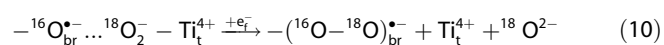
Finally, in step (11) a VB free hole is trapped by the bridging $-(^{16}O-^{18}O)_{br}^{\bullet-}$ radical generated in step (10), its bond to the Ti_t^{4+} cation being broken and one $^{16,18}O_2$ molecule being transferred to the gas phase, thereby leaving behind a bridging oxygen vacancy $(V\left[> {^{16}O_{br}^{2-}}\right])$ that is immediately filled with the $^{18}O^{2-}$ ion onefold-coordinated to its neighboring Ti_t^{4+} cation [Eq. (11)]:

$$-(^{16}O-^{18}O)_{br}^{\bullet-} + Ti_t^{4+} - {^{18}O^{2-}}$$
$$\xrightarrow{+h_f^+} V\left[> O_{br}^{2-}\right] + {^{16,18}O_2^\uparrow(g)} + Ti_t^{4+} - {^{18}O^{2-}} \to > {^{18}O_{br}^{2-}} + Ti_t^{4+} \qquad (11)$$
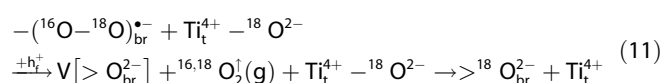
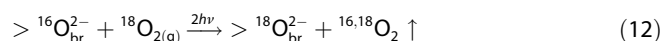As the global Equation (12) indicates, two photons, a $> {^{16}O_{br}^{2-}}$ bridging oxygen and a gas-phase $^{18}O_2$ molecule, are consumed in the generation of a $> {^{18}O_{br}^{2-}}$ bridging oxygen and a $^{16,18}O_2$ molecule:

$$> {^{16}O_{br}^{2-}} + {^{18}O_{2(g)}} \xrightarrow{2h\nu} > {^{18}O_{br}^{2-}} + {^{16,18}O_2}\uparrow \qquad (12)$$

It must be noted that the electron–hole recombination reactions [Eqs. (13) and (14)]:

$$-O_{br}^{\bullet-} + e_f^- \to > O_{br}^{2-} \qquad (13)$$

$$Ti_t^{3+} + h_f^+ \to Ti_t^{4+} \qquad (14)$$

participating in the process and not explicitly included in the mechanistic scheme of Figure 3, are determinant of the POIE efficiency.

Recent experimental and theoretical studies concerning the primary role of molecular oxygen in thermal and photoinduced catalytic surface reactions over TiO_2 give support to some of the reaction steps invoked in Figure 3. On the one hand, Henderson et al.[25] postulated that $HO_2^{\cdot}$ is an intermediate of the reaction between O_2 and $> OH_{br}^-$ bridging hydroxyl groups at (110) TiO_2. This hypothesis was further confirmed by Du et al.,[26] who via high-resolution STM imaging detected the spontaneous dissociation of hydroperoxy species according to Equation (15):

$$HO_2^{\bullet-} \to O_a + -OH_t \qquad (15)$$

where O_a represents an oxygen ad-atom and $-OH_t$ a hydroxyl radical single-bonded to a terminal Ti atom. Experimental evidence that O_2, an efficient electron scavenger, reacts with $> OH_{br}^-$, according to Equation (16):

$$> OH_{br}^- + O_2(g) + 4e_f^- + 3h_f^+ \to -O_{br}^- + -OH_t^- + O_a \qquad (16)$$
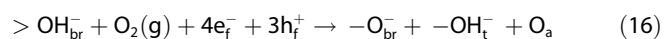
has also been provided by the same authors, which reinforce our thesis that, according to reaction steps (9) and (10), adsorbed $^{18}O_2(g)$ dissociates into $-(^{16}O-^{18}O)_{br}^{\bullet-}$ and $Ti_t^{4+} - {^{18}O^{2-}}$ with the participation of two photons. On the other hand, STM studies by Mezhemy et al.,[27] have evidenced the generation of bridging oxygen vacancies under UV illumination of TiO_2 (110), sustaining the hypothesis formulated in Equation (11).

With respect to the generation of $^{16}O_2(g)$, also observed by Pichat et al.[8] (see Figure 2), the following global reaction [Eq. (17)] should be invoked in analogy with reaction (12):

$$> {^{16}O_{br}^{2-}} + {^{16,18}O_{2(g)}} + 2h\nu \to > {^{18}O_{br}^{2-}} + {^{16}O_2(g)} \qquad (17)$$
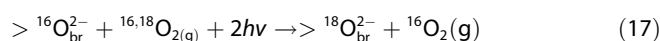
To explain some kinetic details implicit in Figure 2, let us define r_{12} and r_{17} as the rates of reaction steps (12) and (17), respectively. Since r_{17} is proportional to the $^{16,18}O_2(g)$ concentration, for $t \approx 0$, when it is $\left[^{16,18}O_2(g)\right] = 0$ in the gas phase, it should be $r_{17} = 0$, explaining why $^{16}O_2(g)$ is not produced until a certain amount of $^{16,18}O_2(g)$ is present in the gas phase. However, as far as POIE does progress, $^{18}O_2(g)$ in the gas phase is substituted by $^{16,18}O_2(g)$, $> {^{16}O_{br}^{2-}}$ being simultaneously substituted by $> {^{18}O_{br}^{2-}}$ at the TiO_2 surface, so that r_{12} should decrease and r_{17} should increase, as in fact observed in Figure 2. On the other hand, r_{17} grows up as far as $\left[^{16,18}O_2(g)\right]$ increases in the gas phase. Just when zone 2 is reached and $r_{12} \approx r_{17}$, should $\left[^{16,18}O_2(g)\right]$ reach a steady-state value, while $\left[^{16}O_2(g)\right]$ should still increase because of the presence of $> {^{16}O_{br}^{2-}}$ ions at the TiO_2 surface—predictions also confirmed in Figure 2. In conclusion, the proposed mechanism not only ratifies the hypothesis by Courbon et al.[8] that only one surface oxygen is involved in the POIE reaction, but also explains the time dependence of the $^{16,18}O_2(g)$ and $^{16}O_2(g)$ generation from $^{18}O_2(g)$.

4. Tentative Mechanism for POIE between Oxygen Atoms of Gas-Phase $^{16}O_2$ and Adsorbed $H_2^{18}O$

Figure 4 reproduces the experimental results by Muggli and Falconer[17] on the generation rate of $^{16,18}O_2(g)$ when pulses of $^{16}O_2(g)$ are injected over UV-illuminated TiO_2 (Degussa P-25) previously saturated wit a monolayer of $H_2^{18}O$. Apparently, no POIE takes place in the dark, but only when $^{16}O_2(g)$ is pulsed over the UV-illuminated sample. According to the authors, 65% of the adsorbed $H_2^{18}O$ species exchange oxygen with gas-phase $^{16}O_2(g)$ during a 3.5 h experiment, mainly generating $^{16,18}O_2(g)$ and a small amount of $^{18}O_2(g)$. Interestingly, the authors also observed that POIE between oxygen atoms of gas-phase $^{16}O_2(g)$ and those of adsorbed $H_2^{18}O$ immediately stops when ethanol is injected into the system, an effect similar to that obtained by Pichat and co-workers during POIE between $^{18}O_2(g)$ and $> {^{16}O_{br}^{2-}}$ of the TiO_2 surface, in the presence of isobutane[8] and methanol.[18]

The following sequence of reaction steps is proposed to explain the results exposed in Figure 4 with relation to the POIE mechanism [Eqs. (18)–(28)]:
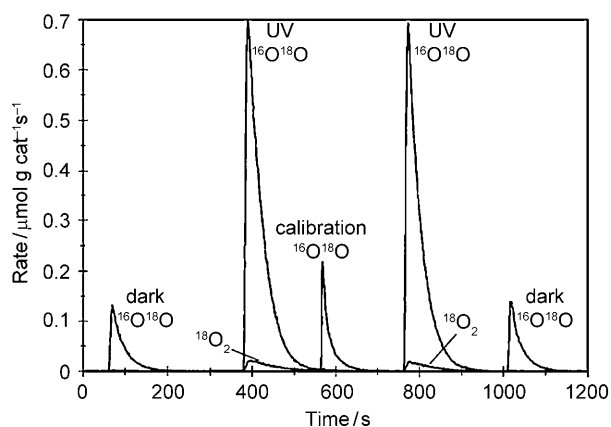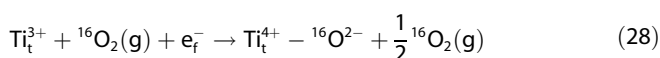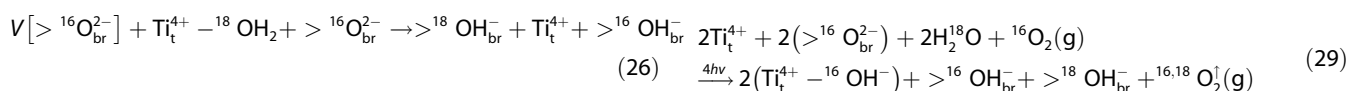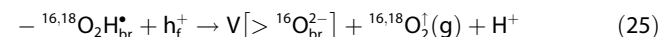
Figure 4. Time evolution of the isotopic gas-phase O$_2$ composition during POIE between oxygen atoms of ^{16}O$_2$(g) and ^{18}OH$_2$ adsorbed onto Degussa P-25 TiO$_2$, in the dark and under UV illumination. Reproduced with permission from ref. [17]. Copyright (1999) Academic Press.

$$2\text{Ti}_t^{4+} + 2\,{}^{18}\text{OH}_2 \rightarrow 2(\text{Ti}_t^{4+} - {}^{18}\text{OH}_2) \tag{18}$$

$$> {}^{16}\text{O}_{br}^{2-} + h_f^+ \rightarrow {}^{16}\,\text{O}_{br}^{\bullet-} \tag{19}$$

$$- {}^{16}\text{O}_{br}^{\bullet-} + h_f^+ \rightarrow V\big[>{}^{16}\,\text{O}_{br}^{2-}\big] + \frac{1}{2}{}^{16}\text{O}_2(\text{g}) \tag{20}$$

$$V\big[>{}^{16}\text{O}_{br}^{2-}\big] + \text{Ti}_t^{4+} - {}^{18}\text{OH}_2 + > {}^{16}\text{O}_{br}^{2-}$$
$$\rightarrow\, > {}^{18}\text{OH}_{br}^- + \text{Ti}_t^{4+} + > {}^{16}\text{OH}_{br}^- \tag{21}$$

$$>^{18}\text{OH}_{br}^- + \text{Ti}_t^{4+} + {}^{16}\text{O}_2(\text{g}) + e_f^- \rightarrow\, > {}^{18}\text{OH}_{br}^-.....{}^{16}\text{O}_2^{\bullet-} - \text{Ti}_t^{4+} \tag{22}$$

$$>^{18}\text{OH}_{br}^-...{}^{16}\text{O}_2^- - \text{Ti}_t^{4+} + h_f^+ \rightarrow\, -{}^{18}\text{OH}_{br}^\bullet.....{}^{16}\text{O}_2^{\bullet-} - \text{Ti}_t^{4+} \tag{23}$$

$$-{}^{18}\text{OH}_{br}^\bullet.......{}^{16}\text{O}_2^- - \text{Ti}_t^{4+} + e_f^- \rightarrow\, -{}^{16,18}\text{O}_2\text{H}_{br}^\bullet + \text{Ti}_t^{4+} - {}^{16}\text{O}^{2-} \tag{24}$$

$$-{}^{16,18}\text{O}_2\text{H}_{br}^\bullet + h_f^+ \rightarrow V\big[>{}^{16}\text{O}_{br}^{2-}\big] + {}^{16,18}\text{O}_2^\uparrow(\text{g}) + \text{H}^+ \tag{25}$$

$$V\big[>{}^{16}\text{O}_{br}^{2-}\big] + \text{Ti}_t^{4+} - {}^{18}\text{OH}_2 + > {}^{16}\text{O}_{br}^{2-} \rightarrow > {}^{18}\text{OH}_{br}^- + \text{Ti}_t^{4+} + >{}^{16}\text{OH}_{br}^- \tag{26}$$

$$\text{Ti}_t^{4+} + e_f^- \rightarrow\, \text{Ti}_t^{3+} \tag{27}$$

$$\text{Ti}_t^{3+} + {}^{16}\text{O}_2(\text{g}) + e_f^- \rightarrow \text{Ti}_t^{4+} - {}^{16}\text{O}^{2-} + \frac{1}{2}{}^{16}\text{O}_2(\text{g}) \tag{28}$$

This mechanism is far more complicated than that schematized in Figure 3 for explaining POIE between $> {}^{16}\text{O}_{br}^{2-}$ and Ti_t^{4+}(g), the main reason for this complexity coming from the fact that adsorbed water cannot be directly photo-oxidized with VB free holes, as pointed out in Section 2. Reaction step (18) shows the adsorption of two H$_2$^{18}O molecules onto terminal Ti_t^{4+} cations. According to steps (19) and (20) $\frac{1}{2}{}^{16}\text{O}_2$(g) is liberated from the TiO$_2$ surface with the participation of two VB free holes successively trapped by one $> {}^{16}\text{O}_{br}^{2-}$ ion, leaving behind a bridging oxygen vacancy. In step (21) an adsorbed H$_2$^{18}O molecule dissociates into ^{18}OH$^-$ and H$^+$; the ^{18}OH$^-$ hydroxyl occu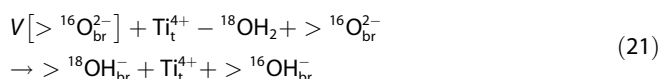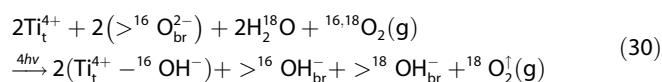pies the bridging oxygen vacancy generated in step (20), giving rise to a $> {}^{18}\text{OH}_{br}^-$ bridging hydroxyl, while the neighboring $> {}^{16}\text{O}_{br}^{2-}$ bridging oxygen ion becomes protonat-

ed. The result is the generation of $> {}^{18}\text{OH}_{br}^-$ and $> {}^{16}\text{OH}_{br}^-$ hydroxyl ions at neighboring bridging surface sites. The mechanism of dissociative adsorption of a water molecule at a bridging oxygen vacancy was first demonstrated via high-resolution STM experiments in 2001 by Schaub et al.[28] and Brookes et al,[29] and further confirmed in 2006 by Wendt et al.[30] Step (22) shows the generation of a Ti_t^{3+} center via the reduction of a fivefold-coordinated Ti_t^{4+} cation with a CB free electron; the electron is further transferred to a ^{16}O$_2$(g) molecule, giving rise to a ^{16}O$_2^{\bullet-}$ adsorbed superoxide radical and regenerating the Ti_t^{4+} ion.[23,24] In step (23) a onefold-coordinated $> {}^{16}\text{O}_{br}^{2-}$ bridging hydroxyl radical is photogenerated via capture of a VB free hole by a $> {}^{16}\text{OH}_{br}^-$ bridging hydroxyl. After trapping a CB free electron, the superoxide generated in step (22) becomes dissociated in step (24), generating one ^{16}O ad-atom that becomes attached to the neighboring $-{}^{18}\text{OH}_{br}^\bullet$ hydroxyl radical, with generation of one $-{}^{16,18}\text{O}_2\text{H}_{br}$ hydroperoxide group at a bridging site and an ^{16}O^{-2} ion adsorbed on a neighboring Ti_t^{4+} ion. Step (25) shows further capture of a VB free hole by the $> {}^{16,18}\text{O}_2\text{H}_{br}^\bullet$ hydroperoxide group generated in step (24), with evolution of a ^{16,18}O$_2$(g) molecule that leaves behind a $V\big[>{}^{16}\text{O}_{br}^{2-}\big]$ bridging oxygen vacancy; the released proton reacts with the ^{16}O^{2-} ion, giving rise to a ^{16}OH$^-$ hydroxyl attached to a Ti_t^{4+} cation. In step (26), which is a repetition of step (21), a Ti_t^{4+}-attached ^{18}OH$_2$ molecule is dissociatively adsorbed in the bridging oxygen vacancy photogenerated in step (25), giving rise to a $> {}^{18}\text{OH}_{br}^-$ bridging hydroxyl, the release of a proton and the appearance of a fivefold-coordinated terminal Ti_t^{4+} ion which is further electro-reduced with a CB free electron in step (27). Finally, as in step (22), in step (28) a new ^{16}O$_2$(g) molecule from the gas phase is adsorbed as a $\text{Ti}_f^{4+} - {}^{16}\text{O}^{2-}$ oxygen ion with the intervention of a CB free electron, $\frac{1}{2}{}^{16}$O$_2$(g) being again liberated from the TiO$_2$ surface. The global reaction, resuming steps (18) to (28), is represented by Equation (29):

$$2\text{Ti}_t^{4+} + 2\big(>^{16}\text{O}_{br}^{2-}\big) + 2\text{H}_2^{18}\text{O} + {}^{16}\text{O}_2(\text{g})$$
$$\xrightarrow{4h\nu} 2\big(\text{Ti}_t^{4+} - {}^{16}\text{OH}^-\big) + >{}^{16}\text{OH}_{br}^- + >{}^{18}\text{OH}_{br}^- + {}^{16,18}\text{O}_2^\uparrow(\text{g}) \tag{29}$$
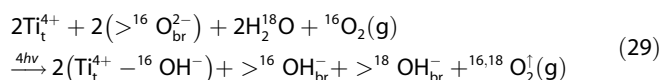
Summing up, four UV photons are needed to generate one ^{16,18}O$_2$(g) species from two ^{18}OH$_2$ surface-bonded water molecules and one ^{16}O$_2$(g) molecule, with the participation of two bridging oxygen ions and two Ti_t^{4+} ions, as well as the photogeneration of two bridging oxygen vacancies, where water molecules are dissociatively adsorbed as a prerequisite of their further photo-oxidation.[28–30] The limiting step for the global reaction, materialized by ^{16,18}O$_2$(g) evolution, should be step (24), where a ^{16,18}O$_2$H$_{br}$ hydro-peroxide group at a bridging position is generated as a precursor of the further evolved ^{16,18}O$_2$(g) molecule.

With respect to the small amount of ^{18}O$_2$(g) detected by Muggli and Falconer[17] (see Figure 4), it may be the result of a POIE mechanism between ^{16}O atoms of ^{16,18}O$_2$ molecules, generated according to Equation (29), and ^{18}O ad-atoms of adsorbed ^{18}OH$_2$ water molecules, according to the following global reaction [Eq. (30)]:

$$2Ti_t^{4+} + 2\left(>^{16}O_{br}^{2-}\right) + 2H_2^{18}O + {}^{16,18}O_2(g)$$
$$\xrightarrow{4h\nu} 2(Ti_t^{4+} - {}^{16}OH^-) + >^{16}OH_{br}^- + >^{18}OH_{br}^- + {}^{18}O_2^{\uparrow}(g) \tag{30}$$

5. POIE in Competition with PO of Organic Species

It has been experimentally confirmed that POIE between oxygen atoms of O_2 gas-phase molecules and oxygen atoms from either the TiO_2 surface or adsorbed water molecules is hindered in the presence of RH_2 organic species prone to be photo-oxidized.[8,17,18] The following explanation can be formulated on the basis of the recently developed Direct-Indirect (D-I) kinetic model for the photo-oxidation of RH_2 species.[31–33]

As shown schematically in Figure 5, for strong electronic interaction of Ti_t^{4+} ions with RH_2 species (specific adsorption), as it is the case for formic acid,[32] RH_2 photo-oxidation mainly
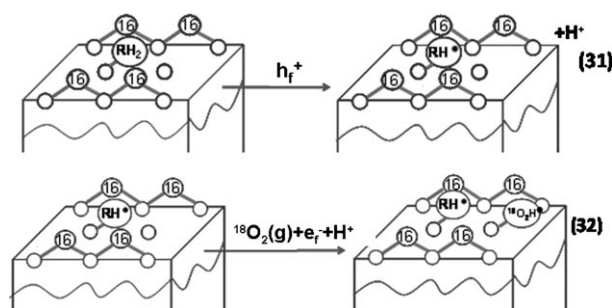

Figure 5. Proposed mechanism for the photo-oxidation of $RH_2(g)$ species specifically adsorbed onto terminal Ti^{4+} ions at the TiO_2–gas interface in competition with POIE between oxygen atoms of $^{18}O_2(g)$ and terminal $>{}^{16}O_{br}^{2-}$ ions. Large white circle: bridging oxygen ion; large grey circle: bridging oxygen radical; small white circle: Ti^{4+} ion; small grey circle Ti^{3+} ion.

takes place via an interfacial direct transfer (DT) mechanism involving inelastic trapping of photogenerated VB free holes by specifically adsorbed RH_2 species, with generation of $RH^\bullet$ radicals and proton liberation [Eq. (31)]:

$$Ti_t^{4+} - RH_2 \xrightarrow{+h_f^+} Ti_t^{4+} - RH^\bullet + H^+ \tag{31}$$
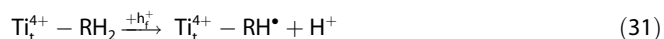
In a second step, oxygen from the gas phase is electro-reduced with CB free electrons, giving rise to adsorbed $^{18}O_2^{\bullet-}$ superoxide radicals that further react with the proton liberated according to Equation (31) to generate hydroperoxide groups chemisorbed on terminal Ti_t^{4+} cations [Eq. (32)]:

$$Ti_t^{4+} + H^+ + {}^{18}O_2(g) \xrightarrow{+e_f^-} Ti_t^{4+} - {}^{18}O_2H^\bullet \tag{32}$$

On the other hand, as schematized in Figure 6, for the case of weak electronic interactions of Ti_t^{4+} ions with RH_2 species (as it is probably the case for phenol[33] and methanol[34] in the presence of water), the D-I model predicts that RH_2 photo-oxidation is the result of a mixture of a DT mechanism, as for the
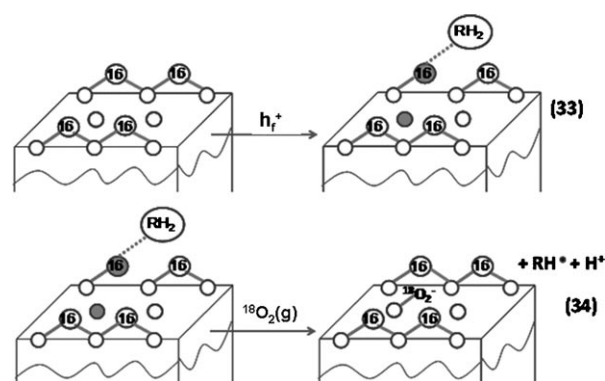

Figure 6. Proposed TiO_2–gas interface mechanism for the photo-oxidation of $RH_2(g)$ species weakly interacting with bridging oxygen ions in competition with POIE between oxygen atoms of $^{18}O_2(g)$ and terminal $>{}^{16}O_{br}^{2-}$ ions. Large white circle: bridging oxygen ion; large grey circle: bridging oxygen radical; small white circle: Ti^{4+} ion; small grey circle: Ti^{3+} ion.

case of formic acid, and an indirect transfer (IT) mechanism involving inelastic trapping of photogenerated VB free holes by bridging oxygen ions, with generation of bridging oxygen radicals, $^{16}O_{br}^{\bullet-}$ (surface-trapped holes) [Eq. (33)]:

$$>{}^{16}O_{br}^{2-}...RH_2 + Ti_t^{4+} \xrightarrow{h_f^+} -{}^{16}O_{br}^{\bullet-}...RH_2 + Ti_t^{4+} \tag{33}$$
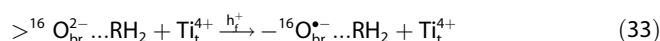
Further adiabatic transfer of the surface-trapped holes to RH_2 molecules leads to the generation of $RH^\bullet$ radicals and proton liberation [Eq. (34)]:

$$-{}^{16}O_{br}^{\bullet-}...RH_2 \xrightarrow{IT} >{}^{16}O_{br}^{2-} + RH^\bullet + H^+ \tag{34}$$
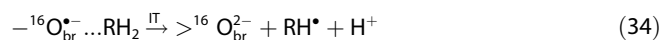
Simultaneously, gas-phase oxygen can be reduced by photogenerated electrons trapped at surface Ti^{4+} sites, giving rise to Ti^{3+} ions [Eq. (35)]:

$$Ti_t^{3+} + {}^{18}O_2(g) \rightarrow +Ti_f^{4+} - {}^{18}O_2^{\bullet-} \tag{35}$$

the global PO reaction being [Eq. (36)]:

$$>{}^{16}O_{br}^{2-}...RH_2 + Ti_t^{4+} + {}^{18}O_2(g)$$
$$\xrightarrow{+h\nu} >{}^{16}O_{br}^{2-} + Ti_t^{4+} - {}^{18}O_2^- + RH^\bullet + H^+ \tag{36}$$
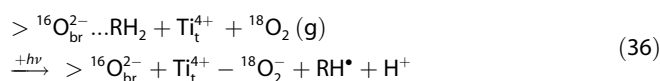
As far as we know, the only experimental data existing in the literature about competition between POIE and PO reactions at TiO_2 surfaces concerns the photo-oxidation of hydrocarbons (isobutane[8] and ethane[12]), ethanol[17] and methanol.[18] While hydrocarbons are expected to scarcely interact with the TiO_2 surface, the interaction of methanol is double, on the one hand through a chemical bond between fivefold-coordinated terminal titanium cations (Ti_t^{4+}) and oxygen anions of the alcohol group, on the other hand through a weak hydrogen bonding with bridging oxygen ions. Further, it is known that water efficiently competes with methanol for adsorption at Ti_t^{4+} sites.[34] Summing up, photo-oxidation of isobutane and ethane is expected to take place exclusively via an IT mechanism, as schematized in Figure 6, while methanol should be

photo-oxidized via a mixture of IT and DT, in competition with the POIE mechanism represented by Equation (11), where $-^{16}O_{br}^{\bullet-}$ bridging oxygen radicals are active surface species.

The fact that POIE is canceled in the presence of physisorbed RH$_2$ species indicates that the rate of reaction (11) must be far lower than the rate of reaction (34). By analogy, in the hypothetical case that POIE would be inhibited in the presence of specifically adsorbed RH$_2$ species, the conclusion to be reached according to the mechanistic scheme of Figure 5 is that the rate of reaction (31) should be far greater than the rate of reaction (11).

5. Conclusions

POIE processes and their competition with the photo-oxidation of RH$_2$ substrate species at the gas–TiO$_2$ interface have been rationalized by invoking the participation of twofold-coordinated bridging oxygen ions as natural surface traps for photogenerated VB free holes, and bridging oxygen radicals as photogenerated surface species active in both POIE and PO reactions. A mechanistic analysis of POIE, both in the presence and absence of adsorbed water, has been developed in terms of the reaction of $>^{16}O_{br}^{2-}$ bridging oxygen ions of the TiO$_2$ surface and oxygen atoms of $^{18}O_2^{\bullet-}$ superoxide species photogenerated by electro-reduction of gas-phase $^{18}O_2(g)$ molecules with free CB electrons. The participation of photoinduced bridging oxygen vacancies as intermediates in the incorporation of water molecules at bridging oxygen sites has also been analyzed on the basis of the D–I kinetic model recently developed in substitution of the classical "Langmuir–Hinshelwood" (L–H) model for heterogeneous photocatalysis.

Glossary of Species Involved in POIE and PO Mechanisms

h_f^+: photogenerated valence band free hole.

e_f^-: photogenerated conduction band free electron.

O_s^{2-}: in general, terminal surface oxygen ion.

$O_s^{\bullet-}$: in general, surface oxygen radical.

$>O_{br}^{2-}$: twofold-coordinated bridging oxygen ion.

$-O_{br}^{\bullet-}$: onefold-coordinated bridging oxygen radical.

$O_2(g)$: gas-phase oxygen molecule.

$-O_2^-$: chemisorbed, onefold-coordinated superoxide ion.

$V[>^{16}O_{br}^{2-}]$: bridging oxygen vacancy.

$O_2^{\uparrow}$: evolved oxygen molecule.

$>OH_{br}^-$: twofold-coordinated bridging hydroxyl ion.

$-OH_{br}^{\bullet}$: onefold-coordinated bridging hydroxyl radical.

$(OH_2)_{ads}$: water molecule adsorbed at a terminal Ti ion.

$OH_{ads}^{\bullet}$: hydroxyl radical adsorbed at a terminal Ti ion.

$-O_2H^{\bullet}$: chemisorbed, onefold-coordinated hydroperoxide radical.

RH$_2$: gas-phase organic molecule liable to be photo-oxidized.

RH$^{\bullet}$: oxidized, gas-phase organic radical.

[1] S. N. Frank, A. J. Bard, *J. Am. Chem. Soc.* **1977**, *99*, 303–304.
[2] S. N. Frank, A. J. Bard, *J. Phys. Chem.* **1977**, *81*, 1484–1488.
[3] J. Peral, X. Domenech, D. F. Ollis, *J. Chem. Technol. Biotechnol.* **1997**, *70*, 117–140.
[4] A. Fujishima, K. Hashimoto, T. Watanabe, *TiO₂ Photocatalysis: Fundamentals and Applications*, BKC Inc., Tokio, **1999**.
[5] P. Pichat, J. Disdier, C. Hoang-Van, D. Mas, G. Goutaillier, C. Gaysse, *Catal. Today* **2000**, *63*, 363–369.
[6] M. Formenti, H. Courbon, F. Juillet, A. Lissatchenko, J. R. Martin, P. Meriandeau, S. J. Teichner, *J. Vacuum. Sci. Technol.* **1972**, *9*, 947–952.
[7] K. Tanaka, *J. Phys. Chem.* **1974**, *78*, 555–556.
[8] H. Courbon, M. Formenti, P. Pichat, *J. Phys. Chem.* **1977**, *81*, 550–554.
[9] H. Courbon, P. Pichat, *Compt. Rend. Acad. Sci. Paris* **1977**, *285*, 171–174.
[10] J. Cunningham, E. L. Goold, J. L. Garcia Fierro, *J. Chem. Soc. Faraday Trans. 1* **1982**, *75*, 785–801.
[11] J. Cunningham, E. L. Goold, E. M. Leahy, *J. Chem. Soc. Faraday Trans. I* **1979**, *75*, 305–313.
[12] S. Sato, T. Kadowaki, K. Yamaguti, *Chem. Phys.* **1984**, *88*, 2930–2931.
[13] S. Sato, *J. Phys. Chem.* **1987**, *91*, 2895–2897.
[14] Y. Yanagisawa, Y. Ota, *Surf. Sci.* **1991**, *254*, L433L436.
[15] L. F. Liao, C. F. Lien, D. L. Shich, M. T. Chen, J. L. Lin, *J. Phys. Chem. B* **2002**, *106*, 11240–11245.
[16] T. L. Thompson, O. Diwald, J. T. Yates Jr, *Chem. Phys. Lett.* **2004**, *393*, 28–30.
[17] D. S. Muggli, J. L. Falconer, *J. Catal.* **1999**, *181*, 155–159.
[18] P. Pichat, H. Courbon, R. Enriquez, T. Y. Tan, R. Amal, *Res. Chem. Intermed.* **2007**, *33*, 239–250.
[19] A. J. Tench, T. Lawson, *Chem. Phys. Lett.* **1970**, *7*, 459–460.
[20] N. B. Wong, J. H. Lundsford, *J. Chem. Phys.* **1972**, *56*, 2664–2667.
[21] P. Salvador, *J. Phys. Chem. C* **2007**, *111*, 17038–17043.
[22] A. Imanishi, T. Okamura, N. Ohashi, R. Nakamura, Y. Nakato, *J. Am. Chem. Soc.* **2007**, *129*, 11569–11578.
[23] E. Puzenat, P. Pichat, *J. Photochem. Photobiol. A* **2003**, *160*, 127–133.
[24] A. Lisachenko, *J. Photochem. Photobiol. A* **2008**, *196*, 127–137.
[25] M. A. Henderson, W. S. Epling, Ch. H. F. Peden, C. L. Perkins, *J. Phys. Chem. B* **2003**, *107*, 534–545.
[26] Y. Du, N. A. Deskins, Z. Zhang, Z. Dohnalek, M. Dupuis, I. Lyubinetsky, *Phys. Rev. Lett.* **2009**, *102*, 096102/1–4.
[27] S. Mezhenny, P. Maksymovich, T. L. Thompson, O. Diwald, D. Stahal, S. D. Walk, J. T. Yates Jr, *Chem. Phys. Lett.* **2003**, *369*, 152–158.
[28] R. Schaub, P. Thostrup, N. Lopez, E. Laegsgaard, I. Stensgaard, J. K. Nørskov, F. Besenbacher, *Phys. Rev. Lett.* **2001**, *87*, 266104/1–4.
[29] I. M. Brookes, C. A. Muryn, G. Thornton, *Phys. Rev. Lett.* **2001**, *87*, 266103/1–4.
[30] S. Wendt, J. Matthiensen, R. Schaub, E. K. Vestergaard, E. Laegsgaard, F. Besenbacher, B. Hammer, *Phys. Rev. Lett.* **2006**, *96*, 066107/1–4.
[31] T. Lana Villarreal, R. Gomez, M. Gonzalez, P. Salvador, *J. Phys. Chem. B* **2004**, *108*, 20278–20290.
[32] D. Monllor Satoca, R. Gomez, M. Gonzalez, P. Salvador, *Catal. Today* **2007**, *129*, 247–255.
[33] J. F. Montoya, J. Velasquez, P. Salvador, *Appl. Catal. B* **2009**, *88*, 50–58.
[34] T. Lana Villarreal, R. Gomez, M. Neuman Spallart, N. Alonso Vante, P. Salvador, *J. Phys. Chem. B* **2004**, *108*, 15172–15181.

Publication 4

"Catalytic Role of Surface Oxygens in TiO_2 Photooxidation Reactions: Aqueous Benzene Photooxidation with $Ti^{18}O_2$ under Anaerobic Conditions". *J. Phys. Chem. Lett.* **2013,** *4* (9), 1415-1422.

Catalytic Role of Surface Oxygens in TiO_2 Photooxidation Reactions: Aqueous Benzene Photooxidation with $Ti^{18}O_2$ under Anaerobic Conditions

Juan Felipe Montoya,[†] Irina Ivanova,[‡] Ralf Dillert,[‡] Detlef W. Bahnemann,[‡] Pedro Salvador,[†] and José Peral*,[†]

[†]Departamento de Química, Universidad Autónoma de Barcelona, 08193 Cerdanyola del Vallés, Spain
[‡]Institut für Technische Chemie, Leibniz Universität Hannover, Callinstrasse 3, D-30167 Hannover, Germany

S *Supporting Information*

ABSTRACT: The important role played in TiO_2 heterogeneous photocatalysis by the two-fold-coordinated TiO_2 surface bridging oxygens ($>O_s^{2-}$ or $>OH_s^-$) has been emphasized. Their ability to trap photogenerated holes and to act as main oxidizing agents, leaving the surface of the catalyst and being part of the intermediates and final reaction products, is probed by using isotopic labeling reactions. In particular, we have studied the aqueous photocatalytic mineralization of benzene in anaerobic conditions using $Ti^{18}O_2$ as the photocatalyst. The reaction evolution has been followed by analysis of the concentration and the isotopic composition of CO_2, the final product of benzene photooxidation. The unique features of this experimental system provide the opportunity for in situ tracing of the fate of $>O_s^{2-}$ or $>OH_s^-$ species during the photocatalytic reaction. Experimental evidence shows that those oxygen atoms are incorporated into CO_2. Participation of surface-trapped holes ($-OH_s^\bullet/-O_s^{\bullet-}$) and the incorporation of surface oxygens into the oxidation products prove the main role played by those species in TiO_2-assisted photocatalytic processes.
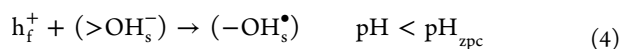
SECTION: Surfaces, Interfaces, Porous Materials, and Catalysis
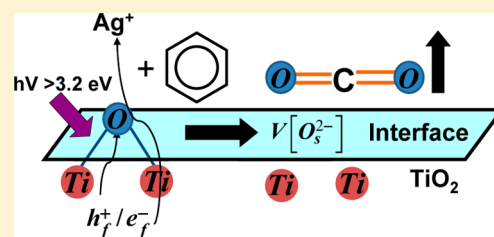
T iO_2 photocatalytic oxidation (PO) of organic molecules has been extensively studied over the last 3 decades.[1−6] Despite this interest, detailed mechanisms of the primary events involved in the PO processes are far from clear, as pointed out in some recent reviews.[5−8] It is generally accepted that TiO_2 excitation with energy larger than the band gap generates electron/hole pairs (eq 1) that can either recombine or photoinduce redox processes.

$$TiO_2 \xrightarrow{h\nu \geq 3.2 \text{ eV}} h_f^+ + e_f^- \qquad (1)$$

The oxidation reactions are initiated by free holes (h_f^+) that are either directly scavenged by chemisorbed organic compounds (eq 2) or trapped by TiO_2 surface lattice oxygen ions, either protonated ($>OH_s^-$) or deprotonated ($>O_s^{2-}$), to generate surface lattice radicals ($-OH_s^\bullet/-O_s^{\bullet-}$) depending on the experimental pH (eqs 3 and 4).[9−11]

$$h_f^+ + (RH_2)_{ads} \rightarrow RH^\bullet + H^+ \qquad (2)$$

$$h_f^+ + (>O_s^{2-}) \rightarrow (-O_s^{\bullet-}) \qquad pH > pH_{zpc} \qquad (3)$$

$$h_f^+ + (>OH_s^-) \rightarrow (-OH_s^\bullet) \qquad pH < pH_{zpc} \qquad (4)$$
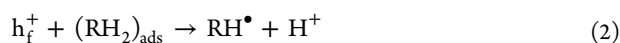
The radical species ($-OH_s^\bullet/-O_s^{\bullet-}$) generated in eqs 3 and 4 can accept an electron from a dissolved organic molecule, producing an organic radical (eq 5)

$$[RH_2]_{aq} + (-OH_s^\bullet/-O_s^{\bullet-}) \rightarrow RH^\bullet + H^+ $$
$$+ (>OH_s^-/>O_s^{2-}) \qquad (5)$$
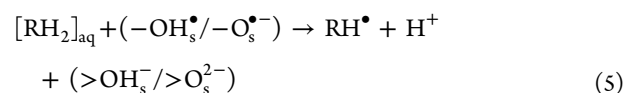
The further oxidation of the organic radicals ($RH^\bullet$) leads in some cases to the production of hydroxylated intermediates ($RH-OH$), which are the first oxidation products of aromatic compounds.[7,12−17] Because the oxygen atom of the $-OH_s^\bullet/-O_s^{\bullet-}$ radical species belongs to the TiO_2 lattice, there is the possibility of incorporation of those oxygens into the reaction products. In fact, this kind of incorporation is well-documented for several photooxidation reactions of organic molecules at the TiO_2 surface carried out under ultrahigh vacuum (UHV) conditions.[6] Furthermore, several studies of photoinduced oxygen isotope exchange between TiO_2 and molecular oxygen (O_2) have demonstrated the reactivity of TiO_2 surface lattice oxygens (O_s) and their ability to be removed from the TiO_2 lattice and to be replaced by gas-phase oxygen atoms under UV illumination.[18−20] It is worth noting that this set of evidence has been obtained for TiO_2 samples under UHV or in the gas phase. However, there are not systematic studies about the reactivity and exchange of O_s during aqueous photocatalytic oxidation reactions, one of the most commonly studied

systems. The use of water as a solvent adds complexity to the unraveling of the reaction mechanisms of heterogeneous photocatalysis because it brings another possible source of oxygen to the scene[14−17] and makes difficult the tracking of the fate of O_s. Two reaction pathways are commonly invoked to explain the generation of hydroxylated intermediates, with the added oxygen atoms coming from water or from O_2 in aqueous solution,[14−17] (1) oxidation of adsorbed water species, either in molecular (H_2O) or dissociated ($OH^−$) form, by photo-generated valence band free holes (h_f^+) according to eq 6.[1−4,21]

$$h_f^+ + (-OH_t^-)_{ads}/(H_2O)_{ads} \rightarrow (OH^\bullet)_{ads}/(OH^\bullet)_{ads} + H^+ \tag{6}$$
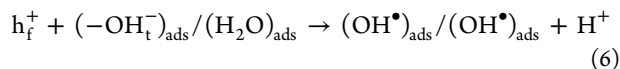
or (2) reduction of molecular oxygen (O_2) by photogenerated conduction band free electrons (e_f^-), leading to the generation of free $OH^\bullet$ radicals, through a multistep reaction involving H_2O_2 as the intermediate species.[16] Besides those two pathways, the oxidation reaction of nonadsorbed water with h_f^+ has been invoked as a possible source of free $OH^\bullet$ radicals.[21] However, electron paramagnetic resonance (EPR) studies of TiO_2 aqueous dispersions have demonstrated that the signal of radical species produced under excitation of the TiO_2 is attributable only to surface radical species $-OH_s^\bullet/-O_s^{\bullet-}$ produced according to eqs 3 or 4.[9−11] Moreover, even if free $OH^\bullet$ radicals are produced from the oxidation of nonadsorbed water molecules, they quickly trap an electron from TiO_2, generating a surface-trapped hole, as has been demonstrated by pulse radiolysis studies on colloidal suspensions of TiO_2.[22,23]

In conclusion, the reaction mechanisms of heterogeneous PO based on TiO_2 in the aqueous phase are hard to study because at least three sources of oxygen exist, the solid surface, the solvent, and the gas-phase oxygen. Recently, isotopic tracing methods have been used to elucidate the oxygen source of hydroxylated products and carbon dioxide (CO_2) evolved during the PO of several aliphatic[24] and aromatic compounds.[14−17] The ratio of oxygen atoms to the reaction products originating from water or O_2 has been experimentally measured by carrying out PO reactions in isotopically labeled water ($H_2^{18}O$) or isotopically labeled oxygen ($^{18}O_2$). Because, in both cases, labeled oxygen was detected in intermediate and final reaction products, several interpretations have been given to the experimental facts. Indeed, the incorporation of labeled oxygen atoms from O_2 into oxidation products has been explained on the basis of photooxidation mechanisms involving either the reaction of the organic radicals ($RH^\bullet$) produced according to eq 2 with O_2-related species (O_2 or $O_2^{\bullet-}$)[15] or by reaction of the organic substrate (RH_2) with free $OH^\bullet$ radicals that originated from O_2 photoelectroreduction.[14,16] On the other hand, two independent mechanistic pathways have been proposed in order to explain the incorporation of labeled O atoms from H_2O into photooxidation products,[14−17,24] (1) reaction of the organic substrate (RH_2) with adsorbed hydroxyl radicals ($OH^\bullet)_{ads}$ produced according to eq 6 and (2) reaction of organic $RH^\bullet$ radicals, generated according to eq 2, with water molecules to produce hydroxylated compounds as reaction intermediates. This multiplicity of mechanisms invoked to explain labeled O atom incorporation into the oxidation products again evinces the complexity of photocatalytic systems.

Although these recent isotopic tracing studies have shed light onto photocatalytic reaction mechanisms, some aspects are still unclear. For instance, the incorporation of TiO_2 surface bridging oxygen ions ($>O_s^{2-}$) into photooxidation products is still an issue that can not be disclosed by the use of $H_2^{18}O$ and/or $^{18}O_2$ isotope-labeled molecules. Moreover, the most recent isotopic tracing studies[14−17,24] disregard the participation of reactions 3 and 4 in the photocatalytic mechanisms, as well as the incorporation of TiO_2 surface lattice oxygen ions ($>O_s^{2-}$ or OH_s^-) into photogenerated products. Furthermore, the incorporation of O atoms from H_2O into photooxidation products has been frequently explained by invoking the generation of ($OH^\bullet)_{ads}$ radicals according to reaction 6, omitting the recently reported data about the thermodynamic and kinetic constraints that make this reaction unlikely.[25,26] The above-mentioned concerns encouraged us to propose an alternative mechanistic pathway that explicitly invokes the participation of the $-OH_s^\bullet/-O_s^{\bullet-}$ radical species generated through reactions 3 and 4.[27]

In order to experimentally test this possible mechanistic pathway, we have developed an alternative strategy. The use of oxygen-isotope-labeled titania[28−31] ($Ti^{18}O_2$) as the photocatalyst for the oxidation of organic compounds and the tracking of the oxygen isotope (^{18}O) incorporated into the oxidation products can be used to elucidate the mechanistic issues just mentioned. Here, we report an isotopic tracing study of CO_2 evolution from benzene photocatalytic oxidation using $Ti^{18}O_2$ as the photocatalyst.

$Ti^{18}O_2$ nanoparticles were prepared following the synthesis method reported by Kavan et al.[28] with some modifications in the hydrolysis of $TiCl_4$. Also, $Ti^{16}O_2$ nanoparticles were synthesized as the reference photocatalyst using the same procedure (details of the synthesis can be found in The Supporting Information).

Both materials were characterized by Raman spectroscopy (RS) and X-ray diffraction (XRD). The spectra of both materials are shown in Figure 1.

The RS of $Ti^{18}O_2$ (Figure 1A) shows peaks at 145, 191, 400, 494, and 610 cm^{-1} that are assigned to the Raman vibrations modes $E_g(1)$, $E_g(2)$, $B_{1g}(1)$, $B_{1g}(2) + A_{1g}$, and $E_g(3)$, respectively.[28,31] The reference material ($Ti^{16}O_2$) exhibits the same peaks, but the frequencies of the vibration modes $E_g(2)$, $B_{1g}(2) + A_{1g}$, and $E_g(3)$ are blue-shifted by 11, 28, and 35 cm^{-1}, respectively. These shifts are in agreement with those recently reported by Kavan et al.[28,31] for isotope-labeled titania with an ^{18}O purity of 97%. The XRD spectra (Figure 1B) of both samples exhibit major peaks at 25.4, 37.8, 48.1, 53.8, and 62.7° that are consistent with the (101), (004), (200), (211), and (213) planes of tetragonal anatase. These assignments are in good agreement with the JCPDS-ICDD standards for anatase (No. 21-1272). The isotopically labeled material ($Ti^{18}O_2$) showed two additional peaks at 27.4 and 36.2° that correspond to the (110) and (101) planes of tetragonal rutile (JCPDS-ICDD standard No. 21-1276). The estimated weight fraction of each crystalline phase was 72.5% for anatase and 27.5% for rutile, calculated according to the method reported by Spurr and Myers.[32] The average crystal size of $Ti^{18}O_2$ was estimated to be 24 nm for anatase and 80 nm for rutile by applying the Scherrer formula on the (101) anatase and (110) rutile diffraction peaks, respectively. With respect to the reference material ($Ti^{16}O_2$), an average crystal size of 19 nm ($2\theta = 25.4°$, (101)) for anatase was estimated, the only crystalline phase detected in that case. Transmission electron microscopy (TEM) micrographs confirm the above-reported features (see the Supporting Information). The specific surface area (S_g), determined from BET nitrogen adsorption isotherms was 32.1 and 52.7 m^2/g for $Ti^{18}O_2$ and $Ti^{16}O_2$, respectively.
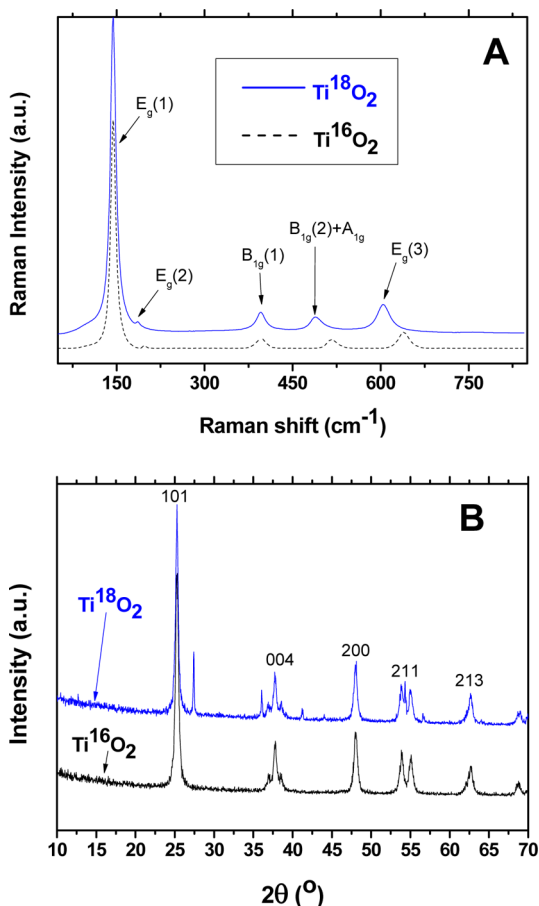
Figure 1. (A) Raman spectra of the synthesized $Ti^{16}O_2$ (black) and $Ti^{18}O_2$ (blue) powders. The excitation line was provided by an Ar^+ laser at 532 nm. The laser power was 2 mW. (B) XRD spectra of the synthesized $Ti^{16}O_2$ (black) and $Ti^{18}O_2$ (blue) powders. In both panels, spectra are separated for clarity, but the intensity scale is the same for both samples.

Because our main objective is to trace the incorporation of ^{18}O from $Ti^{18}O_2$ into the evolved CO_2, a plausible surface isotopic composition of the synthesized $Ti^{18}O_2$ nanoparticles is necessary. It is well-documented that the TiO_2 surface has two kind of hydroxyl groups,[6,21,33−38] bridging hydroxyls ($-OH_t^-$) one-fold-coordinated to Ti^{4+} ions and those two-fold-coordinated hydroxyl ions ($>OH_s^-$) resulting from the protonation of two-fold-coordinated terminal oxygen ions ($>O_s^{2-}$). Therefore, oxygen atoms of $-OH_t^-$ species come from water molecules chemisorbed at the TiO_2 surface, while the oxygen of the $>OH_s^-$ belongs to the TiO_2 lattice. Besides, according to eq 6, hole trapping by water species adsorbed at terminal Ti atoms gives rise to adsorbed hydroxyl radicals, commonly known as $(-OH_t^\bullet)_{ads}$; in contrast, according to eqs 3 and 4, hole trapping by terminal $>OH_s^-$ ions gives rise to surface hydroxyl radicals ($-OH_s^{\bullet-}$). Several studies[35−37] demonstrated that $(-OH_t^-)_{ads}$ groups can be totally removed from the TiO_2 surface by heating up to 623 K, while $>OH_s^-$ groups are stable up to 773 K.[36,39] Therefore, it can be assumed that during the calcination process at 623 K, $>OH_s^-$ groups are not removed from the TiO_2 surface, and their ^{18}O isotopic composition must be the same as that in the bulk (97% purity of ^{18}O). In order to eliminate possible traces of $H_2^{18}O$ that may remain in the synthesis vessel and rehydrate the $Ti^{18}O_2$ surface producing terminal $-^{18}OH_t^-$ ions, the $Ti^{18}O_2$ powder was

washed with $H_2^{16}O$, as it is well-known that oxygen exchange between the $-OH_t^-$ species and water occurs in a quantitative and fast way in the dark at room temperature, while $>OH_s^-$ species are not exchanged under those conditions.[40] Therefore, the surface of the synthesized $Ti^{18}O_2$ can be assumed to be hydroxylated with both labeled two-fold-coordinated surface hydroxyl groups ($>^{18}OH_s^-$) and unlabeled one-fold-coordinated adsorbed hydroxyl groups ($-^{16}OH_t^-$), as illustrated in Scheme 1.

Scheme 1. Representation of the $Ti^{18}O_2$ Hydroxylated Surface[a]
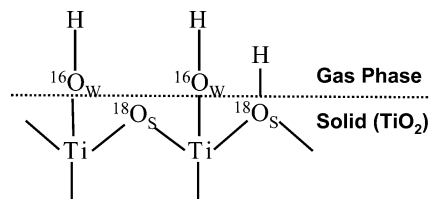
[a]Note that the oxygen of unlabeled adsorbed hydroxyls ($^{16}O_WH$) belongs to chemisorbed water while the oxygen of labeled surface hydroxyls ($^{18}O_sH$) belongs to the TiO_2 lattice.

This isotopic labeling of the $Ti^{18}O_2$ surface hydroxyl groups and the tracking and quantification of the isotopic composition of photooxidation products will allow us to emphasize the importance that reactions 3 and 4 (involving ($>O_s^{2-}$ or $>OH_s^-$)) may have among the possible first steps of the photocatalytic oxidation mechanism.

Benzene has been chosen as a model compound in isotopic tracing studies,[15,16] emphasizing the important role played by O_2 in benzene photooxidation. Because our objective is to distinguish between reaction pathways expressed by eq 6 (involving H_2O) and eq 5 (involving TiO_2 terminal oxygen ions), it is desirable to study PO reactions in the absence of dissolved O_2 in order to suppress the O_2-derived reaction pathways. Several studies have reported benzene photo-oxidation in deoxygenated systems by using either platinum[12] or silver ions[13] (Ag^+) as electron acceptors. It is well-known that Ag^+ species react with e_f^-, leading to the formation and growth of silver nanoparticles on the TiO_2 surface that, in turn, act as a "sink" of new photogenerated conduction band electrons.[41] Therefore, Ag^+ is a suitable electron acceptor for photocatalytic studies in the absence of dissolved O_2.

The photocatalytic anaerobic mineralization of benzene in an argon (Ar)-purged system can be represented by the global reaction depicted in Scheme 2. Note that this reaction can be carried out using as the catalyst $Ti^{18}O_2$ or $Ti^{16}O_2$, and the produced carbon dioxide can be oxygen-isotope-labeled ($C^{16}O^{18}O$) or unlabeled ($C^{16}O_2$). Our objective here is to

Scheme 2. Photocatalytic Anaerobic Mineralization of Benzene[a]
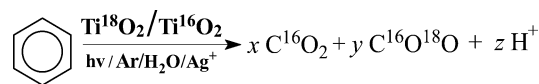
[a]Note that reaction can be carried out using $Ti^{18}O_2$ or $Ti^{16}O_2$ as the photocatalyst, and the main products are labeled ($C^{16}O^{18}O$) or unlabeled ($C^{16}O_2$) carbon dioxide.

study this reaction using both catalysts and tracking both products for each reaction.

Figure 2A and B shows the time evolution of the QMS signals of $C^{16}O_2$ ($m/z = 44$) and $C^{16}O^{18}O$ ($m/z = 46$)

Figure 2. Time evolution of the QMS signal from the $C^{16}O^{18}O$ ($m/z = 46$) and $C^{16}O_2$ ($m/z = 44$) isotopologues of carbon dioxide produced during photocatalytic anaerobic mineralization of benzene with (A) $Ti^{16}O_2$ and (B) $Ti^{18}O_2$. Experimental conditions for both panels are $V_{H_2^{16}O} = 50$ mL, $[AgBF_4]_0 = 10$ mM, $V_{BZ} = 100$ μL, and catalyst load = 50 mg. All experiments were carried out under Ar flow (5 mL/min). Average sampling time interval = 1.04 min.
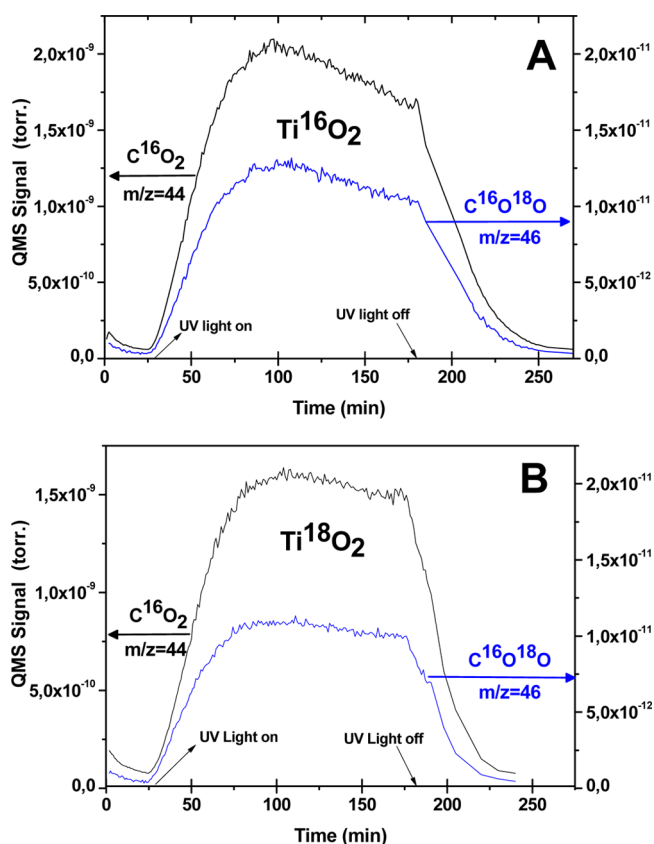
produced from photocatalytic anaerobic mineralization of benzene by using $Ti^{16}O_2$ and $Ti^{18}O_2$ as the photocatalysts, respectively.

No data for $C^{18}O_2$ has been reported because the QMS signal for this species is within the experimental error (around 10^{-13} Torr). As can be seen in the figures, the general behavior is very similar in both experiments. After turning on the UV light ($t = 26$ min), there is a fast production of CO_2 with a steady-state rate being apparently reached after 90 min of illumination. When light is turned off at about 176 min, both CO_2 signals are observed to decay to the background level. The $C^{16}O^{18}O$ detected when using $Ti^{16}O_2$ is due to the natural presence of small amounts of ^{18}O in the water and, consequently, in the synthesized $Ti^{16}O_2$. Attention should be paid to the fact that both signals have an intensity difference of 2 orders of magnitude. The values of the QMS signal of $C^{16}O_2$ are slightly higher in Figure 2A than those in Figure 2B, which is evidence that the reference material ($Ti^{16}O_2$) has a higher photocatalytic activity, something expected because of the higher surface area of $Ti^{16}O_2$ with respect to the labeled $Ti^{18}O_2$ catalyst. By performing a calibration with a standard gas mixture

(1.01% of $C^{16}O_2$ in Ar) under identical experimental conditions, the QMS signal value of $C^{16}O_2$ can be converted into the flow rate (in μmol/h) of the evolved $C^{16}O_2$ gas (see Figure S1, Supporting Information). Note that after a reaction time of 85 min, a steady-state rate of CO_2 production (γ_{CO_2}) of 17.2 and 22.8 μmol/h for $Ti^{18}O_2$ and $Ti^{16}O_2$ was respectively reached.

It is remarkable that the dynamic profile of the $C^{16}O_2$ and $C^{16}O^{18}O$ QMS signals appears to be very similar for the experiments reported in Figure 2A and B, respectively corresponding to $Ti^{16}O_2$ and $Ti^{18}O_2$ samples. Moreover, the production of $C^{16}O^{18}O$ within the first 75 min is practically the same for both samples, suggesting that the $C^{16}O^{18}O/C^{16}O_2$ ratio is higher for $Ti^{18}O_2$ than that for $Ti^{16}O_2$. In order to analyze this fact in detail, the time course of the $C^{16}O^{18}O/C^{16}O_2$ ratio corresponding to experiments of Figure 2A and B is shown in Figure 3.
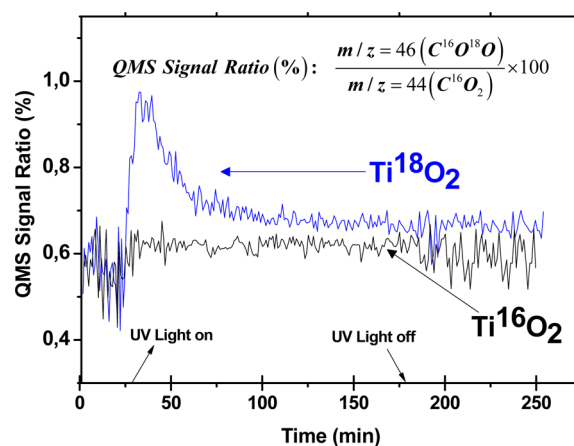
Figure 3. Time evolution of the $C^{16}O^{18}O/C^{16}O_2$ QMS signal ratio from benzene photooxidation experiments reported in Figure 2A and B.

As can be seen, the $C^{16}O^{18}O/C^{16}O_2$ ratio for $Ti^{16}O_2$ experiments of Figure 2A has an average, constant value of about 0.62%, with small fluctuations of around ±0.03% attributable to the instrumental noise. This is in fact a predictable behavior because the amount of $C^{16}O^{18}O$ produced with $Ti^{16}O_2$ should be in agreement with the natural abundance of the $C^{16}O^{18}O$ isotopologue of the carbon dioxide molecule (0.62%). In contrast, the $C^{16}O^{18}O/C^{16}O_2$ ratio obtained from Figure 2B increases rapidly up to 0.97% immediately after the UV light is turned on, remaining constant for about 8 min and then asymptotically decreasing up to 0.62%, the natural isotopic ratio observed for $Ti^{16}O_2$. It is worth noting that after illumination for about 85 min, the signal ratio almost reaches a constant value of about 0.66%. This behavior of the $C^{16}O^{18}O/C^{16}O_2$ ratio indicates that in the experiment with $Ti^{18}O_2$, there is a clear ^{18}O isotopic enrichment of the photoevolved carbon dioxide, beyond the natural level of the $C^{16}O^{18}O$ isotopologue. Because the only possible source of ^{18}O corresponds to terminal ($>^{18}O_s^{2-}$ or $>^{18}OH_s^-$) species of $Ti^{18}O_2$, the experiment unambiguously demonstrates that bridging oxygen ions from the $Ti^{18}O_2$ lattice are incorporated into the evolved CO_2 during photocatalytic anaerobic mineralization of benzene. Because the $H_2^{16}O$ solvent is not isotopically labeled, the participation of $(-OH_t^-)_{ads}/(-H_2O)_{ads}$ terminal species involved in reaction 6 as a source of photogenerated ^{18}O-enriched CO_2 is not

Table 1. Photocatalytic Reaction Scheme[19,27,47]

$$\left\{ TiO_2 \xrightarrow{h\nu \geq 3.2\,eV} h_f^+ + e_f^- \right\} \quad \text{Charge carrier generation}$$

$$\left[\begin{array}{l} h_f^+ + \left(>^{18}O_s^{2-}\right) \longrightarrow \left(-^{18}O_s^{\bullet}\right) \quad\quad pH > pH_{zpc} \\ h_f^+ + \left(>^{18}OH_s^-\right) \longrightarrow \left(-^{18}OH_s^{\bullet}\right) \quad pH < pH_{zpc} \end{array} \right\} \text{Surface trapped holes} \left(h_s^+\right) \text{generation}$$

$$\left\{ h_s^+ + e_f^- \longrightarrow >^{18}O_s^{2-}, >^{18}OH_s^- \right\} \quad \text{Charge carrier recombination}$$

$$\left\{ \left[RH_2 \right]_{aq} + \left(-^{18}OH_s^{\bullet} / -^{18}O_s^{\bullet} \right) \rightarrow RH^{\bullet} + H^+ + \left(>^{18}OH_s^- / >^{18}O_s^{2-} \right) \right\} \text{ Oxidation of not chemisorbed molecules}$$

$$\left\{ \left(RH_2 \right)_{ads} + h_f^+ \rightarrow RH^{\bullet} + H^+ \right\} \quad \text{Oxidation of chemisorbed molecules}$$

$$\left\{ \left(RH_{aq}^{\bullet} \right) + \left(-^{18}O_s^{\bullet -}\right) / \left(-^{18}OH_s^{\bullet}\right) \rightarrow RH^{18}OH + V\left(>^{18}O_s^{2-}\right) \right\} \quad \text{Oxidation of the resulting organic radical}$$

$$\left\{ V\left(>O_s^{2-}\right) + H_2^{16}O \rightarrow \left(>^{16}OH_s^-\right) + H^+ \right\} \text{ Dissociative adsorption of water}$$

possible. It can be further observed in Figure 3 that the ^{18}O carbon dioxide enrichment occurs in the time range of $25 < t < 85$ min. The total amount of $C^{16}O_2$ produced during this time period can be calculated by performing the definite integral (limits $t_a = 25$ min and $t_b = 85$ min) of the curve of $C^{16}O_2$ (in μmol/h) versus time (see Figure S1, Supporting Information), yielding a value of 9.1 μmol for the experiment of Figure 2B. In a similar way, the total amount of evolved $C^{16}O^{18}O$ in the same time range can be calculated from the definite integral of the QMS signal ratio versus time shown in Figure 3. In order to perform this integration, the baseline must be settled at a QMS ratio signal value of 0.62% (natural $C^{16}O^{18}O/C^{16}O_2$ isotopic ratio) in order to subtract the contribution of the $C^{16}O^{18}O$ isotopologue naturally present in the carbon dioxide. A value of 0.17% ^{18}O enrichment in the time range of $25 < t < 85$ min was obtained for the experiment of Figure 2B, which means that 0.0155 μmol of the $C^{16}O^{18}O$ isotopologue is photogenerated. Because all of the ^{18}O atoms of the evolved $C^{16}O^{18}O$ belong to the $Ti^{18}O_2$ surface lattice, it means that 9.33×10^{15} TiO_2 surface lattice oxygen atoms (O_s) are incorporate into the evolved CO_2. Therefore, the surface density of lattice oxygen exchanged atoms (σ_{O_s}) is, approximately, $\sigma_{O_s} = 5.8 \times 10^{11}$ (O_s atoms/cm^2).

In a recent study[20] of photoinduced oxygen isotopic exchange (POIE) on TiO_2 Degussa P-25, it was reported that $\sigma_{O_s} = 2 \times 10^{11}$ (atoms/cm^2). Attention must be paid to the noticeable agreement of both σ_{O_s} values, which seems to indicate that a similar fraction of O_s is exchanged during UV excitation of TiO_2. However, to obtain a quantitatively precise value of σ_{O_s}, further work with different samples and concentrations of $Ti^{18}O_2$ must be developed. In any case, the POIE study demonstrated the existence of a light-induced exchange of surface $>OH_s^-/>O_s^{2-}$ anions. Furthermore, the time evolution of the POIE rate (see Figures 5 and 6 of ref 20) shows the same qualitative behavior as that observed for the ^{18}O enrichment reported in Figure 3, that is, a fast increase immediately after the light is turned on, reaching a maximum that is followed by an asymptotical decay as time further increases. Such POIE behavior has been explained by invoking a mechanism involving h_f^+ capture by $>OH_s^-/>O_s^{2-}$ surface ions with generation of surface $-OH_s^{\bullet}/-O_s^{\bullet -}$ radicals, which further react with gas-phase $^{18}O_2$ molecules.[19,20] Summing up, $-OH_s^{\bullet}/-O_s^{\bullet -}$ radical species are apparently involved in both mechanisms of POIE[19,20] and photooxidation of dissolved organic substrates[27] (see eqs 3 and 4), as is the present case for benzene. This is in agreement with the experimental fact that

POIE is canceled in the presence of dissolved organic molecules to be photooxidized[18] and with the evidence obtained from electron paramagnetic resonance (EPR) experiments demonstrating that TiO_2 surface lattice oxygen ions behave as real photogenerated valence band hole traps.[9-11]

The set of evidence mentioned above encourages us to propose a plausible mechanism to explain the ^{18}O enrichment observed in Figure 3 by invoking the participation of $-^{18}OH_s^{\bullet}/-^{18}O_s^{\bullet -}$ as the primary oxidizing species. This reaction mechanism should take also into account the well-known fact that benzene mineralization to CO_2 involves the photogeneration of hydroxylated aromatic intermediates in the first reaction steps.[7,12,13,15,16] In the proposed mechanism, the photogenerated $-^{18}OH_s^{\bullet}/-^{18}O_s^{\bullet -}$ radical species (eqs 3 and 4) are able to trap electrons from the dissolved organic substrate, yielding an organic radical intermediate, according to reaction 5. Organic radicals can also be generated through reaction 2. In the case of benzene, this is excluded because it requires benzene chemisorption at the TiO_2 surface, which is not the case.[42] The produced organic radicals ($RH^{\bullet}$) can further react with $-^{18}OH_s^{\bullet}/-^{18}O_s^{\bullet -}$ species to generate an ^{18}O isotopically labeled hydroxylated intermediate, leaving behind a terminal oxygen vacancy $V(>^{18}O_s^{2-})$ according to the reaction

$$(RH_{aq}^{\bullet}) + (-^{18}OH_s^{\bullet}/-^{18}O_s^{\bullet -}) \rightarrow RH^{18}OH + V(>^{18}O_s^{2-}) \tag{7}$$
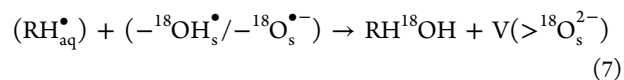
The oxygen vacancy, $V(>^{18}O_s^{2-})$, is quickly filled with a $^{16}OH^-$ ion via dissociative adsorption of a $H_2^{16}O$ molecule from the solvent, according to the reaction

$$V(>O_s^{2-}) + H_2^{16}O \rightarrow (>^{16}OH_s^-) + H^+ \tag{8}$$
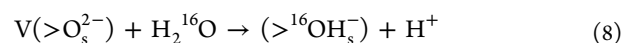
The regeneration of $V(>^{18}O_s^{2-})$ was first demonstrated via high-resolution scanning tunneling microscopy (STM) experiments,[43,44] and is a currently accepted pathway of interaction of water molecules with terminal oxygen vacancies at the TiO_2 surface.[6,45] Noteworthy, reaction 8 implies a continuous enrichment of the $Ti^{18}O_2$ surface with $>^{16}OH_s^-$, a fact that would explain the decrease of the $C^{16}O^{18}O$ signal with time. The replenishment of the oxygen vacancies also closes the catalytic cycle, avoiding the potential collapse of the catalyst surface due to accumulation of photoinduced $V(>^{18}O_s^{2-})$ vacancies and the corresponding surface atomic rearrangement.[45,46]

The $>^{16}OH_s^-$ species generated according to reaction 8 are suitable hole traps that can lead to photogeneration of $-^{16}OH_s^{\bullet}/-^{16}O_s^{\bullet -}$ radical species (eqs 3 and 4), able to further react with organic molecules and organic radicals, according to

reactions 5 and 7, a fact that leads to the generation of $RH^{16}OH$ hydroxylated intermediates. The sequence of elementary steps representing the proposed mechanism is summarized in Table 1.

The expected outcome of the reactions in Table 1 is a mixture of labeled and unlabeled hydroxylated intermediates ($RH^{18}OH$ and $RH^{16}OH$) as the PO reaction proceeds. Further oxidation of hydroxylated aromatic intermediates leads to the production of $C^{16}O_2$, $C^{16}O^{18}O$, and/or $C^{18}O_2$. Because the solvent ($H_2^{16}O$) is a source of $>^{16}OH_s^-$ species (reaction 8), the ratio of the oxidation products ($RH^{18}OH$ and $RH^{16}OH$) and therefore of $C^{16}O_2$, $C^{16}O^{18}O$, and $C^{18}O_2$ will be determined by the ratio between ^{16}O and ^{18}O supplied by the solvent and the $Ti^{18}O_2$ catalyst, respectively. An assessment of such an isotope ratio can be obtained by taking into account that for a mixture of anatase−rutile nanoparticles with S_g = 39.5 m^2/g, similar to our $Ti^{18}O_2$ material, Fujishima et al.[48] reported a surface oxygen density of 1.46 × 10^{15} atoms/cm^2. In our experiments A_{cat} = 16050 cm^2, and consequently, the total number of bridging $>^{18}OH_s^-$ terminal species of the $Ti^{18}O_2$ catalyst at the beginning of the experiment is estimated to be 2.34 × 10^{19}. On the other hand, 50 mL of $H_2^{16}O$ was used as the solvent, providing an approximated amount of 1.67 × 10^{24} unlabeled ^{16}O atoms for reaction. This implies an initial atomic ratio of $^{16}O/^{18}O \approx$ 70000:1 and a total ^{18}O enrichment in the oxidation products that could be as low as 0.0015% (in the unrealistic case that all $H_2^{16}O$ finally participate in the reaction). As discussed before, a higher ^{18}O enrichment (0.17% for $C^{16}O^{18}O$ calculated from data in Figures S1 and 3, Supporting Information) was obtained in our experiment, indicating that the reaction takes place by preferentially using the ^{18}O of the catalyst surface.

It must be highlighted that the here-proposed mechanism is not in contradiction with the data reported by Matsumura et al.[15] and Zhao et al.[16] Indeed, those authors studied the photocatalytic oxidation of benzene in $H_2^{18}O$ and using the $Ti^{16}O_2$ photocatalyst, and they evidence ^{18}O incorporation into the oxidation products in a range of 70−90%. Such a large presence of ^{18}O can be explained by taking into account that with $H_2^{18}O$ as the solvent and $Ti^{16}O_2$ as the catalyst, a low $^{16}O/^{18}O$ ratio was used (around 1:10000) and, consequently, a large majority of ^{18}O was detected in the reaction products. On the contrary, in the experiments reported here, with the $^{16}O/^{18}O$ ratio used at around 70000:1, a minor presence of ^{18}O in the final reaction products should be expected.

According to the findings of the present work, an explanation can be given to the experimental data reported by Zhao's and Matsumura's groups that clearly differs from the mechanistic scheme proposed by those authors. The key point is how the ^{18}O from $H_2^{18}O$ is incorporated into the oxidation products, that is, if it comes from a ^{18}OH radical generated through reaction 6,[14−17,24] or via filling of $Ti^{16}O_2$ photogenerated surface oxygen vacancies with ^{18}O from $H_2^{18}O$ (eq 8) and its subsequent incorporation into oxidation products. The data presented here clearly support the second reaction pathway. Thus, while our mechanistic proposal accounts for the experimental data reported in previous isotopic tracing studies,[14−17,24] the commonly accepted mechanism of formation of hydroxyl radicals through eq 6 does not explain the following independent experimental observations: (a) the incorporation of TiO_2 surface lattice oxygen ions into photooxidation products reported here, (b) the POIE phenomena,[18−20] and (c) the incorporation of TiO_2 surface

lattice oxygen ions into the photooxidation products reported in several surface science studies (SCS) of PO of organic molecules at the TiO_2 surface under UHV conditions.[6,45]

Summing up, experimental evidence has been given here on the incorporation of ^{18}O derived from $Ti^{18}O_2$ surface lattice oxygen ions into CO_2 molecules evolved during the photocatalytic, anaerobic mineralization of benzene. As the reaction proceeds, CO_2 tends to reach its natural isotopic composition, a fact that is attributed to the dissociative adsorption of water into TiO_2 oxygen vacancies photogenerated during the first reaction steps. The whole process can be seen as the consequence of a first step of anodic TiO_2 photocorrosion accompanied by transfer of lattice surface oxygen to the organic molecules, followed by a second healing step where the oxygen vacancies of the surface are replenished by oxygens supplied by water molecules. A mechanistic scheme involving the participation of photogenerated TiO_2 ($-OH_s^\bullet/-O_s^{\bullet-}$) surface radicals as primary oxidizing species accounts for the experimental evidence reported. The use of $Ti^{18}O_2$ nanoparticles and in situ isotopic tracing of the gas-phase products of photocatalytic anaerobic mineralization reactions is shown to constitute a suitable tool in order to gain a deeper understanding of the mechanistic pathways of liquid-phase photocatalysis. The results reported here are in agreement with the evidence reported for the gas-phase POIE phenomena and the SCS of TiO_2 reactions under UHV conditions.

■ ASSOCIATED CONTENT

Ⓢ Supporting Information
Details of experimental procedures; time evolution of the $C^{16}O_2$ production rate (in μmol/h); details of some numerical calculations; and selected TEM images, EDAX spectra, and SAED patterns for both $Ti^{16}O_2$ and $Ti^{18}O_2$ catalysts. This material is available free of charge via the Internet at http://pubs.acs.org.

■ AUTHOR INFORMATION

Corresponding Author
*E-mail: jose.peral@uab.cat. Fax: 34 93 581 2920.

Notes
The authors declare no competing financial interest.

■ ACKNOWLEDGMENTS

■ REFERENCES

(1) Fox, M. A.; Dulay, M. T. Heterogeneous Photocatalysis. *Chem. Rev.* **1993**, *93*, 341−357.

(2) Hoffmann, M. R.; Martin, S. T.; Choi, W.; Bahnemann, D. W. Environmental Applications of Semiconductor Photocatalysis. *Chem. Rev.* **1995**, *95*, 69−96.

(3) Peral, J.; Domenech, X.; Ollis, D. F. Heterogeneous Photocatalysis for Purification, Decontamination and Deodorization of Air. *J. Chem. Technol. Biotechnol.* **1997**, *70*, 117−140.

(4) Fujishima, A.; Zhang, X.; Tryk, D. A. TiO_2 Photocatalysis and Related Surface Phenomena. *Surf. Sci. Rep.* **2008**, *63*, 515−582.

1420

dx.doi.org/10.1021/jz400580b | J. Phys. Chem. Lett. 2013, 4, 1415−1422

(5) Friedmann, D.; Mendive, C.; Bahnemann, D. TiO₂ for Water Treatment: Parameters Affecting the Kinetics and Mechanisms of Photocatalysis. *Appl. Catal., B* **2010**, *99*, 398−406.

(6) Henderson, M. A. A Surface Science Perspective on Photocatalysis. *Surf. Sci. Rep.* **2011**, *66*, 185−297.

(7) Augugliaro, V.; Bellardita, M.; Loddo, V.; Palmisano, G.; Palmisano, L.; Yurdakal, S. Overview on Oxidation Mechanisms of Organic Compounds by TiO₂ in Heterogeneous Photocatalysis. *J. Photochem. Photobiol. C: Photochem. Rev.* **2012**, *13*, 224−245.

(8) Zhang, L.; Mohamed, H. H.; Dillert, R.; Bahnemann, D. Kinetics and Mechanisms of Charge Transfer Processes in Photocatalytic Systems: A Review. *J. Photochem. Photobiol. C: Photochem. Rev.* **2012**, *13*, 263−276.

(9) Howe, R. F.; Grätzel, M. EPR Study of Hydrated Anatase under UV Irradiation. *J. Phys. Chem.* **1987**, *91*, 3906−3909.

(10) Micic, O. I.; Zhang, Y.; Cromack, K. R.; Trifunac, A. D.; Thurnauer, M. C. Trapped Holes on Titania Colloids Studied by Electron Paramagnetic Resonance. *J. Phys. Chem.* **1993**, *97*, 7277−7283.

(11) Dimitrijevic, N. M.; Saponjic, Z. V.; Rabatic, B. M.; Poluektov, O. G.; Rajh, T. Effect of Size and Shape of Nanocrystalline TiO₂ on Photogenerated Charges. An EPR Study. *J. Phys. Chem. C* **2007**, *111*, 14597−14601.

(12) Izumi, I.; Dunn, W. W.; Wilbourn, K. O.; Fan, F. R.; Bard, A. J. Heterogeneous Photocatalytic Oxidation of Hydrocarbons on Platinized Titanium Dioxide Powders. *J. Phys. Chem.* **1980**, *84*, 3207−3210.

(13) Hashimoto, K.; Kawai, T.; Sakata, T. Photocatalytic Reactions of Hydrocarbons and Fossil Fuels with Water. Hydrogen Production and Oxidation. *J. Phys. Chem.* **1984**, *88*, 4083−4088.

(14) Yang, J.; Dai, J.; Chen, C.; Zhao, J. Effects of Hydroxyl Radicals and Oxygen Species on the 4-Chlorophenol Degradation By Photoelectrocatalytic Reactions with TiO₂-Film Electrodes. *J. Photochem. Photobiol. A: Chem.* **2009**, *208*, 66−77.

(15) Bui, T. D.; Kimura, A.; Ikeda, S.; Matsumura, M. Determination of Oxygen Sources for Oxidation of Benzene on TiO₂ Photocatalysts in Aqueous Solutions Containing Molecular Oxygen. *J. Am. Chem. Soc.* **2010**, *132*, 8453−8458.

(16) Li, Y.; Wen, B.; Yu, C.; Chen, C.; Ji, H.; Ma, W.; Zhao, J. Pathway of Oxygen Incorporation From O₂ In TiO₂ Photocatalytic Hydroxylation Of Aromatics: Oxygen Isotope Labeling Studies. *Chem.—Eur. J.* **2012**, *18*, 2030−2039.

(17) Li, Y.; Wen, B.; Ma, W.; Chen, C.; Zhao, J. Photocatalytic Degradation of Aromatic Pollutants: A Pivotal Role of Conduction Band Electron in Distribution of Hydroxylated Intermediates. *Environ. Sci. Technol.* **2012**, *46*, 5093−5099.

(18) Courbon, H.; Formenti, M.; Pichat, P. Study of Oxygen Isotopic Exchange over Ultraviolet Irradiated Anatase Samples and Comparison with the Photooxidation of Isobutane into Acetone. *J. Phys. Chem.* **1977**, *81*, 550−554.

(19) Montoya, J. F.; Peral, J.; Salvador, P. Surface Chemistry and Interfacial Charge-Transfer Mechanisms in Photoinduced Oxygen Exchange at O₂−TiO₂ Interfaces. *ChemPhysChem* **2011**, *12*, 901−907.

(20) Mikhaylov, R. V.; Lisachenko, A. A.; Titov, V. V. Investigation of Photostimulated Oxygen Isotope Exchange on TiO₂ Degussa P25 Surface upon UV−Vis Irradiation. *J. Phys. Chem. C* **2012**, *116*, 23332−23341.

(21) Turchi, C. S.; Ollis, D. F. Photocatalytic Degradation of Organic Water Contaminants: Mechanisms Involving Hydroxyl Radical Attack. *J. Catal.* **1990**, *122*, 178−192.

(22) Lawless, D.; Serpone, N.; Meisel, D. Role of Hydroxyl Radicals and Trapped Holes in Photocatalysis. A Pulse Radiolysis Study. *J. Phys. Chem.* **1991**, *95*, 5166−5170.

(23) Rajh, T.; Saponjic, Z. V.; Micic, O. I. Reactions of Hydrous Titanium Oxide Colloids with Strong Oxidizing Agents. *Langmuir* **1992**, *8*, 1265−1270.

(24) Wen, B.; Li, Y.; Chen, C.; Ma, W.; Zhao, J. An Unexplored O₂-Involved Pathway for the Decarboxylation of Saturated Carboxylic Acids by TiO₂ Photocatalysis: An Isotopic Probe Study. *Chem.—Eur. J.* **2010**, *16*, 11859−11866.

(25) Salvador, P. On the Nature of Photogenerated Radical Species Active in the Oxidative Degradation of Dissolved Pollutants with TiO₂ Aqueous Suspensions: A Revision in the Light of the Electronic Structure of Adsorbed Water. *J. Phys. Chem. C* **2007**, *111*, 17038−17043.

(26) Imanishi, A.; Okamura, T.; Ohashi, N.; Nakamura, R.; Nakato, Y. Mechanism of Water Photooxidation Reaction at Atomically Flat TiO₂ (Rutile) (110) and (100) Surfaces: Dependence on Solution pH. *J. Am. Chem. Soc.* **2007**, *129*, 11569−11578.

(27) Montoya, J. F.; Peral, J.; Salvador, P. Comments on the Published Article "Effects of Hydroxyl Radicals and Oxygen Species on the 4-Chlorophenol Degradation by Photoeletrocatalytic Reactions with TiO₂-Film Electrodes by J. Yang, J. Dai, Ch. Chen, J. Zhao; *J. Photochem. Photobiol. A: Chem.* 208 (2009) 66−77". *J. Photochem. Photobiol. A: Chem.* **2010**, *210*, 215−216.

(28) Kavan, L.; Zukalová, M.; Ferus, M.; Kürti, J.; Koltai, J.; Civis, S. Oxygen-Isotope Labeled Titania: Ti¹⁸O₂. *Phys. Chem. Chem. Phys.* **2011**, *13*, 11583−11586.

(29) Civis, S.; Ferus, M.; Zukalová, M.; Kubát, P.; Kavan, L. Photochemistry and Gas-Phase FTIR Spectroscopy of Formic Acid Interaction with Anatase Ti¹⁸O₂ Nanoparticles. *J. Phys. Chem. C* **2012**, *116*, 11200−11205.

(30) Civis, S.; Ferus, M.; Kubát, P.; Zukalová, M.; Kavan, L. Oxygen-Isotope Exchange between CO₂ and Solid Ti¹⁸O₂. *J. Phys. Chem. C* **2011**, *115*, 11156−11162.

(31) Frank, O.; Zukalová, M.; Laskova, B.; Kurti, J.; Koltai, J.; Kavan, L. Raman Spectra of Titanium Dioxide (anatase, rutile) with Identified Oxygen Isotopes (16, 17, 18). *Phys. Chem. Chem. Phys.* **2012**, *14*, 14567−14572.

(32) Spurr, R. A.; Myers, H. Quantitative Analysis of Anatase-Rutile Mixtures with an X-ray Diffractometer. *Anal. Chem.* **1957**, *29*, 760−762.

(33) Boehm, H. P.; Herrmann, M. Über die Chemie der Oberfläche des Titandioxids. I. Bestimmung des aktiven Wasserstoffs, thermische Entwässerung und Rehydroxylierung. *Z. Anorg. Allg. Chem.* **1967**, *352*, 156−167.

(34) Boehm, H. P. Acidic and Basic Properties of Hydroxylated Metal Oxide Surfaces. *Discuss. Faraday Soc.* **1971**, *52*, 264−275.

(35) Nosaka, A. Y.; Fujiwara, T.; Yagi, H.; Akutsu, H.; Nosaka, Y. Characteristics of Water Adsorbed on TiO₂ Photocatalytic Systems with Increasing Temperature as Studied by Solid-State ¹H NMR Spectroscopy. *J.Phys. Chem. B* **2004**, *108*, 9121−9125.

(36) Nosaka, A. Y.; Nishino, J.; Fujiwara, T.; Ikegami, T.; Yagi, H.; Akutsu, H.; Nosaka, Y. Effects of Thermal Treatments on the Recovery of Adsorbed Water and Photocatalytic Activities of TiO₂ Photocatalytic Systems. *J. Phys. Chem. B* **2006**, *110*, 8380−8385.

(37) Finnie, K. S.; Cassidy, D. J.; Bartlett, J. R.; Woolfrey, J. L. IR Spectroscopy of Surface Water and Hydroxyl Species on Nanocrystalline TiO₂ Films. *Langmuir* **2001**, *17*, 816−820.

(38) Salvador, P. Mechanisms of Water Photooxidation at n-TiO₂ Rutile Single Crystal Oriented Electrodes under UV Illumination in Competition with Photocorrosion. *Prog. Surf. Sci.* **2011**, *86*, 41−58.

(39) Nováková, J. Isotopic Exchange of Oxygen ¹⁸O Between the Gaseous Phase and Oxide Catalysts. *Catal. Rev.—Sci. Eng.* **1971**, *4*, 77−113.

(40) Sato, S. Hydrogen and Oxygen Isotope Exchange Reactions Over Illuminated and Nonilluminated Titania. *J. Phys. Chem.* **1987**, *91*, 2895−2897.

(41) Mohamed, H. H.; Dillert, R.; Bahnemann, D. W. Growth and Reactivity of Silver Nanoparticles on the Surface of TiO₂: A Stopped-Flow Study. *J. Phys. Chem. C* **2011**, *115*, 12163−12172.

(42) Zhou, J.; Dag, S.; Senanayake, S. D.; Hathorn, B. C.; Kalinin, S. V.; Meunier, V.; Mullins, D. R.; Overbury, S. H.; Baddorf, A. P. Adsorption, Desorption, and Dissociation of Benzene on TiO₂ (110) and Pd/TiO₂ (110): Experimental Characterization and First-Principles Calculations. *Phys. Rev. B* **2006**, *74*, 125318/1−125318/11.

(43) Brookes, I. M.; Muryn, C. A.; Thornton, G. Imaging Water Dissociation on TiO₂ (110). *Phys. Rev. Lett.* **2001**, *87*, 266103/1−266103/4.

(44) Schaub, R.; Thostrup, P.; Lopez, N.; Laegsgaard, E.; Stensgaard, I.; Norskov, J. K.; Besenbacher, F. Oxygen Vacancies as Active Sites for Water Dissociation on Rutile TiO$_2$ (110). *Phys. Rev. Lett.* **2001**, *87*, 266104/1−266104/4.

(45) Pang, C. L.; Lindsay, R.; Thornton, G. Chemical Reactions on Rutile TiO$_2$ (110). *Chem. Soc. Rev.* **2008**, *37*, 2328−2353.

(46) Thompson, T. L.; Yates, J. T. Surface Science Studies of the Photoactivation of TiO$_2$-New Photochemical Processes. *Chem. Rev.* **2006**, *106*, 4428−4453.

(47) Monllor-Satoca, D.; Gomez, R.; Gonzalez-Hidalgo, M.; Salvador, P. The "Direct−Indirect" Model: An Alternative Kinetic Approach in Heterogeneous Photocatalysis Based on the Degree of Interaction of Dissolved Pollutant Species with the Semiconductor Surface. *Catal. Today* **2007**, *129*, 247−255.

(48) Kobayakawa, K.; Nakazawa, Y.; Ikeda, M.; Sato, Y.; Fujishima, A. Influence of the Density of Surface Hydroxyl Groups on TiO$_2$ Photocatalytic Activities. *Ber. Bunsen-Ges. Phys. Chem.* **1990**, *94*, 1439−1443.

SUPPORTING INFORMATION

The Catalytic Role of Surface Oxygens in TiO$_2$ Photooxidation Reactions: Aqueous Benzene Photooxidation with Ti^{18}O$_2$ under Anaerobic Conditions

Juan Felipe Montoya[1], Irina Ivanova[2], Ralf Dillert[2], Detlef W. Bahnemann[2], Pedro Salvador[1] and José Peral[1,*]

1.Departamento de Química, Universidad Autónoma de Barcelona, 08193, Cerdanyola del Vallés, Spain.

2. Institut für Technische Chemie, Leibniz Universität Hannover, Callinstrasse 3, D-30167, Hannover, Germany

*Corresponding author, E-mail: jose.peral@uab.cat, Fax: 34 93 581 2920

1. Experimental Methods

1.1 Materials and Reagents

$TiCl_4$ (99.9% purity) packed under Argon gas and sealed with a septum was purchased from Aldrich. This reagent was extracted with a dry syringe an immediately transferred to the vacuum glass apparatus in order to avoid any contamination. Oxygen isotope labeled water ($H_2^{18}O$) was acquired from Cambridge Isotope Laboratories (97% of ^{18}O purity) and used as received. Water purified in a Millipore Milli-Q system was used for the synthesis of the $Ti^{16}O_2$ and as solvent in photocatalytic experiments. Benzene and silver tetrafluoroborate ($AgBF_4$) were analytical reagent grade and used as received without further purification.

1.2 TiO₂ nanoparticles synthesis

Titanium tetrachloride (3.8ml) previously cooled to 2^oC, was injected through a rubber septum in a vacuum glass apparatus (P=30 mbar) immersed in ice ($T = 0^oC$). 1.25 g of oxygen isotope labeled water ($H_2^{18}O$, 97% of ^{18}O) was added slowly through the rubber septum to produce the hydrolysis of the $TiCl_4$ according to reaction 1.

$$TiCl_4(l) + 2H_2^{18}O(l) \rightarrow Ti^{18}O_2(s) + 4HCl(g) \qquad \text{Eq. 1}$$
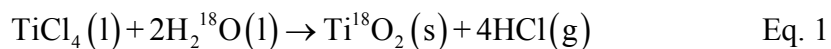
When the reactants where completely mixed a yellow powder was produced. The raw product was heated to 350 ^oC for 2 hours under vacuum. The evolved gas (HCl) was collected in a water trap located at the end of the vacuum line. The final product was a white powder that was cooled at 25 ^oC under vacuum, thoroughly washed with distilled water, filtered and dried by exposition to air at room temperature. $Ti^{16}O_2$ was prepared following the same procedure but using ($H_2^{16}O$) instead of $H_2^{18}O$ as reagent for the hydrolysis reaction (Eq. 1).

1.3 Characterization Techniques

The BET surface area of the samples was determined using a FlowSorb II 2300 (Micromeritics, USA) with a 30 % nitrogen/ 70 % helium gas mixture as adsorbate. Selected area electron-difraction (SAED) patterns and Transmission electron microscopy (TEM) images were acquired in a Jeol-JEM 2011 microscope operated at 200 kV and equipped with an energy dispersive spectrometer (EDS) detector from OXFORD INCA. The recorded images were analyzed using ImageJ software. The samples were dispersed in absolute ethanol before image collection. X-ray diffraction (XRD) spectra were registered on a Rigaku Rotaf ex RU-200B diffractometer (Cu Kα radiation, λ=1.5406 A^0). Raman spectroscopy was carried out using a BRUKER SENTERRA Dispersive Raman Microscope. The spectra were taken to the powder samples exposed to air in the range from 50 to 1555 cm^{-1} using a laser excitation wavelength of 532 nm and a laser power of 2 mW.

1.4 Photocatalytic Experiments

All experiments were carried out in a cylindrical air-tight reactor connected to a gas analyzer (HIDEN HPR-20 QIC) equipped with a quadrupole mass spectrometer (QMS). The reactor had inlet and outlet gas ports connected to a system of valves in order to provide a continuous flow of Argon gas (5 ml/min) through the head space. A fraction of this gas is continuously injected into the QMS analyzer. In all experiments the liquid phase volume was 50 ml and the gas phase volume was 15ml. Temperature was kept constant at $15\pm1\,^{o}C$ using a thermostatic water bath. The suspensions were prepared mixing 50 ml of the solvent ($H_2^{16}O$) with 50 mg of the catalyst ($Ti^{18}O_2$ or $Ti^{18}O_2$) and 100 mg of AgBF$_4$. These suspensions were always magnetically stirred at 400 rpm and purged with Argon gas (flow=30ml/min) for 20 minutes in order to remove dissolved oxygen. Before illumination, Argon gas was circulated through the whole system for 15

minutes at a flow rate of 30 ml/min. Then, the Argon flow was adjusted to the working value of 5 ml/min and the QMS detector was started. The suspension was stirred in the dark for an additional time of 25 minutes in order to achieve a stable ground QMS signal. At the end of this period, the light was turned on. The QMS analyzer was programmed to automatically measure and register the signals of $C^{16}O_2$ (m/z=44), $C^{16}O^{18}O$ (m/z=46), and $C^{18}O_2$ (m/z=48) at time intervals of around 1.04 minutes.

Illumination was carried out with a Xenon Arc lamp. The total photon flux (UV photons, $300nm < \lambda < 390nm$) incident on the reactor in all experiments was $9.81\text{x}10^{17}$ photons/s, as measured by using potassium ferrioxalate actinometry.

2. Mathematical Calculations

2.1 Carbon Dioxide signal conversion

Conversion of the QMS signal of $C^{16}O_2$ (m/z=44) to $C^{16}O_2$ flow units (μmol/h) was performed by registering the QMS signal of a commercial standard mixture of $C^{16}O_2$ (1.01%) in Argon gas that was circulated through the reaction system at several values of flow rate. A calibration curve was obtained and used to convert the QMS signal values reported in Figs. 2A and 2B to gas flow units. The result of this conversion is shown in Fig. S1.

The vertical dashed lines of Fig. S1 depict the integration limits used for the calculation of the total amount of $C^{16}O_2$ produced in the time range of 25<t<85 minutes. The same limits were used in the integration of the signal from Fig. 3 to calculate the ^{18}O enrichment of the evolved carbon dioxide.
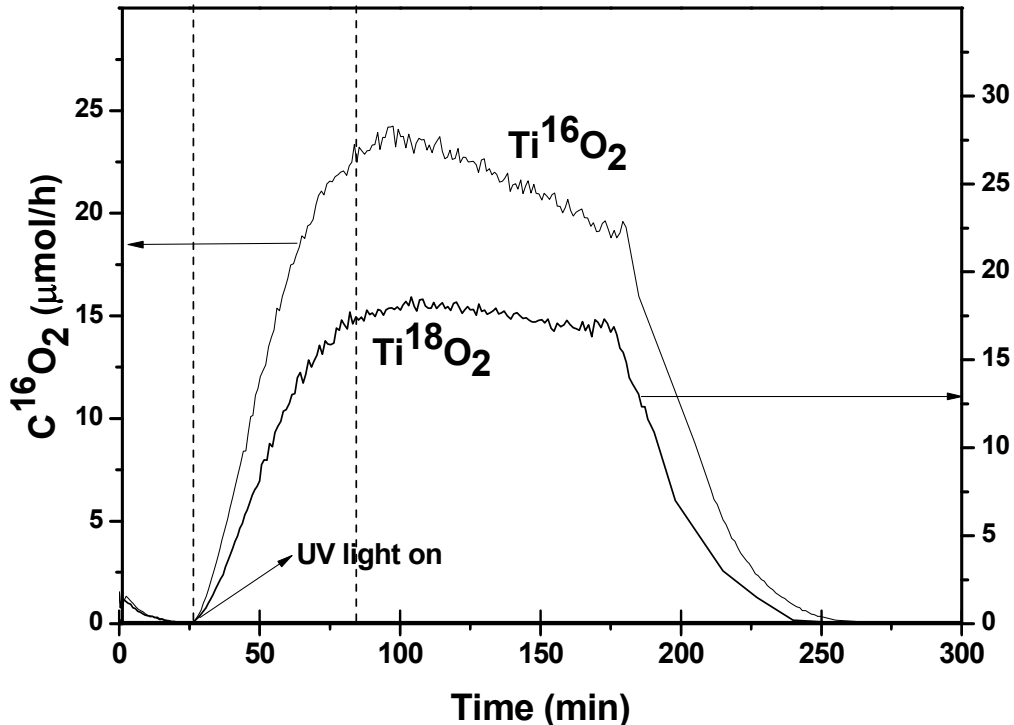
Figure S1. Time evolution of $C^{16}O_2$ production rate $\left(\gamma_{CO_2}\right)$ from PAM of Bz experiments reported in Figures 2A and 2B.

2.2 Isotopic enrichment

As said in the article, all photocatalytic experiments were always repeated by employing as reference a $Ti^{16}O_2$ that was obtained with the same procedure followed for $Ti^{18}O_2$ but using $H_2^{16}O$ as oxygen source of the synthesis. Those reference experiments showed that $C^{16}O^{18}O$ also evolved when using a $Ti^{16}O_2$ catalyst, the reason being the natural presence of a small amount of ^{18}O on $H_2^{16}O$ and, thus, on the synthesized $Ti^{16}O_2$. Figure 3 clearly shows that the background ratio $C^{16}O^{18}O/\ C^{16}O_2$ in the $Ti^{16}O_2$-$H_2^{16}O$ reference experiments is 0.6%. On the other hand, measurements of the isotopic composition of standard CO_2 in contact with water, carried out in our QMS gas analyzer, demonstrate that the natural abundance of the $C^{16}O^{18}O$ isotopologue in the carbon dioxide is also around 0.6% It is also worth noting (Experimental data of Figs. 2A and

3) that the isotopic composition of CO_2 in the reference experiments remains constant and around the 0.6% value either in the dark or under UV lights. Therefore, a value of 0.6% has been taken as the baseline to calculate the ^{18}O isotopic enrichment of CO_2 that can be exclusively attributed to the photocatalytic reaction with $Ti^{18}O_2$.

To calculate the $C^{18}O^{16}O/CO_2$ ratio in the experiments reported in figures 2A and 2B, the QMS signal of $C^{18}O^{16}O$ was divided by the respective signal of CO_2 at each time interval (Eq. 2):

$$\text{QMS signal ratio}\,(\%) = \frac{m/z = 46\,(\mathbf{C^{18}O^{16}O})}{m/z = 44\,(\mathbf{C^{16}O_2})} \times 100 \qquad \text{Eq. 2}$$

Figure 3 illustrates the results of this calculation carried out with the QMS signals of $C^{18}O^{16}O$ and CO_2 of figures 2A and 2B throughout the whole period of time analyzed.

2.3 Estimation of the number of TiO_2 surface lattice oxygen exchanged

The catalytic area of the TiO_2 nanoparticles dispersion in liquid phase can be calculated according to the expression:

$$A_{cat} = x_{cat} \times S_g \qquad \text{Eq. 3}$$

Where, A_{cat} is the catalytic area, x_{cat} is the mass of catalyst and S_g is the specific surface area of the catalyst. For the experiment reported in Fig. 2B $\left(x_{cat} = 0.05\,\text{g}\,;\,S_g = 321000\,\text{cm}^2/\text{g}\right)$ the application of Eq. 7 yields a value of $A_{cat} = 16050\,\text{cm}^2$. The surface density of exchangeable TiO_2 lattice oxygen atoms $\left(\sigma_{O_s}\right)$ can be calculated according to the expression:

$$\sigma_{O_s} = \frac{\text{Number of } O_s \text{ exchanged atoms}}{A_{cat}} \qquad \text{Eq. 4}$$

By replacing the values obtained from fig. 2B into eq. 4 the σ_{O_s} obtained was

$$\sigma_{O_s} = \frac{9.33 \times 10^{15}\,\text{atoms}}{16050\,\text{cm}^2} = 5.81 \times 10^{11}\,\frac{\text{atoms}}{\text{cm}^2} \text{ for the } Ti^{18}O_2 \text{ catalyst.}$$

3. Selected Images of the synthesized nanoparticles obtained by Transmission Electron Microscopy (TEM)

TEM characterization of both $Ti^{16}O_2$ and $Ti^{18}O_2$ catalysts were performed in order to determine the morphological properties and size of the synthesized nanoparticles. During TEM acquisition several spots of the samples were analyzed through Selected-area-electron-diffraction (SAED) and Electron-dispersive X-ray Spectroscopy (EDXS) in order to ascertain the local distribution of crystalline phases and chemical composition, respectively.

TEM micrographs of $Ti^{16}O_2$ reveals that roughly spherical nanoparticles with an average diameter of 22 nm were highly aggregated forming larger moieties. Selected area electron diffraction (SAED) patterns correspond to pure anatase. On the other hand, TEM micrographs of $Ti^{18}O_2$ show the same morphology than the $Ti^{16}O_2$ material, but with average diameters of 26 and 73 nm. The broadening of the SAED patterns suggests the presence of both rutile and anatase phases, in good agreement with the XRD measurements. Finally, electron dispersive X-ray spectroscopy (EDXS) analysis of several spots of the nanoparticles samples showed an average atomic content of 37.96, 61.44 and 0.5% for titanium, oxygen and chlorine atoms, respectively. This suggest that both samples are 99.5% pure TiO_2 with some chlorine impurities that could not be removed during the synthesis process.

Figure S2 show selected images obtained from TEM analysis of the $Ti^{16}O_2$ catalyst. The SAED patterns (panels A and B) reveal main interplanar spacing of 3.5, 2.4, 1.9 and $1.6A^0$. These distances correlate well with the typical anatase interplanar spacing of the planes (101), (004), (200), (211) as it is shown in the insets of the pictures. Panels C to F show TEM images from lower to higher resolution. It can be seen that the nanoparticles are forming aggregates and its shape is roughly spherical. From the image of 50 nm resolution, it was measured an average diameter of 22 nm by performing a statistical analysis of the size distribution observed.

Figure S3 show selected images obtained from TEM analysis of the $Ti^{18}O_2$ catalyst. The SAED patterns (panels A and B) reveal main interplanar spacing of 3.5, 2.4, 1.9 and $1.6A^0$. Although these distances are the same than those of Fig. S2, in this case there is signal broadening which indicates a possible mixing of crystalline phases. Panels C to F show TEM images from lower to higher resolution. It can be seen that the nanoparticles are forming aggregates and its shape is roughly spherical. From the images of 100 and 50 nm resolution, it was determine that the sample was mainly composed of particles with an average diameter of 26 nm but also some bigger particles of around 73 nm were present. The calculated reflection of Fast Fourier Transform (FFT) image obtained from the TEM micrograph of panel F (see inset) reveals interplanar spacing of 3.2 and 3.5 A^0 which are characteristic of rutile (110) and anatase (101) planes, confirming the presence of both phases in this sample.
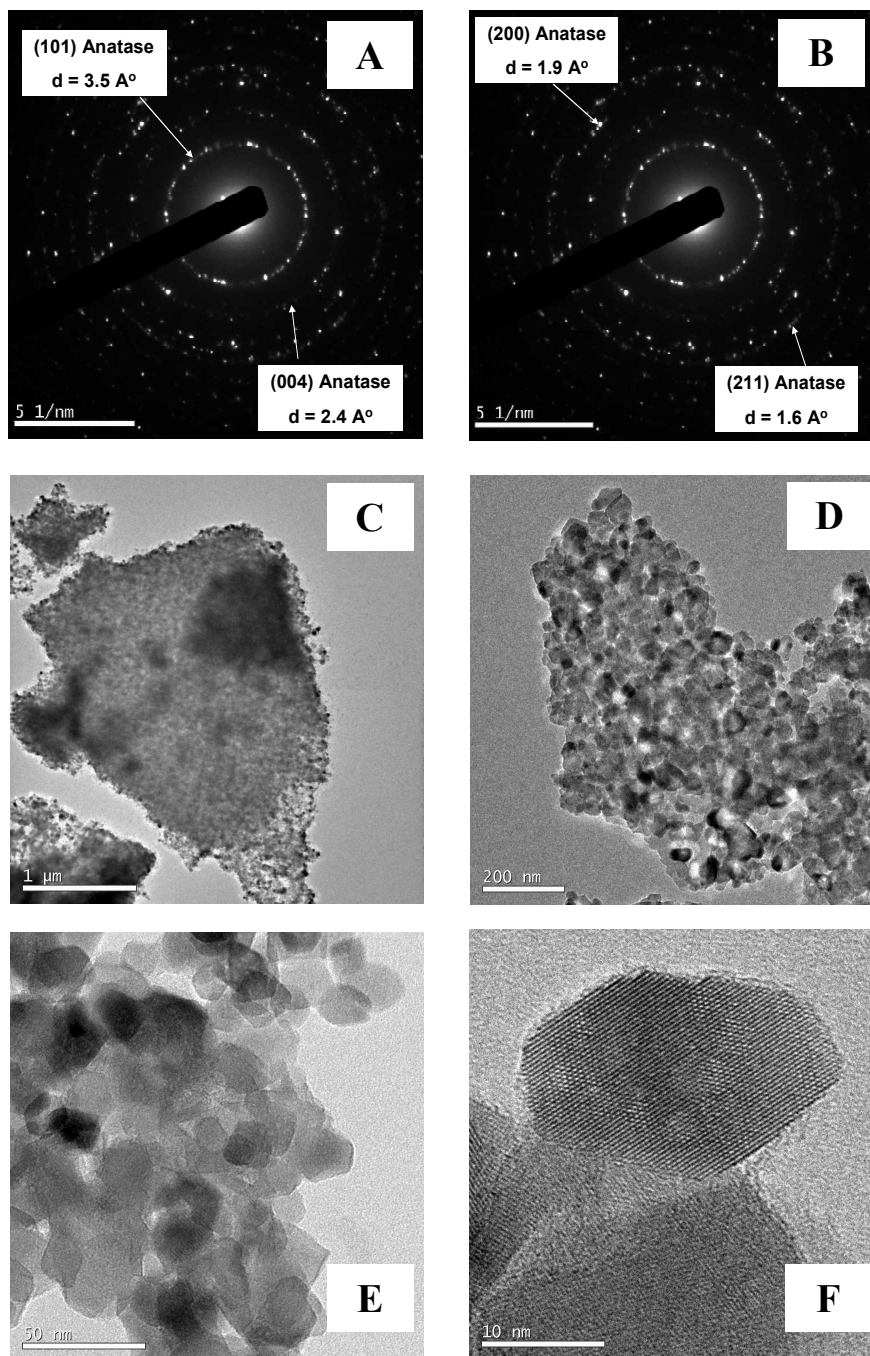
Figure S2. TEM images of Ti^{16}O$_2$ nanoparticles
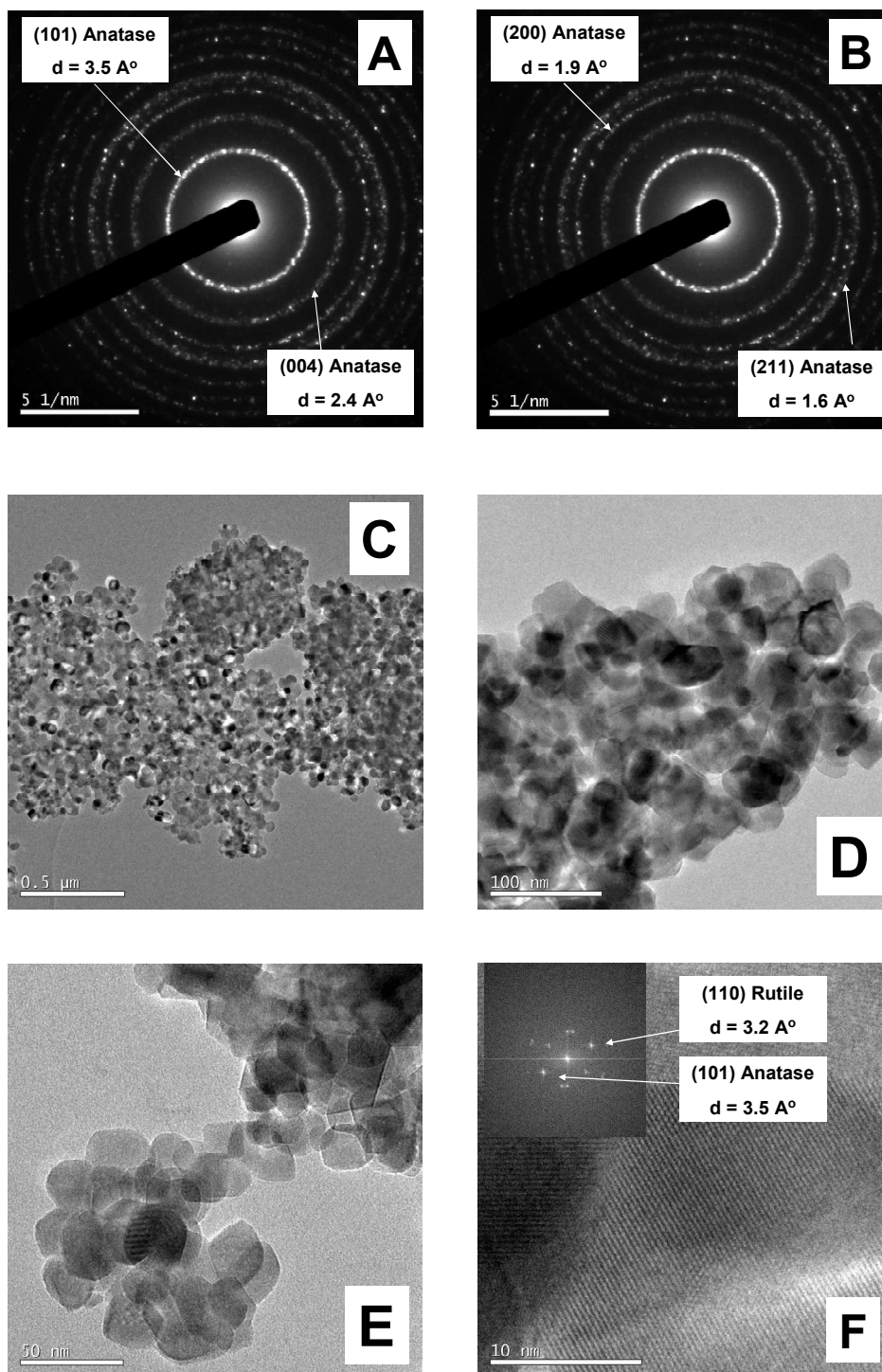
Figure S3. TEM images of Ti^{18}O$_2$ nanoparticles

Figure S4 show a representative EDXS of both Ti^{16}O$_2$ and Ti^{18}O$_2$ catalysts. The average atomic

content calculated from this figure was 37.96, 61.44 and 0.5% for titanium, oxygen and chlorine

atoms, respectively. As it is well known, the quantitative precision of the measurement of oxygen atom by EDXS is limited. For this reason the atomic ratio is not exactly 2:1. However, this analysis indicates that the samples are mainly composed by Ti and O atoms as it was expected. Since HCl is the main reaction byproduct some traces of chlorine were expected as contaminant of the prepared materials.
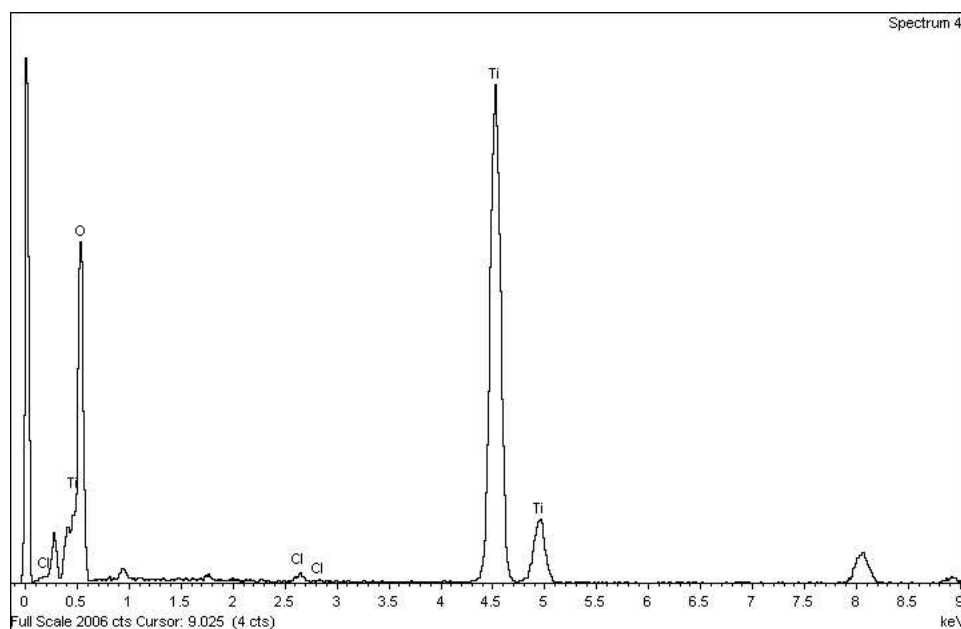
Figure S4. Representative EDXS spectra of the $Ti^{16}O_2$ and $Ti^{18}O_2$ powders. Peaks at 4.3 and 4.8 keV are assigned to the titanium atom and peaks at 0.1 and 0.5 keV to the oxygen atom. The two small peaks at 2.65 and 2.85 keV are assigned to chlorine atom.

CHAPTER 4

CONCLUSIONS AND OUTLOOK

_____

The degree of interaction of several model compounds with bare TiO_2 or F-TiO_2 surfaces were analyzed in detail through spectroscopy techniques and adsorption isotherms. On the other hand, the experimental dependence of the reaction rate on concentration and photon flow for each model compound was studied. It was found that there is a strong correlation between the degree of interaction of the organic substrate with the TiO_2/F-TiO_2 surfaces and their observed kinetic behavior. When the interaction is strong, being chemisorption the main adsorption mode, the organic substrate is photooxidized preferentially via a DT mechanism. In contrast, when the organic substrate is only physisorbed at the TiO_2 surface, it is photooxidized exclusively via an IT mechanism.

If an organic substrate weakly interacts with the TiO_2 surface which mean that only a small proportion of the molecules are able to be chemisorbed being the rest only physisorbed, the photooxidation proceeds by a combination of DT and IT mechanisms. The contribution of each mechanism was found to be dependent on the coverage of the organic substrate at the TiO_2 surface. At higher coverage higher prevalence of the DT mechanisms was observed. These conclusions about the contribution of the DT or IT mechanisms to the photooxidation of the model compounds could be extracted from the analysis of the representations of v_{ox} *vs.* ρ, v_{ox} *vs.* $\rho^{\frac{1}{2}}$, *a vs.* ρ and from photoelectrochemical measurements. In particular, the representations of the new parameter *a* proposed by the D-I model showed their utility to elucidate the working mechanism of charge transfer from analysis of experimental kinetic data.

Besides the above cases, it was found that at high photon flow values the adsorption-desorption equilibrium is perturbed under illumination. A new mathematical expression was formulated to describe the kinetic behavior in that case. The new expression is an extension of the rate equation for DT.

The study of the reactivity of the F-TiO_2 system allowed us inferring that the effect of a TiO_2 surface modification on the reaction rate depends on the charge transfer mechanism that prevails for the oxidation of a particular organic substrate.

In summary, the experimental evidence collected in this work supports the central hypothesis the D-I model: the degree of organic substrate-TiO$_2$ surface interaction plays a crucial role in the kinetics of photocatalytic reactions. Depending on these interactions, the specific organic molecule will be photooxidized by an IT, DT or a combination of both mechanism in different degrees. The mathematical equations proposed by the D-I model accounted for the set of experimental kinetic data collected in this work. The methodology reported here can be used to systematically study the kinetic behavior of different organic substrates and the effects on the reaction rate caused by other types of TiO$_2$ surface modifications different from fluorination.

A comprehensive analysis of literature data about POIE phenomena and isotopic tracing studies of TiO$_2$ photooxidation reactions allowed us to envisage a plausible mechanistic pathway for photocatalytic oxidation reactions that has been overlooked in the past. This pathway involves the participation of the TiO$_2$ surface lattice oxygens (O$_s$) as hole traps, their subsequent incorporation into the photooxidation products, the continuous generation of oxygen vacancies at the TiO$_2$ surface in the course of the photocatalytic process and their healing through dissociative adsorption of O$_2$ and/or H$_2$O to close the catalytic cycle. It is worth noting that unless former mechanistic proposals that assume a "static catalyst surface", our mechanism assumes that the catalytic surface itself is changing and being regenerated in the course of the reaction. This view of the photocatalytic process is more congruent with the findings of SCS on TiO$_2$ surfaces reported in the last decade. Experimental data of TiO$_2$ photooxidation of aromatic compounds under carefully controlled amounts of O$_2$ and/or H$_2$O in the reaction media or using oxygen-isotope-labeled titania (Ti^{18}O$_2$) as catalysts clearly supports this new mechanistic proposal.

Finally, we are convinced that this prominent role assigned to reactive O$_s$ can be systematically used to explain a large body of experimental observations existing in the scientific literature about TiO$_2$ assisted heterogeneous photocatalysis. Nevertheless, further work is required to collect more precise quantitative information about the number of O$_s$ exchanged in the course of a photocatalytic reaction. Moreover, further studies at well defined single crystals of TiO$_2$ rather than nanoparticles are necessary to

elucidate the chemical nature of the O_s exchange in a photocatalytic reaction. This is crucial for the development of new photocatalytic materials with higher amount of reactive O_s, and therefore, higher oxidative efficiency.

CHAPTER 5

ANNEXES

SECTION A

Kinetic Analysis of

Photocatalytic Reactions

Manuscript 1

"Comprehensive Analysis of Kinetics and Mechanisms of TiO$_2$ Photocatalytic Reactions . I) Theoretical approach through the D-I model"

Comprehensive Analysis of Kinetics and Mechanisms of TiO$_2$ Photocatalytic Reactions . I) Theoretical approach through the D-I model

J.F.Montoya[1], J.Peral[1], P. Salvador[1],*

1. Departamento de Química, Universidad Autónoma de Barcelona, 08193, Cerdanyola del Vallés, Spain.

*Corresponding author, E-mail: psalvador@klingon.uab.es

Keywords: photocatalysis; titanium dioxide; interfacial electron transfer mechanisms; photooxidation kinetics; adsorption-desorption equilibrium rupture.

Abstract

The photocatalytic oxidation kinetics of organic species, in both gas phase and liquid semiconductor (sc) suspensions, strongly depends on the electronic interaction strength of substrate species with the sc surface. According to the Direct-Indirect (D-I) model, developed as an alternative to the Langmuir-Hinshelwood (L-H) model (P. Salvador et al., Catalysis Today, 129 (2007) 247.), when chemisorption of dissolved substrate species is not favored and physisorption is the only existing adsorption mechanism, interfacial hole transfer takes place via an indirect transfer (IT) mechanism, the photooxidation rate exponentially depending on the incident photon flux ($v_{ox} = v_{ox}^{IT} \propto \rho^n$), with n=1/2 under high enough photon flux (standard experimental conditions), whatever the substrate concentration, $\left[\left(RH_2 \right)_{aq} \right]$. In contrast, under simultaneous physisorption and chemisorption of substrate species, hole capture takes place via a combination of indirect transfer (IT) and direct transfer (DT) mechanism ($v_{ox} = v_{ox}^{IT} + v_{ox}^{DT}$), with $v_{ox}^{DT} \propto \rho^n$, being n=1 for low enough ρ values, as long as adsorption-desorption equilibrium conditions existing in the dark are maintained under illumination, and monotonically decreasing towards n=0 as ρ increases and adsorption-desorption equilibrium becomes broken. This behaviour invalidates the frequently invoked axiom that the reaction order (exponent n) exclusively depends on the photon flux intensity, being in general n=1 for low ρ values and n=1/2 for high illumination intensities, independently of the nature of the sc-substrate electronic interaction. On the basis of a detailed analysis of the parameter defined as $a = \dfrac{\left(v_{ox} \right)^2}{2 \left[(RH_2)_{aq} \right] \rho}$, an experimental test is developed in order to quantify the influence of both interfacial hole transfer mechanisms DT and IT in the photooxidation kinetics. An estimation of the photon flux critical value where adsorption-desorption equilibrium of chemisorbed substrate species becomes broken and the reaction order starts to decreases from n=1 towards n=0, is presented.

1. Introduction

TiO$_2$ photocatalysis has received an increasing attention during the last 30 years as a solar light assisted potential technology for environmental decontamination via photooxidation of pollutants present both in air [1] and water.[2] However, and in spite that a considerable effort has been done in order to establish mechanistic and kinetic fundamentals existing behind photocatalytic reactions, this objective is still far of being reached.

A handicap in this respect concerns the almost "robotic" use of the classical Langmuir-Hinshewoold (L-H) kinetic model as a suitable tool for the kinetic analysis of photocatalytic reactions.[3-8] Some recognized objections to the use of the L-H model are: (1) the a priori assumption that the adsorption-desorption equilibrium of substrate species existing in the dark is not disturbed under illumination, no mater the substrate concentration and/or photon flux used; (2) the lack of physical meaning of the intervening, L-H kinetic rate constants; (3) the non explicit intervention of the photon flow as an experimental parameter in kinetic expressions, hindering the reaction rate dependence on the photon flux to be predicted; (4) the assumption that the chemical nature of the sc surface is not modified during photocatalytic reactions; (5) the omission of the degree of electronic interaction of substrate species with the semiconductor surface, a parameter strongly affecting photooxidation kinetics, contradicting the experimental evidence shown in the second part of this publication that the photooxidation rate of physisorbed organic species weakly interacting with the TiO$_2$ surface, as it is for instance benzene in organic medium, is far lower than that of strongly chemisorbed molecules, like formic acid in aqueous medium. [9]

On the one hand, the recent application of new techniques to the study of chemical surface reactions at atomic scale, as it is the case of Scanning Tunnelling Microscopy (STM), has provided essential information not only about the role that TiO$_2$ rutile surface defects, like bridging oxygen vacancies, play as chemically active surface centers, but on chemical changes taking place at the TiO$_2$ surface during photocatalytic reactions. [13-15] On the other hand, from UV photoinduced oxygen isotopic exchange (POIE) involving anatase nanoparticles in contact with O$_2$, experimental evidence has

been obtained that two-fold coordinated bridging oxygen atoms $(>O_{br}^{2-})$ of the TiO_2 surface are exchanged with oxygen atoms of oxygen molecules, and that such POIE reactions are blocked in the presence of organic molecules prone to be photooxidized.[16-18]. Moreover, experimental evidence exists that one-fold coordinated bridging oxygen radicals $(-O_{br}^{\cdot-})$ photogenerated via inelastic trapping of valence band free holes (h_f^+) by terminal, two-fold coordinated bridging oxygen ions $(>O_{br}^{2-})$, behave as labile surface oxygen species able to capture electrons from physisorbed molecules via an adiabatic, interfacial charge transfer mechanism, leading in some cases to an oxidation process where bridging oxygen atoms of the TiO_2 surface are incorporated into substrate species. This seems to be the case in the photooxidation of benzene to phenol [19] and 4-chloropenol to catechol and or hydroquinone.[20]

Another stubborn controversy in TiO_2 photocatalysis is that concerning the nature of photoinduced radical species active in the photooxidation of organic substrates in aqueous dissolution. From MIES and UPS spectral analysis of hydrated , well defined TiO_2 rutile surfaces, it has been recently shown that the photooxidation of adsorbed water species, is hindered both thermodynamically and kinetically,[21, 22] contradicting the generalized assumption that besides free OH radicals originated from the electroreduction of dissolved oxygen molecules, the photooxidation of chemisorbed water leads to adsorbed OH radicals acting as primary oxidizing species in TiO_2 photocatalytic reactions. [2, 23-25]

A new, comprehensive approach to TiO_2 photocatalysis should necessarily involve the development of an autoconsistent mechanistic model able to take into account the nature of those physicochemical phenomena behind involved photoreactions. With this aim in mind, during the last years we have developed the Direct-Indirect (D-I) model as an alternative to the L-H model.[5, 26] Depending on the type of electronic interaction of substrate species with the sc surface, the D-I model contemplates two well defined types of interfacial charge transfer mechanisms. On the one hand, for strong electronic interaction (chemisorption) of dissolved substrate species (Lewis basic species) with terminal Ti^{IV} ligands of the TiO_2 surface (Lewis acid sites), the D-I model assumes

that photooxidation is mainly based in an inelastic, interfacial direct transfer (DT) mechanism of photogenerated valence-band (VB) free holes (h_f^+) to Ti^{IV} anchored substrate species. On the other hand, for weak interaction (physisorption) of substrate species with the TiO_2 surface, the D-I model assumes an interfacial indirect transfer (IT) mechanism involving two successive steps: in a first step h_f^+ holes are inelastically trapped by terminal $> O_{br}^{2-}$ ions, with generation of surface $- O_{br}^{·-}$ radicals; in a second step surface trapped holes are isoenergetically transferred to physisorbed substrate species according to the Marcus-Gerischer model for adiabatic electron transfer at the sc-electrolyte interface.[27-29] Involved interfacial charge transfer mechanisms are schematised in Figure 1. IT is the only working mechanism in the absence of chemisorption, as it is the case for benzene,[9] but always coexist with the DT mechanism when chemisorption takes place. Generally DT prevails on IT, although the contribution of both mechanisms can be comparable in some special cases, as will be shown in part 2) of this publication.

In contrast with the L-H model, the D-I model allows to develop photooxidation kinetic expressions where both the photon flux and the substrate concentration are explicitly present, allowing the photooxidation rate dependence on both experimental variables to be predicted. On the one hand, the D-I model rejects the participation of $OH^·$ radicals generated via direct photooxidation of water species chemisorbed at terminal Ti^{IV} ions with h_f^+ holes, considering photogenerated $- O_{br}^{·-}$ radicals as TiO_2 surface active oxidant species. On the other hand, Ti^{IV} surface ions are not only considered as chemisorption sites for substrate species but as trapping sites for conduction band electrons (e_f^-).

Because of the complexity involved in real photocatalytic systems, the applicability of the D-I model to the analysis of experimental kinetic data is not always a simple task. A main problem concerns the influence of adsorption-desorption equilibrium rupture under high enough illumination intensity conditions on the photon flux dependence of

the photooxidation rate, as first raised by Ollis in 2005 [8] and further assumed by the D-I model.[5] An apparent problem of the D-I model concerns the difficulty to discern between DT and IT charge transfer mechanisms from photooxidation kinetic measurements under non-equilibrated adsorption-desorption conditions (high enough illumination intensity). Our objective here is twofold: on the one hand we pretend to get information about the experimental conditions (photon flux and substrate concentration) under which the rupture of the adsorption-desorption equilibrium existing at darkness is broken under illumination, leading to a drastic photooxidation kinetic change in those cases were DT is the prevailing interfacial charge transfer mechanism; on the other hand, we will try to quantify to what extent DT and IT mechanisms contribute to photooxidation reactions. In part 2) of this publication, a comparative photooxidation kinetic analysis of model organic molecules, like benzene and phenol dissolved in acetonitrile, and formic acid , 4-chlorophenol, and phenol dissolved in water will be performed in order to verify the applicability of the D-I model under both equilibrated and non-equilibrated adsorption-desorption conditions.

2.-Interfacial charge transfer mechanisms involved in the D-I model.

a) The IT mechanism

As defined in previous publications, [5, 26] when IT is the only possible electron transfer mechanism between dissolved substrate species and the sc surface, in the absence of chemisorption, the initial photooxidation rate dependence on the photon flux and substrate concentration is defined by the expression:

$v_{ox} =$

$$v_{ox}^{IT} = \frac{d\left[(RH_2)_{aq}\right]}{dt}\Bigg|_{(t\to0)} = \left[\left(a^{IT}\left[(RH_2)_{aq}\right]\right)^2 + 2a^{IT}k_0\rho\left[(RH_2)_{aq}\right]\right]^{1/2} - a^{IT}\left[(RH_2)_{aq}\right]$$

(1)

, where $a^{IT} = \dfrac{k_{ox}^{IT} k_{red}^{'} [O_2]_{aq}}{4k_{r,1}^{'}}$ is a constant parameter with real physical meaning, that

depends on the kinetic rate constants k_{ox}^{IT} and $k_{red}^{'}$ associated to the adiabatic electron

transfer mechanism from physisorbed RH_2 molecules to $-O_{br}^{-}$ radicals and from

terminal Ti^{III} ions to dissolved O_2 molecules, respectively, as well on the $k_{r,1}^{'}$ rate

constant for recombination of e_f^{-} electrons with $-O_{br}^{-}$ surface trapped holes;

$\left[(RH_2)_{aq} \right]$ represents the concentration of dissolved substrate species, either in water or

in any other solvent, and ρ the incident photon flux. For high enough illumination

intensities within the standard experimental range ($\rho \geq 1 \times 10^{15}$ photon/s), such that

$2a^{IT} k_0 \rho \left[(RH_2)_{aq} \right] \gg \left(a^{IT} \left[(RH_2)_{aq} \right] \right)^2$, i.e., for $\rho \gg \dfrac{a^{IT} \left[(RH_2)_{aq} \right]}{2k_0}$, eq. (1) becomes:

$$v_{ox}^{IT} \approx \left(2k_0 a^{IT} \left[(RH_2)_{aq} \right] \right)^{1/2} \rho^{1/2} \qquad (2)$$

Note that according to (2), v_{ox}^{IT} vs. $\rho^{1/2}$ plot is linear above a critical ρ_c value; below ρ_c

the linearity is lost and $\dfrac{dv_{ox}^{IT}}{d\rho^{1/2}}$ increases as ρ decreases, in such a way that $v_{ox}^{IT} = 0$ for

$\rho = 0$. This behaviour will be further analyzed

b) The DT mechanism

For strong electronic interaction of substrate species with terminal Ti^{IV} atoms, i.e., under

chemisorption conditions,, DT uses to be the prevailing photooxidation mechanism.

Furthermore, if equilibrated adsorption-desorption of substrate species is fulfilled, the

photooxidation rate then becomes: [5, 26]

$$v_{ox} = v_{ox}^{DT} = \dfrac{d[(RH_2)ads]}{dt}\bigg|_{(t\to0)} = \dfrac{k_{ox}^{DT} \left[(RH_2)_{ads} \right] k_0 \rho}{k_1^{'} \left[O_{br}^{2-} \right] + k_{ox}^{DT} \left[(RH_2)_{ads} \right]} \qquad (3)$$

, where the concentration of chemisorbed substrate species, $\lfloor (RH_2)_{ads} \rfloor$, is described by the appropriate adsorption isotherm.

Representations of v_{ox}^{DT} *vs.* ρ are shown in Figure 3. As can be seen, the main difference between eq. (2) and eq. (3) concerns the predicted photon flux reaction order n (photon flux exponent value): n=1/2 for v_{ox}^{IT} and $\rho > 1x10^{10}$ .photons/ s and n=1 for v_{ox}^{DT} and for a ρ lower than a limiting value depending on the system, , in such a way that a clear experimental distinction between IT and DT as prevailing photooxidation mechanism is an easy task from a simple analysis of the v_{ox} *vs.* ρ plot.

A typical example of DT photooxidation kinetics (i.e., n=1) is that corresponding to water dissolved formic acid, a substrate able to become strongly anchored to the TiO_2 surface in competition with water molecules. [14,30] Literature examples where IT is the prevailing mechanism (i.e., n=1/2) is the photopolymerization of methyl metacrylate on ZnO,[31] as well as the photooxidation of organic species like chloroform, [32] and methyl viologen in aqueous dissolution.[33]

Against the D-I model assumption that the reaction order strongly depends on the type of sc-substrate electronic interaction, it is generally admitted in photocatalysis that the value of the exponent n exclusively depends on the photon flux intensity, being in general n=1 for low enough ρ values and n=1/2 for high enough illumination intensity. [25] This assumption contradicts, for instance, the experimental evidence that within a similar photon flux range ($10^{-9} < \rho < 10^{-5}$ Einstein L^{-1} min^{-1}), it is n=1 for formic acid,[30] while $n = \dfrac{1}{2}$ for chloroform. [32]

In spite that the D-I model contemplates two well defined electron transfer mechanisms, DT and IT, where n=1 and $n = \dfrac{1}{2}$, respectively, as we will show in part 2) of this publication there are cases where 0.5<n<1, an apparent incongruence attributable to the existence of adsorption-desorption equilibrium rupture in cases where chemisorption exists and $v_{ox}^{DT} \geq v_{ox}^{IT}$.

3.- DT photooxidation kinetics under non-equilibrated adsorption-desorption of chemisorbed substrate species: photooxidation rate dependence on photon flux and substrate concentration.

Usually, photocatalytic kinetic models, including the LH model, have been developed under the assumption that the adsorption-desorption equilibrium existing in the dark is not perturbed under illumination, an assumption only valid under low enough illumination intensity. However, any auto-consistent, photocatalytic kinetic model should take into account that the steady state concentration of chemisorbed substrate species stongly depends on the photon flux. According to the LH model, and considering that $OH^.$ radicals generated from the photooxidation of water molecules behave as primary photooxidizing species, Ollis recently developed a pseudo-steady-state kinetic analysis based on the existence of non-equilibrated adsorption of reactants.[8] The author arrives to the following expression for the photon flux dependence of the photooxidation rate (r):

$$r = \frac{k_{cat}^{app} k_{diss}^{app} [RH_2]_{aq}}{k_{diss}^{app} + [RH_2]_{aq}} \tag{4}$$

While in eq. (4) the concentration of dissolved substrate species, $[RH_2]_{aq}$, explicitly appears as an independent experimental variable, the photon flux only appears implicit in the apparent rate constant, k_{cat}^{app}, and in the dissociation constant, k_{diss}^{app}, both being considered to depend on the photon flux. The fact that the photon flux is not explicitly present in eq. (4) represents an important drawback of Ollis analysis. This problem is avoided when the pseudo-steady-state approach proposed by Ollis is incorporated into the D-I model, and h_f^+ holes, instead of $OH^.$ radicals generated from the photooxidation of TiO_2 adsorbed water molecules, are considered as primary photooxidizing species of chemisorbed substrate molecules. The following explicit photon flux dependent expression is then obtained for the concentration of adsorbed substrate species:[5]

$$\left[\left(\mathrm{RH_2}\right)_{ads}\right] = \cfrac{K_{ads}\mathrm{b}\left[\left(\mathrm{RH_2}\right)_{aq}\right]}{1 + K_{ads}\left[\left(\mathrm{RH_2}\right)_{aq}\right] + \cfrac{\mathrm{k_{ox}^{DT}}}{\mathrm{k_{-1}}}\cfrac{\mathrm{k_0'}\rho}{\mathrm{k_1'}\left[\mathrm{O_{br}^{2-}}\right] + \mathrm{k_{ox}^{DT}}\left[\left(\mathrm{RH_2}\right)_{ads}\right]}}$$

(5)

, where $\mathrm{k_{-1}}$ is the diffusion constant of substrate species from the sc surface towards the solution and $\mathrm{k_0'}$ is an empirical constant mainly depending on the nature of the catalyst and the reactor geometry, the remaining parameters being as previouly deffined. A detailed description of the obtention of eq.(5) is given in the Appendix.

As pointed out in Figure 1, and against the thesis recently defended by S. Valencia et al.,[34] the back reaction of electroreduction of photogenerated $\mathrm{RH^{\cdot}}$ radicals to $\mathrm{RH_2}$ molecules is not considered in obtaining eq.(5); as much as we are dealing with initial photooxidation rates and $\mathrm{RH^{\cdot}}$ concentration is negligible vs. $\mathrm{RH_2}$ concentration, such a back reaction cannot have any influence on the adsorption-desorption equilibrium breaking taking place under high enough illumination intensities.

Note that for low enough ρ values, such that $\cfrac{\mathrm{k_{ox}^{DT}}}{\mathrm{k_{-1}}}\cfrac{\mathrm{k_0'}\rho}{\mathrm{k_1'}\left[\mathrm{O_{br}^{2-}}\right] + \mathrm{k_{ox}^{d}}\left[\left(\mathrm{RH_2}\right)_{ads}\right]} \ll 1 + K_{ads}\left[\left(RH_2\right)_{aq}\right]$, i.e., under equilibrated adsorption-desorption conditions, eq.(5) becomes:

$$\left[RH_2\right]_{ads} =$$

$$\cfrac{K_{ads}b\left[RH_2\right]_{aq}k_1'\left[O_{br}^{2-}\right] + K_{ads}b\left[RH_2\right]_{aq}k_{ox}^{DT}\left[RH_2\right]_{ads}}{K_{ads}k_1'\left[O_{br}^{2-}\right]\left[RH_2\right]_{aq} + k_1'\left[O_{br}^{2-}\right] + K_{ads}\left[RH_2\right]_{aq}k_{ox}^{DT}\left[RH_2\right]_{ads} + k_{ox}^{DT}\left[RH_2\right]_{ads} + \cfrac{k_{ox}^{DT}}{k_{-1}}k_0'\rho}$$ (6)

; eq.(6) can be further transformed into the second order equation :

$$\left[RH_2\right]_{ads}^2\left(K_{ads}\left[RH_2\right]_{aq}k_{ox}^{DT} + k_{ox}^{DT}\right) +$$

$$\left[RH_2\right]_{ads}\left(K_{ads}k_1'\left[O_{br}^{2-}\right]\left[RH_2\right]_{aq} + k_1'\left[O_{br}^{2-}\right] + \cfrac{k_{ox}^{DT}}{k_{-1}}k_0'\rho - K_{ads}b\left[RH_2\right]_{aq}k_{ox}^{DT}\right)$$ (7)

$$-K_{ads}b\left[RH_2\right]_{aq}k_1'\left[O_{br}^{2-}\right] = 0$$

. The only solution with physical meaning of eq. (7) is that corresponding to the expression:

$$\left[\left(RH_2\right)_{ads}\right]=\frac{-\left(X\rho-H\right)+\left\{\left(X\rho\text{-}H\right)^2+A\right\}^{1/2}}{L} \qquad (8)$$

, where $\quad X=\dfrac{k_0^{'}k_{ox}^{DT}}{k_{-1}}, \quad H=\gamma b-\alpha-\beta, \quad L=2(\gamma+k_{ox}^{DT}) \quad$ and $\quad A=4\alpha b(\gamma+k_{ox}^{DT}),$ being

$$\alpha=K_{ads}k_1^{'}\left[O_{br}^{2-}\right]\left[\left(RH_2\right)_{aq}\right] \quad, \qquad \beta=k_1^{'}\left[O_{br}^{2-}\right] \qquad \text{and} \qquad \gamma=K_{ads}k_{ox}^{DT}\left[\left(RH_2\right)_{aq}\right].$$

Importantly, the parameters with real physical meaning intervening in eq. (8) have well deffined values and cannot be considered as adjustable parameters .

Note that, as expected, for low enough ρ values, such that $A\gg(X\rho-H)^2,$ the adsorption-desorption equilibrium is re-established and $\left[\left(RH_2\right)_{ads}\right]$ becomes photon flux independent..

Analysis of parameters involved in eq. (8)

Figure 3 illustrates the influence of parameters $k_{ox}^{DT},\ k_1^{'}\left[O_{br}^{2-}\right],K_{ads},\ \left[\left(RH_2\right)aq\right]$ and b, on the photon flux dependence of $\left[\left(RH_2\right)_{ads}\right],$ as obtained from eq. (8). In general, it can be seen how the adsorption-desorption equilibrium existing in the dark (ρ =0) becomes broken as ρ increases, leading to a pronounced monotonous decrease of both $\left[\left(RH_2\right)_{ads}\right]$ and $\dfrac{d\left[\left(RH_2\right)_{ads}\right]}{d\rho}$. Other relevant features of figure 2 are the following: 1) for constant ρ, $\left[\left(RH_2\right)_{ads}\right]$ is observed to increase as $K_{ads},\ k_1^{'}\left[O_{br}^{2-}\right]$ and b increase, while it is observed to decrease as k_{ox}^{DT} increases; 2) the decrease of k_{ox}^{DT} and b leads to a clear decrease of $\dfrac{d\left[\left(RH_2\right)_{ads}\right]}{d\rho},$ indicating that adsorption is the limiting step in DT photooxidation of substrate species; the opposite tendency is observed when K_{ads} and $k_1^{'}\left[O_{br}^{2-}\right]$ decrease.

Figure 4 shows the photon flux influence on the adsorption isotherms ($\left[(RH_2)_{ads}\right]$ vs. $\left[(RH_2)_{aq}\right]$ plot) under broken adsorption-desorption equilibrium conditions. As expected, an increasing deviation from the adsorption isotherm at darkness ($\rho=0$) is observed as the photon flow grows up. Further, $\dfrac{d[RH_2]_{ads}}{d[RH_2]_{aq}}$ is observed to increase for low enough $[RH_2]_{aq}$ values, while it decreases for high enough $[RH_2]_{aq}$ values; such a change in tendency of $\dfrac{d[RH_2]_{ads}}{d[RH_2]_{aq}}$, which defines the transition from equilibrate to non-equilibrated adsorption-desorption of substrate species, becomes shifted towards higher $[RH_2]_{aq}$ values as the photon flux increases.

The DT photooxidation rate under non-equilibrated adsorption-desorption conditions, expressed by eq. (9), is obtained by substituting into eq. (3) the expression for $\left[(RH_2)_{ads}\right]$ in eq. (8)

$$v_{ox}^{DT} = \frac{k_{ox}^{DT} \dfrac{\left\{(X\rho\text{-}H)^2 + A\right\}^{1/2} - (X\rho - H)}{L}\rho}{k_1'\left[O_{br}^{2-}\right] + k_{ox}^{DT} \dfrac{\left\{(X\rho\text{-}H)^2 + A\right\}^{1/2} - (X\rho - H)}{L}} \tag{9}$$

As expected, under low enough ρ values, such that

$$(X\rho - H)^2 \ll A \tag{10}$$

, when equilibrated adsorption-desorption is recovered, a linear dependence of v_{ox}^{DT} on the photon flux is predicted by eq. (9).

Since it is in general $k_{ox}^{DT} \ll k_1'\left[O_{br}^-\right]$ and $\left[(RH_2)_{ads}\right] \ll \left[O_{br}^-\right]$, it must be expected that $k_{ox}^{DT}\left[(RH_2)_{ads}\right] \ll k_1'\left[O_{br}^-\right]$, in such a way that eq. (9) leads to the following expression for v_{ox}^{DT}:

$$v_{ox}^{DT} \approx \frac{k_{ox}^{DT}}{k_1'\left[O_{br}^-\right]}\left[\frac{\left\{X^2\rho^4 - 2XH\rho^3 + H^2\rho^2 + A\rho^2\right\}^{1/2} - X\rho^2 + H\rho}{L}\right] \tag{9_1}$$

For low enough ρ values, such that

$$H^2\rho^2 >> X^2\rho^4, 2XH\rho^3, A\rho^2 \; ; \; A\rho^2 >> X^2\rho^4, 2XH\rho^3 \text{ and } |H\rho >>|X\rho^2 \qquad (9_2)$$

, eq. (9_1) becomes:

$$v_{ox}^{DT} \approx \frac{k_{ox}^{DT}}{k_1'[O_{br}^-]} \frac{\left\{H^2 + A^2\right\}^{1/2} + H}{L} \rho^1 \qquad (9_3)$$

, indicating that a photooxidation rate order n=1 prevails under low enough illumination intensity. In contrast, as ρ increases and the adsorption-desorption equilibrium becomes broken, so that $X^2\rho^4 > 2XH\rho^3 > H^2\rho^2 > A\rho^2$, eq. (9_3) is no valid anymore, the lineal dependence of v_{ox}^{DT} on ρ disappears and $\dfrac{d\, v_{ox}^{DT}}{d\rho}$ starts to progressively decrease, in such a way that $\dfrac{d\, v_{ox}^{DT}}{d\rho} \to 0$ (v_{ox}^{DT} approaches a constant value), which is equivalent to say that $v_{ox}^{DT} \propto \rho^0$ (a zero photooxidation rate order is reached). But considering that n=1 for low enough ρ, while n=0 under high enough ρ, a reaction order $0 \leq n \leq 1$ is expected for intermediate photon flux values, contradicting the frequently invoked universal axiom that independently of the nature of the sc-substrate electronic interaction, the photooxidation rate order exclusively depends on the photon flux intensity, being in general n=1 and n=1/2 for low enough and high illumination intensities, respectively. This behaviour is illustrated in the double exponential plot of v_{ox}^{DT} vs. ρ , for variable substrate concentration, shown in Figure 5A in logaritmic scale. Interestingly, it can be seen that the transition from n=1 towards n=0 is shifted towards higher ρ values as $[RH_2]_{aq}$ increases. For comparison, a similar plot of v_{ox}^{IT} vs. ρ for variable substrate concentration, according to eq.(2), is shown in Figure 5B. As expected, for high enough illumination intensity ($\rho \geq 10^{13} cm^{-2} s^{-1}$), $\log v_{ox}^{IT}$ depends linearly on ρ, in agreement with eq. (2)

4.- The $\dfrac{(v_{ox})^2}{2\rho\left[(RH_2)_{aq}\right]}$ vs. ρ plot under variable substrate concentration**:** a simple experimental test for differentiating DT from IT mechanism.

For high enough illumination intensity values, within the standard experimental range, it can be written according to eq. (2) that:

$$a^{IT} \equiv \frac{k_{ox}^{IT} k_{red}'\left[O_2\right]_{aq}}{4k_{r,1}'} = \text{const} = \frac{\left(v_{ox}^{IT}\right)^2}{2\left[(RH_2)_{aq}\right]\rho} \qquad (10)$$

, indicating that when the photooxidation kinetics is governed by an IT mechanism $\dfrac{\left(v_{ox}^{IT}\right)^2}{2\left[(RH_2)_{aq}\right]\rho}$ does not depend on the photon flux, whatever the substrate concentration.

.- *The a_{ap}^{DT} parameter.*

By analogy with the a^{IT} parameter for the IT mechanism, defined by eq. (10), the following apparent a_{ap}^{DT} parameter can be defined for the DT mechanism :

$$a_{ap}^{DT} = \frac{\left(v_{ox}^{DT}\right)^2}{2\left[(RH_2)_{aq}\right]\rho} \qquad (11)$$

, such that

$$\frac{d\,a_{ap}^{DT}}{d\rho} = \frac{1}{2\rho\left[(RH_2)_{aq}\right]}\left[2v_{ox}^{DT}\frac{d(v_{ox}^{DT})}{d\rho} - \frac{\left(v_{ox}^{DT}\right)^2}{\rho}\right] \qquad (12)$$

In congruence with the admitted existence of a stronger electronic interaction of terminal Ti^{IV} lattice cations with $> O_{br}^{2-}$ bridging oxygen anions than with $(RH_2)_{aq}$,

dissolved substrate species, it is reasonable to assume that $k_1^{'} \gg k_{ox}^{d}$, and therefore that

$k_1^{'}\left[O_{br}^{2-}\right] \gg k_{ox}^{d}\left[(RH_2)_{ads}\right]$, eq. (3) becoming:

$$v_{ox}^{DT} = \frac{k_{ox}^{DT}\left[(RH_2)_{ads}\right]\,\rho}{k_1^{'}\left[O_{br}^{2-}\right]}$$

, so that

$$\frac{(v_{ox}^{DT})^2}{\rho} \approx \left(\frac{k_{ox}^{DT}\left[(RH_2)_{ads}\right]}{k_1^{'}\left[O_{br}^{2-}\right]}\right)^2 \rho \qquad (13)$$

. Similarly, eqs.(12) and (13) can be transformed into eq.(12_1) and eq.(13_1),

respectively, $a_{ap}^{DT} \approx \dfrac{1}{2\left[(RH_2)_{aq}\right]}\left(\dfrac{k_{ox}^{DT}\left[(RH_2)_{ads}\right]}{k_1^{'}\left[O_{br}^{2-}\right]}\right)^2 \rho \qquad (12_1)$

$\dfrac{d\,a_{ap}^{DT}}{d\,\rho} \approx \dfrac{\left(k_{ox}^{DT}\right)^2}{2\left[(RH_2)_{aq}\right]\left(k_1^{'}\left[O_{br}^{2-}\right]\right)^2}\left\{\left[(RH_2)_{ads}\right]^2 + 2\rho\left[(RH_2)_{ads}\right]\dfrac{d\left[(RH_2)_{ads}\right]}{d\rho}\right\} \qquad (13_1)$

Two cases can be considered:

 a) Low enough photon flux, such that $(X\rho - H)^2 \ll A$ in eq.(8) and

$\left[(RH_2)_{ads}\right]$ does not depend on the photon flux. Moreover, according to eq. (12_1)

a_{ap}^{DT} does depend linearly on ρ and according to eq. (13_1) $\dfrac{d\,a_{ap}^{DT}}{d\rho} > 0$.

 b) High enough photon flux, such that $(X\rho - H)^2 \gg A$ in eq. (8).

On the one hand we know from Fig. 2 that $\left[(RH_2)_{ads}\right]$ decreases as ρ increases; on the

other hand, from eq. (3) the following relationships can be obtained

$$\frac{d\left(v_{ox}^{DT}\right)}{d\rho} \approx \frac{k_{ox}^{DT}}{k_1'\left[O_{br}^{2-}\right]}\left(\left[(RH_2)_{ads}\right]+\rho\frac{d\left[(RH_2)_{ads}\right]}{d\rho}\right) \tag{14}$$

$$, \; v_{ox}^{DT}\frac{d\left(v_{ox}^{DT}\right)}{d\rho} \approx \left(\frac{k_{ox}^{DT}}{k_1'\left[O_{br}^{2-}\right]}\right)^2\left[(RH_2)_{ads}\right]\rho\left(\left[(RH_2)_{ads}\right]+\rho\frac{d\left[(RH_2)_{ads}\right]}{d\rho}\right) \tag{15}$$

$$\text{and} \quad \frac{\left(v_{ox}^{DT}\right)^2}{\rho} \approx \left(\frac{k_{ox}^{DT}}{k_1'\left[O_{br}^{2-}\right]}\right)^2\left[(RH_2)_{ads}\right]^2\rho \tag{16}$$

By substituting eq. (14) and eq. (16) into eq.(12), the following expression for $\dfrac{d\,a_{ap}^{DT}}{d\rho}$ is

inferred:

$$\frac{d\,a_{ap}^{DT}}{d\rho} = \frac{\left[(RH_2)_{ads}\right]}{2\left[(RH_2)_{aq}\right]}\left(\frac{k_{ox}^{DT}}{k_1'\left[O_{br}^{2-}\right]}\right)^2\left(\left[(RH_2)_{ads}\right]+2\rho\frac{d\left[(RH_2)_{ads}\right]}{d\rho}\right) \tag{17}$$

Let us analyze eq. (~~19~~ 17) in detail. Since under non-equilibrated adsorption-desorption conditions (i.e., for high enough photon flux) $\dfrac{d\left[(RH_2)_{ads}\right]}{d\rho}$<0 (see Figure 2),

eq. (17) allows to say that $\dfrac{d\,a_{ap}^{DT}}{d\rho}$<0 for $\left[(RH_2)_{ads}\right]< 2\rho\dfrac{d\left[(RH_2)_{ads}\right]}{d\rho}$. In contrast,

under equilibrated adsorption-desorption conditions (i.e., for low enough photon flux)

$\dfrac{d\,a_{ap}^{DT}}{d\rho}$>0. Therefore, eq. (17) necessarily predicts the existence of an intermediate

photon flux value where $\dfrac{d\,a_{ap}^{DT}}{d\rho}$=0, or in other words, $a_{ap}^{DT}(\rho)$ must go through a

maximum for a photon flux $\rho_{max} = \left| \dfrac{\left[(RH_2)_{ads} \right]}{2 \dfrac{d\left[(RH_2)_{ads} \right]}{d\rho}} \right|$ (18),   such that

$$\left[(RH_2)_{ads} \right] = \left| 2\rho_{max} \dfrac{d\left[(RH_2)_{ads} \right]}{d\rho} \right|.$$

Moreover, Fig. 3 indicates that $\left[(RH_2)_{ads} \right]$ increases, while $\dfrac{d\left[(RH_2)_{ads} \right]}{d\rho}$ decreases,

when $\left[(RH_2)_{aq} \right]$ increases, which means according to eq. (18) that the ρ_{max} should

also increase with substrate concentration. In conclusion, for low enough ρ values,

under equilibrated adsorption-desorption conditions, we find that $a_{ap}^{DT} \propto \rho^n$ with n=1

(i.e., a_{ap}^{DT} increases linearly with the photon flux). However, when high enough ρ

values are reached and equilibrated adsorption-desorption is broken, the lineal

dependence of a_{ap}^{DT} on ρ is lost, a_{ap}^{DT} reaches a maximum value for $\rho = \rho_{max}$ and

starts to decrease for $\rho > \rho_{max}$. Moreover, under constant photon flux, a_{ap}^{DT} is

found to decreases when $\left[(RH_2)_{aq} \right]$ increases, while ρ_{max} is observed to shift towards

higher photon flux values. This is in fact the behaviour observed in figure 6 for the

dependence of a_{ap}^{DT} on ρ, under variable $\left[(RH_2)_{aq} \right]$, as obtained by combining eq.(8)

and eq.(12_1).

    .- *The* a_{ap}^{IT+DT} *parameter.*

Let us now consider those cases where both mechanisms IT and DT contribute to the

photooxidation of substrate species, so that $v_{ox} = v_{ox}^{IT} + v_{ox}^{DT}$, a common situation when

chemisorption of substrate species exist.

It can be defined in this case

$$a_{ap}^{IT+DT} = \frac{\left(v_{ox}^{IT}+v_{ox}^{DT}\right)^2}{2\rho[RH_2]_{aq}} = \frac{\left(v_{ox}^{IT}\right)^2+\left(v_{ox}^{DT}\right)^2+2v_{ox}^{IT}\,v_{ox}^{DT}}{2\rho\left[(RH)_{aq}\right]} = a^{IT}+a_{ap}^{DT}+\frac{v_{ox}^{IT}\,v_{ox}^{DT}}{\rho\left[(RH)_{aq}\right]} \qquad (19)$$

Obviously, parameters a^{IT} and a_{ap}^{DT}, described respectively by eqs. (10) and (11),

appear as two extreme cases of eq.(19), $a_{ap}^{IT+DT} \approx \frac{\left(v_{ox}^{IT}\right)^2}{2\rho\left[RH_2\right]_{ads}} \equiv a^{IT}$ for $v_{ox}^{IT} >> v_{ox}^{DT}$ and

$a_{ap}^{IT+DT} \approx \frac{\left(v_{ox}^{DT}\right)^2}{2\rho\left[RH_2\right]_{ads}} \equiv a_{ap}^{DT}$ for $v_{ox}^{IT} << v_{ox}^{DT}$. Figure 7 shows the influence of a^{IT} on the

a_{ap}^{IT+DT} *vs.* ρ plot, under constant value of the concentration of substrate species

$\left(\left[(RH_2)_{aq}\right]=5x10^{17}\ cm^{-3}\right)$ and other parameters involved in eq. (19); a_{ap}^{DT} is shown for

comparison. It can be seen that the qualitative behaviour is the same of that observed in

Figure 8. This demonstrates that the indirect transfer mechanism does not change the

foregoing tendencies.

5.- Conclusions

A) In the absence of chemisorption the photooxidation of substrate species exclusively

takes place via an IT mechanism, the photooxidation rate under high enough

illumination intensity (standard experimental conditions) being $v_{ox} \equiv v_{ox}^{IT} \propto \rho^{1/2}$. B)

When chemisorption of substrate species takes place and DT prevails on IT,

i.e., $v_{ox}^{DT} >> v_{ox}^{IT}$, it is $v_{ox} \equiv v_{ox}^{DT} \propto \rho^1$ for low enough illumination intensity where

equilibrated adsorption-desorption conditions takes place; in contrast, under high

enough illumination intensity, when adsorption-desorption equilibrium rupture is

induced, the surface concentration of sc adsorbed substrate species is found to decrease

with ρ at the same time that the photooxidation reaction order decreases from n=1

towards n=0 as ρ increases, in such a way that unambiguous differentiation between

the DT and the IT mechanism is not always possible. C) The analysis of the photon flux and substrate concentration dependence of the experimental parameter defined as

$$a = \frac{\left(v_{ox}\right)^2}{2\left[\left(RH_2\right)_{aq}\right]\rho}$$ allows to unequivocally determine the nature of the prevailing

photooxidation mechanism taking place at the sc-electrolyte/ interface during the photocatalytic reaction, DT, IT or a combination of both. So, in the absence of chemisorption (physisorption is the only existing adsorption mechanism), the parameter a is found to be independent of both ρ and $\left[\left(RH_2\right)_{aq}\right]$; however, when chemisorption and physisorption coexist and DT is not negligible vs. IT ($v_{ox}^{DT} \geq v_{ox}^{IT}$), the parameter a appears to increase linearly with the photon flux for low enough ρ values, as long as the adsorption-desorption equilibrium existing in the dark is maintained under illumination; however, as the photon flux increases a critical photon flux value, ρ_{max}, is found, where $\frac{d\,a}{d\rho}=0$, indicating that parameter a goes through a maximum for $\rho = \rho_{max}$ (i.e., $\frac{d\,a}{d\rho}>0$ for $\rho < \rho_{max}$ while $\frac{d\,a}{d\rho}<0$ for $\rho > \rho_{max.}$), finally, ρ_{max} value is found to increase as $\left[\left(RH_2\right)_{aq}\right]$ increases.

References

[1]   J. Peral, X. Domenech, D. F. Ollis, *J. Chem. Technol. Biotechnol.* **1997**, 70, 117.

[2]   M. R. Hoffmann, S. T. Martin, W. Choi, D. W. Bahnemann, *Chem. Rev.* **1995**, 95, 69.

[3]   A. V. Emeline, V. K. Ryabchuk, N. Serpone, *J. Phys. Chem.B* **2005**, 109, 18515.

[4]   D. Friedmann, C. Mendive, D. Bahnemann, *Appl. Catal. B: Environ.* **2010**, 99, 398.

[5]   D. Monllor-Satoca, R. Gomez, M. Gonzalez-Hidalgo, P. Salvador, *Catalysis Today* **2007**, 129, 247.

[6]   B. Ohtani, *Chemistry Letters* **2008,** 37, 216.

[7]   C.Turchi, D. Ollis, *J.Catal.,* **1990**, 122, 178.

[8]   D. Ollis, *J. Phys. Chem. B* **2005**, 109, 2439.

[9]   J. Zhou, S. Dag, S. D. Senanayake, B. C. Hathorn, S. V. Kalinin, V. Meunier, D. R. Mullins, S. H. Overbury, A. P. Baddorf, *Phys.Rev.B* **2006,** 74, 125318.

[10] T. D. Bui, A. Kimura, S. Ikeda, M. Matsumura, *App. Cat. B: Environ.* **2010,** 94, 186.

[11] H. Park, W. Choi, *Cat. Today* **2005,** 101, 291.

[12] T. D. Bui, A. Kimura, S. Ikeda, M. Matsumura, *J Am. Chem. Soc.* **2010,** 132, 8453..

[13] T. L. Thompson, J. T. Yates, *Chem. Rev.* **2006**, 106, 4428.

[14] C. L. Pang, R. Lindsay, G. Thornton*, Chem. Soc. Rev.* **2008**, 37, 2328.

[15] F. Besenbacher, J. V. Lauritsen, T. R. Linderoth, E. Lµgsgaard, R. T. Vang, S. Wendt, *Surf. Sci* **2009,** 603, 1315.

[16] H.Courbon, M.Formenti, P.Pichat, *J.Phys.Chem.* **1977,** 81, 550.

[17] P.Pichat, H.Courbon, R.Enriquez, T.Y.Tan, R.Amal, *Res.Chem.Intermed.* **2007,** 33, 239.

[18] J.F.Montoya, J.Peral, P.Salvador, *Chem.Phys.Chem.***2011**,12,901.

[19] J.F.Montoya, J.Peral, P.Salvador, (SPEA 7).

[20] J.F.Montoya, J.Peral, P.Salvador, *J.Photochem. Photobiol. A: Chem.* **2010**, 210, 215.

[21] P. Salvador, *J.Phys. Chem. C* **2007**, 111, 17038.

[22] A. Imanishi, T. Okamura, N. Ohashi, R. Nakamura, Y. Nakato, *J. Am. Chem. Soc*. **2007**, 129, 11569.

[23] P.Pichat, *Appl. Catal B: Environ.* **2010**, 99, 428.

[24] X. Zhang, D.A. Tryk, A. Fujishima, *Surf. Sci. Rep.* **2008,** 63, 515.

[25] S.Malato, P.Fernandez Ibañez, M.I.Maldonado, J.Blanco, W.Gernjak, *Cat. Today* **2009**, 147,1.

[26] T. L. Villarreal, R. Gomez, M. Gonzalez, P. Salvador, *J. Phys. Chem. B* **2004,** 108, 20278.

[27] R.H. Marcus, *J. Chem. Phys.* **1956,** 24, 966.

[28] H. Gerischer in "Advances in Electrochemistry and Electrochemical Engineering", vol. I, p. 139.; ed: P. Delahay; Interscience, New York, 1961.

[29] H. Gerischer, *Surf. Sci.* **1969,** 18, 97.

[30] J. F. Montoya, J. A. Velasquez, P. Salvador, *Appl. Catal. B: Environ.* **2009,** 88, 50

[31] A.J.Hoffman, H.Yee, G. Mills, M.R. Hoffmann, *J.Phys.Chem.* **1992**, 96,5540

[32] C.Kormann, D.W.Bahnemann, M.R.Hoffmann, *Environ.Sci.Technol.* **1991,** 25, 494

[33] I.N.Martinov, E.N.Savinov, *J.Photochem.Photobiol. A : Chem.* **2000,** 134, 219.

[34] S.Valencia, F.Cataño, L.Rios, G.Restrepo, J.Martín, *Appl. Catal. B: Environ.* **2011, 111,** 300.

[35] J. F. Montoya, J.Peral, P. Salvador, *Appl. Catal. B: Environ.* **2012**, 111, 649

Appendix

Ollis proposes eq. (A1) to describe the photooxidation rate of adsorbed substrate species onto the sc surface under pseudo steady-state, non-equilibrated adsorption-desorption conditions [8]

$$\frac{d\theta_A}{dt} = k_1 \left[RH_2 \right]_{aq} (1-\theta_A) - k_{-1}\theta_A - k_{ox}^{DT}\theta_A = 0 \tag{A1}$$

, where θ_A represents the fraction of semiconductor surface sites covered with substrate species, while and k_1 and k_{-1} are the respective diffusion constants of dissolved species from the sc surface towards the electrolyte bulk and viceversa.

From eq. (A1) the following expression is obtained for θ_A:

$$\theta_A = \frac{k_1 \left[RH_2 \right]_{aq}}{k_1 \left[RH_2 \right]_{aq} + k_{-1} + k_{ox}^{DT}} \tag{A2}$$

But considering a L-H isotherm type for the adsorption of substrate species and taking into account that

$$v_{ox} = -\frac{d\left[\left(RH_2 \right)_{ads} \right]}{dt} = k_{LH}\theta_A \tag{A3}$$

, where k_{LH} represents the L-H apparent kinetic constant, the following expression is obtained for the photooxidation rate,

$$v_{ox} = k_{LH} \frac{\frac{k_1}{k_{-1}}\left[(RH_2)_{aq}\right]}{\frac{k_1}{k_{-1}}\left[(RH_2)_{aq}\right] + \frac{k_{LH}}{k_{-1}}} \qquad (A4)$$

Finally, considering that $\frac{k_1}{k_{-1}} = (K_{ads})_{dark}$, the adsorption constant of substrate species at

darkness, the following equation is obtained:

$$v_{ox} = k_{LH} \frac{(k_{ads})_{dark}\left[(RH_2)_{aq}\right]}{(k_{ads})_{dark}\left[(RH_2)_{aq}\right] + \frac{k_{LH}}{k_{-1}}} \qquad (A5)$$

Eq. (A5), describing Ollis modified version of the photocatalytic L-H model under non-equilibrated adsorption-desorption conditions, presents significant drawbacks. On the one hand it does not take into account the degree of electronic interaction (chemisorption or physisorption) existing between substrate species and the sc surface; on the other hand, $OH^{\cdot}$ radicals generated from the direct photooxidation of water molecules, are considered as primary photooxidizing species,[7,8] which is a questionable hypothesis.[21]

Eq. (A5) can be adapted to the DT mechanism of the D-I model under two premises:[5] 1) the existence of strong electronic interaction (chemisorption) of substrate species with Ti_s^{IV} ions of the TiO_2 surface, 2) oxidizing species participating in the

photooxidation process are not photogenerated $OH^{\cdot}$ radicals, as assumed by Ollis, but valence band free holes (h_f^+), in such a way that DT photooxidation rate is described as $v_{ox}^{DT} = k_{ox}^{DT}\left[h_f^+\right]\left[(RH_2)_{ads}\right]$,[5] where the rate constant k_{ox}^{DT}, with a real physical meaning ($k_{ox}^{DT} = \sigma v$, σ and v being the cross section for hole capture by $(RH_2)_{ads}$ species and the thermal speed of electrons within the sc, respectively), is used in substitution of the apparent rate constant k_{LH} used by Ollis.[8] Taking into account these premises, the surface concentration of chemisorbed substrate species becomes:

$$[PhO]_{ads} = \theta_A \times b = \frac{K_{ads} b [PhO]_{aq}}{1 + K_{ads}[PhO]_{aq} + \frac{k_{ox}^d\left[h_f^+\right]}{k_{-1}}} \qquad (A6)$$

, where b is the actual density of sc surface sites (Ti_s^{IV} ions) available for chemisorption

of substrate species and $\left[h_f^+\right] = \frac{k_0' \rho}{k_i'\left[O_{br}^{2-}\right] + k_{ox}^d[PhO]_{ads}}$ the concentration of

photogenerated valence band free holes, k_0' being an empirical constant depending on the nature of the catalyst and the reactor geometry.[26] Eq. (A6) finally becomes:

$$[PhO]_{ads} = \theta_A \times b = \frac{K_{ads}b[PhO]_{aq}}{1+K_{ads}[PhO]_{aq} + \dfrac{k_{ox}^{d}}{k_{-1}} \dfrac{k_0'\rho}{k_1'[O_{br}^{2-}] + k_{ox}^{d}[PhO]_{ads}}} \qquad (A7)$$

List of acronyms

a^{IT} : indirect transfer parameter defined according to eq. 1.

a_{ap}^{DT} : apparent direct transfer parameter.

a_{ap}^{IT+DT} : apparent (direct + indirect) transfer parameter.

b: semiconductor surface sites available for chemisorption of dissolved substrate species.

DT: electric charge, interfacial direct transfer mechanism.

e_f^- : conduction band free electrons.

h_f^+ : valence band free holes.

IT: electric charge, interfacial indirect transfer mechanism.

k_{ads} : chemisorption constant.

k_{-1} : diffusion constant of dissolved substrate species from the sc surface towards the electrolyte.

k_{ox}^{IT} : indirect transfer photooxidation rate constant.

k_{ox}^{DT} : direct transfer photooxidation rate constant.

k_{red}' : recombination rate constant of conduction band free electrons with electrolyte dissolved O_2 molecules.

k_1' : diffusion constant of dissolved substrate species from the electrolyte towards the semiconductor surface.

k_o' : empirical , photon absorption constant.

k_{r_1}' : interfacial recombination rate constant of conduction band free electrons with $-O_{br}^{\cdot-}$ radicals.

$[O_2]_{aq}$: concentration of electrolyte dissolved O_2 molecules.

$>O_{br}^{2-}$: TiO_2 surface bridging oxygen ions.

$-O_{br}^{\cdot-}$: TiO_2 surface bridging oxygen radicals.

$[(RH_2)_{aq}]$: concentration of dissolved substrate species, either in water or any other solvent.

$[(RH_2)_{ads}]$: concentration of semiconductor adsorbed substrate species.

v_{ox} : photooxidation rate.

v_{ox}^{DT} : direct transfer mechanism photooxidation rate.

v_{ox}^{IT} : indirect transfer mechanism photooxidation rate.

Θ_a : fraction of semiconductor surface sites covered with chemisorbed substrate species.
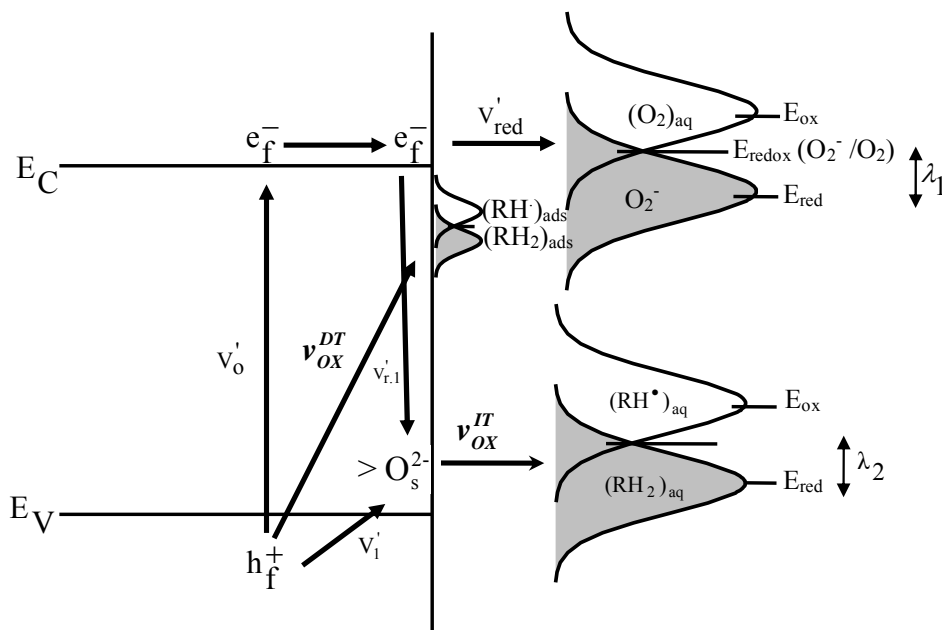

Figure 1. D-I model diagram showing TiO_2 energy levels and primary interfacial reactions involving: electroreduction of dissolved O_2 molecules with CB electrons, at a rate v'_{red} , photooxidation of physisorbed RH_2 species via an adiabatic IT mechanism of surface trapped holes (h_s^+), identified with O_s^-/O_{br}^- terminal oxygen radicals, at a rate v_{ox}^{IT} , and photooxidation of chemisorbed, $(RH_2)_{ads}$ substrate species with VB free holes (h_f^+)**,** via an inelastic DT mechanism, at a rate v_{ox}^{DT}; λ represents the reorganization energy according to the Gerischer model for electron transfer at the sc-electrolyte interface.[28,29] Since we are dealing with initial photooxidation rates, the back reaction of electroreduction of photogenerated $RH^•$ radicals with CB electrons is considered to be negligible and therefore is not included in the diagram.[35] Reproduced with permission from reference 30. Copyright (2009) Elsevier.
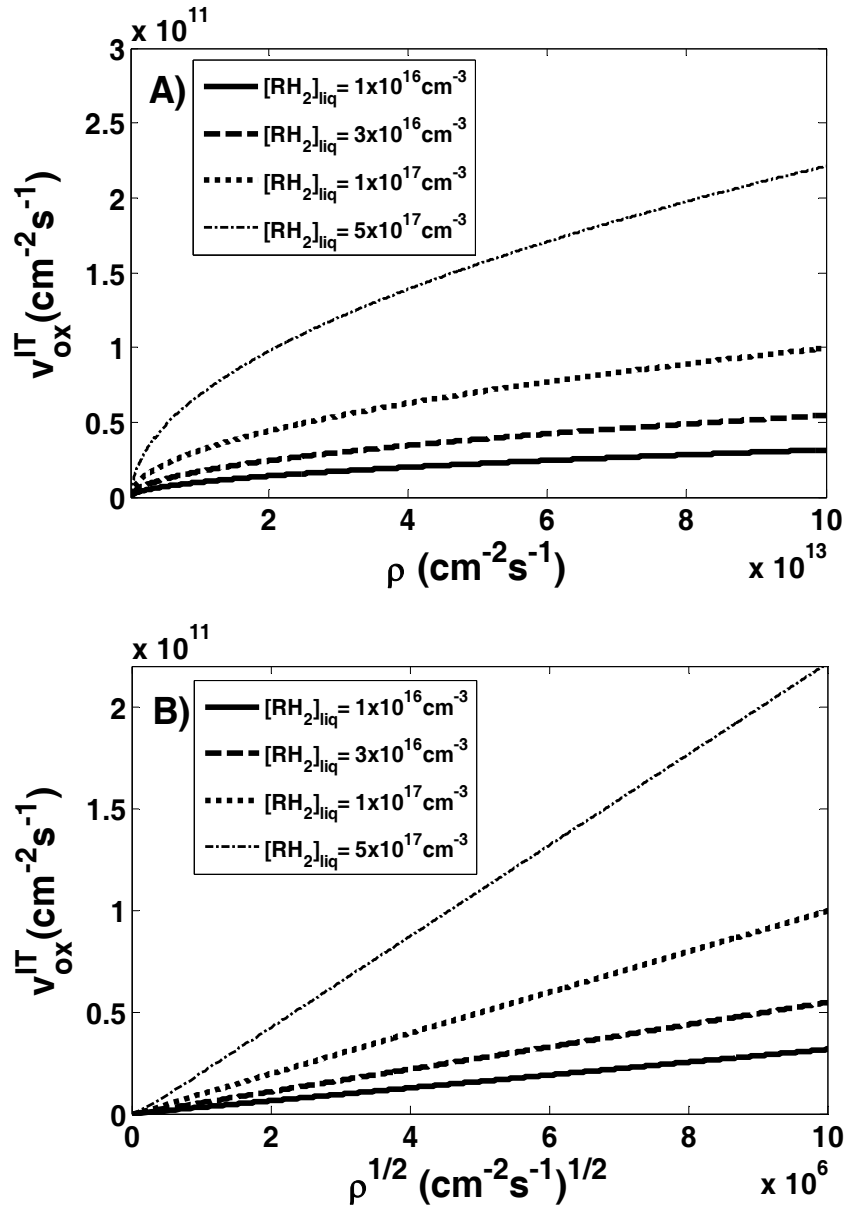
Figure 2. Plots of v_{ox}^{IT} vs. ρ (A) and v_{ox}^{IT} vs. $\rho^{1/2}$ (B), according to eq. (1) and eq. (1'), respectively , for $0 < \rho < 10^{14} \text{cm}^{-2} \text{s}^{-1}$, with $k_0 a^{IT} = 5.0 x 10^{-10} cms^{-1}$ and $\left[\left(RH_2 \right)_{liq} \right] = 10^{16}, \, 3x10^{16}, \, 10^{17} \text{ and } 5x10^{17} \text{cm}^{-3}$.
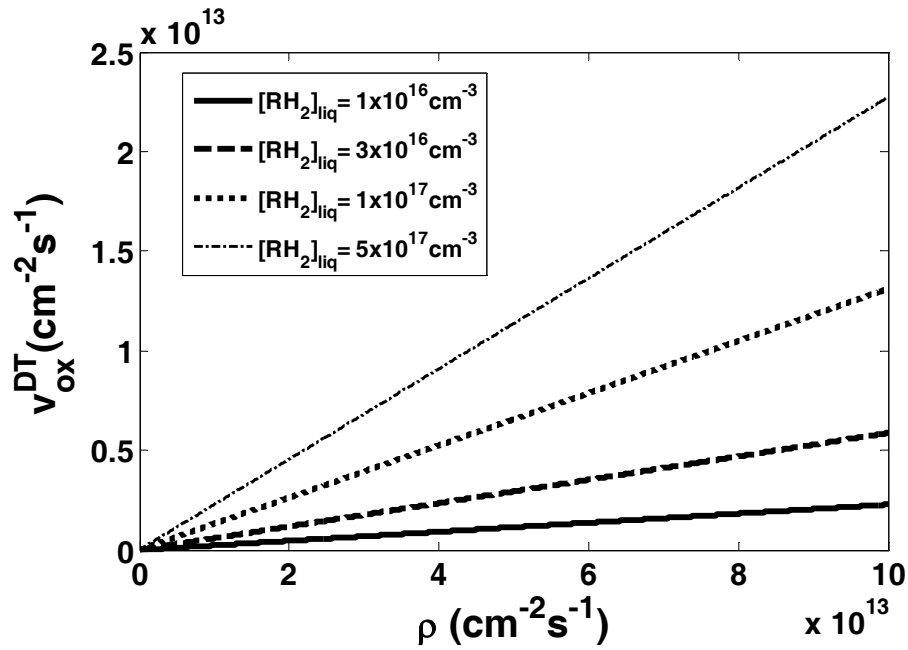
Figure 3. v_{ox}^{DT} vs. ρ plot according to eq. (2") , for $0 < \rho < 10^{14}$ cm^{-2} s^{-1} . K_{ads}=8.91X10^{-18}cm^3 , b=1.391x10^{15}cm^{-2}, $\dfrac{k_0 k_{ox}^{DT}}{k_1'\left[O_s^{2-}\right]} = 2\text{x}10^{-16}$ cm^2 , under substrate concentration values $\left[\left(RH_2\right)_{liq}\right] = 10^{16},\ 3\text{x}10^{16},\ 10^{17}$ and $5\text{x}10^{17}$cm^{-3}.
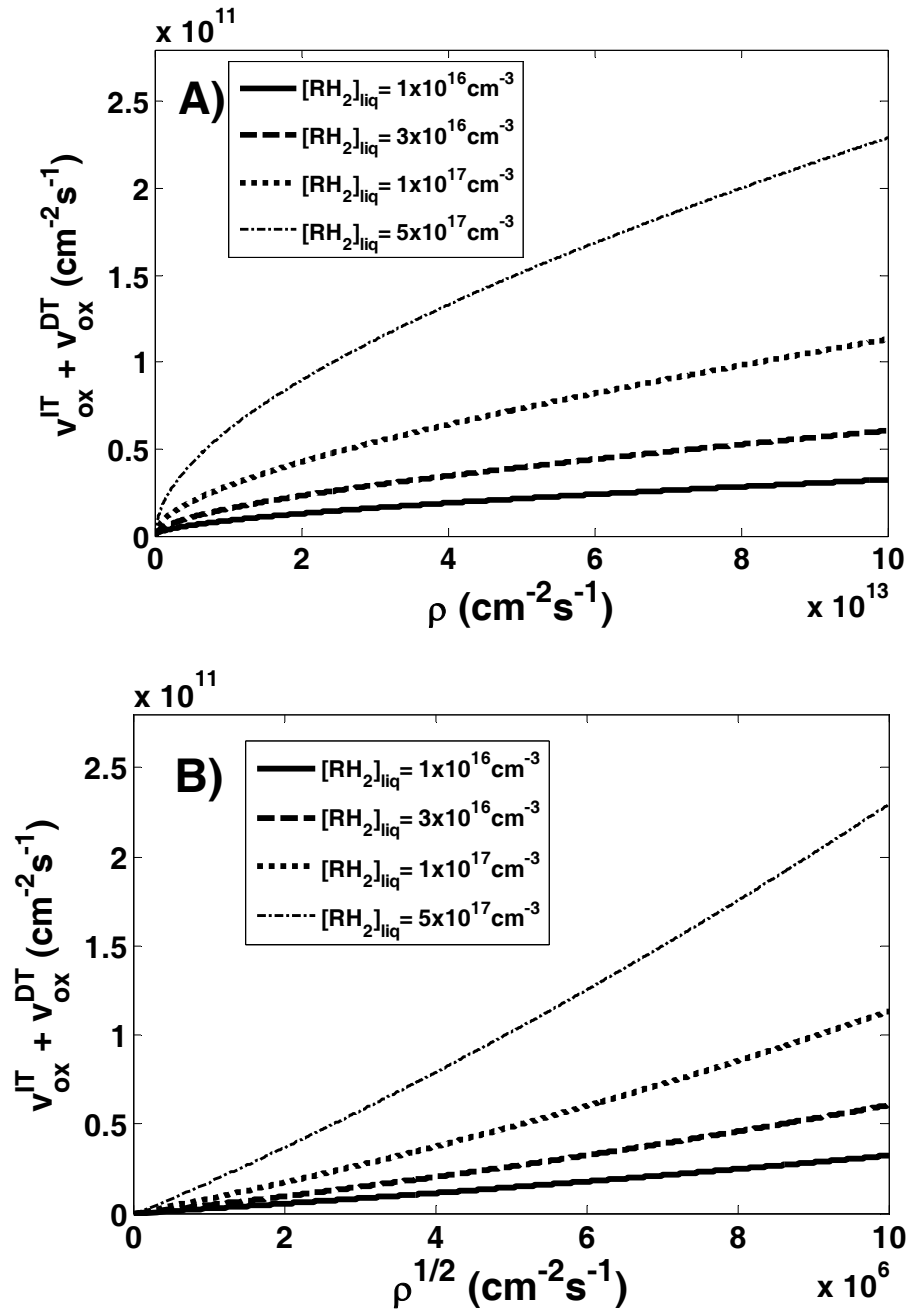
Figure 4. Plots of $v_{ox}^{IT}+v_{ox}^{DT}$ vs. ρ (A) and $v_{ox}^{IT}+v_{ox}^{DT}$ vs. $\rho^{1/2}$ (B), according to eq. (3), for $0< \rho <10^{14} cm^{-2}s^{-1}$, $k_0 = 0.1$, $a^{IT} = 3.3x10^{-9}\,cm\,s^{-1}$, $k_{ox}^{DT} = 1.42x10^{-8}\,cm^3 s^{-1}$, $K_{ads}=1.33X10^{-17} cm^3$, b=9.39x10^{13} cm^{-2} and $k_1^{'}[O_s^{2-}]= 2.36x10^8\,cm\,s^{-1}$, under 3 substrate concentration values $[(RH_2)_{liq}]=10^{16}$, $3x10^{16}$, 10^{17} and $5x10^{17} cm^{-3}$, respectively.
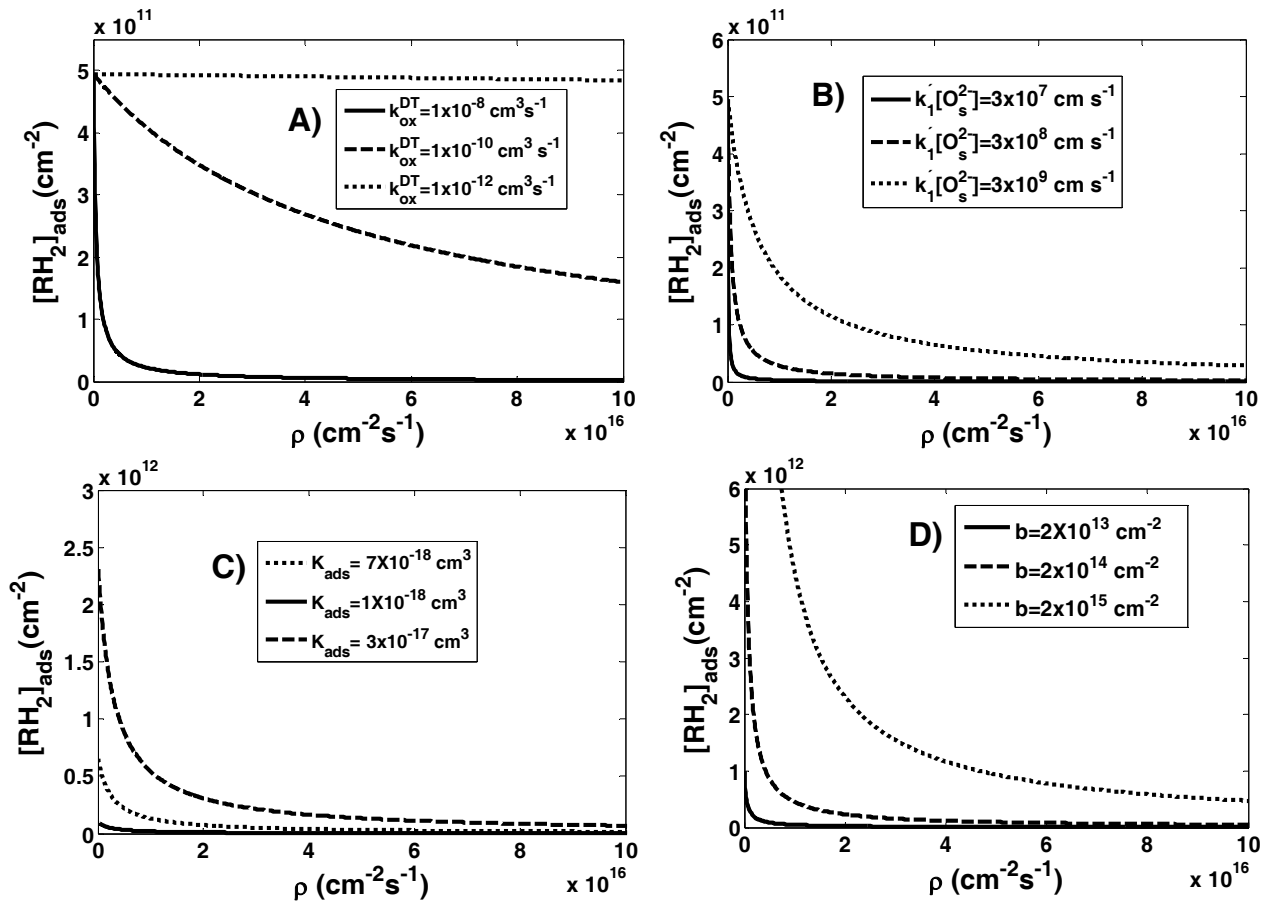
Figure 5. Influence of parameters: k_{ox}^{DT} (A), $k_1'\left[O_s^{2-}\right]$ (B), $\mathbf{K_{ads}}$ (C) and b (D), on the photon flux dependence of the concentration of adsorbed substrate species, according to eq. (10).

$K_{ads}= 5.2\times10^{-18}$ cm^3 in (A), (B),and (D); b=10^{13} cm^{-2} in (A), (B), (C); $k_{ox}^{DT}=10^{-8}$ cm^{3}s^{-1} in (B), (C), and (D); and $k_1'\left[O_s^{2-}\right]=2.36\times10^8$cm s^{-1} in (A), (C), (D). Common values of the remaining parameters are: $\left[RH_2\right]_{liq} = 10^{16}$ cm^{-3}, $k_1=10^{-20}$ cm^{3}s^{-1} and $k_0= 10^{-1}$.
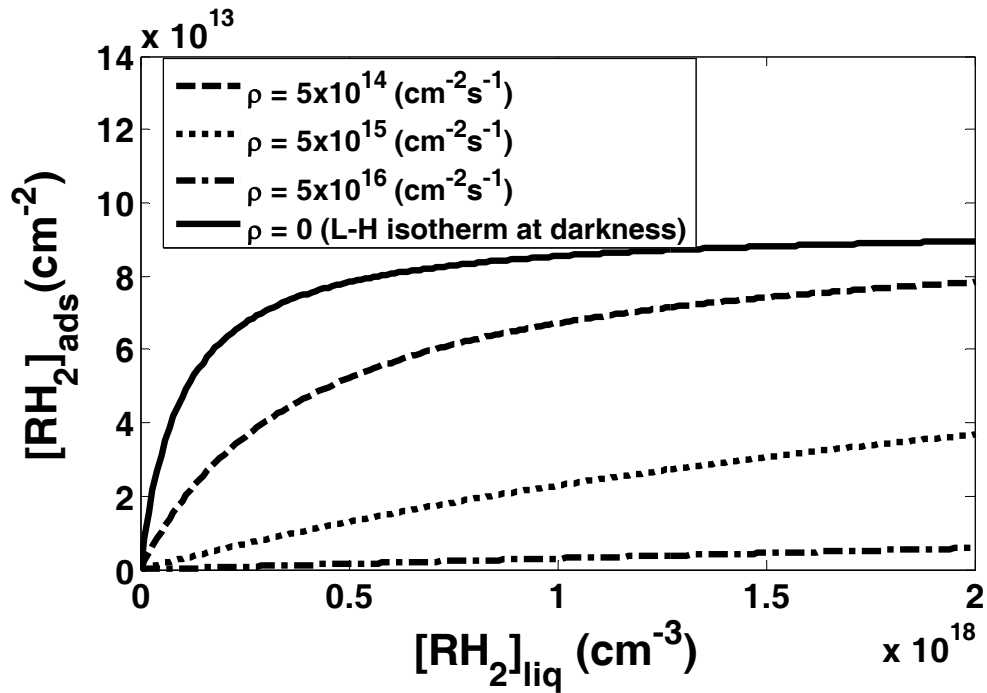
Figure 6. Effect of illumination intensity on the relationship between concentration of adsorbed and dissolved substrate species, according to eq. (8). The L-H isotherm at darkness corresponds to $\rho = 0$. Parameters used are: $k_1' \left[O_s^{2-} \right] = 2.36 \times 10^8$ cm s^{-1}; $b = 9.4 \times 10^{13}$ cm^{-2}; $k_1 = 10^{-20}$ cm^{3}s^{-1}; $k_{ox}^{DT} = 1.42 \times 10^{-8}$ cm^3 s^{-1}; $k_0 = 10^{-1}$; $K_{ads} = 1 \times 10^{-17}$ cm^3.
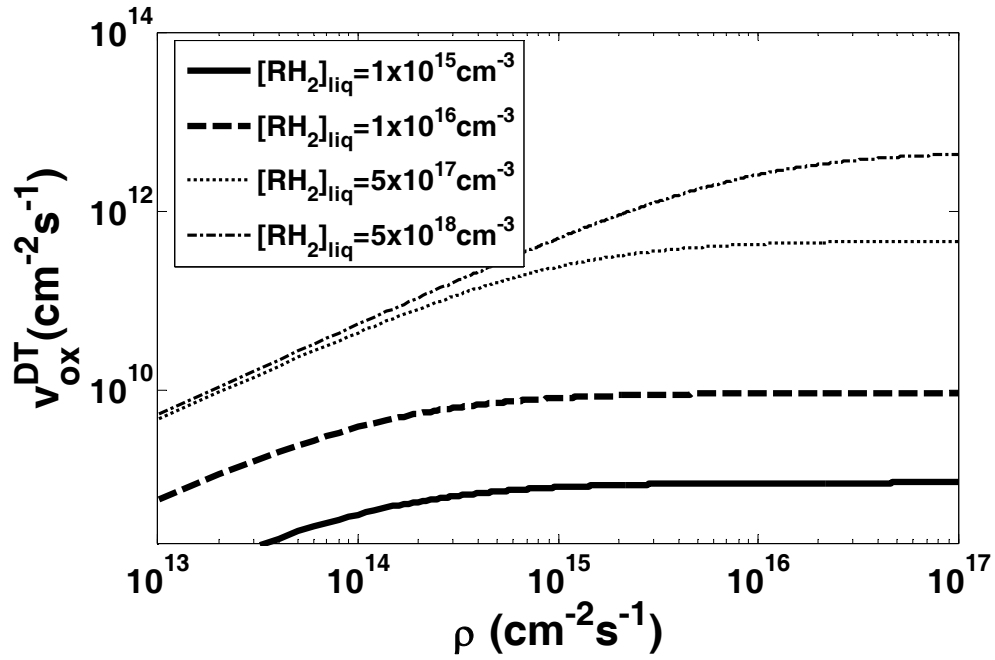
Figure 7. Logarithmic representation of the v_{ox}^{DT} dependence on the photon flux according to eq. (9_1) for $10^{13} < \rho < 10^{17}$ cm^{-2}s^{-1}, $k_0 = 0.1$, K_{ads}=1.33x10^{-17}cm^3 , $k_1' \left[O_s^{2-} \right] = 2.36$x10^8 cm s^{-1}, b=9.39x10^{13}cm^{-2}, and $k_{ox}^{DT} = 1.42$x10^{-8} cm^{3}s^{-1} , under 10^{15}, 10^{16}, 5x10^{17}cm^{-3}, 5x10^{18} cm^{-3} substrate concentration values.
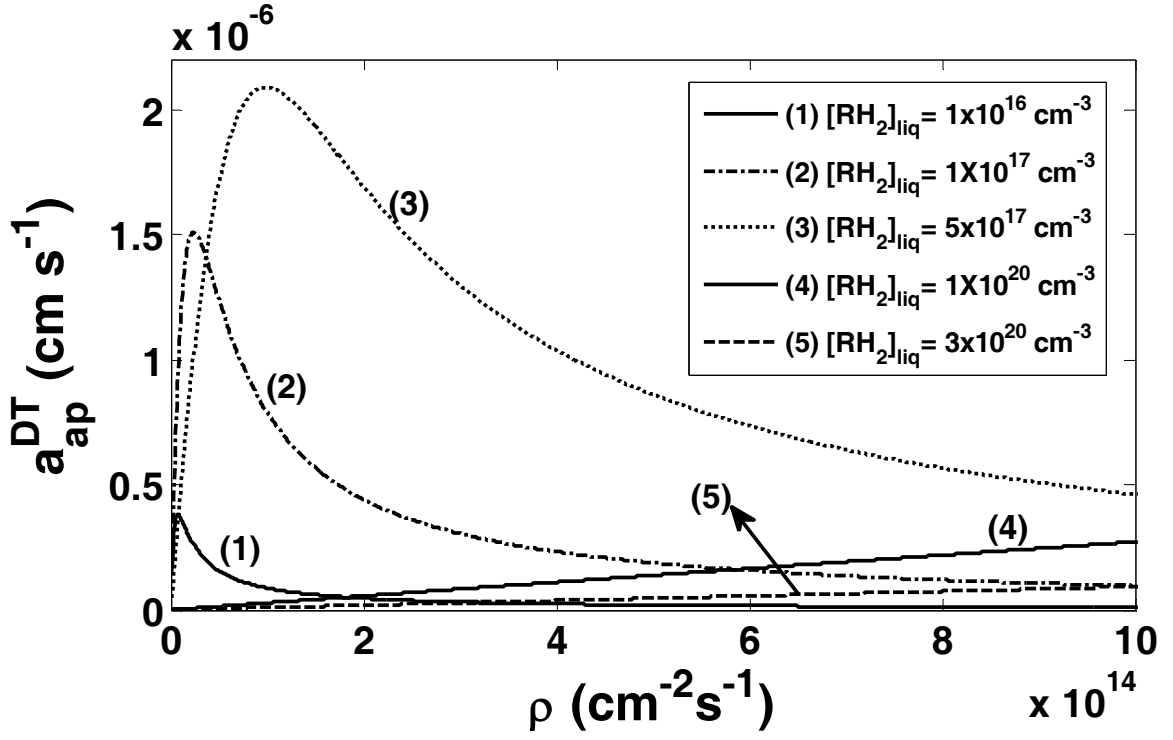
Figure 8. a_{ap}^{DT} photon flux dependence for $0 < \rho < 10^{15}$, obtained from eq. (11) and the following parameters: $K_{ads} = 8.9 \times 10^{-18}$ cm^3; $b = 1.4 \times 10^{15} cm^{-2}$; $k_1' \left[O_s^{2-} \right] = 2.36 \times 10^8 cms^{-1}$; $k_1 = 1 \times 10^{-20} cm^3 s^{-1}$; $k_{ox}^{DT} = 5 \times 10^{-7} cm^3$ s^{-1} and $k_0 = 0.1$.
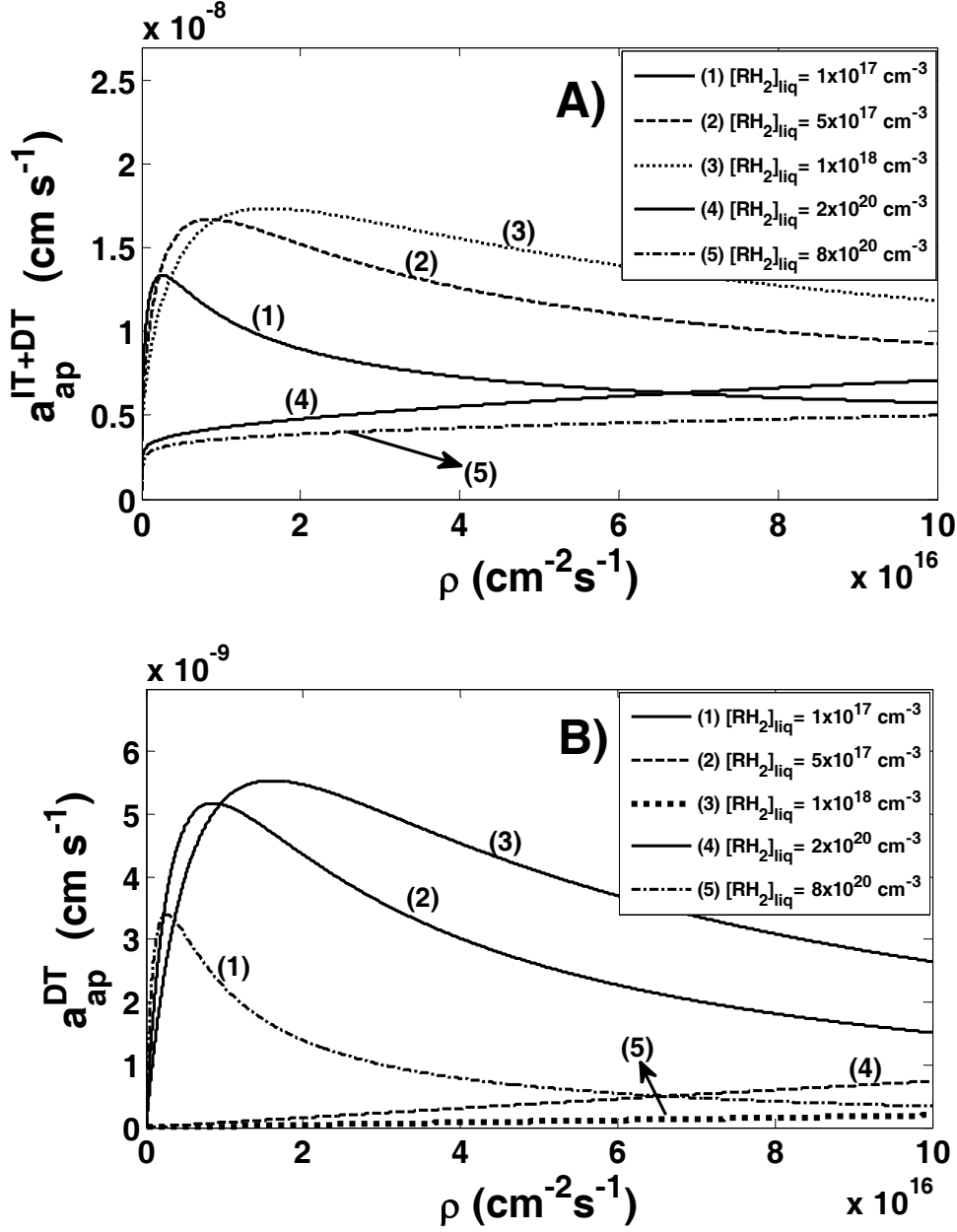
Figure 9. Comparative plot of the photon flux dependence of a_{ap}^{IT+DT} (A) and a_{ap}^{DT} (B), for $0 < \rho < 10^{17}$, obtained from eq. (11) for $a^{IT} = 3.3 \times 10^{-9}$ cms^{-1}, and the following values of the parameters involved in eq. (19): $K_{ads} = 1.33 \times 10^{-17}$ cm^3; $b = 9.39 \times 10^{13}$ cm^{-2}; $k_1 = 9 \times 10^{-20}$ cm^{3}s^{-1} ; $k_{ox}^{DT} = 1.42 \times 10^{-8}$ cm^{3}s^{-1} $\quad \dfrac{k_0 k_{ox}^{DT}}{k_1^{'} \left[O_s^{2-} \right]} = 6 \times 10^{-18}$ cm^{3}s^{-1} and $k_0 = 0.1$

Manuscript 2

"Comprehensive Analysis of Kinetics and Mechanisms of TiO$_2$ Photocatalytic Reactions . II) Experimental Validation of the D-I model"

Comprehensive Analysis of Kinetics and Mechanisms of TiO$_2$ Photocatalytic Reactions . II) Experimental validation of the D-I model

Juan Felipe Montoya[1], José Peral[1], and Pedro Salvador[1,*]

1.Departamento de Química, Universidad Autónoma de Barcelona, 08193 Cerdanyola del Vallés, Spain.

*Corresponding author, E-mail: psalvador@klingon.uab.es

Keywords: Kinetics; Mechanisms; Photocatalysis; D-I Model; Charge Transfer

Abstract

The interactions of three model compounds, dissolved in water or acetonitrile, with the TiO_2 surface were analyzed in detail through spectroscopy techniques and adsorption isotherms. It was found the following order in the interaction strength: formic acid (FA) > phenol (PhO) > benzene (BZ). The main adsorption mode of FA is chemisorption; of BZ is physisorption while PhO is adsorbed via both modes.

These interactions modes have consequences in the kinetic behavior: phenol in water is photooxidized via a combination of indirect transfer (IT) and direct transfer (DT) mechanisms which have rate values within the same order of magnitude. In contrast, the contribution of the DT mechanism to the photooxidation of phenol in acetonitrile is higher, being estimated that the rate values of the DT mechanism are at least one order of magnitude higher than those of the IT. FA was found to be predominantly photooxidized via a DT mechanism. Finally, BZ is exclusively photooxidized via a IT mechanism.

The representations of the new parameter *a* proposed by the D-I model showed their utility to elucidate the working mechanism of charge transfer from analysis of experimental kinetic data. Additional representations of *a vs.* ρ of aqueous phenol photooxidation data reported by Emeline et al. allowed to analyse in detail the case of adsorption equilibrium disruption, a situation evidenced by the several maxima observed at the curves of the functions of *a vs.* ρ.

The experimental evidence collected in this work supports the central hypothesis the D-I model: the degree of organic substrate-TiO_2 surface interactions plays a crucial role in the kinetics of photocatalytic reactions. Depending on these interactions, the specific organic molecule will be photooxidized by an IT, DT or a combination of both mechanism in different degrees.

1. INTRODUCTION

Titanium dioxide (TiO$_2$) photocatalytic oxidation of organic molecules is a largely studied process that has been regarded as a promising technology for environmental remediation.[1-4] It has been demonstrated in extensive degradation studies employing many different model compounds that most of the organic contaminants present in water and even in air can be fully decomposed.[1,2,5-7] Despite this potential applicability, the development of more efficient photocatalytic systems is required in order to achieve large scale implementation of photocatalysis as an oxidation technology.[4]

It is commonly accepted that the photocatalytic process is initiated by interfacial redox reactions that involve charge carriers, namely electrons $\left(e_f^-\right)$ and holes $\left(h_f^-\right)$, that are generated when the TiO$_2$ is exposed to light with energy larger than the band gap (eq 1).

$$TiO_2 \xrightarrow{\text{hv} \geq 3.2\text{eV}} h_f^+ + e_f^- \qquad (1)$$
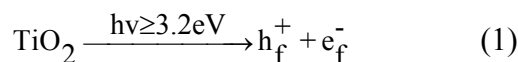
Oxidation reactions are initiated by holes, species that, at TiO$_2$ have a high oxidation potential. [1-4,8] Due to their role as initiators of oxidation reactions, the study of the dynamics of this charge carriers is of seminal importance to achieve a sound and comprehensive understanding of the photocatalysis phenomena.[8] After the generation step (eq. 1), free holes can follow several pathways, including recombination, trapping by chemisorbed organic molecules (eq 2), or trapping by TiO$_2$ surface lattice oxygens (O$_s$), according to reactions 3 and 4. [9-13]

$$h_f^+ + \left(RH_2\right)_{ads} \rightarrow RH^{\bullet} + H^+ \qquad (2)$$

$$h_f^+ + \left(> O_s^{2-}\right) \longrightarrow \left(-O_s^{\bullet\bullet}\right) \quad pH > pH_{zpc} \qquad (3)$$

$$h_f^+ + \left(> OH_s^-\right) \longrightarrow \left(-OH_s^{\bullet}\right) \quad pH < pH_{zpc} \qquad (4)$$
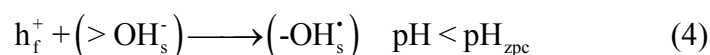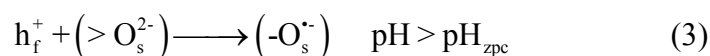
Reaction 2 implies an oxidation of a chemisorbed organic molecule $\left(\left[RH_2\right]_{ads}\right)$ via a direct transfer (DT) mechanism[11,13,14] while the surface radicals $\left(-OH_s^{\bullet}/-O_s^{\bullet\bullet}\right)$ generated trough eqs 3 and 4 can further oxidize dissolved organic molecules $\left(\left[RH_2\right]_{liq}\right)$ via an indirect transfer (IT) mechanism, according to eq 5. [11,13,15-19]

$$\left[RH_2\right]_{liq} + \left(-OH_s^{\bullet}/-O_s^{\bullet\bullet}\right) \rightarrow RH^{\bullet} + H^+ + \left(> OH_s^-/> O_s^{2-}\right) \qquad (5)$$
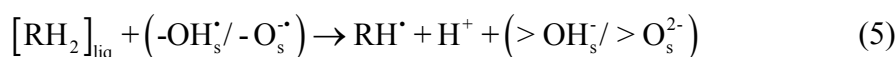
It is worth noting that the DT (eq 2) and IT (eq 5) photooxidation mechanisms have several important differences: (1) the DT mechanism implies an ultrafast nonequilibrium hole transfer before thermalization of the photoexcited energy while the IT implies an equilibrated hole transfer across the TiO_2-liquid interface; [8,13] (2) while chemisorption is a prerequisite for DT mechanism, it is not necessary in the case of IT; [11,13,15,16] (3) the two types of oxidations are carried out at different active sites: DT occurs at Ti^{4+} surface ions which are the sites for chemisorption of organic molecules via a covalent bonding between an organic molecule and a Ti^{4+} ion. On the other hand, the active sites for IT are the O_s which trap the photogenerated holes before their interfacial transfer to the organic molecule[9,10,12,13,17-19] (eqs 3 to 5). The above set of differences testifies that DT and IT are markedly different processes. However, both types of mechanisms lead to a similar distribution of photooxidation products and can simultaneously coexist, making difficult to distinguish between them. [13,20] This distinction is critical because both kind of mechanisms leads to a different type of kinetic equations[11,13,15] and their respective efficiency can be improved by different types of TiO_2 surface modifications[16]. Moreover, design and scaling-up of photoreactors for practical applications requires a trustworthy kinetic model as a fundamental input[21-27].

For a long time, kinetic analysis of TiO_2 photocatalytic reactions have largely relied on rate equations with the same analytical form as the Langmuir-Hinshewoold (L-H) model. [1,2,5,6,14,28] Despite its wide application in photocatalysis, the use of the classical L-H kinetic model has been put under question for multiple factors.[4,13,29-37] As an alternative, one of us have recently developed the Direct-Indirect (D-I) kinetic model which is based on the degree of interaction of the organic species with semiconductor surface. [11,13] Hence, according to this model, the existence or absence of chemisorption of the organic molecule at the TiO_2 surface is a critical parameter that determine the kinetic behavior. As a consequence, an experimental testing of the D-I model requires a previous exhaustive study of the adsorption modes of the specific organic compound at the TiO_2 surface.

In the last decade, there has been an extraordinary growth of surface science studies (SCS), especially those employing scanning tunneling microscopy (STM), devoted to

understand the relationships between the surface properties and the photochemical events triggered by TiO_2 excitation. [38-40] The deeper understanding of the TiO_2 surface chemistry furnished by these SCS gives useful information for kinetic and mechanistic studies of photocatalytic reactions. However, this set of results must be used with care for the interpretation of liquid-phase photocatalytic data because these SCS were carried out under ultra-high vacuum (UHV) conditions. As a result, the application of this body of knowledge is not straightforward, due to the drastic change introduced by the solvent. [4] Despite this limitation, some information about the binding sites, structure, coverage, and stability of several adsorbates at TiO_2 is useful for application to kinetic studies. Spectroscopy techniques, in particular Fourier transformed infrared (FTIR)[41-50] and diffuse reflectance UV-vis spectroscopy (DRUVS)[51], have been extensively used in the last years to monitor the interaction, structure and reactivity of several organic substrates onto the TiO_2 surface even in the presence of a solvent. Consequently, the use of these experimental techniques combined with the fundamental findings of SCS is useful to elucidate the details of the adsorption modes of a specific organic compound at the TiO_2 surface. This elucidation is the starting point of any kinetic study because the crucial role of adsorption phenomena on kinetics of photocatalytic reactions. [11,13]

In this study, FTIR and DRUVS are used to study the adsorption behavior at the TiO_2 surface of several model compounds, i.e. benzene (BZ), phenol (PhO), and formic acid (FA), dissolved in water or acetonitrile. The results obtained with these spectroscopy techniques combined with the interpretation of the adsorption isotherms allow us to propose plausible structures of these organic molecules at the TiO_2 surface. Subsequently, a complete kinetic study is carried out for each model compound using one or both solvents. It was found that there is a direct correlation between the adsorption modes and the kinetic behavior in agreement with the predictions of the D-I model. The whole body of experimental kinetic data reported here fits well to the D-I kinetic equations applicable to the different combinations of charge transfer mechanisms discussed in the first part of this publication: pure IT, combination of DT and IT at different ratios, prevalence of DT, and DT under adsorption-desorption equilibrium rupture. Altogether, constitute a general experimental validation of the D-I

model and an illustration of its applicability as a tool to differentiate between charge transfer mechanisms from the analysis of experimental kinetic data.

2. EXPERIMENTAL METHODS

2.1 Materials

TiO_2 was purchased from Aldrich (purity 99.7%, average particle size: 25 nm, 100% anatase, BET area=55 m^2/g). The same TiO_2 powder was used for all the kinetic studies and the spectroscopy measurements.

All other reagents were analytical grade and used as received without further purification. All aqueous solutions were prepared with deionized water from a SARTORIUS ARIUM 611 apparatus $\left(conduc\tan ce = 18\,M\Omega\,cm^{-1} \right)$

2.2 High Performance Liquid Chromatographic (HPLC) Analysis

In the kinetic and adsorption experiments the time evolution of the concentration of the organic substrate was monitored by HPLC. The details of the HPLC system, the chromatographic method, and procedure of treatment of the samples are given in the document of supporting info, appendix A.

2.3 Kinetics Experiments

TiO_2 powder was dispersed in 100 ml of the desired solvent (C_{cat}=0.5 g/L) by sonication and shaking in an ultrasonic cleaning bath for 15 minutes. The pH in the case of the aqueous suspensions was adjusted to 3 by adding a standard solution of $HClO_4$. An aliquot of a stock solution (5000 ppm) of the organic substrate was subsequently added in order to reach the desired initial concentration. The suspensions were covered with foil and left under stirring at 300 rpm overnight in order to reach adsorption equilibrium. Irradiation experiments were carried out in borosilicate glass cylindrical reactors (I.D.=6 cm, h=7cm) illuminated on the top by an assembly of 6 UV-A lamps (Philips Cleo 15W, emission: $300 < \lambda < 400\,nm$, $\lambda_{max} = 365\,nm$). The photon flow was regulated by changing the distance between the reactor and the set of lamps. At each distance the photon flow was measured by potassium ferrioxalate actinometry following

a standard procedure.[52] The light intensity of the set of lamps was routinely monitored with a UV-A radiometer in order to guarantee the stability of the photon flow of the lamps. They were also allowed to reach a stable light intensity by turning them on 10 minutes before the starting of each experiment and putting a dark screen between them and the reactor.

Before illumination, 1 ml of sample of the equilibrated suspensions was taken for analysis, being this the initial equilibrium concentration reported in Fig. 3 to 6. The reactor was filled with 100 ml of the equilibrated suspension; magnetically stired (300 rpm) and bubbled with air. After, the dark screen was removed, samples were withdrawn at different time intervals depending on the experimental conditions and the organic substrate. Each organic substrate experiment was repeated three times, and this allowed to estimate an experimental error of $e = \pm 12\%$ in the measurement of the initial reaction rates (see supporting info file, appendix B).

Control experiments carried out for each organic substrate showed that there was no observable decrease of the concentration due to air stripping or photolysis. Temperature of the liquid phase was periodically monitored being always $25 \pm 2\ ^{o}C$.

2.4 Attenuated Transmission Reflectance FTIR Spectroscopy (ATR-FTIR)

The monitoring of the interactions of the organic substrates with the TiO_2 surface was made by using the *in situ* ATR-FTIR technique[41-49].The spectra were recorded on a BOMEM MB122 instrument equipped with a liquid N_2-cooled MTC-A (mercury–tellurium–cadmium) detector and a Pike Technologies horizontal ATR unit with a ZnSe crystal. The dimensions of the trapezoidal ZnSe-ATR element were 6.8 x 72 mm^2 long on the horizontal probe face, 4 mm thick, and the angle of incidence was 45°. The number of reflections on the upper face was 9. The interferometer and the infrared light path were constantly purged with Argon. The final spectral resolution was 4 cm^{-1}. Each final spectrum was an average of 80 scans. Baseline corrections were made in order to eliminate minor fluctuations due to instrumental instability. The spectra were not smoothed and no ATR corrections were made. The details of solution compartment employed for the measurements can be found elsewhere[46]. The material of the solution compartment was POM (Polyoxymethylene) and the window of the reactor was

borosilicate glass. These materials were chemically resistant to the studied solutions; hence no interferences in the spectra due to the materials degradation were detected. The solutions were not recirculated and the temperature was monitored during spectra collection, being $21\pm2^{o}C$. For the measurements with aqueous solutions the pH was adjusted to 3 by adding a solution of $HClO_4$ and the ionic strength was fixed by adding KNO_3 (10 mM).

10 ml of the solvents, either water (pH 3, 10 mM KNO_3) or acetonitrile were introduced in the solution compartment. After two minutes a spectrum was collected and taken as the background. After collection of the background the solvent was replaced by 10 ml of the test solution. Sequential spectra were collected during 60 minutes taking one spectrum each 60 seconds. The final spectrum corresponds to that of the pure solutions (spectrum a) showed in Figures 2A, 2B and 2C. After the study of the solutions on the bare crystal, its surface was covered with a TiO_2 thin layer following a procedure previously described.[46] For the study of the organic solutions the films were prepared with the same procedure but using TiO_2 suspensions in acetonitrile. After coating the crystal the same procedure was repeated to collect the background and to study the adsorption of the substrate on the TiO_2 surface. Since no change in the intensity of the bands was observed after 1 hour this time was considered enough to reach the adsorption equilibrium.

2.5 Diffuse Reflectance UV-Vis Spectroscopy (DRUVS)

TiO$_2$ samples for DRUVS analysis were prepared as follows: 2 g of TiO_2 powder were dispersed in 100 ml of the solvent (water or acetonitrile) by simultaneous shaking and sonication for 15 minutes in an ultrasonic cleaning bath. An aliquot of 5ml of a stock solution (10000 ppm) of the organic substrate was subsequently added to the suspension giving an initial concentration of the substrate of 476 ppm. The pH in the case of the aqueous suspensions was adjusted to 3 by adding a standard solution of $HClO_4$. The suspensions were covered with foil and stirred in the dark at 300 rpm during 24 hours. The TiO_2 powder was recovered by filtering the suspension with Nylon filter membranes (0.45 μm pore size) and dried at 60 ^{o}C for 1 hour. The spectra of the resulting powders were measured in a UV-Vis spectrophotometer (Varian Cary

100) equipped with a diffuse reflectance attachment and a certificate diffuse reflectance standard (Labsphere). The spectra of TiO_2 without adsorbed organic substrates were taken from samples of TiO_2 powders prepared in the same way described above, but without addition of any organic solution to the TiO_2 suspensions.

3. **RESULTS AND DISCUSSION**

3.1 Spectroscopy study of substrate-semiconductor surface interactions

The DRUVS spectra of the pure anatase TiO_2 powder and those of TiO_2 in contact with solvents without dissolved organic substrates were totally identical (Figure 1, spectra 1a). It can be seen that the anatase sample absorbs at wavelengths in the region of $\lambda < 390\,nm$, and this behavior remains unchanged when the sample is in contact with a pure solvent (either water or acetonitrile). The spectrum of the sample of the same TiO_2 powder in contact with a solution of benzene dissolved in acetonitrile (TiO_2/Bz, spectrum 1b) also shows absorbance in the region of $\lambda < 390\,nm$, evidencing that either there is no surface complex formation or, if it is formed, it does not absorb in the visible region. In contrast, the TiO_2 powders in contact with solutions of phenol show a shift in the onset of light adsorption to higher wavelengths. It is remarkable the difference in this red shift depending on the solvent: while the anatase powder in contact with an aqueous solution of phenol (TiO_2/H_2O/PhO, spectrum 1c) shows a red shift of 20 nm (absorbs in the region of $\lambda < 410\,nm$), the same powder in contact with phenol dissolved in acetonitrile (TiO_2/ACN/PhO, spectrum 1d) shows a shift of 90 nm (absorbs in the region of $\lambda < 480\,nm$).
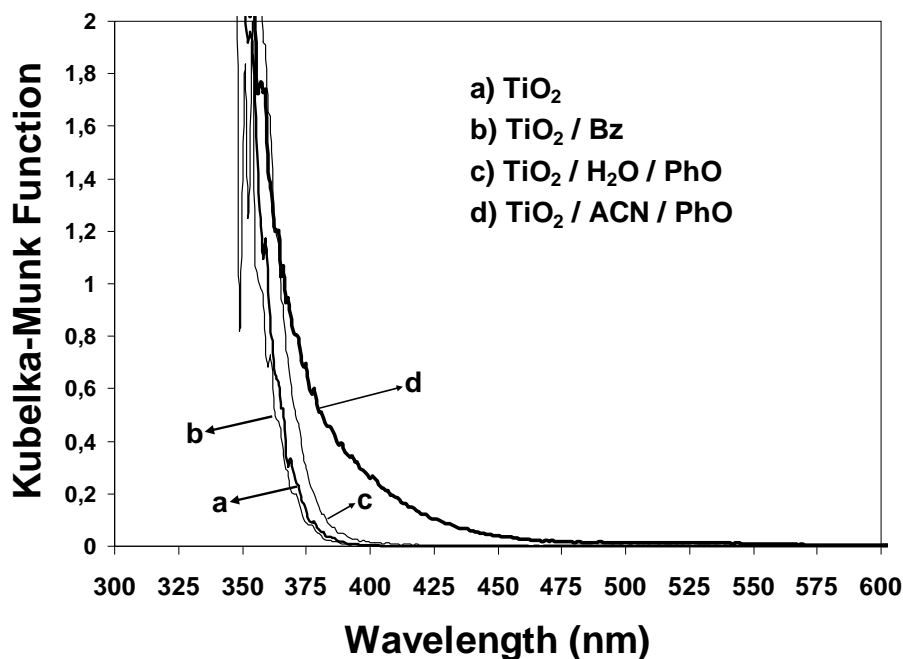
Figure 1. DRUVS spectra of anatase TiO_2 powders previously in contact with pure solvents (a) or different organic substrates (b-d).

The observed visible light adsorption of the samples TiO_2/PhO evinces the formation of a surface complex (SC).[51] The most probably structure of the SC in the case of phenolic compounds is the formation of a covalent bonding between the oxygen of the phenol molecule and a Ti (IV) site (phenolate link). [48,53] This kind of surface complexation enables the visible light absorption trough ligand to metal charge transfer (LMCT) between the organic substrate (ligand) and the Ti (IV) site on the surface [54-55]. Since the structure of the visible light absorbing SC must be equal for phenol chemisorbed on TiO_2 independently of the solvent, the observed dependence of the red shift onset on the solvent (20 and 90 nm, for water and acetonitrile respectively) is attributed to a solvent dependent surface density of the SC. While in the TiO_2/H_2O/PhO sample the phenol molecules are less effectively chemisorbed at the TiO_2 surface due to the competition of water for the Ti (IV) sites, in the TiO_2/ACN/PhO sample the phenol molecules can be easily chemisorbed at the TiO_2 surface, since acetonitrile is not expected to compete for the Ti (IV) sites due to its weak interaction with the TiO_2 surface[56]. This means that a higher surface density of the SC is expected when the TiO_2 powder is exposed to

contact with a solution of phenol dissolved in acetonitrile leading to a higher red shift in the absorption spectra. It is worth noting that our TiO_2/substrate samples were obtained by filtration of the TiO_2 powder equilibrated with the substrate in solution, therefore the surface density of the SC corresponds to the adsorbed equilibrium concentration. The above procedure differs with that used by Kim and Choi[51] who obtained the TiO_2 samples for DRUVS measurements by solvent evaporation, forcing in this way the absorption of large amounts of substrate molecules on the TiO_2 surface. Under those conditions a surface density of the SC higher than that of adsorbed equilibrium concentration is expected. This explains the higher shift observed by that group in the absorption spectrum of the sample TiO_2/H_2O/PhO sample, which absorbs in the region of $\lambda < 530\,nm$, with respect to that observed in Figure 1.

In summary, the higher red shift in the absorption spectrum observed for the sample TiO_2/ACN/PhO is due to a higher surface density of the SC with respect to the case of the sample TiO_2/H_2O/PhO. The above means that when solutions of phenol of the same concentration are in contact with TiO_2, a higher amount of phenol gets chemisorbed when the solvent is acetonitrile instead of water. This behavior implies that phenol chemisorption is favored by the use of acetonitrile as solvent because in that case there is no competition between the phenol molecules and water for the Ti (IV) sites on the surface.

In order to get further spectroscopy evidence of the aforementioned facts, an ATR-FTIR study of the semiconductor-substrate interactions was carried out. In Figure 2A (spectrum a) five bands located at 1153, 1169, 1223, 1261, 1366, 1474 and 1501 cm^{-1} can be identified for an organic solution of phenol. These bands are assigned to[48,57-60]: $\delta(CH)$ (1153); $\delta(CH), \delta(OH) + \delta(CH)$ (1169); $\delta(OH)$ (1223); $\nu(CO)$ (1261); $\nu(CC) + \nu(CO)$ (1366); $\nu(CC)$ (1474); $\delta(CH) + \nu(CC)$ (1501). On the other hand, the main bands for an acid aqueous solution of phenol (Figure 2B, spectrum a) are located at: 1242 ($\nu(CO)$); 1377 ($\nu(CC) + \nu(CO)$); 1477 ($\nu(CC)$) and 1501 ($\delta(CH) + \nu(CC)$). There are two shoulders, one of them at 1192 ($\delta(OH)$), and the other at 1269 ($\nu(CO)$) cm^{-1}.

The differences in the spectra of the solutions of Figures 2A and 2B in the region between 1100 and 1300 cm^{-1}, can be explained by the different speciation of phenol depending on the solvent. Since the pK$_a$ of phenol in aqueous solution is 9.98 [ref. 61], at pH 3 the protonated species predominated. In contrast, for phenol dissolved in acetonitrile there is a mixture of both types of species (protonated and deprotonated). In the spectrum (a) of Figure 2A the existence of the protonated species is evidenced by the band at 1223 cm^{-1} attributed to a $\delta(OH)$ mode[57], while the band at 1261 cm^{-1} corresponds to the $\nu(CO)$ mode of the deprotonated species. In the spectrum a of Figure 2B at 1269 cm^{-1} there is only a small shoulder due to the almost complete absence of deprotonated species. In contrast, there is a broad and intense band at 1242 cm^{-1} which corresponds to the $\nu(CO)$ mode of the protonated species. This broad band does not allow a clear identification of the band assigned to the $\delta(OH)$ mode (1223 cm^{-1}).
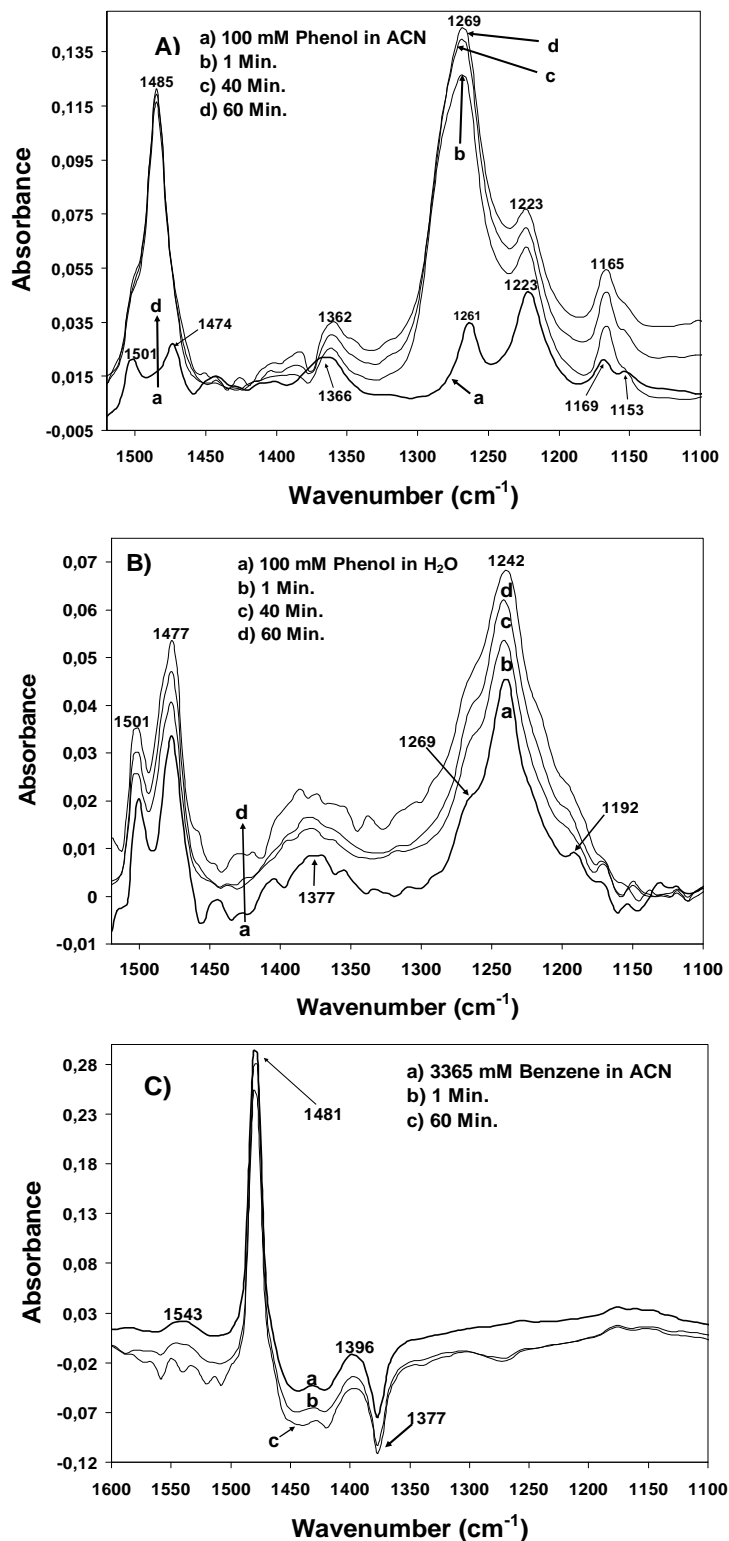
Figure 2. ATR-FTIR spectra of: A) a 100 mM solution of phenol dissolved in acetonitrile in the absence (a) and in the presence of a film of TiO_2 anatase at different times of contact between the organic substrate and TiO_2 (b-d); B) a 100 mM solution of Phenol dissolved in water (pH 3) in the absence (a)

and in the presence of a film of TiO_2 anatase at different times of contact between the organic and TiO_2 (b-d); C) a 3365 mM solution of Benzene dissolved in acetonitrile in the absence (a) and in the presence of a film of TiO_2 anatase at different times of contact between the organic and TiO_2 (b and c).

After the contact of the phenol solutions with the TiO_2 surface (spectra b-d of Figures 2A and 2B) some changes in the spectral features, and an intensity increase of the bands, which is directly related to the degree of coverage of the TiO_2 surface by the organic substrate, [62] can be noticed. A comparison between these spectra and those of the pure solutions help to envisage the structure and the degree of coverage of each adsorbate at the TiO_2 surface. For phenol there are two main adsorption modes: molecular and dissociative adsorption. In the former case, the phenol molecules remain intact and weakly interact with the TiO_2 surface (physisorption) while in the latter the phenol molecules are deprotonated and the oxygen of the alcohol moiety makes a covalent bond to a Ti (IV) site (chemisorption). The pronounced and fast increase in the intensity of the band at 1261 cm^{-1} in the presence of the TiO_2 film (spectra b-d, Figure 2A), evinces an increase in the surface density of deprotonated species of phenol due to the formation of a SC at the TiO_2 surface. This feature is characteristic of dissociative adsorption of phenol since in this case the adsorbed phenol molecules become deprotonated. In contrast, the smaller intensity increase in the band at 1223 cm^{-1} shows that the presence of TiO_2 produced almost no change in the spectral features of the protonated species of phenol. This means that the main spectral changes introduced by the presence of TiO_2 arise from the chemisorption of phenol on the semiconductor surface. Thus, the main adsorption mode of phenol dissolved in acetonitrile is dissociative adsorption (chemisorption) which implies an inner sphere complexation of phenol with the TiO_2 surface. This interpretation of the FTIR spectra is in agreement with the results obtained by the DRUVS spectra of Figure 1.

The changes produced in the aromatic ring bands of the organic solution of phenol, located at 1474 and 1501 cm^{-1} (spectrum a, Figure 2A) after the contact with the anatase TiO_2 film (spectra b-d, Figure 2A), also attest the formation of a surface complex. These two bands, characteristic of a pure phenol solution, completely disappeared and

were replaced by one broader and more intense band centered at 1485 cm^{-1} that correspond to the aromatic ring vibration of the adsorbate.

The spectra of Figure 2A exhibit minor changes with respect to the time of contact (spectra b-d) which indicates that adsorption equilibrium is reached rapidly. Since acetonitrile is not expected to compete with phenol for the Ti (IV) sites[56], this can be adsorbed very fast reaching the equilibrium state almost immediately.

When phenol in aqueous solution is put in contact with the TiO$_2$ layer there is a competition between phenol and water molecules for the Ti (IV) sites. This competitive adsorption explains the higher time needed to reach the equilibrium state for the case of the aqueous solutions of phenol (spectra b-d, Figure 2B) with respect to the organic solutions (spectra b-d, Figure 2A). Although in the former case there is an intensity increase in the bands after the contact of the phenol solutions with the TiO$_2$ layer, this increase is not as pronounced as in the case of the organic solutions, evincing a lower surface density of phenol molecules at the TiO$_2$ surface when water is used as solvent. Moreover, all the bands of Figure 2B increase in the same proportion and the ratio between their intensities remains unchanged. Hence, the spectral features of the TiO$_2$/H$_2$O/PhO are identical to those of the spectrum of the pure aqueous solution of phenol. This indicates that the main adsorption mode of phenol in aqueous solution is molecular adsorption (physisorption) because in this case the structure of the phenol molecules remains unmodified after the contact with the TiO$_2$ layer. All the above facts demonstrated the hindering of the chemisorption of phenol due to the competition of water for the Ti (IV) sites. This interpretation is in agreement with the results obtained by DRUVS spectra of Figure 1.

In the spectra of Figure 2C the main bands are located at 1377 ($\nu(CC)$); 1396 ($\nu(CC)$); and 1481 cm^{-1} ($\nu(CC)$). All the bands remain unchanged after exposition of the organic solution of benzene (spectrum a, Figure 2C) to the TiO$_2$ layer (spectra b and c). It is worth mentioning that the baseline of each spectrum was shifted in order to help the visualization because otherwise the spectra would have been totally superposed. The lack of changes in the intensity of the bands observed in the spectra of Figure 2C reveals the absence of chemisorption of benzene at the TiO$_2$ surface. This conclusion is in agreement with those reported by Baddford and coworkers[63] who studied benzene

adsorption at the TiO$_2$ surface by a combination of STM, temperature programmed desorption (TPD) and theoretical calculations; concluding that benzene has a very low binding energy (-67 kJ/mol) and a high mobility on the TiO$_2$ surface, being both typical hallmarks of physisorption. Moreover, that group found no dissociative reactivity of benzene on the TiO$_2$ surface which means that benzene molecules remains unchanged after the interaction with TiO$_2$. This set of observation clearly indicates that benzene is only physisorbed at the TiO$_2$ surface.

ATR-FTIR spectra of formic acid was not studied here because we reported them in previous publications[15,16]. Formic acid even in aqueous solution strongly interacts with the TiO$_2$ surface, and, consequently, chemisorption is its main adsorption mode. This means that formic acid is able to displace the water molecules adsorbed at the surface in order to form a formiate complex at the surface. This complex is formed through two covalent bonds between the two oxygens of the FA molecule and two Ti(IV) sites[39]. The Ti-O bond lengths of FA chemisorbed on TiO$_2$ have been quantitatively measured by scanned energy mode photoelectron diffraction (PhD) being 2.08 A^o for both Ti-O bonds while the bond length of Ti-O from water chemisorption was found to be 2.21 A^o [39], indicating a weaker covalent interaction. Hence, formic acid is able to be chemisorbed at the TiO$_2$ surface in spite of the competition of large amounts of water (see more details of the discussion in the supporting info, appendix A).

The information about the structure and the degree of coverage of the adsorbates provided by the spectroscopy techniques (Figures 1 and 2) must correlate with the quantitative information furnished by adsorption isotherms. The values of the constants of the Langmuir type isotherms obtained from the study of adsorption of solutions of FA and PhO at the anatase TiO$_2$ surface are reported in Table 1. (See experimental details, figures, calculations and deeper discussion of the adsorption isotherms in the supporting info, appendix A). It is worth mentioning, that data of benzene dissolved in acetonitrile is not included in Table 1 since the adsorbed concentration of this compound was negligible and the data did not fit to the Langmuir isotherm equation. This behavior is not surprising because, as already discussed, benzene showed a very weak interaction with the TiO$_2$ surface.

Table 1. Langmuir adsorption constants of phenol (dissolved in water or acetonitrile) and formic acid.

Isotherm	K_{ads} (cm^3/molec.)	b (molec./nm^2)	Kads*b (cm)
Phenol in Water (TiO$_2$/PhO/H$_2$O)	1.328 x 10^{-17}	0.9390	0.00125
Formic Acid (TiO$_2$/FA/H$_2$O)	8.915 x 10^{-18}	13.91	0.0124
Phenol in Acetonitrile (TiO$_2$/PhO/ACN)	3.961 x 10^{-18}	9.234	0.00366

From Table 1 it can be deduced that the values of a complete monolayer coverage of the organic substrates (parameter "b" third column) follow the order: b (TiO$_2$/FA/H$_2$O)> b (TiO$_2$/PhO/ACN)> b (TiO$_2$/PhO/H$_2$O). The values of $K_{ads}b$ (fourth column of Table 1) reflect that the tendency to form a monolayer under adsorption equilibrium conditions follows the order: $K_{ads}b$ (TiO$_2$/FA/H$_2$O)> $K_{ads}b$ (TiO$_2$/PhO/ACN)> $K_{ads}b$ (TiO$_2$/PhO/H$_2$O).

These quantitative parameters show that adsorption of formic acid is highly favored and it covers a high proportion of the TiO$_2$ surface (aprox. 70% of the total adsorption sites (n_T) considering them as n_T= 20 sites/nm^2 for anatase nanoparticles[64]) even in the presence of water. On the other hand, phenol has adsorption constants highly dependent on the solvent. While in acetonitrile chemisorption of phenol is favored and the coverage is relative high (aprox. 46% of the total adsorption sites) in water the adsorption is hindered and the coverage is poor (aprox. 4.7 % of the total adsorption sites). This can be explained by the different role played by each solvent in the competition for the Ti (IV) adsorption sites.

In general, the quantitative information furnished by the adsorption isotherms is in agreement with the conclusions obtained from spectroscopy data of Figures 1 and 2.

To summarize: a) benzene is only physisorbed at the TiO$_2$ surface; b) the main adsorption mode of aqueous formic acid is chemisorption; c) phenol can be

chemisorbed or physisorbed; d) the degree of phenol chemisorption depends on the solvent: water hinders chemisorption of phenol due to the competition for the Ti (IV) sites whereas acetonitrile allows chemisorption of phenol in a higher extent because this solvent weakly interacts with the TiO_2 surface. Scheme 1 illustrates the substrate-TiO_2 surface interactions of these model compounds.

Scheme 1. Organic substrate-TiO_2 surface interactions of the model compounds[a]
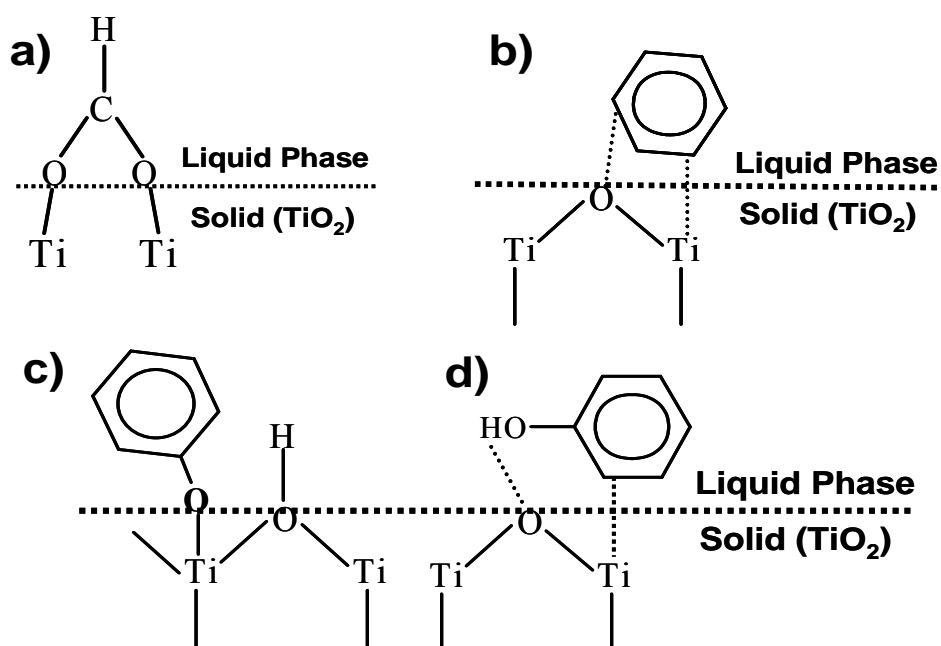
[a] a)Formic acid chemisorption; b) benzene physisorption; c) phenol chemisorption; d) phenol physisorption. Solid lines represent covalent bonding while dashed lines represent weak interactions (like Van der Waals interactions).

3.2 Kinetic study

At this point, the implications of the aforementioned TiO_2-organic substrate interactions on the kinetic behavior of each model compound can be analyzed. To do this, the dependence of the initial reaction rate on photon flow and concentration was investigated for each organic substrate dissolved in water or acetonitrile.

In the absence of chemisorption, the organic substrate must be photooxidated via a pure IT mechanism, represented by eq. 2-I (from now on, equations numbers followed by the

notation (-I) refer to the correspondent equation at the first part of this publication[65]). Figure 3A and B show the representation of the initial reaction rate $\left(v_{ox}\right)$ vs. photon flow $\left(\rho\right)$ and v_{ox} vs. $\left(\rho^{\frac{1}{2}}\right)$, respectively, for experimental kinetic data of benzene photooxidation and their respective fitting to eq 2-I for each concentration studied.
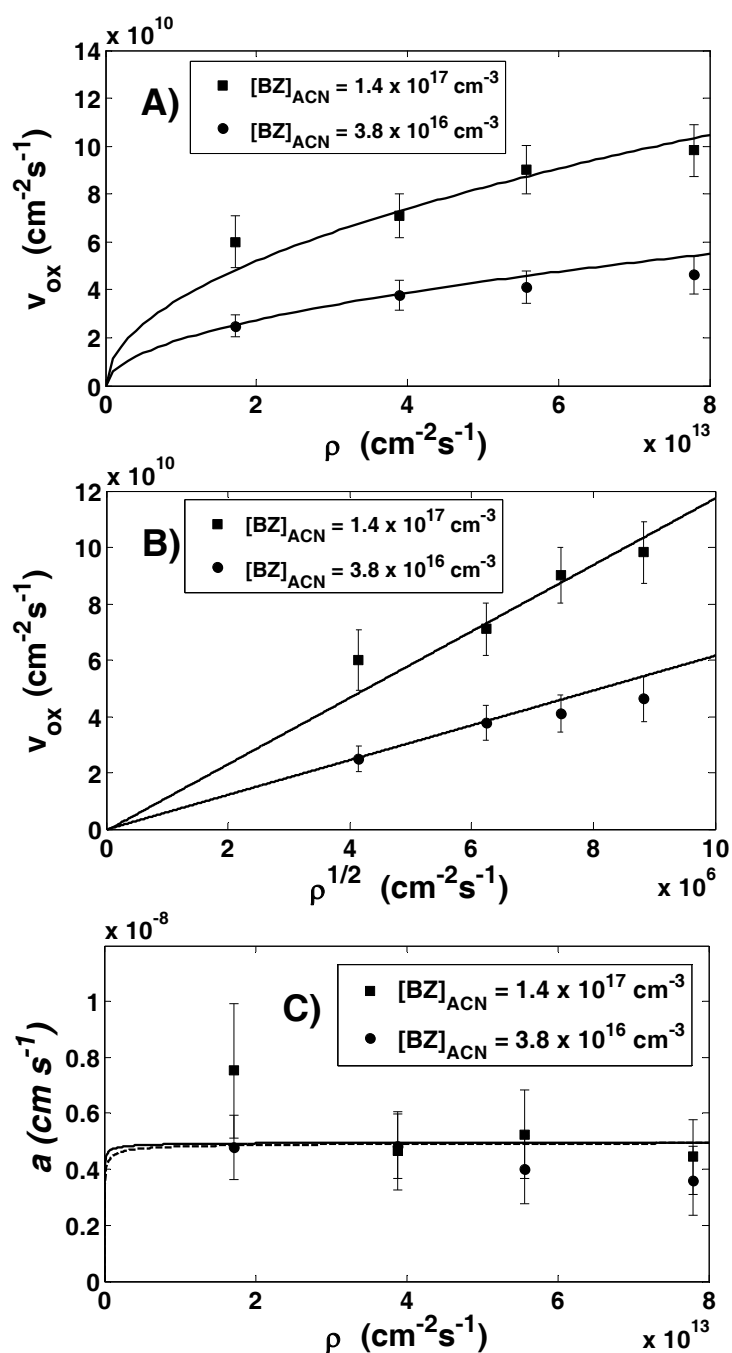
Figure 3. (A) Initial reaction rate $\left(v_{ox} \right)$ of benzene (BZ) photooxidation in acetonitrile (ACN) as a function of (A) photon flow $\left(\rho \right)$ and (B) the square root of photon flow $\left(\rho^{\frac{1}{2}} \right)$. The solid lines are the theoretical representation of v_{ox}^{IT} calculated from eq. 2-I. (C) Experimental parameter "*a*" (eq 6) as a function of ρ. The solid and dashed lines correspond to the theoretical representation of a^{IT} **vs** ρ for both concentrations calculated from eq 7.

The fitting parameters used in all panels were: $k_0 = 0.1$; $A_{cat} = 1x10^4 \ cm^2$; $a^{IT} = 5x10^{-9} \ cm/s$.

From Figure 3A it can be observed that benzene photooxidation fits well to the mathematical function that represents a pure IT mechanism (eq 2-I). As explained before, eq 2-I predicts a square root dependence of the initial reaction rate $\left(v_{ox} \right)$ on photon flow $\left(\rho \right)$ when $\rho \gg \dfrac{a^{IT} \left[\left(RH_2 \right)_{aq} \right]}{2k_0}$. As a result, a representation of $\left(v_{ox} \right)$ vs. $\left(\rho^{\frac{1}{2}} \right)$ must be linear, for high enough ρ values. This kind of behavior is observed in Figure 3B where the experimental data of benzene photooxidation fits to straight lines for both concentrations in the whole experimental range $\left(1.7x10^{13} \leq \rho \leq 7.8 \times 10^{13} \ photons/cm^2 \ s \right)$. This clearly demonstrates that v_{ox} for benzene photooxidation has a square root dependence on ρ, as predicted by the D-I model for an organic substrate that is only physisorbed at the TiO_2 surface. This type of dependence was reported before for other organic substrates such as chloroform[66] and methylviologen, [67] two compounds that, because of their chemical structure, are likely candidates of physisorption onto the TiO_2 surface. It is noticeable that eq 2-I, in contrast with the L-H model, explicitly includes the photon flow and predicts this type of kinetic behavior. Moreover, we would like to stress that the kinetic data reported in Figure 3 fits to a kinetic equation (eq 2-I) with a completely different analytical expression from that deduced from the L-H model. This contradicts the dogma which states that kinetic data of photocatalytic reactions always fits to a L-H type kinetic equation. [31]

Experimental kinetic data of Figure 3A was used to calculate the experimental values of the parameter "a" according to eq 6 (see details of calculations in the document of supporting info, appendix B).

$$a = \frac{\left(v_{ox}\right)^2}{2k_0 A_{cat}\rho\left[RH_2\right]_{liq}} \qquad (6)$$

A representation of a vs. ρ is shown in Figure 3C. Assuming that the only working mechanism for benzene photooxidation is the IT, the corresponding theoretical equation that represents a^{IT} is:

$$a^{IT} = \frac{\left(v_{ox}^{IT}\right)^2}{2k_0\rho\left[RH_2\right]_{liq}} \qquad (7)$$

Figure 3C shows that the values of a^{IT} calculated from eq 7 tend to converge at a constant value of $5x10^{-9}$ cm/s for both initial concentrations of benzene when $\rho > 0.5x10^{13}\ cm^{-2}s^{-1}$. As expected for high enough photon flow, a^{IT} is a constant independent of the photon flow and the concentration. For lower values of photon flow $\left(0 < \rho < 0.5x10^{13}\ cm^{-2}s^{-1}\right)$ the condition of $\rho \gg \dfrac{a^{IT}\left[\left(RH_2\right)_{aq}\right]}{2k_0}$ is not fulfilled and $a^{IT} \to 0$ as $\rho \to 0$. Since all our experimental data was acquired at $\rho > 0.5x10^{13}\ cm^{-2}s^{-1}$ a constant value of a must be obtained. Actually, the experimental values of a showed a reasonably good fitting to the horizontal lines that represent a^{IT} vs. ρ for $\rho > 0.5x10^{13}\ cm^{-2}s^{-1}$. It has to be pointed out that the error bars are higher in Figure 3C than those of Figure 3A and B because when eq 6 is applied to calculate a the experimental error associated to the variable $\left(v_{ox}\right)$ is duplicated due to error propagation derived from the mathematical calculations ($e = \pm 24\%$, see details in appendix B). Despite these relative large error bars, the calculated value of $a = 5\times10^{-9}\ cm/s$ fits well the kinetic data as it evinced by the good fitting showed in Figure 3A and B using this value. Moreover, the qualitative behavior of a showed in

Chapter 5

Figure 3C is characteristic of a pure IT mechanism as it is clear that $\dfrac{da}{d\rho}$ is not positive

as would be expected when the DT mechanism operates.

As discussed before, formic acid (FA) strongly interacts with the TiO$_2$ surface, almost forming a monolayer (aprox. 70%). Under these circumstances, a prevalence of a direct transfer (DT) mechanism would be expected. Eq 3-I predicts a linear dependence of v_{ox}^{DT} on ρ for a pure DT mechanism. As a result, a representation of v_{ox}^{DT} vs. ρ must be linear. Figure 4A shows the representation of v_{ox} vs. ρ for experimental kinetic data of FA photooxidation and the corresponding fitting to eqs 2-I and 3-I for each concentration studied. It can be seen that v_{ox} has a linear dependence on ρ, as the curves that represent v_{ox}^{DT} vs. ρ are straight lines that tend to the origin. This behavior suggests that in the FA photooxidation the DT mechanism prevails although some contribution of the IT mechanism can not be totally disregarded because chemisorbed molecules always coexist with physisorbed ones. However, based on the theoretical expected value of the kinetic constant of IT $\left(k_{ox}^{IT}\right)$ it can be assumed that the contribution of the IT mechanism should be negligible in this case. Indeed, k_{ox}^{IT} has an exponential activation energy term associated to the energy difference between the top of the valence band of TiO$_2$ (E$_v$) and the redox potential of the organic substrate (E$_{redox}$) that is oxidized (see eq 2 of ref. 13). In contrast, the DT considers an inelastic charge transfer mechanism and its kinetic constant $\left(k_{ox}^{DT}\right)$ does not contain activation energy term. As a consequence, when the activation energy is higher than 1 eV, as is the case for $\text{FA}\left(\Delta E=E_{red}\text{-}E_S\approx1.08V\right)$, the kinetic constant k_{ox}^{IT} must be several orders of magnitude lower than k_{ox}^{DT} (i.e. $k_{ox}^{DT}>>k_{ox}^{IT}$). Several studies of charge carrier dynamics of several TiO$_2$-adsorbate systems have demonstrated that direct hole transfer is an ultrafast process that occurs in the femtosecond scale, being even in the same time scale of recombination.[8] Thus, these experimental data confirms that $k_{ox}^{DT}>>k_{ox}^{IT}$. If the surface coverage of a chemisorbed molecule is high as in the case of FA on anatase TiO$_2$ under the studied conditions, the relationship between the kinetic constants

$\left(k_{ox}^{DT} >> k_{ox}^{IT} \right)$ necessarily implies the same relationship between the rates, i.e. $v_{ox}^{DT} >> v_{ox}^{IT}$ as can be inferred from eqs 2-I and 3-I. In order to confirm this thesis for the case of FA, a representation of a vs. ρ from experimental data of Figure 4A was made (Figure 4B). Initially, and assuming that both mechanisms coexist, the corresponding theoretical equation that represents a^{DT+IT} is:

$$a^{DT+IT} = \frac{\left(v_{ox}^{DT+IT} \right)^2}{2k_0 \rho [RH_2]_{liq}}$$ (8)

If $v_{ox}^{DT} >> v_{ox}^{IT}$ for FA photooxidation, then $a_{ap}^{IT+DT} \approx a_{ap}^{DT}$. As mentioned elsewhere[65], if the adsorption equilibrium is not broken under illumination, a_{ap}^{DT} linearly depends on ρ, $\dfrac{da}{d\rho}$ must be positive, and the straight lines that represent a_{ap}^{DT} vs. ρ must tend to the origin. Indeed, this is the kind of behavior that can be observed in Figure 4B indicating that FA is preferentially photooxidized via a DT mechanism without adsorption-desorption equilibrium rupture.
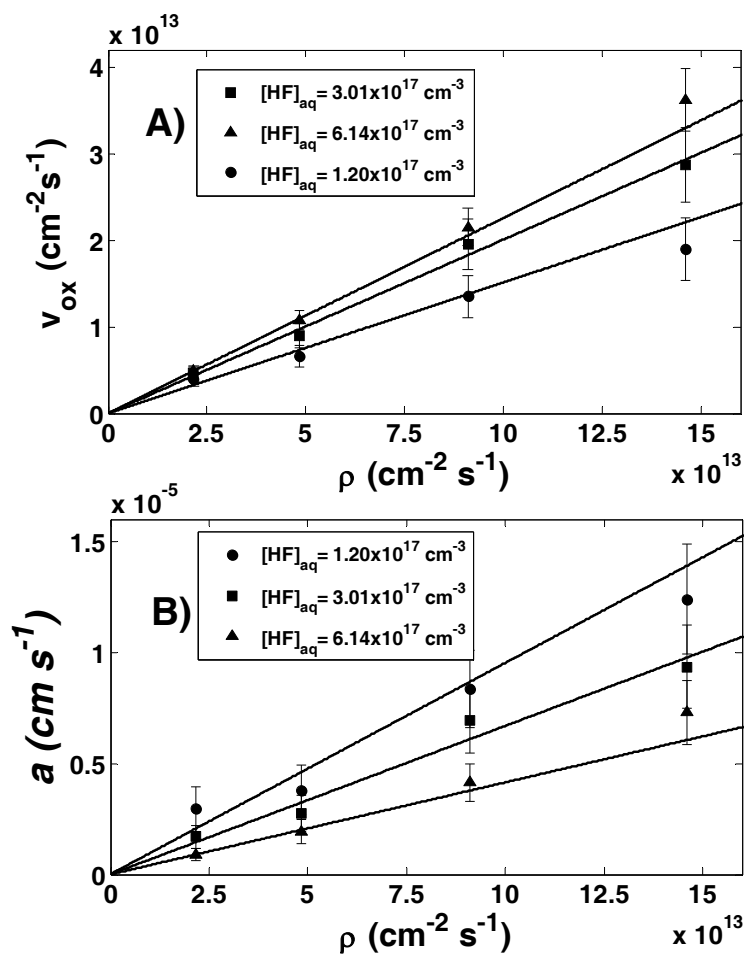
Figure 4. A) Initial reaction rate $(\mathbf{v_{ox}})$ of aqueous formic acid (HF) photooxidation as a function of photon flow $(\mathbf{\rho})$. The solid lines are the theoretical representation of $v_{ox}^{IT} + v_{ox}^{DT}$ calculated from eqs. 2-I and 3-I. B) Experimental parameter "*a*" (eq 6) as a function of $\mathbf{\rho}$. The solid lines correspond to the theoretical representation of $\mathbf{a^{IT+DT}}$ **vs** $\mathbf{\rho}$ calculated from eq 8.The fitting parameters used in both panels were: k_0 = 1; A_{cat} = $6x10^2$ cm²; K_{ads}=8.91x10⁻¹⁸cm³,b=1.39x10¹⁵cm⁻ ;$k_{ox}^{DT} = 5.85x10^{-8}cm^3 s^{-1}$;$a^{IT} = 1x10^{-14}$ **cm** / **s** ; $\mathbf{k_1'}\left[\mathbf{O_s^{2-}}\right] = 2.36x10^8$**cms**$^{-1}$

By replacing the fitting parameters of Figure 4A and B in eqs 2-I, 3-I, and 8 it was found that the $\dfrac{a_{ap}^{DT}}{a_{ap}^{IT}}$ and $\dfrac{v_{ox}^{DT}}{v_{ox}^{IT}}$ ratios are aproximately 10^9. Although this ratio values are not quantitatively exact due to the lack of knowledge of the exact values of several

fitting parameters, they clearly show that for FA $v_{ox}^{DT} \gg v_{ox}^{IT}$ because experimental data

can only be fitted with a set of parameters that always yield very high $\dfrac{a_{ap}^{DT}}{a_{ap}^{IT}}$ and $\dfrac{v_{ox}^{DT}}{v_{ox}^{IT}}$

ratios. In conclusion, FA photooxidation is a paradigmatic case where a DT mechanism prevails.

On the other hand, the photonic efficiency (PE) of a photooxidation process is:[68]

$$\zeta\left(\%\right)=\frac{v_{ox}}{\rho}\times100 \qquad\qquad (9)$$

Applying eq. 9 to experimental data of Figures 3A and 4A, it was found that the range of PE for benzene photooxidation is $0.063 < \zeta\left(\%\right) < 0.35$ while for formic acid is $12.9 < \zeta\left(\%\right) < 22.7$. This astonishing difference in the photonic efficiencies illustrate the great contrast between the photooxidation via DT or IT mechanisms. While FA is readily oxidized via direct hole trapping (eq 2), benzene oxidation requires a first step of surface hole trapping (eqs 3 and 4) followed by a step of interfacial hole transfer (eq 5). As a consequence, FA oxidation is fast and effectively competes with recombination yielding high values of PE.

Comparing Figures 3 and 4 it can be seen that $\mathbf{v}_{ox} \propto \rho^{\frac{1}{2}}$ for benzene while $\mathbf{v}_{ox} \propto \rho$ for FA within a similar photon flow range. This behavior contradicts the common assertion which states that in general $\mathbf{v}_{ox} \propto \rho$ for low enough ρ values while $\mathbf{v}_{ox} \propto \rho^{\frac{1}{2}}$ for high enough ρ values. Our data demonstrate that the dependence of $\mathbf{v}_{ox}$ on ρ can be explained invoking two different charge transfer mechanisms that lead to different kinetic equations. In summary, FA is preferentially oxidized via a DT mechanism with a high PE and a linear dependence of the initial rate on photon flow $\left(\mathbf{v}_{ox} \propto \rho\right)$. Benzene is oxidized via a IT mechanism, with a low PE and a square root dependence of the initial rate on photon flow $\left(\mathbf{v}_{ox} \propto \rho^{\frac{1}{2}}\right)$. This set of differences

illustrates the main features of each charge transfer mechanism disclosed by the kinetic analysis of photooxidation of these model organic molecules.

After the analysis of the main features of DT and IT mechanisms is time to explore in detail one of the most common situation in photocatalysis, namely the photooxidation of an organic molecule via both mechanisms operating simultaneously. Since DT requires chemisorption of the organic substrate at the TiO_2 surface, this mechanism can be hindered avoiding chemisorption as much as possible. As already discussed, this is the case for phenol in aqueous solution. Figure 5 depicts kinetic data of aqueous phenol photooxidation.
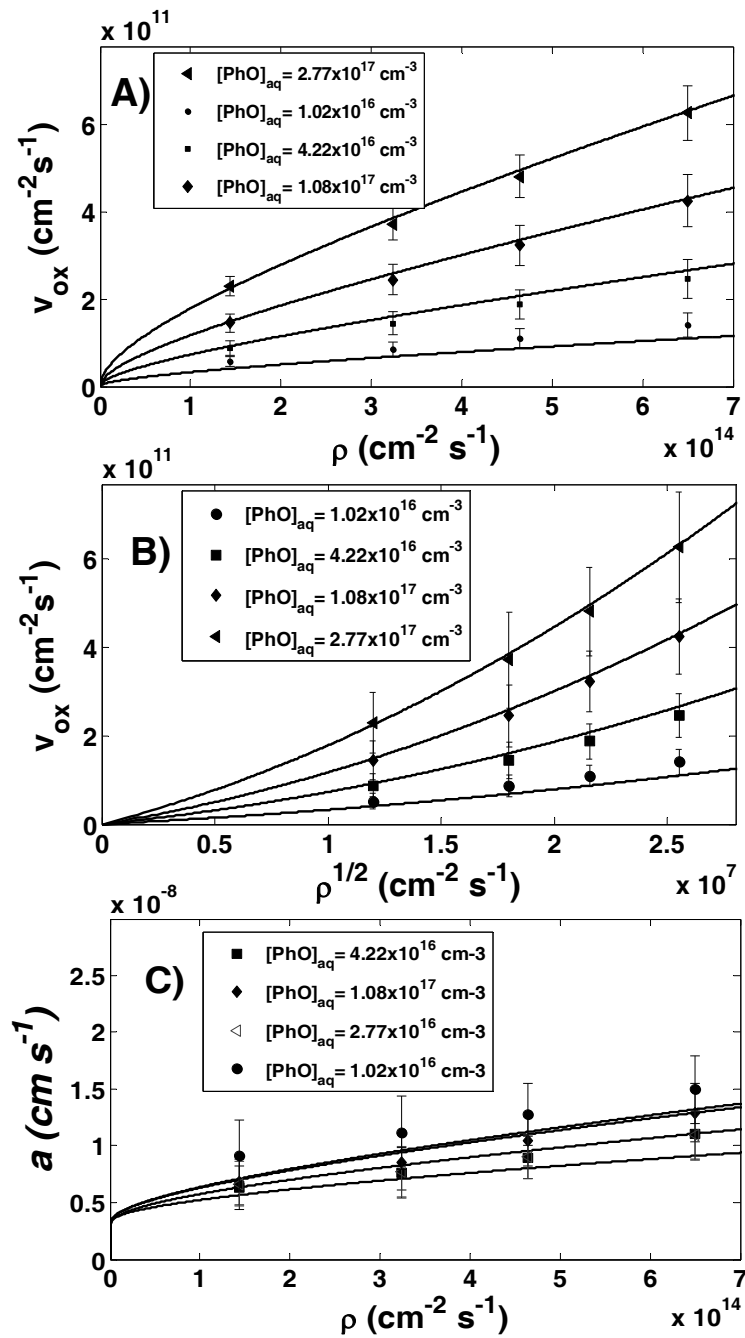
Figure 5. Initial reaction rate $\left(\mathbf{v_{ox}} \right)$ of aqueous phenol (PhO) photooxidation as a function of: (A)

photon flow $\left(\rho \right)$ and (B) the square root of photon flow $\left(\rho^{\frac{1}{2}} \right)$. The solid lines are the theoretical

representation of $v_{ox}^{DT} + v_{ox}^{IT}$ calculated from eqs. 2-I and 3-I. C) Experimental parameter "*a*" (eq 6) as a

function of ρ. The solid lines correspond to the theoretical representation of $\mathbf{a^{IT+DT}}$ **vs** ρ calculated

from eq 8. The fitting parameters used in all panels were: $k_0 = 0.1$; $A_{cat} = 1.2 \times 10^3$ cm^2; $K_{ads} = 1.33 \times 10^{-17}$

cm^3,   b=9.39x10^{13} cm^{-2}, $k'_1 \left[O_S^{2-} \right] = 2.36x10^8 \, cms^{-1}$; $k_{ox}^{DT} = 1.42x10^{-8} cm^3 s^{-1}$.

$a^{IT} = 3.3x10^{-9} \, cm/s$.

Figure 5A shows a nonlinear dependence of v_{ox} on ρ unlike the linear behavior observed in Figure 4A. This indicates that DT is not the prevalent mechanism as was discussed for FA photooxidation. Figure 5B demonstrates that there is no square root dependence of v_{ox} on ρ because the curves that represent v_{ox} **vs.** $\rho^{\frac{1}{2}}$ are not straight lines like in the case of benzene photooxidation (Figure 3B). In fact, the analysis of both figures leads to the conclusion that $v_{ox} \propto \rho^n$ with $0.5 < n < 1$. This kind of experimental dependence of the initial rate on photon flow suggests that phenol is simultaneously oxidized by DT and IT mechanisms. In order to explore this hypothesis in detail, the experimental kinetic data of Figure 5A was used to calculate the value of the parameter a within the range of photon flow and concentrations studied (Figure 5C). It was found that a linearly increases as ρ increases, i.e. $\dfrac{da}{d\rho} > 0$ as is expected for a DT mechanism without adsorption-desorption equilibrium rupture. However, unlike the straight lines of Figure 4B, the solid lines of Figure 5C do not point to the origin and have a relative low slope which resembles more to the horizontal lines observed in Figure 3C. In general, the behavior of the parameter a observed in Figure 5C has some similarities with both Figures 3C and 4B which is symptomatic of photooxidation via a mixture of both mechanisms.

By replacing the fitting parameters of Figure 5 in eqs 2-I and 3-I it was found that the $\dfrac{v_{ox}^{DT}}{v_{ox}^{IT}}$ ratio is in the range $0.3 < \dfrac{v_{ox}^{DT}}{v_{ox}^{IT}} < 1$ for the experimental range of photon flow studied $\left(1.5x10^{14} \le \rho \le 6.7 \times 10^{14} \, \textbf{\textit{photons/cm}}^2 \, \textbf{\textit{s}} \right)$. This ratio values evince that for aqueous phenol $v_{ox}^{DT} \approx v_{ox}^{IT}$ because experimental kinetic data of Figure 5A can only be fitted with a set of parameters that always yield v_{ox}^{DT} *and* v_{ox}^{IT} values that have the same order of magnitude.

It seems contradictory to postulate that $v_{ox}^{DT} \approx v_{ox}^{IT}$ because as mentioned before $k_{ox}^{DT} >> k_{ox}^{IT}$. However, in the case of aqueous phenol $\left[RH_2 \right]_{liq} >> \left[RH_2 \right]_{ads}$ due to chemisorption hindering as already discussed above. Analyzing in detail eqs 2-I and 3-I, it can be inferred that the magnitude of v_{ox}^{IT} depends on both k_{ox}^{IT} and $\left[RH_2 \right]_{liq}$ whereas v_{ox}^{DT} depends on both k_{ox}^{DT} and $\left[RH_2 \right]_{ads}$. Therefore, even if $k_{ox}^{DT} >> k_{ox}^{IT}$ it is possible to get similar values of v_{ox}^{DT} and v_{ox}^{IT} if the difference between the kinetic constants is compensate by a low surface coverage of the organic substrate, i.e. very low values of $\dfrac{\left[RH_2 \right]_{ads}}{\left[RH_2 \right]_{liq}}$. In summary, for aqueous phenol low surface coverage leads to low v_{ox}^{DT} values which at the same time leads to a situation where $v_{ox}^{DT} \approx v_{ox}^{IT}$ in spite of $k_{ox}^{DT} >> k_{ox}^{IT}$.

The PE for kinetic data of Figure 5A is in the range $0.02 < \zeta \left(\% \right) < 0.18$. These low values of PE in the case of aqueous phenol are indicative of DT hindering because higher values of PE would be expected for photooxidation through a preferential DT mechanism as in the case of FA.

If it is true that the DT mechanism is hindered as a consequence of the low coverage of the TiO_2 surface by phenol molecules when the solvent is water, the use of acetonitrile as solvent must promote DT because a higher surface coverage will be reached using this solvent. With this idea in mind, we carried out the same kinetic studied showed in Figure 5 but using acetonitrile instead of water as solvent. The experimental kinetic data are reported in Figure 6.
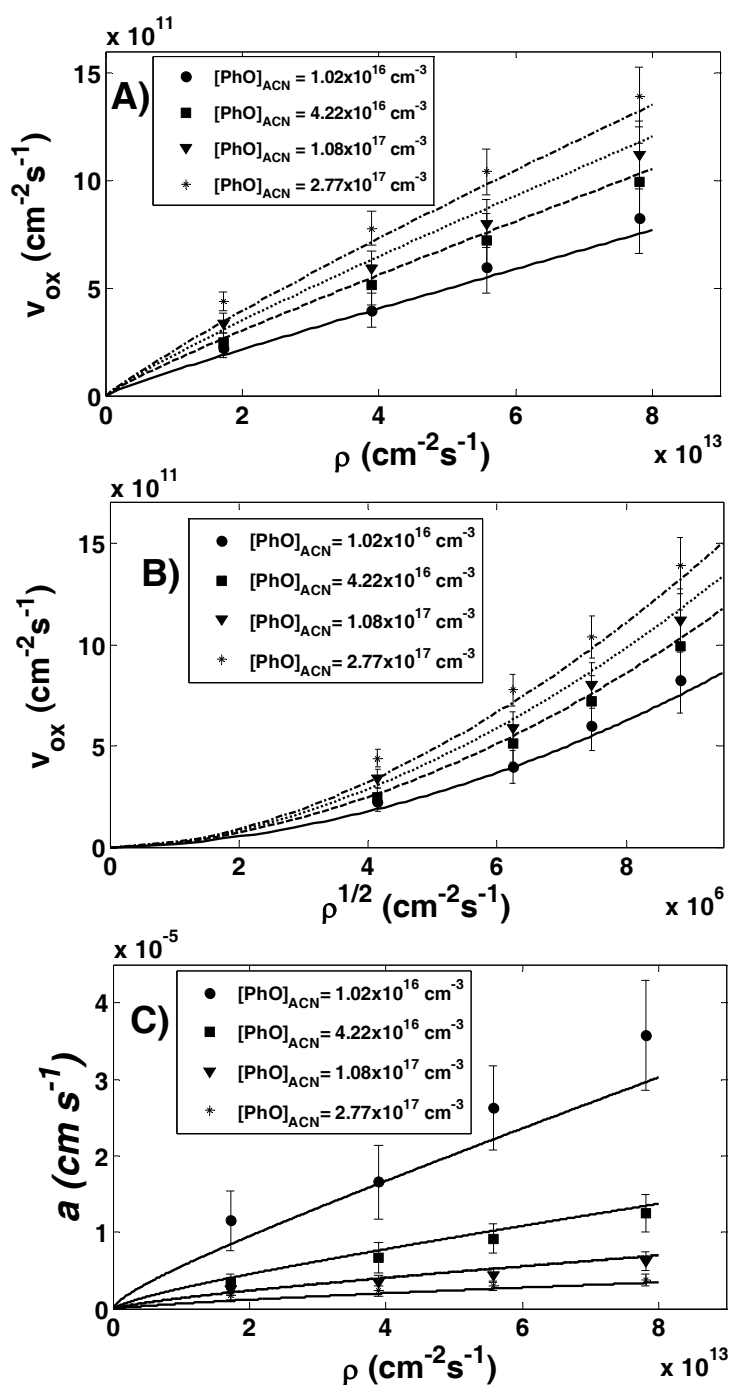
Figure 6. Initial reaction rate $\left(\mathbf{v}_{ox} \right)$ of phenol (PhO) photooxidation in acetonitrile (ACN) as a function

of: (A) photon flow $\left(\rho \right)$ and (B) the square root of photon flow $\left(\rho^{\frac{1}{2}} \right)$. The solid lines are the

theoretical representation of $v_{ox}^{DT} + v_{ox}^{IT}$ calculated from eqs. 2-I and 3-I. C) Experimental parameter "*a*"

(eq 6) as a function of ρ. The solid lines correspond to the theoretical representation of $\mathbf{a^{IT+DT}}$ **vs** ρ

calculated from eq 8. The fitting parameters used in all the panels were: $k_0 = 0.012$; $A_{cat} = 1.0 \times 10^4$ cm^2;

$K_{ads} = 3.96 \times 10^{-18}$ cm^3, $b = 9.23 \times 10^{14}$ cm^{-2}, $k_1' \left[O_s^{2-} \right] = 2.36 \times 10^8$ cms^{-1}; $k_{ox}^{DT} = 1.5 \times 10^{-5} cm^3 s^{-1}$.

$a^{IT} = 6 \times 10^{-7} cm/s$

Again, a nonlinear dependence of $\mathbf{v}_{ox}$ on ρ and $\rho^{\frac{1}{2}}$ can be inferred from Figure 6A and B, respectively. This evince that like in the preceding case $\mathbf{v}_{ox} \propto \rho^{\mathbf{n}}$ with $0.5 < \mathbf{n} < 1$, a typical experimental dependence observed for photooxidation via a mixture of both DT and IT mechanism. However, the curves depicted in Figure 6A and B have higher slopes than those of Figures 5A and B, namely, $\dfrac{dv_{ox}}{d\rho}$ *and* $\dfrac{dv_{ox}}{d\rho^{\frac{1}{2}}}$ are higher for the photooxidation of phenol in acetonitrile with respect to aqueous phenol. This is symptomatic of a higher contribution of the DT mechanism to the photooxidation of phenol when is dissolved in acetonitrile instead of water.

The experimental dependence of the parameter a on photon flow and concentration is shown in Figure 6C. It can be seen that $\dfrac{da}{d\rho} > 0$ and there is no maxima in the curves as is expected for a DT mechanism without adsorption-desorption equilibrium rupture. Although this general features are similar to those of Figure 5C there are two important differences: the slope $\left(\dfrac{da}{d\rho} \right)$ of each curve is higher in Figure 6C and each straight line has a higher tendency to point to the origin. These two aspects are characteristic of the DT mechanism as discussed for FA photooxidation (Figure 4B).

By replacing the fitting parameters of Figure 6 in eqs 2-I and 3-I it was found that the $\dfrac{v_{ox}^{DT}}{v_{ox}^{IT}}$ ratio is in the range $1.5 < \dfrac{v_{ox}^{DT}}{v_{ox}^{IT}} < 6.5$ for the experimental range of photon flow studied $\left(1.7 \times 10^{13} \le \rho \le 7.8 \times 10^{13} \, \textbf{photons}/\textbf{cm}^2 \, \textbf{s} \right)$. On the other hand, the PE for kinetic data of Figure 6A is in the range $1.1 < \zeta \left(\% \right) < 2.2$. It is remarkable that both

$\dfrac{v_{ox}^{DT}}{v_{ox}^{IT}}$ and $\zeta(\%)$ values increase at least one order of magnitude with respect to those of

obtained from Figure 5.

These high values attest that in the photooxidation of phenol in acetonitrile $v_{ox}^{DT} > v_{ox}^{IT}$.

In principle, it is surprising the drastic change introduced by the solvent in the kinetics of phenol photooxidation. However, this change can be rationalized in terms of the severe alteration in the phenol-TiO_2 surface interaction attributable to the solvent. As previously discussed, a higher surface coverage is expected when phenol is dissolved in acetonitrile instead of water. This means higher values of $\dfrac{[RH_2]_{ads}}{[RH_2]_{liq}}$ in the former case

than in the latter. These higher values necessarily lead to higher values of v_{ox}^{DT} because eq 2-I implies that v_{ox}^{DT} increases as $[RH_2]_{ads}$ increases. The growth of v_{ox}^{DT} leads to the remarkable growth in $\zeta(\%)$ observed for phenol photooxidation in acetonitrile because as aforementioned $k_{ox}^{DT} >> k_{ox}^{IT}$ which means that photooxidation by this mechanism should be more efficient.

In a recent publication[19] we assert that photooxidation of organic substrates by free $OH^{\bullet}$ radicals originated from water oxidation (see eq 6 of ref. 19) do not play a significant role in photocatalysis, in agreement with similar claims made by other groups[37,69,70] However, the presence of dissolved molecular oxygen (O_2) brings a new possibility for the production of free $OH^{\bullet}$ radicals via a multistep photoreduction reaction (see the complete reaction sequence in eqs 1 to 5 of ref. 71):

$$O_2 + e_f^- + H^+ \rightarrow\rightarrow\rightarrow OH^{\bullet} \qquad (10)$$
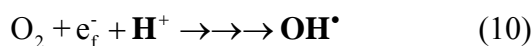
It is worth noting that reaction 10 requires protons (for instance the pK_a of the second reaction step is 4.8[71]). This means that reaction 10 will be favored by the use of water at acid pH as solvent and hindered by the use of acetonitrile as solvent. In spite of this, the initial reaction rate of phenol photooxidation in acetonitrile is 10 times higher than aqueous phenol. This demonstrates that at least at the initial steps of the photocatalytic process (when $t \rightarrow 0$), the oxidation by free $OH^{\bullet}$ radicals produced from eq 10 do not play a significant role in the photooxidation of the organic substrate. Moreover, if we

accept that the production of free $OH^\bullet$ radicals via direct water oxidation by holes is possible (eq 6 of ref. 19), this reaction again should be favored by the use of water as solvent instead of acetonitrile. However, the experimental evidence collected here reveals that phenol is oxidized faster in acetonitrile. In consequence, the oxidation of phenol by free $OH^\bullet$ radicals produced from water oxidation by holes plays not a significant role. In a more general view, the higher photonic efficiencies observed for phenol photooxidation in acetonitrile with respect to those in water can be readily explained in terms of the stronger substrate-TiO_2 surface interaction, and considering as primary reaction steps the oxidation of the organic substrate by either free (eq 2) or surface trapped (eqs 3 to 5) holes. In contrast, the commonly invoke oxidation mechanism through $OH^\bullet$ radicals would produce an opposite experimental behavior with respect to the actually observed. Thus, this kinetic study constitutes additional evidence against the crucial role assigned in some studies to organic photooxidation by free $OH^\bullet$ radicals.

At the first part of this publication, [65] it was discussed that under high enough photon flow the adsorption-desorption equilibrium can be disrupted. When this happens, some maxima in the functions of a *vs.* ρ must be observed (see Figures 8-I and 9-I).[65] Herein, no maxima can be observed in Figures 3C, 4B, 5C and 6C. This mean that our experimental kinetic data was acquired at low enough photon flow values to keep the adsorption equilibrium under illumination. In contrast, kinetic data of aqueous phenol photooxidation reported by Emeline et al.[30] is representative of a situation where the adsorption equilibrium is disrupted under illumination. This can be deduced from the representation of a *vs.* ρ (see figure 13 of ref. 30) made by us in a previous publication where we analyzed in detail Emeline et al. data. [30] At that time, we made the hypothesis that phenol was oxidized via a pure IT mechanism. However, we found and apparent contradiction because the parameter a was not constant as would be expected. In contrast, we found that a was dependent on photon flow and concentration. To explain that behavior we suggested there that despite the weak interaction of aqueous phenol with the TiO_2 surface the contribution of the DT mechanism to the initial reaction rate could be not negligible as initially supposed. The data of Figure 5 provide experimental

support to corroborate that hypothesis because as already discussed it was found that $v_{ox}^{DT} \approx v_{ox}^{IT}$ for aqueous phenol photooxidation.

This dependence of the parameter **a** on photon flow and concentration of Emeline et al. data[30] is illustrated in Figure 7. Some maxima in the representation of **a vs. ρ** at different concentrations can be seen. This evinces that, in this case, phenol is photooxidized by a mixture of IT and DT under adsorption-desorption equilibrium rupture.

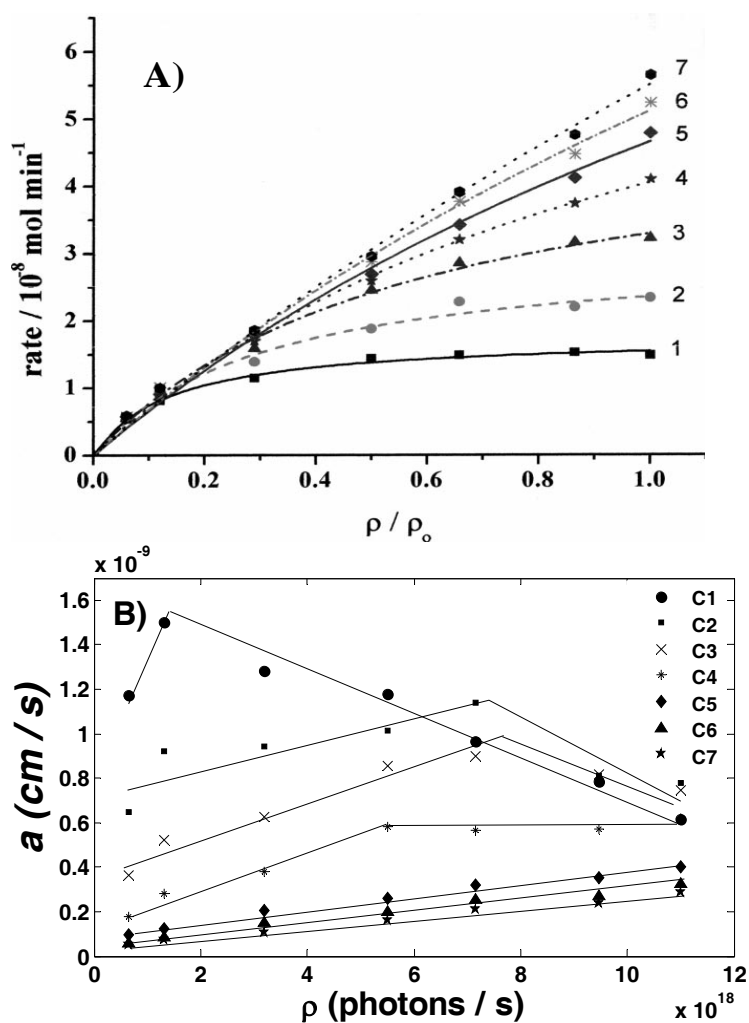**Figure 7**. Representation of: A) initial reaction rate as a function of photon flow ρ for aqueous phenol photooxidation (Figure 3 of ref. 30, reproduced with permission of Elsevier); B) representation of **a vs.** ρ calculated from kinetic data of panel A. Initial concentrations reported by Emeline et al.[30] were: C_1=0.027mM, C_2=0.053mM, C_3=0.106mM, C_4=0.213mM, C_5=0.427mM, C_6=0.638mM, C_7=0.851mM.

The parameter $\boldsymbol{a}$ of panel (B) was calculated with eq 6. Fitting parameters used: $k_0=0.1$, $A_{cat}=1 \times 10^3$ cm^2 and $A_{irr}=100$ cm^2.

The values of the parameter $\boldsymbol{a}$ showed in Figure 7B are not quantitatively exact because some experimental parameters necessary to calculate them such as irradiated area (A_{irr}) and volumen of the reactor was not reported (see details of calculations in supporting info, appendix B).[30] However, beyond the quantitative values of $\boldsymbol{a}$, the important thing is the qualitative behavior observed in Figure 7B which resembles the theoretical one reported in Figures 8-I and 9-I. Moreover, independently of the values assigned to the constants (k_0, A_{cat}, A_{irr}) the qualitative behavior observed in Figure 7B remains unchanged. This reinforces the utility of making $\boldsymbol{a}$ *vs.* ρ representations from the experimental kinetic data in order to elucidate the charge transfer mechanism operative in each specific case.

4. CONCLUSIONS

The interactions of three model compounds, dissolved in water or acetonitrile, with the TiO$_2$ surface were analyzed in detail through spectroscopy techniques and adsorption isotherms. It was found that FA strongly interacts with the TiO$_2$ surface even in the presence of water, being chemisorption the main adsorption mode. As a consequence FA is photooxidized preferentially via a DT mechanism. In contrast, benzene is only physisorbed at the TiO$_2$ surface, being photooxidized exclusively via an IT mechanism. The kinetic analysis of these two paradigmatic cases allows to disclosing the main hallmarks of each photooxidation mechanism by separate. The interaction of phenol with the TiO$_2$ surface was found to be dependent on the solvent due to the competition between the solvent and the phenol molecules for the adsorption sites at the TiO$_2$ surface. While phenol in water weakly interacts with the TiO$_2$ surface because of chemisorption hindering by the competition of water for the Ti(IV) adsorption sites, phenol in acetonitrile showed a stronger interaction. These interactions modes have consequences in the kinetic behavior: phenol in water is photooxidized via a combination of IT and DT mechanisms which have rate values within the same order of magnitude. In contrast, the contribution of the DT mechanism to the photooxidation of

phenol in acetonitrile is higher, being estimated that the rate values of the DT mechanism are at least one order of magnitude higher than those of the IT.

These conclusions about the contribution of the DT or IT mechanisms to the photooxidation of the model compounds could be extracted from the analysis of the representations of v_{ox} *vs.* ρ, v_{ox} *vs.* $\rho^{\frac{1}{2}}$, and a *vs.* ρ. In particular, the representations of the new parameter a proposed by the D-I model showed their utility to elucidate the working mechanism of charge transfer from analysis of experimental kinetic data.

Besides the above cases analyzed from our experimental data, there is another possible situation: the adsorption-desorption equilibrium rupture under illumination. This can occur at a higher photon flow range than that used in this study. From the representation of a *vs.* ρ of aqueous phenol photooxidation data reported by Emeline et al. [30], it could be inferred that adsorption equilibrium is disrupted in that case as is evinced by the several maxima at the curves of the functions of a *vs.* ρ.

The experimental evidence collected in this work supports the central hypothesis the D-I model: the degree of organic substrate-TiO$_2$ surface interactions plays a crucial role in the kinetics of photocatalytic reactions. Depending on these interactions, the specific organic molecule will be photooxidized by an IT, DT or a combination of both mechanism in different degrees.

The methodological procedure used in this work to study organic substrate-TiO$_2$ surface interactions and to analyze kinetic data could be applied to the study of any organic photooxidation. This will allow elucidating the extent of participation of each charge transfer mechanism in each particular situation. As a result, a more rational design of strategies to improve the efficiency of the photocatalytic process could be implemented because the efficiency of each charge transfer mechanism can be improved through different types of surface modifications. [16]

ASSOCIATED CONTENT

Supporting Information

Details of HPLC methods and analysis; adsorption isotherms; calculation of adsorption constants and additional discussion about adsorption of the model molecules at the TiO_2 surface can be found in the appendix A. Details of some numerical procedures to calculate initial reaction rates, the parameter a , and unit conversions can be found in appendix B. This material is available free of charge via the Internet at http://pubs.acs.org.

ACKNOWLEDGMENTS

References

(1) Hoffmann, M. R.; Martin, S. T.; Choi, W.; Bahnemann, D. W. Environmental Applications of Semiconductor Photocatalysis. *Chemical Reviews* **1995,** *95* (1), 69-96.

(2) Peral, J.; Domenech, X.; Ollis, D. F. Heterogeneous photocatalysis for purification, decontamination and deodorization of air. *Journal of Chemical Technology and Biotechnology* **1997,** *70* (2), 117-140.

(3) Fujishima, A.; Zhang, X.; Tryk, D. A. TiO2 photocatalysis and related surface phenomena. *Surface Science Reports* **2008,** *63* (12), 515-582.

(4) Friedmann, D.; Mendive, C.; Bahnemann, D. TiO2 for water treatment: Parameters affecting the kinetics and mechanisms of photocatalysis. *Applied Catalysis B: Environmental* **2010,** *99* (3-4), 398-406.

(5) Matthews, R. W. Kinetics of photocatalytic oxidation of organic solutes over titanium dioxide. *Journal of Catalysis* **1988,** *111* (2), 264-272.

(6) Matthews, R. W. Photooxidation of organic impurities in water using thin films of titanium dioxide. *J. Phys. Chem.* **1987,** *91* (12), 3328-3333.

(7) Alfano, O. M.; Bahnemann, D.; Cassano, A. E.; Dillert, R.; Goslich, R. Photocatalysis in water environments using artificial and solar light. *Catalysis Today* **2000,** *58* (2-3), 199-230.

(8) Zhang, L.; Mohamed, H. H.; Dillert, R.; Bahnemann, D. Kinetics and mechanisms of charge transfer processes in photocatalytic systems: A review. *Journal of Photochemistry and Photobiology C: Photochemistry Reviews* **2012,** *13* (4), 263-276.

(9) Howe, R. F.; Gratzel, M. EPR study of hydrated anatase under UV irradiation. *J. Phys. Chem.* **1987,** *91* (14), 3906-3909.

(10) Micic, O. I.; Zhang, Y.; Cromack, K. R.; Trifunac, A. D.; Thurnauer, M. C. Trapped holes on titania colloids studied by electron paramagnetic resonance. *J. Phys. Chem.* **1993,** *97* (28), 7277-7283.

(11) Villarreal, T. L.; Gomez, R.; Gonzalez, M.; Salvador, P. A Kinetic Model for Distinguishing between Direct and Indirect Interfacial Hole Transfer in the Heterogeneous Photooxidation of Dissolved Organics on TiO_2 Nanoparticle Suspensions. *J. Phys. Chem. B* **2004,** *108* (52), 20278-20290.

(12) Dimitrijevic, N. M.; Saponjic, Z. V.; Rabatic, B. M.; Poluektov, O. G.; Rajh, T. Effect of Size and Shape of Nanocrystalline TiO2 on Photogenerated Charges. An EPR Study. *J. Phys. Chem. C* **2007,** *111* (40), 14597-14601.

(13) Monllor-Satoca, D.; Gomez, R.; Gonzalez-Hidalgo, M.; Salvador, P. The "Direct-Indirect" model: An alternative kinetic approach in heterogeneous photocatalysis based on the degree of interaction of dissolved pollutant species with the semiconductor surface. *Catalysis Today* **2007,** *129* (1-2), 247-255.

(14) Turchi, C. S.; Ollis, D. F. Photocatalytic Degradation Of Organic Water Contaminants: Mechanisms Involving Hydroxyl Radical Attack. *Journal of Catalysis* **1990,** *122* (1), 178-192.

(15) Montoya, J. F.; Velasquez, J. A.; Salvador, P. The direct-indirect kinetic model in photocatalysis: A reanalysis of phenol and formic acid degradation rate dependence on photon flow and concentration in TiO2 aqueous dispersions. *Applied Catalysis B: Environmental* **2009,** *88* (1-2), 50-58.

(16) Montoya, J. F.; Salvador, P. The influence of surface fluorination in the photocatalytic behaviour of TiO2 aqueous dispersions: An analysis in the light of the direct-indirect kinetic model. *Applied Catalysis B: Environmental* **2010,** *94* (1-2), 97-107.

(17) Montoya, J. F.; Peral, J.; Salvador, P. Comments on the published article "Effects of hydroxyl radicals and oxygen species on the 4-chlorophenol degradation by photoeletrocatalytic reactions with TiO2-film electrodes by J. Yang, J. Dai, Ch. Chen, J. Zhao; J. Photochem. Photobiol. A: Chem. 208 (2009) 66-77". *Journal of Photochemistry and Photobiology A: Chemistry* **2010,** *210* (2-3), 215-216.

(18) Montoya, J. F.; Peral, J.; Salvador, P. Surface Chemistry and Interfacial Charge-Transfer Mechanisms in Photoinduced Oxygen Exchange at O_2-TiO_2 Interfaces. *ChemPhysChem* **2011,** *12* (5), 901-907.

(19) Montoya, J. F.; Ivanova, I.; Dillert, R.; Bahnemann, D. W.; Salvador, P.; Peral, J. Catalytic Role of Surface Oxygens in TiO2 Photooxidation Reactions: Aqueous Benzene Photooxidation with Ti18O2 under Anaerobic Conditions. *J. Phys. Chem. Lett.* **2013,** *4* (9), 1415-1422.

(20) Minero, C.; Mariella, G.; Maurino, V.; Pelizzetti, E. Photocatalytic Transformation of Organic Compounds in the Presence of Inorganic Anions. 1. Hydroxyl-Mediated and Direct Electron-Transfer Reactions of Phenol on a Titanium Dioxide-Fluoride System. *Langmuir* **2000,** *16* (6), 2632-2641

(21) Cassano, A. E.; Martin, C. A.; Brandi, R. J.; Alfano, O. M. Photoreactor Analysis and Design: Fundamentals and Applications. *Ind. Eng. Chem. Res.* **1995,** *34* (7), 2155-2201

(22) Dillert, R.; Cassano, A. E.; Goslich, R.; Bahnemann, D. Large scale studies in solar catalytic wastewater treatment. *Catalysis Today* **1999,** *54* (2-3), 267-282.

(23) Cassano, A. E.; Alfano, O. M. Reaction engineering of suspended solid heterogeneous photocatalytic reactors. *Catalysis Today* **2000,** *58* (2-3), 167-197.

(24) Sagawe, G.; Brandi, J.; Bahnemann, D.; Cassano, A. E. Photocatalytic reactors for treating water pollution with solar illumination. I: A simplified analysis for batch reactors. *Chemical Engineering Science* **2003,** *58* (12), 2587-2599

(25) Sagawe, G.; Brandi, J.; Bahnemann, D.; Cassano, E. Photocatalytic reactors for treating water pollution with solar illumination. II: A simplified analysis for flow reactors. *Chemical Engineering Science* **2003,** *58* (12), 2601-2615.

(26) Sagawe, G.; Brandi, R. J.; Bahnemann, D.; Cassano, A. E. Photocatalytic reactors for treating water pollution with solar illumination. III: a simplified analysis for recirculating reactors. *Solar Energy* **2004,** *77* (5), 471-489.

(27) Mueses, M. A.; Machuca-Martinez, F.; Puma, G.L. Effective quantum yield and reaction rate model for evaluation of photocatalytic degradation of water contaminants in heterogeneous pilot-scale solar photoreactors. *Chemical Engineering Journal* **2013,** *215*, 937-947.

(28) Minero, C.; Catozzo, F.; Pelizzetti, E. Role of adsorption in photocatalyzed reactions of organic molecules in aqueous titania suspensions. *Langmuir* **1992,** *8* (2), 481-486.

(29) Minero, C. Kinetic analysis of photoinduced reactions at the water semiconductor interface. *Catalysis Today* **1999,** *54* (2-3), 205-216.

(30) Emeline, A. V.; Ryabchuk, V.; Serpone, N. Factors affecting the efficiency of a photocatalyzed process in aqueous metal-oxide dispersions: Prospect of distinguishing between two kinetic models. *Journal of Photochemistry and Photobiology A: Chemistry* **2000,** *133* (1-2), 89-97.

(31) Emeline, A. V.; Ryabchuk, V. K.; Serpone, N. Dogmas and Misconceptions in Heterogeneous Photocatalysis. Some Enlightened Reflections. *J. Phys. Chem. B* **2005,** *109* (39), 18515-18521.

(32) Ollis, D. F. Kinetics of Liquid Phase Photocatalyzed Reactions: An Illuminating Approach. *The Journal of Physical Chemistry B* **2005,** *109* (6), 2439-2444.

(33) Ollis, D. Kinetic Disguises in Heterogeneous Photocatalysis. *Topics in Catalysis* **2005,** *35* (3), 217-223.

(34) Mills, A.; Wang, J.; Ollis, D. F. Kinetics of Liquid Phase Semiconductor Photoassisted Reactions: Supporting Observations for a Pseudo-Steady-State Model. *The Journal of Physical Chemistry B* **2006,** *110* (29), 14386-14390.

(35) Mills, A.; Wang, J.; Ollis, D. F. Dependence of the kinetics of liquid-phase photocatalyzed reactions on oxygen concentration and light intensity. *Journal of Catalysis* **2006,** *243* (1), 1-6.

(36) Ohtani, B. Preparing Articles on Photocatalysis-Beyond the Illusions, Misconceptions, and Speculation. *Chemistry Letters* **2008,** *37* (3), 216-229.

(37) Minero, C.; Bedini, A.; Maurino, V. Glycerol as a probe molecule to uncover oxidation mechanism in photocatalysis. *Applied Catalysis B: Environmental* **2012,** *128* (0), 135-143.

(38) Thompson, T. L.; Yates, J. T. Surface Science Studies of the Photoactivation of TiO2New Photochemical Processes. *Chemical Reviews* **2006,** *106* (10), 4428-4453.

(39) Pang, C. L.; Lindsay, R.; Thornton, G. Chemical reactions on rutile TiO2(110). *Chemical Society Reviews* **2008,** *37* (10), 2328-2353.

(40) Henderson, M. A. A surface science perspective on photocatalysis. *Surface Science Reports* **2011,** *66* (6-7), 185-297.

(41) Hug, S. J.; Sulzberger, B. In situ Fourier Transform Infrared Spectroscopic Evidence for the Formation of Several Different Surface Complexes of Oxalate on TiO2 in the Aqueous Phase. *Langmuir* **1994,** *10* (10), 3587-3597.

(42) Weisz, A. D.; García Rodenas, L.; Morando, P. J.; Regazzoni, A. E.; Blesa, M. A. FTIR study of the adsorption of single pollutants and mixtures of pollutants onto titanium dioxide in water: oxalic and salicylic acids. *Catalysis Today* **2002,** *76* (2-4), 103-112.

(43) Araujo, P. Z.; Mendive, C. B.; Rodenas, L. A. G.; Morando, P. J.; Regazzoni, A. E.; Blesa, M. A.; Bahnemann, D. FT-IR-ATR as a tool to probe photocatalytic interfaces. *Colloids and Surfaces A: Physicochemical and Engineering Aspects* **2005,** *265* (1-3), 73-80.

(44) Lana-Villarreal, T.; Rodes, A.; Perez, J. M.; Gomez, R. A Spectroscopic and Electrochemical Approach to the Study of the Interactions and Photoinduced Electron Transfer between Catechol and Anatase Nanoparticles in Aqueous Solution. *Journal of the American Chemical Society* **2005,** *127* (36), 12601-12611.

(45) Mendive, C. B.; Bahnemann, D. W.; Blesa, M. A. Microscopic characterization of the photocatalytic oxidation of oxalic acid adsorbed onto TiO2 by FTIR-ATR. *Catalysis Today* **2005,** *101* (3GÇô4), 237-244.

(46) Mendive, C. B.; Bredow, T.; Blesa, M. A.; Bahnemann, D. W. ATR-FTIR measurements and quantum chemical calculations concerning the adsorption and photoreaction of oxalic acid on TiO2. *Phys. Chem. Chem. Phys.* **2006,** *8* (27), 3232-3247.

(47) Mendive, C. B.; Bredow, T.; Feldhoff, A.; Blesa, M.; Bahnemann, D. Adsorption of oxalate on rutile particles in aqueous solutions: a spectroscopic, electron-microscopic and theoretical study. *Phys. Chem. Chem. Phys.* **2008,** *10* (14), 1960-1974.

(48) Horikoshi, S.; Miura, T.; Kajitani, M.; Hidaka, H.; Serpone, N. A FT-IR (DRIFT) study of the influence of halogen substituents on the TiO2-assisted photooxidation of phenol and p-halophenols under weak room light irradiance. *Journal of Photochemistry and Photobiology A: Chemistry* **2008,** *194* (2-3), 189-199.

(49) Mendive, C. B.; Bredow, T.; Feldhoff, A.; Blesa, M. A.; Bahnemann, D. Adsorption of oxalate on anatase (100) and rutile (110) surfaces in aqueous systems: experimental results vs. theoretical predictions. *Phys. Chem. Chem. Phys.* **2009,** *11* (11), 1794-1808.

(50) Minella, M.; Faga, M. G.; Maurino, V.; Minero, C.; Pelizzetti, E.; Coluccia, S.; Martra, G. Effect of Fluorination on the Surface Properties of Titania P25 Powder: An FTIR Study. *Langmuir* **2009**.

(51) Kim, S.; Choi, W. Visible-Light-Induced Photocatalytic Degradation of 4-Chlorophenol and Phenolic Compounds in Aqueous Suspension of Pure Titania: Demonstrating the Existence of a Surface-Complex-Mediated Path. *The Journal of Physical Chemistry B* **2005,** *109* (11), 5143-5149.

(52) Hatchard, C. G.; Parker, C. A. A New Sensitive Chemical Actinometer. II. Potassium Ferrioxalate as a Standard Chemical Actinometer. *Proceedings of the Royal Society of London. Series A. Mathematical and Physical Sciences* **1956,** *235* (1203), 518-536.

(53) Orlov, A.; Watson, D. J.; Williams, F. J.; Tikhov, M.; Lambert, R. M. Interactions of 4-Chlorophenol with TiO2 Polycrystalline Surfaces: A Study of Environmental Interfaces by NEXAFS, XPS, and UPS. *Langmuir* **2007,** *23* (19), 9551-9554.

(54) Wang, Y.; Hang, K.; Anderson, N. A.; Lian, T. Comparison of Electron Transfer Dynamics in Molecule-to-Nanoparticle and Intramolecular Charge Transfer Complexes. *The Journal of Physical Chemistry B* **2003,** *107* (35), 9434-9440.

(55) Tachikawa, T.; Tojo, S.; Fujitsuka, M.; Majima, T. Photocatalytic One-Electron Oxidation of Biphenyl Derivatives Strongly Coupled with the TiO2 Surface. *Langmuir* **2004,** *20* (7), 2753-2759.

(56) Knorr, F. J.; Mercado, C. C.; McHale, J. L. Trap-State Distributions and Carrier Transport in Pure and Mixed-Phase TiO2: Influence of Contacting Solvent and Interphasial Electron Transfer. *J. Phys. Chem. C* **2008,** *112* (33), 12786-12794.

(57) Greaves, S. J.; Griffith, W. P. Vibrational spectra of catechol, catechol-d2 and -d6 and the catecholate monoanion. *Spectrochimica Acta Part A: Molecular Spectroscopy* **1991,** *47* (1), 133-140.

(58) H. Gunzler, H.U. Gremlich, IR Spectroscopy. An Introduction, Wiley–VCH, 2002

(59) Zierkiewicz, W.; Michalska, D.; Zeegers-Huyskens, T. r. s. Molecular Structures and Infrared Spectra of p-Chlorophenol and p-Bromophenol. Theoretical and Experimental Studies. *The Journal of Physical Chemistry A* **2000,** *104* (50), 11685-11692.

(60) Zierkiewicz, W.; Michalska, D.; Czarnik-Matusewicz, B.; Rospenk, M. Molecular Structure and Infrared Spectra of 4-Fluorophenol: A Combined Theoretical and Spectroscopic Study. *The Journal of Physical Chemistry A* **2003,** *107* (22), 4547-4554.

(61) Stradins, J.; Hasanli, B. Anodic voltammetry of phenol and benzenethiol derivatives.: Part 1. Influence of pH on electro-oxidation potentials of substituted phenols and evaluation of pKa from anodic voltammetry data. *Journal of Electroanalytical Chemistry* **1993,** *353* (1-2), 57-69.

(62) Roddick-Lanzilotta, A. D.; Connor, P. A.; McQuillan, A. J. An In Situ Infrared Spectroscopic Study of the Adsorption of Lysine to TiO2 from an Aqueous Solution. *Langmuir* **1998,** *14* (22), 6479-6484.

(63) Zhou, J.; Dag, S.; Senanayake, S. D.; Hathorn, B. C.; Kalinin, S. V.; Meunier, V.; Mullins, D. R.; Overbury, S. H.; Baddorf, A. P. Adsorption, desorption, and dissociation of benzene on TiO_2 (110) and Pd/TiO_2 (110) : Experimental characterization and first-principles calculations. *Phys. Rev. B* 2006, *74* (12), 125318.

(64) Kobayakawa, K.; Nakazawa, Y.; Ikeda, M.; Sato, Y.; Fujishima, A. Influence of the Density of Surface Hydroxyl-Groups on TiO_2 Photocatalytic Activities. *Berichte der Bunsen-Gesellschaft-Physical Chemistry Chemical Physics* 1990, *94* (12), 1439-1443.

(65) Montoya, J. F.; Peral, J.; Salvador, P. Comprehensive Analysis of Kinetics and Mechanisms of TiO_2 Photocatalytic Reactions . I) Theoretical approach through the D-I model. Manuscript submitted for publication.

(66) Kormann, C.; Bahnemann, D. W.; Hoffmann, M. R. Photolysis of chloroform and other organic molecules in aqueous titanium dioxide suspensions. *Environmental Science & Technology* 1991, *25* (3), 494-500.

(67) Martyanov, I. N.; Savinov, E. N. Photocatalytic steady-state methylviologen oxidation in air-saturated TiO2 aqueous suspension: Initial photonic efficiency and initial oxidation rate as a function of methylviologen concentration and light intensity. *Journal of Photochemistry and Photobiology A: Chemistry* **2000,** *134* (3), 219-226.

(68) Serpone, N.; Terzian, R.; Lawless, D.; Kennepohl, P.; Sauvé, G. v. On the usage of turnover numbers and quantum yields in heterogeneous photocatalysis. *Journal of Photochemistry and Photobiology A: Chemistry* **1993,** *73* (1), 11-16.

(69) Lawless, D.; Serpone, N.; Meisel, D. Role of hydroxyl radicals and trapped holes in photocatalysis. A pulse radiolysis study. *J. Phys. Chem.* **1991,** *95* (13), 5166-5170.

(70) Rajh, T.; Saponjic, Z. V.; Micic, O. I. Reactions of hydrous titanium oxide colloids with strong oxidizing agents. *Langmuir* **1992,** *8* (5), 1265-1270.

(71) Li, Y.; Wen, B.; Yu, C.; Chen, C.; Ji, H.; Ma, W.; Zhao, J. Pathway of Oxygen Incorporation from O2 in TiO2 Photocatalytic Hydroxylation of Aromatics: Oxygen Isotope Labeling Studies. *Chem. Eur. J.* **2012,** *18* (7), 2030-2039.

SUPPORTING INFORMATION

Comprehensive Analysis of Kinetics and Mechanisms of TiO$_2$ Photocatalytic Reactions . II) Experimental validation of the D-I model

Juan Felipe Montoya[1], José Peral[1], and Pedro Salvador[1,*]

1.Departamento de Química, Universidad Autónoma de Barcelona, 08193 Cerdanyola del Vallés, Spain.

*Corresponding author, E-mail: psalvador@klingon.uab.es

Keywords: Kinetics; Mechanisms; Photocatalysis; D-I Model; Charge Transfer

Appendix A. ADSORPTION STUDY

1. Experimental

1.1 Materials

All reactants were analytical grade and were used without further purification (purity >99%). TiO_2 was purchased from Aldrich (purity 99.7%, mean particle size: 25 nm, 100% anatase, BET area=55 m^2/g). Water was purified in a Millipore Mill-Q system $(resistivity \geq 18\,M\Omega\,cm)$.

1.2 Analytical methods

a) Adsorption isotherm of phenol dissolved in acetonitrile was obtained analyzing the concentration of samples in a high performance liquid chromatography (HPLC) system composed of a LCP 4100 ECOM Tech Lab pump and a LCD 2084 ECOM Techlab UV Detector adjusted to 280 nm. The stationary phase was a Hypersil ODS column (25cm Long. x 4.6 mm i.d., 5 μm particles) working at room temperature. The mobile phase was a mixture of acetonitrile and water (40:60 %v/v) adjusted to pH 3 by adding H_3PO_4. The flow rate was kept constant at 0.8 ml/min. The retention time of phenol peak was 6.65 min. A calibration curve (R^2=0.9977) was obtained by injecting patrons of 8 different concentrations of phenol (in a range from 0 to 30 ppm) using a mixture of water and ACN (50:50 %v/v) as solvent.

b) Analysis of samples from the study of adsorption of phenol in aqueous solutions was carried out in a HPLC system which comprises a LC-10AT Shimadzu pump and a diode array detector (Agilent, G1315B) adjusted to 280 nm. The stationary phase was the same Hypersil column mentioned above working at room temperature. The mobile phase was a mixture of acetonitrile and water (60:40 %v/v) adjusted to pH 3 by adding H_3PO_4. The flow rate was kept constant at 0.5 ml/min. The retention time of phenol peak was 7.54 min. A calibration curve (R^2=0.9992) was obtained by injecting patrons

of 8 different concentrations of phenol (in a range from 0 to 20 ppm) using as solvent a mixture of water and ACN (50:50 %v/v). Formic acid (FA) samples were analyzed at the same HPLC system using as stationary phase an Aminex HPX-87H column and 0.01 M H_2SO_4 aqueous solution as mobile phase. The flow rate was kept constant at 0.6 ml/min. The detector was adjusted to 210 nm. The retention time of FA peak was 14.1 min. A calibration curve (R^2=0.9986) was obtained by injecting patrons of FA aqueous solutions at eight different concentrations (in a range from 0 to 20 ppm).

1.3 Experimental Procedure

a) Adsorption isotherm of phenol dissolved in ACN: 8 solutions of different concentrations of phenol dissolved in ACN were prepared in 25 ml volumetric flasks. Two aliquots of 1 ml were taken and analyzed by HPLC in order to determine the initial concentration of phenol (C_o). Then, each solution was added to opaque plastic containers with 0.0125 g of TiO_2 and was put under stirring at 300 rpm. Temperature was periodically monitored being 23 +/- 1 ^{o}C throughout the experiment. After 24 hours two samples of 1 ml were taken, filtered through Nylon syringe filters (pore size: 45 μm), diluted with 1 ml of water and analyzed by HPLC in order to get the value of the equilibrium concentration (C_{eq}). In a previous experiment a solution of phenol (C_o=0.35 mM) was put in contact with TiO_2 in the dark under the same experimental conditions described above, taking samples at time intervals of 15 min in the first hour, every two hours until eight hours, and finally at 20 and 24 hours of adsorption time. It was found that a steady state concentration is reached after two hours being this the time needed to achieve adsorption equilibrium.

b) Adsorption isotherm of phenol dissolved in water: 8 aqueous solutions of different concentrations of phenol were prepared in 50 ml volumetric flasks. The initial pH was adjusted to 3.0 by adding $HClO_4$ and it remained constant along the experiment. Ionic strength was adjusted by adding KNO_3 (0.01 M). Two aliquots of 1 ml were taken and analyzed by HPLC in order to determine the initial concentration of phenol (C_o). Then, each solution was added to opaque plastic containers with 0.096 g of TiO_2 and was left under stirring at 300 rpm. Temperature was periodically monitored being 23 +/- 1 ^{o}C

throughout the experiment. After 24 hours two samples of 1 ml were taken, filtered through cellulose acetate syringe filters (pore size: 45 μm), diluted with 1 ml of acetonitrile and analyzed by HPLC in order to get the value of the equilibrium concentration (C_{eq}). Preliminary experiments showed that adsorption equilibrium was reached within two hours.

c) Adsorption isotherm of formic acid (FA) dissolved in water: 6 aqueous solutions of different concentrations of FA were prepared in 50 ml volumetric flasks. The initial pH was adjusted to 3.0 by adding $HClO_4$ and it remained constant along the experiment. Two aliquots of 1 ml were taken and analyzed by HPLC in order to determine the initial concentration of FA (C_o). Then, each solution was added to opaque plastic containers with 0.096 g of TiO_2 and was left under stirring at 300 rpm. Temperature was periodically monitored being 23 +/- 1 ^{o}C throughout the experiment. After 24 hours two samples of 1 ml were taken, filtered through cellulose acetate syringe filters (pore size: 45 μm), and analyzed by HPLC in order to get the value of the equilibrium concentration (C_{eq}). Preliminary experiments showed that adsorption equilibrium was reached within one hour.

Results

The amount of organic molecules absorbed per mass of TiO_2 (C_{ads}) was calculated using eq. 1.

$$C_{ads} = \frac{\left(C_0 - C_{eq}\right) \times V}{W} \times 6.022 x 10^{23}$$
Eq. 1

In eq. 1 the concentrations are expressed in molar units, V is the total volume of the suspension (in Liters) and W is the weight of catalyst (in grams).

Figure 1 shows the adsorption isotherms of formic acid, and phenol dissolved in water and acetonitrile, and benzene dissolved in acetonitrile. It is worth nothing that the amount of benzene absorbed on TiO_2 is negligible and the difference in concentration calculated according to eq. 1 are within the experimental error of the HPLC instrument.
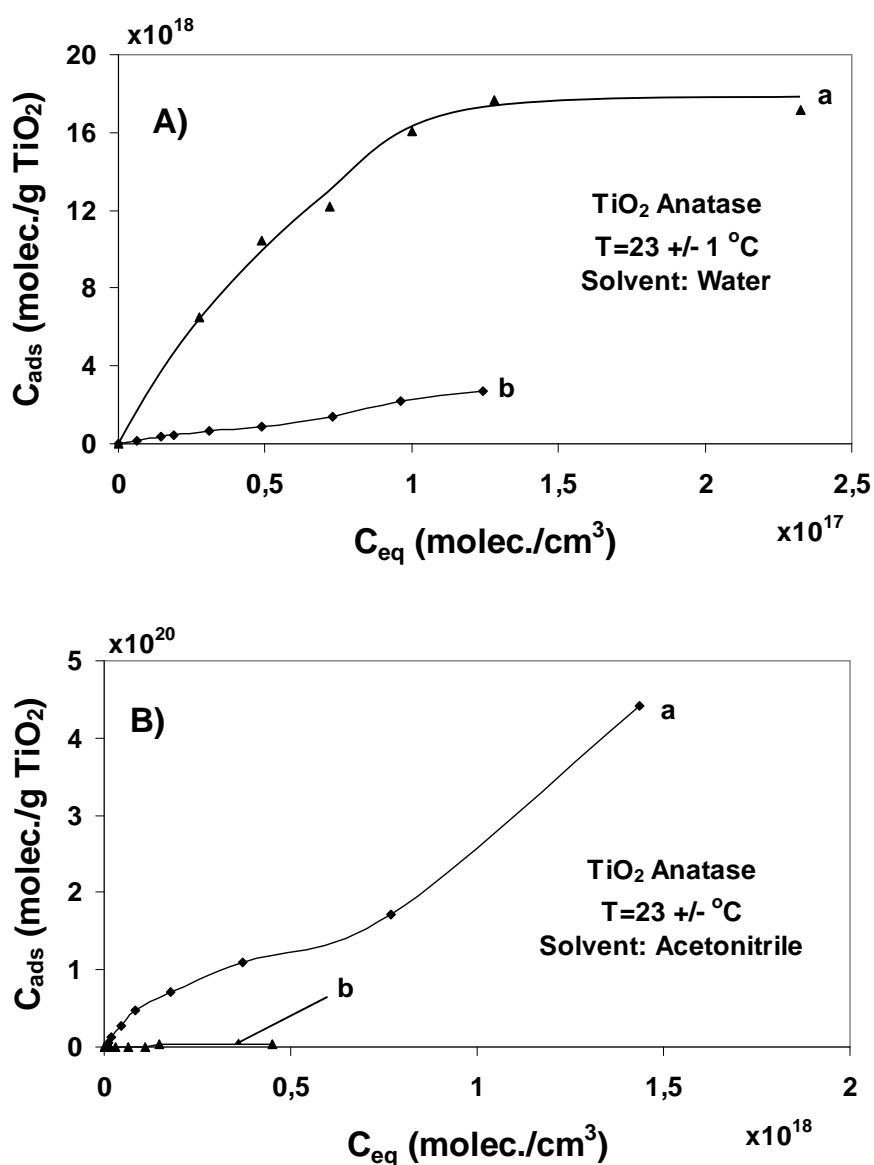
Figure 1. A) Adsorption isotherms of aqueous solutions of FA (a) and phenol (b) on TiO$_2$ anatase. B) Adsorption isotherms of phenol (a) and benzene (b) dissolved in acetonitrile on TiO$_2$ anatase.

It has been reported that TiO$_2$ forms particle agglomerates (PAs) when it is dispersed in a solvent[1-5]. The size of each PA depends on the solvent and the type of TiO$_2$ sample. The average diameter of the PAs (D$_a$) of anatase TiO$_2$ in acetonitrile is D$_a$=78 +/- 6 nm[1]

while those dissolved in water have an average diameter of D_a = 650 +/- 250 nm[2-4] for samples of pure anatase with a primary particle size lower than 100 nm. Assuming that the PAs of TiO_2 have a spherical shape, the volume of each PA with a diameter of 78 and 650 nm is calculated to be 2.48×10^{-16} and 1.44×10^{-13} cm^3 respectively. Considering that the mass density of anatase TiO_2 is 3.894 g/cm^3, the total number of PAs per gram of catalyst in acetonitrile and water is calculated to be 1.033×10^{15} and 1.79×10^{12} PAs/g respectively. The surface area of each PA in acetonitrile and water is 1.91×10^{-10} and 1.33×10^{-8} cm^2/PA respectively. The specific surface area (S_g) of anatase TiO_2 suspended in water and acetonitrile can be obtained by multiplying the respective surface area of each PA by the number of PAs per gram of catalyst. It was calculated a S_g=197303 cm^2/g for TiO_2 suspensions in acetonitrile and S_g=23807 cm^2/g for suspensions in water. These specific surface areas are lower than the BET area reported by the manufacturer of the TiO_2 (S_g=550000 cm^2/g). Since BET area is measured with the sample of TiO_2 exposed to vacuum, agglomeration of particles is not expected, hence the value of S_g measured by BET must be higher than those calculated for TiO_2 suspended in liquid phase. Using the same procedure described above and taking into account that the primary particle size (D_p) of our TiO_2 sample is D_p=25 nm, the specific surface area of TiO_2 exposed to vacuum is calculated to be S_g=616332 cm^2/g which is in good agreement with the value measured by BET.

The amount of molecules adsorbed per catalyst area ($\left[RH_2 \right]_{ads}$) can be calculated with eq. 2.

$$\left[RH_2 \right]_{ads} = \frac{C_{ads}}{S_g} \quad \left(\frac{molec.}{cm^2} \right) \qquad \text{Eq. 2}$$

Figure 2 shows the adsorption isotherms obtained using eq. 2 and the values of S_g calculated for each solvent to transform de values of the ordinate axis of fig. 1.
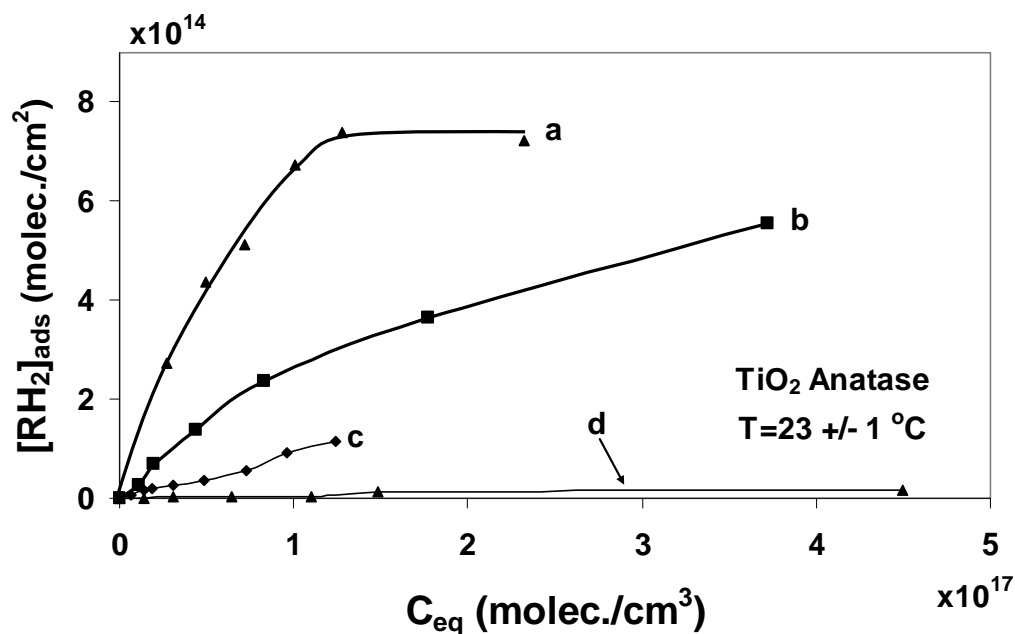
Figure 2. A) Adsorption isotherms of different organic molecules on TiO_2 anatase: a) FA dissolved in water; b) phenol dissolved in acetonitrile; c) phenol dissolved in water; d) benzene dissolved in acetonitrile.

The linearized form of the Langmuir isotherm equation (eq. 3) is expressed by eq. 4.

$$\left[RH_2 \right]_{ads} = \frac{K_{ads} b C_{eq}}{1 + K_{ads} C_{eq}} \qquad \text{Eq. 3}$$

Where K_{ads} is the Langmuir adsorption constant and b is the maximum amount of organic molecules adsorbed per catalyst area.

$$\frac{C_{eq}}{\left[RH_2 \right]_{ads}} = \frac{1}{K_{ads} b} + \frac{C_{eq}}{b} \qquad \text{Eq. 4}$$

According to eq. 4 a representation of $\dfrac{C_{eq}}{\left[RH_2 \right]_{ads}}$ vs. C_{eq} must be linear whit a slope

equal to $\dfrac{1}{b}$ and an intercept equal to $\dfrac{1}{K_{ads} b}$. From eq. 4 it can be inferred that the

inverse of the intercept with the ordinate axis is equal to the relation between the

adsorbed and dissolved organic molecules $\left(\dfrac{\left[RH_2 \right]_{ads}}{C_{eq}} \right)$ when the equilibrium

concentration (C_{eq}) tends to zero, this is expressed in eq. 5:

$$\frac{1}{\mathbf{int\, ercept}} = K_{ads}b = \left(\frac{\left[RH_2 \right]_{ads}}{C_{eq}} \right)_{C_{eq} \to 0} \qquad \text{Eq. 5}$$

A higher value of $\left(\dfrac{\left[RH_2 \right]_{ads}}{C_{eq}} \right)_{C_{eq} \to 0}$ reflects a higher tendency of the adsorbate to

cover the surface when it reach the adsorption equilibrium. Therefore, the higher the

value of $K_{ads}b$ the higher the tendency of a particular adsorbate to cover the surface

under equilibrium conditions.

Figure 3 shows the isotherms of fig. 2 linearized according to eq. 4. Only five points of

each isotherm fitted to a linear behavior. These points are within the range of C_{eq} where

the organic molecule is chemisorbed at TiO_2 surface following a Langmuir type

adsorption. The points of the adsorption isotherm of benzene could not be fitted to eq.

4. Since benzene only is physisorbed[6] (non covalent interaction) at the TiO_2 surface it is

not expected a Langmuir type adsorption because this implies that chemisorption takes

place. The absence of chemisorption of benzene dissolved in acetonitrile at the anatase

TiO_2 surface is supported by our FTIR spectra of Figure 2C which show that there is no

change in the bands of benzene in the spectral region of 1100-1600 cm^{-1} when it is put

in contact with a TiO_2 film, unlike the changes observed in the bands of phenol in
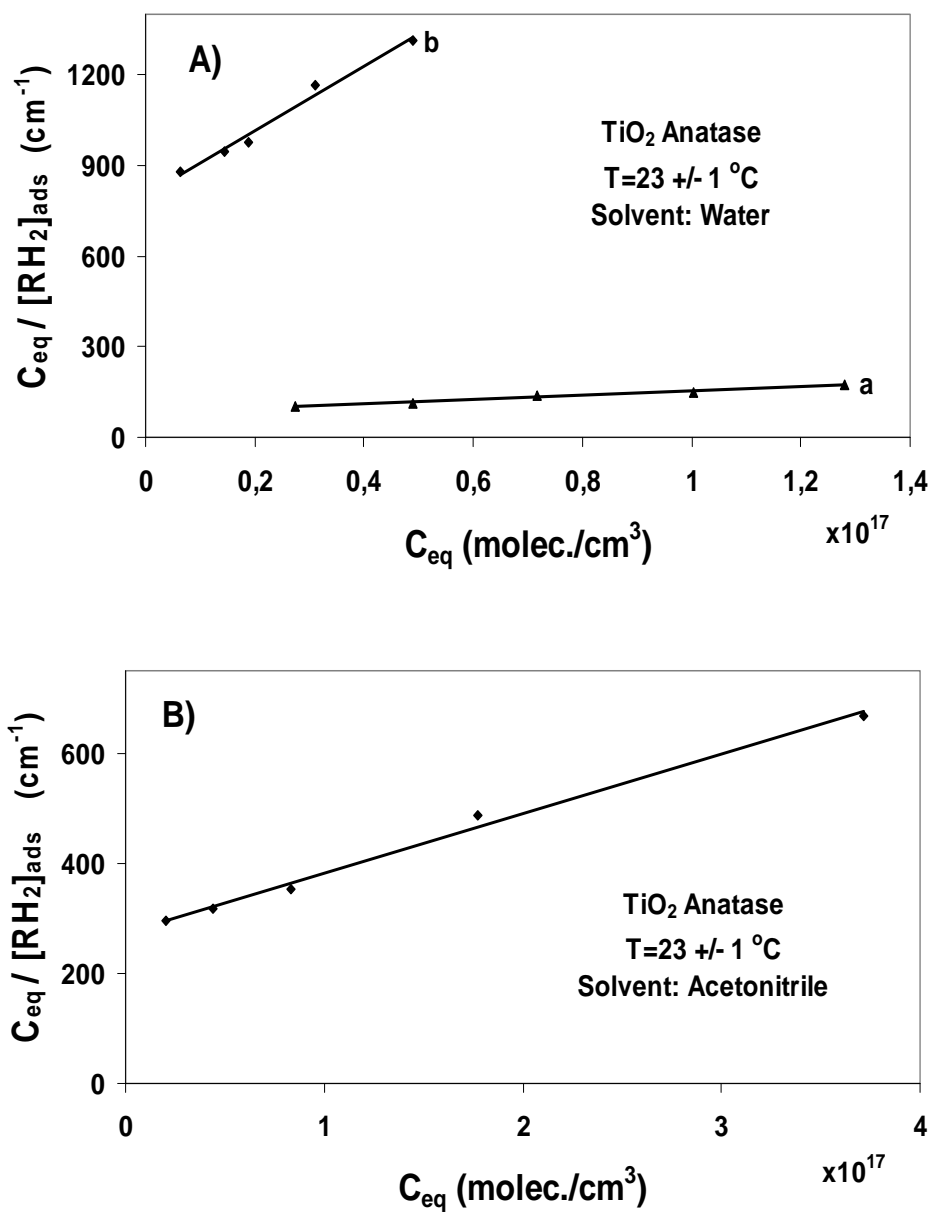
Figures 2A and 2B.

Figure 3. Linear fitting of adsorption isotherms of fig. 2 to eq. 4: A) aqueous solutions of FA (a) and phenol (b) on TiO_2 anatase and B) phenol dissolved in acetonitrile on TiO_2 anatase.

The parameters of each linear fitting of Fig. 3 are showed in Table 1. This parameters where used to calculate the values of K_{ads} and b of each adsorption isotherm reported in Table 2.

Table 1. Fitting parameters of straight lines of Fig. 3

Isotherm	Slope (cm^2/g)	Intercept (cm^{-1})	R^2
Phenol in Water	1.065 x 10^{-14}	801.86	0.9820
Formic Acid	7.186 x 10^{-16}	80.640	0.9732
Phenol in Acetonitrile	1.083 x 10^{-15}	273.41	0.9936

Table 2. Constants of eq. 4 calculated with the parameters reported in Table 1.

Isotherm	K$_{ads}$ (cm^3/molec.)	b (molec./cm^2)	Kads*b (cm)
Phenol in Water	1.328 x 10^{-17}	9.390 x 10^{13}	0.00125
Formic Acid in water	8.915 x 10^{-18}	1.391 x 10^{15}	0.0124
Phenol in Acetonitrile	3.961 x 10^{-18}	9.234 x 10^{14}	0.00366

The values of $K_{ads}b$ showed in Table 2 reflect that the tendency to cover the surface under equilibrium conditions follows the order: Formic acid in water > Phenol in acetonitrile > Phenol in water.

Fujishima and coworkers[7] reported that the maximum amount of fluorine ions absorbed at different anatase TiO$_2$ samples is in a range of: $1.72x10^{15}\frac{molec.}{cm^2} \leq b_{F^-} \leq 2.24x10^{15}\frac{molec.}{cm^2}$. Since fluorine ions have a small atomic size and strongly adsorbs on the TiO$_2$ surface it is expected a complete coverage of the TiO$_2$ adsorption sites [7-10]. If we consider the average value of fluorine surface density

as one monolayer (1 ML = 2 x 10^{15} sites/cm^2) it means that the maximum coverage of formic acid reported in Table 2 is 0.696 ML while the maximum coverage of phenol dissolved in acetonitrile is 0.462 ML and that of phenol in water is 0.047 ML. The maximum coverage of formic acid reported here is slightly higher than that reported for rutile single crystal surface which is approximately 0.5 ML[11]. The coverage of each substrate a the monolayer is not equal to 1.0 ML in any case because in liquid phase the solvent molecules, largely exceeding the organic substrate concentration, can compete for the adsorption sites.

The dependence of phenol maximum coverage on the solvent can be rationalized in terms of competitive adsorption between the phenol molecules and the solvent for the TiO_2 adsorption sites (Ti (IV) surface sites). Serpone and coworkers[12] found in a FTIR diffuse reflectance (DRIFT) study that phenol and halophenols interaction with the TiO_2 surface produce a significant change in the C-O stretching band, $\nu\,(\boldsymbol{C-O})$ in the spectral range 1100-1350 cm^{-1}. Based on this observation, they proposed that phenol and halophenols adsorption on TiO_2 takes place through a bond between its oxygen and a Ti^{IV} surface site. This is in agreement with the findings of Orlov and coworkers[13] who found by mean of photoelectron spectroscopy techniques (UPS and XPS) that 4-chlorophenol is attached to the TiO_2 surface via a phenolate link (Ti-O$_{ph}$ bond with a 70° angle with respect to surface plane), with the carbon framework intact and no scission of the C-Cl bond. This adsorption mode is stable at temperatures below 473K. Although there are not reports of surface science studies of interaction between phenol and TiO_2[14] the same interaction mode is expected because experimental data obtained by mean of temperature programmed desorption (TPD) and Scanning Tunneling Microscopy (STM) for 10 different alcohols shows that they follow a general pattern characterized by two adsorption modes: dissociative adsorption (chemisorption) at the TiO_2 surface through a chemical bond between the Ti^{IV} sites and the oxygen of the alcohol or molecular adsorption (physisorption)[11].

It is well known that water can be dissociatively adsorbed (chemisorption) at the TiO_2 surface trough a bond between its oxygen and a Ti^{IV} surface site or can be moleculary

adsorbed (physisorption) [11,14-16] . TPD spectra of water on TiO_2 show two peaks at 265 and 490 K that are assigned to the molecular and dissociative adsorption modes respectively. These peaks in the case of methanol are located at 295K and 480 K and have very similar values for other 10 alcohols[11]. The small difference (10K) between the peaks assigned to the dissociative adsorption mode of water and alcohols suggests that they have a similar binding energy to the TiO_2 surface. Therefore, water is able to compete with phenol for the Ti^{IV} surface sites. In aqueous solutions of phenol (1 mM) the molar ratio between water and phenol is around 55000, hence it is expected an effective displacement of phenol adsorbed at Ti^{IV} surface sites by water molecules. This kind of displacement was recently demonstrated by mean of Sum Frequency Generation (SFG) spectroscopy for the case of methanol adsorbed on TiO_2 anatase which is removed in a high extent from the TiO_2 surface by water molecules when the molar ratio between water and methanol is ≥ 300[17].

In contrast, acetonitrile (ACN) is not expected to displace phenol molecules chemisorbed at the TiO_2 surface because photoluminescence measurements have shown that ACN weakly interacts with the anatase TiO_2 surface[18].

The drastic change in the in the C-O stretching band, $\nu (C-O)$ of phenol dissolved in acetonitrile when interacts with an anatase TiO_2 film (Figure 2A) and the small change observed in the same band for phenol dissolved in water (Figure 2B) support the above conclusions.

The high value of the maximum coverage (0.696 ML) obtained for formic acid in aqueous solution implies that water can not effectively displace the molecules of formic acid adsorbed at the TiO_2 surface with the same efficiency that it displaces phenol molecules. This behavior is expected because formic acid adsorbs dissociatively (chemisorption) on TiO_2 with both of its oxygens strongly bonded to two adjacent Ti^{IV} surface sites[11]. The bond length has been quantitatively measured by scanned energy mode photoelectron diffraction (PhD) being 2.08 A^o for both Titanium-Oxygen bonds (Ti-O) bonds while the bond length of Ti-O from water chemisorption was found to be 2.21 A^o [11], indicating a weaker covalent interaction. Hence, formic acid is able to be chemisorbed at the TiO_2 surface in spite of the competition of large amounts of water. This conclusion is supported by our FTIR measurements which show a drastic change

in the stretching band of the COO group (ν ($\boldsymbol{O-C-O}$), 1577 cm^{-1}) of formic acid in aqueous solution when it is put in contact with a TiO$_2$ film[19] evidencing the formation of a surface formiate complex. Other authors have reached the same conclusion for other carboxylic acids by mean of FTIR measurements: Bahnemann and coworkers[20-23] reported the formation of several surface oxalate complex from adsorption of aqueous solutions of oxalic acid at anatase and rutile TiO$_2$ surfaces; Blesa and coworkers[24] reported the formation of several surface complex from adsorption of aqueous solutions of oxalic and salisylic acid at the TiO$_2$ surface.

Another important evidence of the strong interaction of carboxylic acids with the TiO$_2$ surface was obtained from SFG spectroscopy measurements[17], which showed that acetic acid is overwhelmingly adsorbed at the anatase TiO$_2$ surface in spite of the competition of large amounts of water while under the same conditions methanol is displaced from the TiO$_2$ surface by the water molecules.

Summing up: formic acid strongly interacts (chemisorption) with the TiO$_2$ surface even in aqueous solution while the strength of phenol interaction depends on the solvent, being strong when it is dissolved in acetonitrile (the main absorption mode is chemisorption) and weaker when it is dissolved in water because of the competition of water for the Ti^{IV} surface sites. Since a slight change in the C-O stretching band, ν ($\boldsymbol{C-O}$) of phenol in aqueous solution is observed in figure 2B, and also five points of the adsorption isotherm of phenol in water (Figure 3A) fitted to the Langmuir equation, it can be concluded that although chemisorption of phenol is hindered by the competition of water it is not completely suppressed. This means that both modes of adsorption at the TiO$_2$ surface coexist in the case of phenol aqueous solutions: chemisorption and physisorption. An analogous conclusion was reported for adsorption of methanol at the anatase TiO$_2$ surface[17]. Finally, the only possible mode of interaction of benzene with the TiO$_2$ surface is physisorption[6]. The interaction modes of these molecules with the TiO$_2$ surface are illustrated in the scheme 1.

   Scheme 1. Interaction modes of three organic molecules with the TiO$_2$ surface[a]
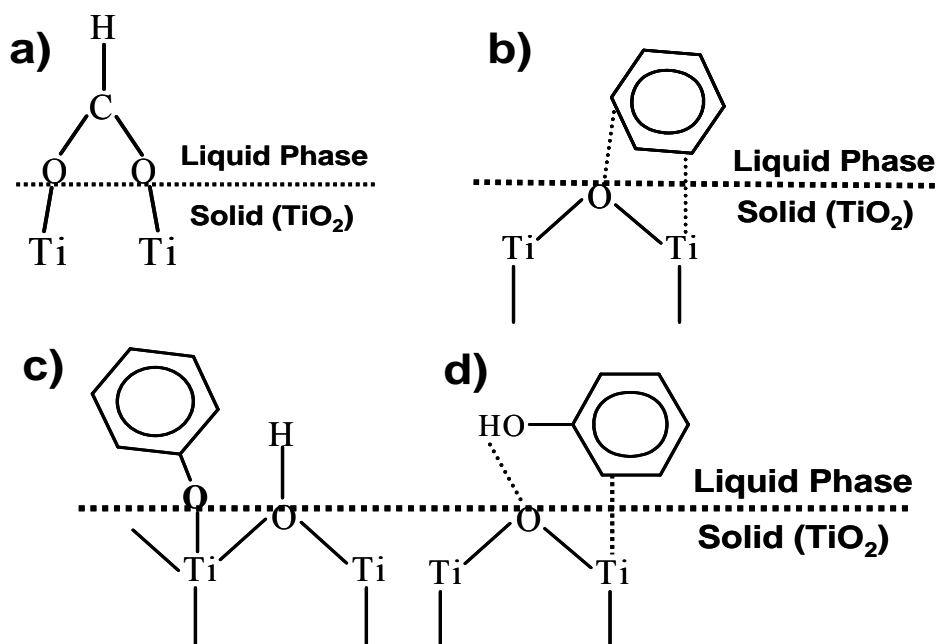
ᵃ a) formic acid chemisorption; b) benzene physisorption; c) phenol chemisorption; d) phenol physisorption. Solid lines represent covalent bonding while dashed lines represent weak interactions (like Van der Waals interactions).

References

1. J. U. Wieneke, B. Kommoβ, O. Gaer, I. Prykhodko, M. Ulbricht. *Ind. Eng. Chem. Res.* **2012**, *51*, 327-334.

2. M.I. Cabrera, O. M. Alfano, A. E. Cassano. *J. Phys. Chem.* **1996**, *100*, 20043-20050.

3. T. A. Egerton, R. W. Harrison, S. E. Hill, J. A. Mattinson, H. Purnama. *Journal of Photochemistry and Photobiology A: Chemistry* **2010**, *216*, 268-274.

4. V. Nu Hoai Nguyen, R. Amal, D. Beydoun. *Chemical Engineering Science* **2005**, *60*, 5759-5769.

5. C. B. Mendive, D. Hansmann, T. Bredow, D. Bahnemann. *J. Phys. Chem. C* **2011**, *115*, 19676-19685.

6. J. Zhou, S. Dag, S. D. Senanayake, B. C. Hathorn, S. V. Kalinin, V. Meunier, D. R. Mullins, S. H. Overbury, A. P. Baddorf. *Phys. Rev. B* **2006**, *74*(12), 125318.

7. K. Kobayakawa, Y. Nakazawa, M. Ikeda, Y. Sato, A. Fujishima, *Ber. Bunsenges. Phys. Chem.* **1990**, *94*, 1439.

8. C. Minero, G. Mariella, V. Maurino, E. Pelizzetti. *Langmuir* **2000**, *16*(6), 2632-2641.

9. M. Minella, M. G. Faga, V. Maurino, C. Minero, E. Pelizzetti, S. Coluccia, G. Martra. *Langmuir* **2009**.

10. J. F. Montoya, P. Salvador. *Applied Catalysis B: Environmental* **2010**, *94*(1-2), 97-107.

11. C. L. Pang, R. Lindsay, G. Thornton. *Chemical Society Reviews* **2008**, *37*(10), 2328-2353

12. S. Horikoshi, T. Miura, M. Kajitani, H. Hidaka, N. Serpone. *Journal of Photochemistry and Photobiology A: Chemistry* **2008**, *194*(2-3), 189-199.

13. A. Orlov, D. J. Watson, F. J. Williams, M. Tikhov, R. M. Lambert. *Langmuir* **2007**, *23*(19), 9551-9554.

14. M. A. Henderson. *Surface Science Reports* **2011**, *66*(6-7), 185-297

15. M. A. Henderson. *Surface Science Reports* **2002**, *46*(1-8), 1-308.

16. U. Diebold. *Surface Science Reports* **2003**, *48*(5-8), 53-229.

17. C. Wang, H. Groenzin, M. J. Shultz. *Journal of the American Chemical Society* **2005**, *127*(27), 9736-9744.

18. F. J. Knorr, C. C. Mercado, J. L. McHale. *J. Phys. Chem. C* **2008**, *112*(33), 12786-12794.

19. J. F. Montoya, J. A. Velasquez, P. Salvador. *Applied Catalysis B: Environmental* **2009**, *88*(1-2), 50-58.

20. C. B. Mendive, T. Bredow, M. A. Blesa, D. W. Bahnemann. *Phys. Chem. Chem. Phys.* **2006**, *8*(27), 3232-3247.

21. C. B. Mendive, T. Bredow, A. Feldhoff, M. Blesa, D. Bahnemann. *Phys. Chem. Chem. Phys.* **2008**, *10*(14), 1960-1974.

22. C. B. Mendive, T. Bredow, A. Feldhoff, M. A. Blesa, D. Bahnemann. *Phys. Chem. Chem. Phys.* **2009**, *11*(11), 1794-1808.

23. P. Z. Araujo, C. B. Mendive, L. A. G. Rodenas, P. J. Morando, A. E. Regazzoni, M. A. Blesa, D. Bahnemann. *Colloids and Surfaces A: Physicochemical and Engineering Aspects* **2005**, *265*(1-3), 73-80.

24. A. D. Weisz, L. García Rodenas, P. J. Morando, A. E. Regazzoni, M. A. Blesa. *Catalysis Today* **2002**, *76*(2-4), 103-112.

SUPPORTING INFORMATION

Comprehensive Analysis of Kinetics and Mechanisms of TiO$_2$ Photocatalytic Reactions . II) Experimental validation of the D-I model

Juan Felipe Montoya[1], José Peral[1], and Pedro Salvador[1,*]

1.Departamento de Química, Universidad Autónoma de Barcelona, 08193 Cerdanyola del Vallés, Spain.

*Corresponding author, E-mail: psalvador@klingon.uab.es

Keywords: Kinetics; Mechanisms; Photocatalysis; D-I Model; Charge Transfer

Appendix B. Conversion of units and calculations

In figures 3A, 4A, 5A and 6A the values in the abscise axis were those of the incident photon flow (ρ) measured by Potassium Ferrioxalate actinometry following a standard experimental procedure[1]. On the other hand, the experimental initial reaction rate (ν_{ox}) values in the ordinate axis were calculated in each case from the experimental plot of the concentration of the organic substrate versus time (C vs. t) by fitting a mathematical function to the experimental data and calculating the absolute value of the first derivate of the concentration with respect to time when the time is equal to zero, hence:

$$v_{ox} = \left| \left(\frac{dC}{dt} \right)_{t=0} \right|.$$

Some typical experimental plots and its fitting to a mathematical function are shown in Figures 1 and 2.

The plot shows Phenol Concentration (ppm) on the y-axis versus t (min) on the x-axis, with the fitted equation:

$$y = -0.0012x^3 + 0.0415x^2 - 0.6359x + 6.5026$$
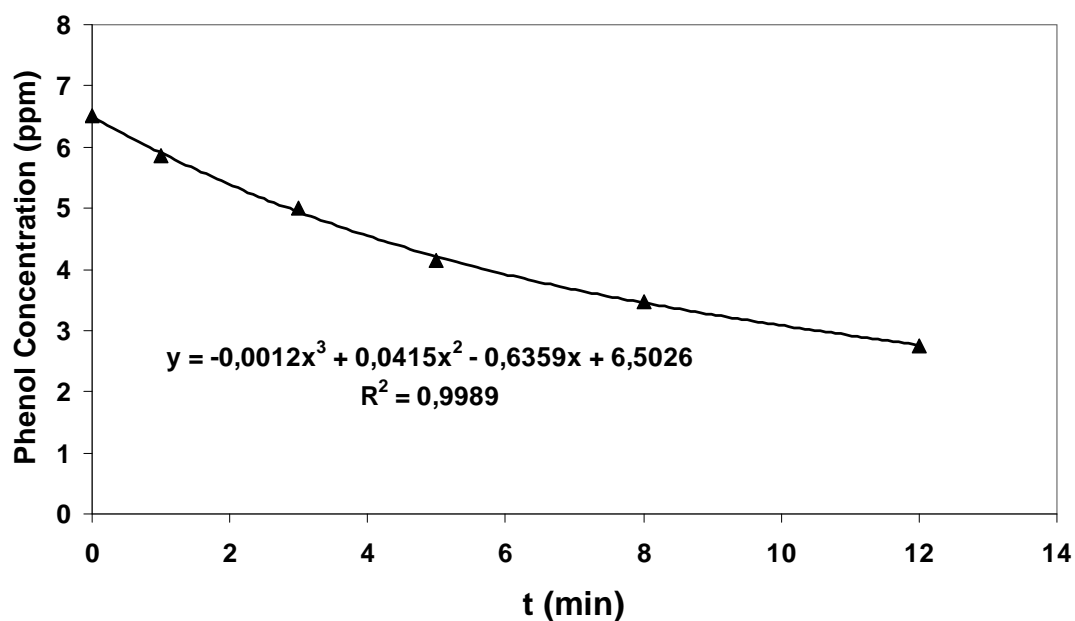$$R^2 = 0.9989$$

Figure S1. Example of a typical concentration vs. time plot from photocatalytic oxidation of phenol. The points correspond to experimental data while the solid line corresponds to the fitting to the mathematical function showed in the graphic. The experimental conditions were: $\rho = 5.57 x 10^{17} \dfrac{photons}{s}$; catalyst

load=0.5 g/L of anatase TiO_2; Initial equilibrium concentration of phenol ($[PhO]_{ACN}$ = 0.070 mM); solvent: acetonitrile; Reactor volume: 0.1 L. Irradiated area of the reactor: 40 cm².
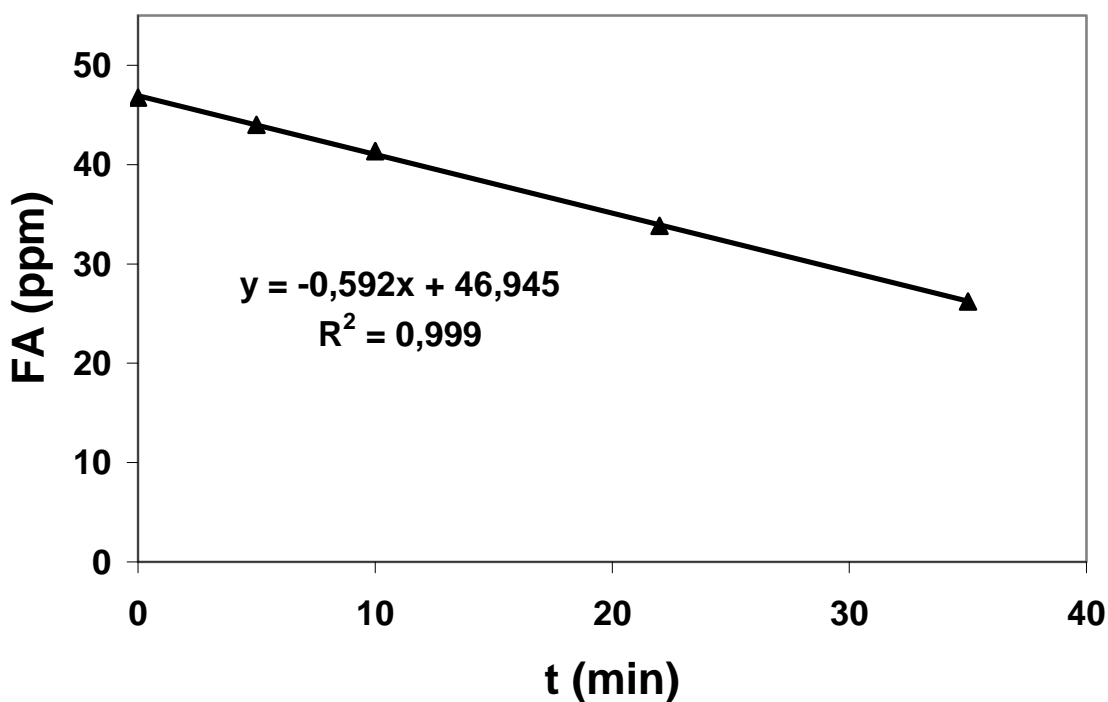

Figure S2. Example of a typical concentration vs. time plot from photocatalytic oxidation of formic acid (FA). The points correspond to experimental data while the solid line corresponds to a fitting to the mathematical function showed in the graphic. The experimental conditions were: $\rho = 2.91x10^{16} \dfrac{photons}{s}$; catalyst load=0.5 g/L of anatase TiO_2; Initial concentration of formic acid ($[FA]_{H_2O}$ = 1.02 mM); solvent: water; Reactor volume: 0.05 L. Irradiated area of the reactor: 58.9 cm²

In the fitting equations of Figures S1 and S2, "y" represents the concentration of the organic molecule (in ppm) and "x" represents the time of reaction (in minutes). The value of $\left|\left(\dfrac{dy}{dx}\right)_{x=0}\right|$ corresponds to the initial reaction rate (v_{ox}).

From the equation reported in Figure S1 it can be calculated that $\left|\left(\dfrac{dy}{dx}\right)_{x=0}\right| = 0.6359\,\dfrac{ppm}{min}$ while from the equation in Figure S2 $\left|\left(\dfrac{dy}{dx}\right)_{x=0}\right| = 0.592\,\dfrac{ppm}{min}$.

The respective conversion of units for Figure S1 is:

$$v_{ox} = \left|\left(\frac{dy}{dx}\right)_{x=0}\right| = 0.6359\,\frac{mg}{L*min} \times 0.1L \times \frac{1mmol}{94.11mg} \times \frac{1min}{60s} \times \frac{6.022 \times 10^{20}\,molec.}{1mmol} = 6.782x10^{15}\,\frac{molec.}{s}$$

While unit conversion for Figure S2 is:

$$v_{ox} = \left|\left(\frac{dy}{dx}\right)_{x=0}\right| = 0.592\,\frac{mg}{L*min} \times 0.05L \times \frac{1mmol}{46.03mg} \times \frac{1min}{60s} \times \frac{6.022 \times 10^{20}\,molec.}{1mmol} = 6.456x10^{15}\,\frac{molec.}{s}$$

Theoretical estimations of the initial reaction rates with the D-I model are given in units of $\dfrac{molec.}{cm^2 s}$. Thus, an additional step is required in order to express the experimental initial reaction rate according to the units of the D-I model.

The catalytic area of the TiO_2 nanoparticles dispersed in liquid phase can be calculated according to the expression:

$$A_{cat} = x_{cat} \times S_g \qquad \text{Eq. S1}$$

Where, A_{cat} is the catalytic area, x_{cat} is the mass of catalyst and S_g is the specific surface area of the catalyst (S_g) in a particular solvent. As calculated in appendix A, S_g=197303 cm^2/g for TiO_2 suspensions in acetonitrile and S_g=23807 cm^2/g for suspensions in water.

For the experiment reported in Figure S1:

$$A_{cat} = x_{cat} \times S_g = 0.05g \times 197303\,\frac{cm^2}{g} = 9865cm^2 \approx 10000cm^2 \qquad \text{(Eq. S2)}$$

For the experiment reported in Figure S2:

$$A_{cat} = x_{cat} \times S_g = 0.025g \times 23807\,\frac{cm^2}{g} = 595cm^2 \approx 600cm^2 \qquad \text{(Eq. S3)}$$

By dividing the values of v_{ox} calculated for Figures S1 and S2 by the values of A_{cat} calculated in eqs S2 and S3, respectively, it can be calculated that:

$$v_{ox} = 6.78x10^{15}\frac{molec.}{s} \times \frac{1}{A_{cat}} = \frac{6.78x10^{15}}{10000}\frac{molec.}{cm^2 s} = 6.78x10^{11}cm^{-2}s^{-1}$$

For the experiment reported in Figure S1, whereas:

$$v_{ox} = 6.46x10^{15}\frac{molec.}{s} \times \frac{1}{A_{cat}} = \frac{6.46x10^{15}}{600}\frac{molec.}{cm^2 s} = 1.08x10^{13}cm^{-2}s^{-1}$$

For the experiment reported in Figure S2.

All the initial reaction rates reported in Figures 3A, 4A, 5A and 6A were calculated following the aforementioned procedure. In all cases a similar fitting to that of Figures S1 and S2 were made taking at least five experimental points of the plot (C vs. t). These points were measured within a time of reaction enough to achieve a reduction of the initial concentration of the organic molecule of approximately 50%. From figures S1 and S2 it can be seen that these times of reaction were different depending on the organic molecule and the experimental conditions. The experimental error (e) was estimated to be $e = \pm 12\%$ by calculating the deviations in the values of v_{ox} for selected experiments repeated three times. This error is the sum of the instrumental error of the HPLC system and the error introduced by the mathematical manipulations made to calculate the values of $\left|\left(\dfrac{dy}{dx}\right)_{x=0}\right|$ from the experimental curves of concentration versus time (Figures S1 and S2)

It is worth nothing that fitting equations reported in Figures S1 and S2 have no physical meaning; therefore they were only used to obtain the values of the experimental initial reaction rates and were not used to analyze the kinetic phenomena.

In a similar way the photon flow measured by actinometry was converted to specific photon flow per unit area of catalyst. For instance the photon flow reported in Figure S1 is:

$$\rho = 5.57x10^{17}\frac{photons}{s} \times \frac{1}{A_{cat}} = \frac{5.57x10^{17}}{10000}\frac{photons}{cm^2 s} = 5.57x10^{13}cm^{-2}s^{-1}$$

All the photon flows reported in Figures 3 to 6 were calculated in an analogous way, using in each case the respective value of A_{cat} calculated according to the specific experimental conditions.

The values of the initial concentrations were converted in each case from milimolar units (mM) to $\dfrac{molec.}{cm^3}$. For instance the units conversion applied for data of Figure S1 was:

$$[PhO]_{ACN} = 0.070mM \times \frac{1L}{1000cm^3} \times \frac{6.022 \times 10^{20} molec.}{1mi\lim ol} = 4.22 \times 10^{16} \frac{molec.}{cm^3} = 4.22 \times 10^{16} cm^{-3}$$

All the initial concentration values reported in Figures 3 to 6 were calculated in an analogous way.

The experimental values of a reported in Figures 3C, 4B, 5C and 6C were calculated by replacing the respective experimental values of v_{ox}, ρ and $[RH_2]_{liq}$ in equation 6. Because the experimental error of v_{ox} is $e = \pm 12\%$, the error of the parameter a calculated according to eq. 6 is $e = \pm 24\%$ due to the propagation of error associated with the calculation of the value of $(v_{ox})^2$, the term in the numerator of eq 6. This mathematical operation yields an error in the value of the parameter a that is the double of the initial experimental error of v_{ox} $(e = \pm 12\%)$.

The experimental error in the values of both v_{ox} and a are illustrated in Figures 3 to 6 by error bars at each experimental point.

Bahnemann and coworkers[2] have reported that the TiO_2 particle agglomerates (PA) formed when the TiO_2 is dispersed in a solvent are broken by exposition of the suspension to light. It means that the estimated values of S_g for TiO_2 suspensions in acetonitrile and water only remains constant in the dark. When the suspension is illuminated as it is the case in the kinetic experiments, the value of S_g can increase due to the breaking of PA. The upper limit of the increase of S_g is given by the BET surface area of the catalyst, which is the specific surface area of the catalyst exposed to vacuum (no PA formation at all). This means that the range of the value of S_g for TiO_2

suspensions in acetonitrile exposed to ligth is $197303 \frac{cm^2}{g} \leq S_g \leq 550000 \frac{cm^2}{g}$, while in water is $23807 \frac{cm^2}{g} \leq S_g \leq 550000 \frac{cm^2}{g}$.

The above means that the values of A_{cat} used in Figures 3 to 6 can change during the course of the kinetic experiment. Therefore, the experimental values of the parameter $\boldsymbol{a}$ and $\boldsymbol{v}_{ox}$ are not quantitatively exact. However, the qualitative behavior observed in the Figures 3 to 6 remains unchanged for whatever value of S_g assumed to calculate $\boldsymbol{a}$ and $\boldsymbol{v}_{ox}$. The same can be said about the value assumed for k_0. However, we would like to stress that all the parameters involved in the D-I model have a well defined physical meaning. Thus, even if the exact value of a specific parameter is not known, the values used for kinetic fitting must be within a range where the parameter has physical sense. For instance: $0 \leq \boldsymbol{k}_0 \leq 1$, being $\boldsymbol{k}_0 = 0$ when the whole incident light in the reactor is not absorbed by the catalyst and $\boldsymbol{k}_0 = 1$ when the whole light is absorbed by the catalyst. Therefore the values of $\boldsymbol{k}_0$ assumed to fit the kinetic data must be in the range $0 \leq \boldsymbol{k}_0 \leq 1$. The same reasoning applies for each fitting parameter reported in Figures 3 to 6.

To calculate the values of the parameter $\boldsymbol{a}$ showed in Figure 7B it was necessary to suppose the values of the volume of the reactor, the irradiated area (A_{irr}), k_0, and A_{cat} because any of this information is reported in the article of Emeline et. al.[3]. In that article they reported the photon flow per irradiated area of the reactor (in $\frac{photons}{cm^2 s}$). To convert that units to $\frac{photons}{s}$ it was necessary to assume a value for the irradiated area (A_{irr}=100 cm^2) and this value was multiplied by each photon flow of Figure 7A, obtaining in this way the values in the abscise axis reported in Figure 7B.

On the other hand, an example of a typical conversion of the reaction rate values reported in Figure 7A is shown in eq. 5:

$$v_{ox} = 1.8x10^{-8} \frac{mol}{min} \times \frac{6.022 \times 10^{23} molec.}{1mol} \times \frac{1min}{60s} \times \frac{1}{1000cm^2} = 1.807x10^{14} \frac{molec.}{cm^2 s} = 1.81x10^{14} cm^{-2} s^{-1}$$

All the reaction rate values of Figure 7A were converted to units of $cm^{-2}s^{-1}$ following the same procedure in order to use them for the calculations of the values of the parameter a reported in Figure 7B. These values of v_{ox} were replaced in eq 6 to calculate the values of the parameter a reported in Figure 7B. It was also assumed in these calculations that $k_0 = 0.1$ and $A_{cat} = 1000$ cm^2. Again, we would like to stress that although the values assumed for the parameters affect the quantitative values of the parameter a, the qualitative behavior remains unchanged for whatever value assigned to the constants.

References

1. C.G. Hatchard and C.A. Parker; *Proc. R. Soc. Lond. A* **(1956)**, 235, 518.
2. C. B. Mendive, D. Hansmann, T. Bredow, D. Bahnemann. *J. Phys. Chem. C* **2011**, *115*(40), 19676-19685.
3. A. V. Emeline, V. Ryabchuk, N. Serpone. *Journal of Photochemistry and Photobiology A: Chemistry* **2000**, *133*(1-2), 89-97.

SECTION B

Mechanisms of Photocatalytic Reactions

Manuscript 3

"About the Capital Role of TiO$_2$ Surface Lattice Oxygens in Liquid Phase

Photocatalytic Reactions"

About the Capital Role of TiO$_2$ Surface Lattice Oxygens in Liquid Phase Photocatalytic Reactions

J.F. Montoya,[1] D.W. Bahnemann,[2] J.Peral, [1,]* and P. Salvador, [1,]*

1. Departamento de Química, Universidad Autónoma de Barcelona, 08193, Cerdanyola del Vallés, Spain.
2. Institut für Technische Chemie, Leibniz Universität Hannover, Callinstrasse 3, D-30167 Hannover,

Germany

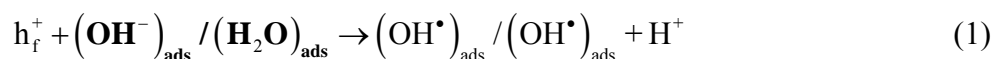*Corresponding authors, E-mails: jose.peral@uab.cat, psalvador@klingon.uab.es

Abstract

Several mechanisms have been proposed over the last three decades to explain the elementary steps of liquid phase photocatalytic oxidation reactions. None of them has taken into the account the possibility of TiO_2 surface lattice oxygens (O_s) incorporation into the photogenerated products. Herein, we study in detail two paradigmatic TiO_2-assisted photocatalytic reactions, water splitting and aromatic compounds oxidations. Experiments were carried out under carefully controlled amounts of oxygen and/or water, and also in the presence of oxygen-isotope labeled catalyst ($Ti^{18}O_2$). It was demonstrated the feasibility of production of CO_2 in the absence of O_2 and H_2O using just the O_s as the source of oxygen atoms. Later, isotopic tracing experiments with $Ti^{18}O_2$ demonstrated that in fact the O_s species were exchanged during the course of the photooxidation reactions. The experimental evidence collected in this work has allowed us proposing new mechanistic pathways for both reactions which explicitly involves hole trapping by O_s species, their incorporation into the reaction products, generation of oxygen vacancies at the TiO_2 surface lattice, and the subsequent healing of the catalyst surface with oxygen atoms from O_2 and/or H_2O to close the catalytic cycle. The new mechanisms considers that the catalytic surface is continuously changing in the course of the photocatalytic reactions, challenging earlier interpretations of photocatalysis phenomena that assumed a "static" catalytic surface.

Keywords: Oxygen Isotope Labelled Titania, $Ti^{18}O_2$, Surface Oxygens, Benzene Photooxidation, Photocatalysis Reaction Mechanism.

1. INTRODUCTION

Titanium Dioxide (TiO$_2$) has been extensively studied, especially in the last three decades.[1-13] This semiconductor has been applied for solar energy conversion,[5,14] the development of building materials with super-hydrophilic surface properties,[6,8] photooxidation of organic pollutants in gas[3] and liquid phase,[1,2,4,8,11,12] and photochemical hydrogen production from water[7,15]. Despite this wide range of applications, a comprehensive understanding of the phenomena involved in TiO$_2$ photochemistry remains elusive. [13] In the last decade, surface science studies (SCS) of TiO$_2$ have shed light onto the mechanism of photocatalytic reactions at atomic scale[6,9,10]. This SCS have demonstrated the crucial role of the semiconductor surface, in particular its properties and interactions with substrates, in the photochemical events triggered by TiO$_2$ excitation with light of energy higher than the band gap. However, the important findings of these SCS have rarely been applied to the elucidation of reaction mechanisms of the most typical photocatalytic systems, namely those in which the semiconductor interacts with substrates in gas or liquid phase, because of the ultra high vacuum (UHV) conditions required by the instrumental techniques used in those SCS. However, although the results of the SCS must be used with care for the interpretation of photocatalytic phenomena in gas or liquid phase[16], it is a necessity to apply this body of knowledge to the formulation of plausible photocatalytic reaction mechanisms. For instance, new insights into the mechanisms of water photooxidation reaction on TiO$_2$ have been achieved by a detailed interpretation of electron photoemission spectra (EPS) of water adsorbed at rutile TiO$_2$ surfaces[17-20]. In particular, the commonly assumed reaction of direct oxidation of water, either dissociatively or molecularly adsorbed, by holes (eq 1) has been called into question. [17-20]

$$h_f^+ + \left(\mathbf{OH^-}\right)_{\mathbf{ads}}/\left(\mathbf{H_2O}\right)_{\mathbf{ads}} \rightarrow \left(OH^\bullet\right)_{ads}/\left(OH^\bullet\right)_{ads} + H^+ \tag{1}$$

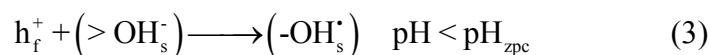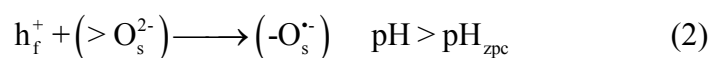In those studies the authors claimed that the reaction expressed by eq 1 is thermodynamically and kinetically hindered[17-20], therefore they proposed alternative mechanisms of water photooxidation based on nucleophilic attack[17,18] (NA) and redox photooxidation (RP) mechanisms[20]. The formulation of the primary reaction steps considered by both mechanisms make use of the information provided by SCS at single-

crystal-rutile TiO_2 surfaces using techniques such as atomic force microscopy[19] (AFM), scanning tunneling microscopy,[6,9,10,21,22] (STM) and EPS.[9,10,21] Although both mechanisms have important differences, both consider the TiO_2 surface lattice oxygens (O_s) as the primary trapping sites of photogenerated holes and also propose that the primary intermediate species of water photooxidation reaction are several types of O_s radical species.[17,18,20] Further, one of us proposed that O_s are incorporated in the final oxidation product, i.e molecular oxygen (O_2).[20] Hence, lattice oxygen vacancies $\mathbf{V}\left[\mathbf{O_s}\right]$ at the TiO_2 surface must be produced during the water photooxidation reaction[20], but they are rapidly healed through dissociative adsorption of water at $\mathbf{V}\left[\mathbf{O_s}\right]$ sites [9,10,21,22].

Important consequences are derived from these findings because the above mentioned discoveries open the way to proposed new mechanistic pathways for TiO_2 photocatalytic reactions. In particular, a mechanistic route including the participation of the O_s and the $\mathbf{V}\left[\mathbf{O_s}\right]$ sites into the sequence of elementary steps of photocatalytic oxidation seems plausible.

An old and not still closed debate in photocatalysis is the role played by hydroxyl radicals $\left(OH^\bullet\right)_{ads}$, produced according to eq 1, in the oxidation of organic compounds. Several research teams have stated that $\left(OH^\bullet\right)_{ads}$ radicals, or even free hydroxyl radicals $\left(OH^\bullet\right)_{free}$ produced from oxidation of nonabsorbed water by free holes $\left(h_f^+\right)$, are one of the major oxidizing agents in photocatalytic reactions. [1-3,23-34] The main evidence that support this thesis is the detection by electron paramagnetic resonance (EPR) spectroscopy of $OH^\bullet$ species in UV irradiated TiO_2 aqueous suspensions[23,31,33] and the detection of hydroxylated reaction intermediates, especially during the photooxidation of aromatic compounds. [25-30,32,34] However, other EPR studies demonstrated that the h_f^+ are trapped at the O_s (eqs 2 and 3) and did not produced $OH^\bullet$ radicals. [35-37]

$$h_f^+ + \left(> O_s^{2-}\right) \longrightarrow \left(-O_s^{\bullet-}\right) \quad pH > pH_{zpc} \qquad (2)$$

$$h_f^+ + \left(> OH_s^-\right) \longrightarrow \left(-OH_s^\bullet\right) \quad pH < pH_{zpc} \qquad (3)$$

Moreover, Nosaka et al.[38] detected no $\left(OH^{\bullet}\right)_{\text{free}}$ radicals by EPR in illuminated TiO_2 aqueous suspensions, challenging earlier interpretations of the EPR spectra made by other authors. Furthermore, even if $\left(OH^{\bullet}\right)_{\text{free}}$ are produced from oxidation of nonabsorbed water, they quickly trap an electron from TiO_2 generating a surface-trapped hole $\left(\text{-}OH_s^{\bullet}/\text{-}O_s^{\bullet-}\right)$, as has been demonstrated by pulse radiolysis studies on colloidal suspensions of TiO_2. [39,40]

Although the detection of hydroxylated aromatic intermediates is an experimental fact, [25-30,32,34] it is not a conclusive proof of the prevalence of hydroxyl-radical-chemistry (HRC), triggered by $\left(OH^{\bullet}\right)_{\text{ads}}$ species generated according to eq. 1, in photocatalytic oxidation reactions. Hydroxylation can also take place via reactions of organic radical cations[41,42], generated by single electron transfer (SET) of a chemisorbed organic substrate to a free hole (eq 4), with water, O_2 , and/or O_2-derived radicals[43] (see scheme 1 of ref. 43).

$$h_f^+ + \left(RH_2\right)_{\text{ads}} \rightarrow RH^{\bullet} + H^+ \qquad (4)$$

The importance of the reactions paths initiated by SET in aromatics hydroxylation was highlighted by Kamat et al.[44] and Rabani et al.[45]. More recently, Jenks and coworkers have analyzed in detail the reaction products distribution from TiO_2-assisted aromatic degradation of several model compounds[46-49]. Those authors made a clear distinction between SET-derived and HRC-derived reaction products. On the other hand, Zhao et al.[34,43,50] and Matsumura et al.[51] scrutinized in detail these reactions by using oxygen-isotope-labeled water ($H_2^{18}O$) and/or labeled molecular oxygen ($^{18}O_2$) as tracers. Both groups found that oxygen atoms of the hydroxylated products are originated from water or O_2 with ratios that depend on reaction conditions. A recent study[43] has clearly demonstrated that O_2 incorporation into the hydroxylated products involves multistep O_2 electro-reduction to produce $\left(OH^{\bullet}\right)_{\text{free}}$ species in the bulk of the solution (eq 5, see the complete reaction sequence in ref. 43) that subsequently react with the dissolved aromatic compounds.

$$O_2 + 3e_f^- + 2\mathbf{H}^+ \rightarrow\rightarrow\rightarrow \left(\mathbf{OH}^{\bullet}\right)_{\mathbf{free}} + \mathbf{OH}^- \qquad (5)$$

The reaction pathway of eq 5 was commonly overlooked in the past[43]. As a consequence, the HRC-derived products detected in TiO_2 photooxidation of aromatics were considered as a proof of $OH^{\bullet}$ radical production from reaction 1.[29] The aforementioned recent evidence against the reaction 1 and the findings of Zhao et al.[43] strongly suggest that the HRC-derived products detected in past studies[25-30,32,34,44-49] were produced in the bulk of the aqueous solution by reaction of the aromatics with $\left(\mathbf{OH^{\bullet}}\right)_{\mathbf{free}}$ species generated according to eq 5. In summary, O_2 incorporation into the hydroxylated products occurs in the bulk of the aqueous solution, it is initiated by electrons, and it is produced through HRC. In contrast, the incorporation of oxygen atoms from water into the hydroxylated products must occur at the TiO_2 surface and is initiated by holes, being responsible for the generation of SET-derived products. [43,51] However, it is not still clear how the oxygen atom from water is incorporated into the hydroxylated products. Even the most recent studies[43] and reviews[52] on the topic of aromatics photooxidation still state that this incorporation is initiated by reaction 1 as initial step. Nevertheless, there is another possible incorporation pathway not considered before. [53] This new pathway of aromatics photooxidation considers the reaction of the organic radical cations with the TiO_2 lattice radical species $\left(\text{-OH}_s^{\bullet}\right)/\left(\text{-O}_s^{\bullet-}\right)$ generated in reactions 2 or 3 (eq. 6)

$$\left(RH_{aq}^{\bullet}\right)+\left(\text{-OH}_s^{\bullet}/\text{-O}_s^{\bullet-}\right)\rightarrow RHO_sH+V\left[O_s\right] \qquad (6)$$

It is worth noting that reaction 6 implies incorporation of the O_s into the hydroxylated products. Later, the $V\left[O_s\right]$ sites produced in eq 6 are healed through dissociative adsorption of water regenerating the catalyst surface. [9,10,21,22] This step implies an oxygen atom transfer from the water molecules to the TiO_2 surface lattice. Finally when these new TiO_2 surface lattice oxygen atoms react with other $\left(RH_{aq}^{\bullet}\right)$ species according to eq. 6 a hydroxylated intermediate is produced. In this reaction product the oxygen atom of the hydroxyl group belongs to the water molecule.

In summary, this new mechanistic pathway has subtle but important differences with the traditional one. It states that hydroxylation is produced by oxygen atom transfer from the TiO_2 lattice to the aromatic molecules, while water heals the $V\left[O_s\right]$ sites leaved

behind, thus favoring incorporation of oxygen atoms from water into the hydroxylated products as the reaction proceeds. In contrast, the traditional mechanism invokes the production of $\left(OH^{\bullet}\right)_{ads}$ according to reaction 1 and subsequent hydroxyl radical attack to the aromatic molecule.

In this study, we report the photooxidation of aromatics under carefully controlled amounts of oxygen and/or water. These reactions conditions allowed tuning the possible reaction mechanisms involved in the reaction: evacuation of O_2 suppresses the reaction pathway initiated by eq 5 while anhydrous conditions inhibit the possibility of the reaction pathway initiate by eq 1. In this way, we could gain a better understanding of each reaction mechanism by separate. Later, isotopic tracing studies of reaction products from several aromatic compounds photooxidation using isotope-labeled-titania[53-55] ($Ti^{18}O_2$) as catalyst allowed demonstrating the participation of O_s into the photocatalytic reaction. Finally, an isotopic tracing study of the water photooxidation confirmed that in the O_2 evolved from this reaction there is a fraction of oxygen atoms that belongs to the TiO_2 lattice. These set of results constitute evidence that supports a new mechanistic pathway in photocatalysis[53] which explicitly invokes the generation of TiO_2 surface lattice radicals $\left(-OH_s^{\bullet}\right)/\left(-O_s^{\bullet -}\right)$, the incorporation of O_s into the reaction products, the production of $V[O_s]$ sites at the catalyst surface and its subsequently healing with oxygen atoms from water and/or molecular oxygen molecules.

2. EXPERIMENTAL

2.1 Materials

TiO_2 (anatase nanoparticles $\left(D_p \leq 25nm\right)$; purity 99.7%; surface area 55 m^2/g determined by BET) was purchased from Aldrich. Anhydrous acetonitrile (ACN) packed with Argon (biotech grade, $\leq 0.001\%$ w.t. water) was purchased from Aldrich and used as received in non-aqueous experiments. Water $\left(resistivity \geq 18\,M\Omega\,cm\right)$ was purified in a Millipore Milli-Q system. Molsieves (3A^o, Aldrich) were dried at 350 ^{o}C for 24 hours before each experimental running[56]. Benzene, phenol, benzaldehyde, benzoic acid and silver tetrafluoroborate were analytical reagent grade and used as

received without further purification. For isotopic tracing (IT) experiments, ^{18}O labeled titania ($Ti^{18}O_2$) and unlabeled $Ti^{16}O_2$ nanoparticles were synthesized and characterized following a procedure reported elsewhere. [53]

2.2 TiO$_2$ Dehydration and water analysis

Photocatalytic experiments carried out with a controlled amount of water require a previous step of TiO$_2$ dehydration. To achieve this, the following procedure was performed: the anatase powder was added to the photoreactor (PR) and heated at 623K under flow of dry air (< 3 ppm water) for 2 hours. Then, it was cooled at 200 ^{o}C, sealed with a rubber septum, and cooled to room temperature under flow of Helium. This procedure completely removes terminal hydroxyl $\left(-\mathbf{O_w H^-} \right)$, but preserves bridging hydroxyl $\left(> \mathbf{O_s H^-} \right)$ groups.[57-60]

Karl Fischer (KF) analysis was carried out for samples taken before and after some photocatalytic experiments. Aliquots of around 10 g of the solvent were extracted from the reactor through the rubber septum and analyzed in an automatic Karl Fischer titrator (CRISON TitroMatic KF 2S).

2.3 Photocatalytic Experiments

Photocatalytic benzene mineralization (PBM) experiments were carried out in a cylindrical air-tight reactor connected to a thermal conductivity detector gas chromatography system (GC-TCD). The reactor had inlet and outlet ports connected to a system of valves in order to bubble helium gas when it was required. In all PBM experiments the volume of both the liquid and the gas phase were 25 ml. Temperature was kept constant at $24 \pm 1 \, ^oC$ using a thermostatic water bath.

For experiments under a controlled amount of water the following procedure was followed: (1) the commercial TiO$_2$ was dehydrated inside the photo-reactor (PR) according to the aforementioned method; (2) 0.5 g of 3A^o Molsieves freshly dried and still hot (at 350 ^{o}C) were added to the PR inside the oven at 200 ^{o}C; (3) the whole system (PR + Molsieves + TiO$_2$ powder) was sealed with a rubber septum, filled with Helium gas and cooled to room temperature. (4) Anhydrous solutions of silver ions and aliquots of pure benzene (both dissolved in ACN and pre-dried with 3A^o Molsieves

according to a reported drying protocol[56]) were injected through the rubber septum. (5) 40 ml of the anhydrous solvent were injected and Helium gas was bubbled for 30 minutes under magnetic stirring (400 rpm). (6) The flow of Helium gas was removed, an aliquot of water was injected with a micro syringe if necessary, and 15 ml of the liquid phase was extracted for KF analysis after 30 minutes of stirring in the dark. The gas phase was analyzed by GC-TCD. This analysis yields the amounts of O_2 and H_2O before starting the photocatalytic reaction. When the desired water concentration in the PR was higher than $0.560\,mM$ (the minimum possible water concentration in anhydrous acetonitrile[56]) the step two was omitted, i.e. in those cases Molsieves were not added to the reaction system.

After completing the above 6 steps the light was turned on. Illumination was carried out with four 25W Philips fluorescent UV lamps. IR and radiation with $\lambda < 300nm$ were filtered by a Pyrex glass jacket with water recirculation. The total photon flux (UV photons, $300nm < \lambda < 390nm$) incident on the reactor in all experiments was $\rho = 8.76 \times 10^{16}$ **photons/s**, as measured by potassium ferrioxalate actinometry[61].

Isotopic tracing experiments were carried out in an experimental system previously described using synthesized $Ti^{18}O_2$ and $Ti^{16}O_2$ nanoparticles as catalysts.[53] The aforementioned drying protocol (section 2.2) was applied to both catalysts for experiments performed in anhydrous solvent under a controlled amount of water.

2.4 Analytical methods

O_2 and CO_2 in the gas phase were monitored at different times of reaction using a Shimadzu GC-TCD (Model 2014). A Carboxen 1000 colum (4.5m X 1/8" X 2.1 mm) was used as stationary phase. Helium was used as carrier gas. The GC was temperature programmed as follows: the temperature of injector and the detector were held at 50 ^{o}C and 100 ^{o}C, respectively. GC oven temperature was set at 40 ^{o}C for 5 minutes and then it was increased to 85 ^{o}C at 10°C/min. The final temperature was held for 14 minutes. Linear calibration curves of concentration versus peak area where performed for CO_2 and O_2. The concentration range of both curves were 0.032 to 12 mM which is

equivalent to a range of 0.8 to 300 μmol of the measured gas in the system (Gas phase volume = 0.025L). The detection limit for both gases was therefore 0.8 μmol.

In IT experiments the gas phase was monitored (every 1 minute) by a gas analyzer equipped with a quadrupole mass spectrometer (QMS) from HIDEN analytical (Model HPR-20 QIC). The QMS was programmed to register and collect the signal of the $C^{18}O_2$ ($m/z = 48$), $C^{18}O^{16}O$ ($m/z = 46$), and $C^{16}O_2$ ($m/z = 44$) isotopologues of carbon dioxide (CO_2) in experiments of aromatics photooxidation. On the other hand, in experiments of water photooxidation, the QMS signals of the $^{18}O_2$ ($m/z = 36$), $^{18}O^{16}O$ ($m/z = 34$), and $^{16}O_2$ ($m/z = 32$) isotopologues of molecular oxygen (O_2) were monitored.

The ^{18}O content of liquid phase intermediate products from benzaldehyde photooxidation was determined with a gas chromatograph coupled to a mass spectrometer (Shimadzu GC/MS-QP 5000). A Rxi-5 ms (L=30 m, d=0.32 mm) capillary column was used. Operating temperatures were programmed as follows: injection temperature, 250°C; oven temperature, 50°C (hold 3 min); from 50 to 280°C at a rate of 25°C/min (hold 3 min), then, from 280 to 300°C at a rate of 5°C/min; 280 °C (hold 3 min); in split mode with split ratio of 3; injection volume (3.0 μL) with helium as a carrier gas (at 1.5 mL//min). A high performance liquid chromatography (HPLC) system composed of a LCP 4100 ECOM Tech Lab pump and a LCD 2084 ECOM Techlab UV Detector adjusted to 230 nm was used to measure the concentration of benzaldehyde and benzoic acid (BA). The stationary phase was a Hypersil ODS column (25cm Long. x 0.46 mm i.d., 5 μm particles) working at room temperature. The mobile phase was a mixture of acetonitrile and water (40:60 %v/v) adjusted to pH 3 by adding H_3PO_4. The flow rate was kept constant at 1 ml/min. The retention time was 5.1 and 7.4 min for BA and benzaldehyde peaks, respectively. The reaction products adsorbed on the TiO_2 powder were also analyzed after they were extracted from the TiO_2 surface. For the extraction, 30 mg of the powder was recovered by centrifugation at the end of the photocatalytic reaction, then it was mixed with 5 ml of a solution of KF (0.044 M) and $HClO_4$ (0.05 M) dissolved in acetonitrile and stirred for 30 minutes. Finally, the liquid phase was analyzed by HPLC and GC-MS to determine the concentration and the ^{18}O content of the reaction products, respectively.

3. RESULTS AND DISCUSSION

3.1 Blank Experiments

A series of experiments were carried out in order to determine the potential contribution of processes others than TiO_2-assisted aromatic compounds (AC) photocatalytic oxidation. First, experiments of photolysis were carried out illuminating several solutions of 100 μL of the AC dissolved in acetonitrile, in the presence of oxygen (O_2) or with $AgBF_4$ (17mM) in Helium atmosphere. In all cases CO_2 was not detected within a period of 100 hours of UV irradiation. The absence of CO_2 production demonstrates that homogeneous reactions and/or photolysis have a negligible contribution to the oxidation process. On the other hand, deoxygenated-TiO_2 suspensions (20 g/L of TiO_2 in acetonitrile; 10mM of the AC; 17 mM of $AgBF_4$) were submitted to continuous stirring in the dark. Again CO_2 was not detected in the gas phase. This means that possible processes occurring in the dark such as homogeneous oxidation reactions of benzene and/or acetonitrile with Ag^+ ions had a negligible contribution to the observed CO_2 evolution.

In the experiments carried out in Helium atmosphere, some traces of O_2 (< 1 μmol) due to impurities could be detected. Hence, it was necessary to check if this residual content of O_2 was enough to promote the AC photocatalytic oxidation. In all cases, no CO_2 production for experiments performed in Helium atmosphere (O_2 < 1 μmol) and in the absence of silver ions (Ag^+) was observed. Consequently, the experiments developed in Helium can be considered anaerobic in spite of the small residual amount of oxygen impurities detected ([O_2]< 0.04 mM).

3.2 PBM under controlled amounts of water

TiO_2 exposed to moisture is hydroxylated [29,57-59,62]. According to theoretical calculations[63] and solid state ^{1}H-NMR spectra,[58,59] water on anatase surface forms a 3D hydrogen-bonding-network with two stable layers: one of low mobility at coverage up to 3 monolayers (ML) and an outermost layer with high mobile water molecules at coverage higher than 3 ML. Nosaka et. al.[59] have estimated that the stable layer has a total number of water molecules of 1.6×10^{15} molec./cm^2. According to this estimation,

0.5 g of our anatase sample (A_{cat}=275000 cm^2, see calculation of catalyst area (A_{cat}) in the Supporting Information) has 4.4×10^{20} molecules of water forming the stable water layer, which is equivalent to a total mass weight of 13.15 mg. The weight difference measured several times of 0.5000 g of our anatase TiO$_2$ sample, before and after the aforementioned TiO$_2$ thermal treatment (section 2.2), was 22 +/- 1 mg, indicating that all surface adsorbed water was completely removed. This conclusion is in agreement with detailed studies of anatase TiO$_2$ dehydration which state that at temperatures of 623K (for 1 hour) all the surface adsorbed water is removed but the O_s are preserved. [57-60] This is of seminal importance in our experiments because our main objective is to elucidate the role of the O_s in the photocatalytic reactions. Scheme 1 shows the composition of the anatase TiO$_2$ surface before and after the thermal treatment.

Scheme 1. Surface Structure of Anatase TiO$_2$ before and after Thermal Treatment [a]
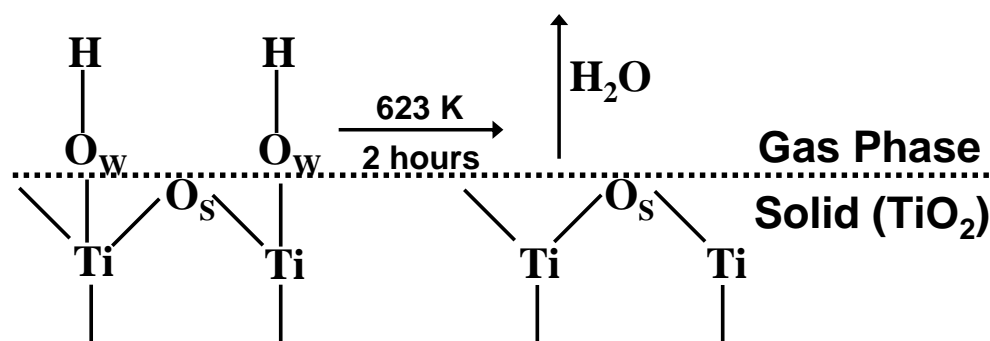
[a] Before thermal treatment the TiO$_2$ surface is composed of terminal hydroxyl $\left(-\mathbf{O_w H^-}\right)$ and bridging hydroxyls $\left(>\mathbf{O_s H^-}\right)$ groups. After heating the $-\mathbf{O_w H^-}$ groups are removed but the $>\mathbf{O_s H^-}$ remain attached to the TiO$_2$ surface. It is worth noting that the oxygen atoms of terminal hydroxyls $\left(\mathbf{O_w}\right)$ belong to chemisorbed water while the oxygen atoms of bridging hydroxyls $\left(\mathbf{O_s}\right)$ belong to the TiO$_2$ lattice.

Once the TiO$_2$ surface was free of terminal hydroxyls $\left(-\mathbf{O_w H^-}\right)$ we studied the photooxidation of benzene in anhydrous solvent (acetonitrile) and anaerobic conditions. Therefore, the only source of oxygen atoms in the photo-reactor was the TiO$_2$ lattice.

However, some water or O_2 due to residual impurities in the solvent or in the gas phase could not be neglected. Actually, we have carefully quantified the traces of O_2 and H_2O in order to take their contribution into account.

Figure 1 shows the CO_2 evolution from PBM under different concentrations of dissolved water $\left(\left[H_2O\right]\right)$ in the solvent. The lowest value of $\left[H_2O\right]$ is the minimum concentration of dissolved water that could be achieved using the best drying protocol reported for acetonitrile[56]. In other experiments, higher $\left[H_2O\right]$ values were achieved adding an aliquot of water to the reaction system. For the lowest value of water concentration $\left(\left[H_2O\right] = 0.560\,\text{mM}\right)$ the production rate of CO_2 $\left(\gamma_{CO_2}\right)$ was 0.39 μmol/h within the first 20 hours, decreasing gradually to zero as time increased. At t >90 h a steady state concentration of 1000 μM of CO_2 was reached, as it was checked by taking a sample at longer illumination time (t=140 h). The final concentration of CO_2 was more than three times higher to that stoichiometrically possible (300 μM of CO_2) if it would be assumed that all the oxygen atoms from O_2 and H_2O initially present in the system are incorporated into the photogenerated CO_2. Thus, the above results can only be explained taking into account the contribution of the TiO_2 lattice as a source of oxygen atoms.
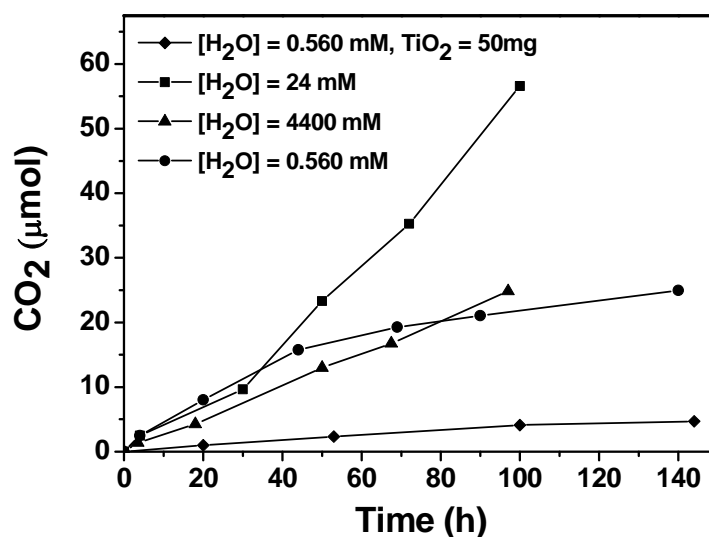

Figure 1. Time evolution of CO_2 from anaerobic benzene photooxidation under controlled amounts of water. Experimental conditions are $V_{ACN} = 25\,\text{ml}$, $\left[AgBF_4\right]_0 = 17\text{mM}$, Benzene = 50 μL, Catalyst

load=500 mg (unless otherwise specified), $\rho = 8.76 \times 10^{16}$ photons/s . Experiments were carried out under stagnant Helium atmosphere (O_2<1 μmol, maximum impurity level in the gas phase detected by GC-TCD).

At higher water concentrations, roughly constant values of γ_{CO_2} $(t \leq 100h)$ could be calculated by performing a linear regression to the CO_2 vs. time curves. This regression furnishes values for γ_{CO_2} of 0.25 and 0.52 μmol/h for experiments with $[H_2O]$ values of 4400 and 24 mM, respectively. In those cases no steady state concentration of CO_2 was observed. Thus, the increase in the $[H_2O]$ values does not lead to a proportional increase of γ_{CO_2}.

Because in the absence of water and O_2, the production of CO_2 should be limited by the available amount of O_s, and additional experiment with a lower catalyst load (50mg) was carried out. In the first 20 hours no CO_2 was detected (detection limit 0.8 μmol) and the steady state concentration of CO_2 (at t >100 h) was 180 μM. This experiment demonstrated that a depletion in the catalyst load leads to a decrease in both the steady state concentration of CO_2 and γ_{CO_2}. This effect can be directly attributed to the depletion of O_s initially present in the system.

3.3 Effect of electron acceptors

Normally, photocatalytic reactions are carried out in the presence of molecular oxygen (O_2). It is generally accepted that O_2 acts as an electron scanvenger[64]. Figure 2A shows the time evolution of CO_2 from PBM in the presence of two electron scavengers[65,66]: silver ions (Ag^+) and O_2. It can be seen that in the experiment performed in Helium atmosphere the γ_{CO_2} value is more than one order of magnitude slower than that of the reaction performed in the presence of O_2. Moreover, the steady state concentration of CO_2 is much higher $\left([CO_2] = 8100 \mu M\right)$ in the presence of O_2 than in its absence $\left([CO_2] = 1000 \mu M\right)$.
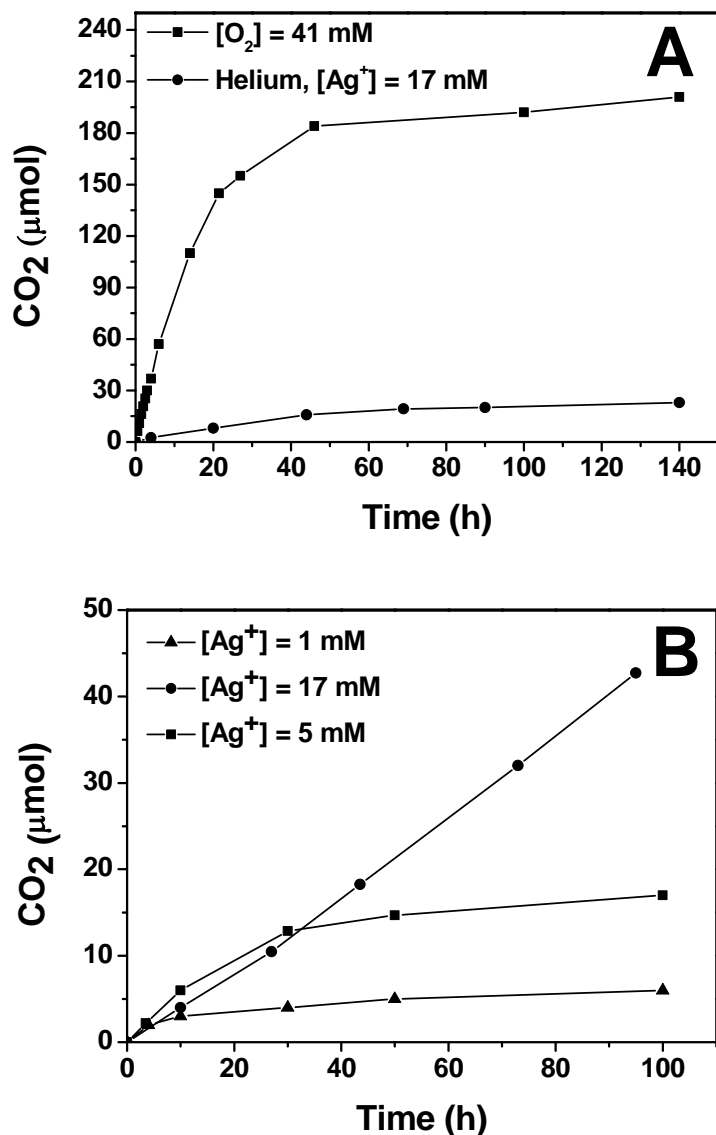
Figure 2. Time evolution of CO_2 evolved from Benzene photooxidation with different electron acceptors**.** **(A)** Silver ions (in helium atmosphere) or molecular oxygen (O_2) as electron acceptors; $[H_2O] = 0.560$ mM. (B) Effect of different concentrations of silver ions (under Helium atmosphere); $[H_2O] = 24$ mM. Experimental conditions for both panels are $V_{ACN} = 25$ml, Benzene = 50 μL, Catalyst load =500 mg, $\rho = 8.76 \times 10^{16}$ photons/s.

Bahnemann et. al. have reported the second order rate constants for the reaction of anatase TiO_2 conduction band free electrons $\left(e_f^-\right)$ with O_2[66] and Ag^+ ions.[65] The values of these constants for the first reaction step (single electron transfer) are $2x10^4$ $M^{-1}s^{-1}$ and $3.74x10^4 M^{-1}s^{-1}$ for O_2 and Ag^+, respectively. According to those constant values, if

the value of γ_{CO_2} would depend on the rate of e_f^- scavenging, then the value of γ_{CO_2} should be higher in the presence of Ag^+ than that in the presence of O_2. The experimental data reported in Figure 2A shows an opposite tendency, i.e. γ_{CO_2} is overwhelmingly higher in the presence of O_2 $\left(\gamma_{CO_2} = 9.69 \mu mol/h\right)$ than in the presence of Ag^+ $\left(\gamma_{CO_2} = 0.39 \mu mol/h\right)$. This fact demonstrate that in this case the value of γ_{CO_2} depends mainly on the reactions initiated by holes $\left(\mathbf{h}^+\right)$ instead of those initiated by e_f^-.

According to eqs 3 and 4 holes are trapped at O_s. Therefore, the O_s are necessary to promote reactions initiated by $\mathbf{h}^+$. For experiments of Figure 2A, the O_s species must be consumed as they are incorporated into the photogenerated CO_2. In the presence of O_2 the consumed O_s can be replaced via dissociative adsorption of O_2 at $\mathbf{V}[\mathbf{O_s}]$ sites[9,10] while in its absence the O_s can not be replaced. As a result, γ_{CO_2} must be higher in the presence of O_2 as it was actually observed in Figure 2A. The possibility of O_2 being incorporated in the final CO_2 through the intermediate formation of $\left(OH^\bullet\right)_{free}$ radicals by O_2 electroreduction (eq. 5) has to be discharged here because acetonitrile is unable to supply the protons needed for $\left(OH^\bullet\right)_{free}$ production (see eq. 5 and ref 43).

Although in the experiments with Ag^+ ions the γ_{CO_2} values are low, their presence is totally necessary to scavenge the electrons in anaerobic conditions as it is evidence by Figure 2B. Increasing the concentration of Ag^+ under the same experimental conditions produce and increase of the steady concentration of CO_2 (at t >50 h) from 200 to 650 μM for $[Ag^+]$ values of 1 and 5 mM, respectively. Moreover, at the highest $[Ag^+]$ value no steady state concentration of CO_2 was observed within the reaction period of 100 hours. The maximum concentration of CO_2 $\left([\mathbf{CO_2}] = 1700 \, \mu\mathbf{M}\right)$ observed in this last experiment (at t=100 h) is much higher than in the others. Despite this large difference in the $[\mathbf{CO_2}]$ values at long illumination times (t > 10 h), a similar value of γ_{CO_2} (around $0.45 \, \mu mol/h$) was observed during the first 10 hours of irradiation. Therefore,

the main changes in the behavior of CO_2 evolution are observed at long illumination times (t > 10 h). Thus, the observed depletion of γ_{CO_2} (at t>10h) at low $[Ag^+]$ values can be mainly attributed to the consumption of the available Ag^+ ions in the system as the photocatalytic reaction proceed. In agreement with this, no CO_2 was produced in the absence of Ag^+ ions as mentioned before (section 3.1).

3.4 Isotopic Tracing (IT) experiments

Experiments in anhydrous and anaerobic conditions seem to indicate that O_s species are involved in the oxidation of organic compounds to CO_2. In order to get direct experimental evidence of this hypothesis, isotopic tracing experiments were carried out. As we have reported earlier[53] the use of oxygen-isotope-labeled titania ($Ti^{18}O_2$) as photocatalyst and the analysis of the isotopic composition of the evolved CO_2 from organic compounds photooxidation provides an opportunity for in situ tracing of the fate of O_s species during photocatalytic oxidation reactions.

Figure 3 shows the isotopic composition and concentration of the CO_2 evolved from PBM reaction carried out in anaerobic conditions and using acetonitrile as solvent.
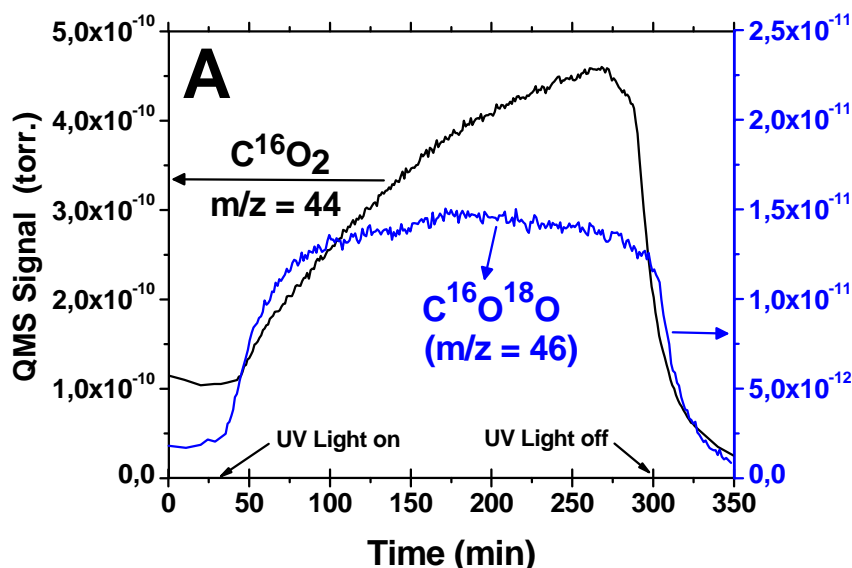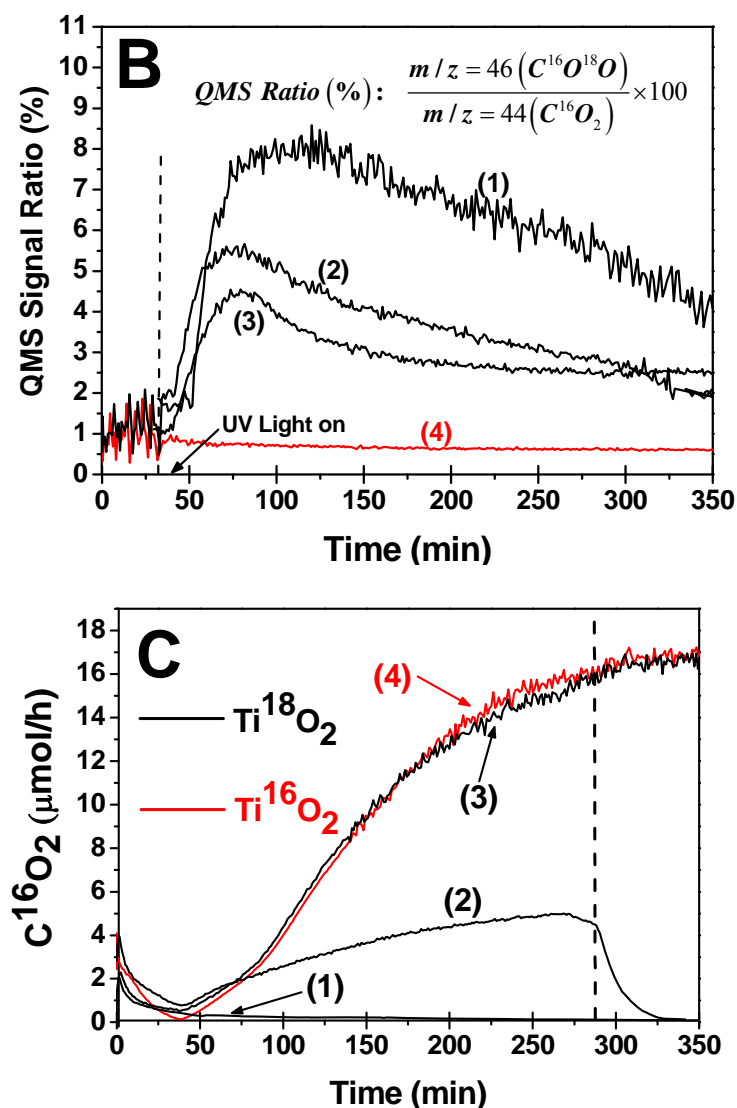
Figure 3. (A) Time evolution of the QMS signal of the $C^{16}O^{18}O$ (*m/z = 46*) and $C^{16}O_2$ (*m/z = 44*) isotopologues of carbon dioxide evolved from photocatalytic anaerobic mineralization of benzene with $Ti^{18}O_2$; $[H_2O] = 10\ \text{mM}$. (B) Time evolution of the $C^{16}O^{18}O/C^{16}O_2$ QMS signal ratio from benzene photooxidation experiments with $Ti^{18}O_2$ (curves 1,2 and 3 (black)) and $Ti^{16}O_2$ (curve 4 (red)). The concentrations of water are $[H_2O] = 0.560\ \text{mM}$ (1), $[H_2O] = 10\ \text{mM}$ (2), $[H_2O] = 24\ \text{mM}$ (3), and $[H_2O] = 24\ \text{mM}$ (4). (C) Time evolution of $C^{16}O_2$ production rate (γ_{CO_2}) from PAM of benzene experiments reported in panel B. Experimental conditions for all panels are $V_{ACN} = 50\ \text{mL}$, Volume of Benzene = 100 μL, Catalyst load=50 mg, $[AgBF_4]_0 = 10\text{mM}$, $\rho = 9.81 \times 10^{17}$ photons/s . All experiments were carried out under Ar flow (5 mL/min). Average sampling time interval = 1.04 min.

Figure 3A illustrates the time evolution of the QMS signal of the $C^{18}O^{16}O$ (*m/z = 46*), and $C^{16}O_2$ (*m/z = 44*) isotopologues of carbon dioxide (CO_2) evolved during a

representative PBM experiment. Although the QMS signal of $C^{18}O_2$ (*m/z = 48*) was also monitored, it is not reported in Figure 3A because that signal was around the detection limit of the QMS instrument.

It is evident from Figure 3A that the time profiles of the $C^{18}O^{16}O$ and $C^{16}O_2$ QMS signals have a different shape. In contrast, the time profile of the QMS signal for both isotopologues was almost identical in a PBM experiment carried out in almost identical conditions but using water as solvent (see Figure 2 of ref. 53). Thus, the solvent has a significant effect on the isotopic composition of the evolved CO_2.

The time profile of the $C^{18}O^{16}O$ QMS signal of Figure 3A shows that after the light is turned on there is a fast production of $C^{18}O^{16}O$ until a steady state QMS signal is reached at around 125 minutes. In contrast, the $C^{16}O_2$ QMS signal increase at a slower rate and no steady state rate was observed during the course of the experiment (until 300 minutes). These features of the QMS signals suggest that immediately after turning on the UV light, there is a fast enrichment of the evolved CO_2 with isotopically labeled oxygen (^{18}O). As the reaction proceeds (t > 100 min) the $C^{18}O^{16}O$/ $C^{16}O_2$ ratio tends to decrease as can be inferred from the constant value of the $C^{18}O^{16}O$ QMS signal reached at t = 125min while the value of the $C^{16}O_2$ QMS signal continues the increase. With the purpose to explore this aspect in detail, we calculated the $C^{18}O^{16}O$/ $C^{16}O_2$ ratio during the course of several PBM experiments using labeled ($Ti^{18}O_2$) or unlabeled ($Ti^{16}O_2$) titania as photocatalyst. The results of these calculations are depicted in Figure 3B (see details of calculation method in the Supporting Information). Before turning on the lamp (t < 30 min) the $C^{18}O^{16}O$/ $C^{16}O_2$ ratio was markedly affected by signal noise in all experiments and thereby it is not possible to distinguish any clear difference. After the UV light was turned on a different behavior could be observed for the various experimental conditions studied. When $Ti^{16}O_2$ was used as photocatalyst a constant value of $0.7 \pm 0.05\%$ for the $C^{18}O^{16}O$/ $C^{16}O_2$ ratio was obtained regardless of the experimental conditions. This constant ratio value is in close agreement with our previously reported results and represents the natural $C^{18}O^{16}O$/ $C^{16}O_2$ ratio of carbon dioxide at the atmosphere and in water [53]. In contrast, experiments with $Ti^{18}O_2$ as catalyst showed a fast increase of the $C^{18}O^{16}O$/ $C^{16}O_2$ ratio values immediately after the light was turned on, reaching a maximum at around 90 minutes and followed by a slow

decrease at longer illumination times. Noteworthy, the values of the maxima observed in Figure 3B strongly depend on the amount of water present in the system. It could be observed that the maxima values increase as $[H_2O]$ values decrease. This experimental trend is in agreement with our previous results[53] where a much lower maximum $C^{18}O^{16}O/C^{16}O_2$ ratio value was observed (ratio max. = 0.96%, see Figure 3 of ref. 53) under the same experimental conditions but using pure water as solvent. On the other hand, in the experiments reported in Figure 3B the $C^{18}O^{16}O/C^{16}O_2$ ratio values slowly decrease and do not reach the natural $C^{18}O^{16}O/C^{16}O_2$ ratio values of CO_2 $(0.7 \pm 0.05\,\%)$ within the time range studied (t < 350 minutes). In contrast, when the experiment is carried out in pure water as solvent the $C^{18}O^{16}O/C^{16}O_2$ ratio value rapidly decreases from its maximum (0.96%) to the natural ratio value of CO_2 after one hour of reaction (see Figure 3 of ref. 53).

Hence, the use of an anhydrous solvent leads to a significant increase in the $C^{18}O^{16}O/C^{16}O_2$ ratio, being this increment more pronounced as the water concentration decreases.

In order to get quantitative information about the total amount of CO_2 evolved during the studied reactions, a calibration of the $C^{16}O_2$ QMS signal was performed by using a standard CO_2 gas. Figure 3C shows the calculated rate of CO_2 evolution $(\gamma_{CO_2}$ in μmol/h$)$ for experiments of curves 1 to 4 from Figure 3B. An opposite trend to that observed for the $C^{18}O^{16}O/C^{16}O_2$ ratio values of Figure 3B can be seen here, i.e. the γ_{CO_2} increases as the $[H_2O]$ increases.

From Figure 3B it is evident that the isotopic enrichment does not stop even at illumination times as long as 350 minutes. Therefore, the ^{18}O isotopic enrichment was quantified within a well defined time range (35 <t <270 min). This period of time starts from the onset of the ^{18}O isotopic enrichment (t = 35 min, represented by a vertical dashed line in Figure 3B) and finishes at a long enough time that allows to reach an almost stable value of γ_{CO_2} in all the experiments (t = 270 min, represented by a vertical dashed line in Figure 3C).

The total amount of $C^{16}O_2$ produced during the selected time period can be calculated by performing the definite integral (limits $t_a = 35$ min and $t_b = 270$ min) of the curve of $C^{16}O_2$ (in μmol/h) versus time (Figure 3C). This calculation yielded values of 0.4, 8.30, 30.5 and 32 μmol of $C^{16}O_2$ for curves 1, 2, 3 and 4, respectively. In a similar way, the ^{18}O isotopic enrichment can be calculated from the definite integral of the QMS signal ratio versus time showed in Figure 3B. In order to perform this integration, the baseline must be settled at a QMS ratio signal value of 0.7% (the natural $C^{16}O^{18}O/C^{16}O_2$ isotopic ratio of CO_2) in order to subtract the contribution of the $C^{16}O^{18}O$ isotopologue naturally present in the carbon dioxide. The calculated values of ^{18}O enrichment in the time range of $35 < t < 270$ min were 6.0, 3.9, 3.1 and 0.0 % for curves 1, 2, 3, and 4, respectively.

By combining the above results, we can calculate the amount of the $C^{16}O^{18}O$ isotopologue photogenerated at each experiment. Values of 0.024, 0.32, 0.95, and 0.0 μmol of $C^{16}O^{18}O$ were found for curves 1, 2, 3 and 4 (of Figure 3B and C), respectively. Because all of the ^{18}O atoms of the evolved $C^{16}O^{18}O$ belong to the $Ti^{18}O_2$ surface lattice, it means that 1.45×10^{16}, 1.93×10^{17}, 5.72×10^{17} and 0.0 TiO_2 surface lattice oxygen atoms (O_s) were incorporate into the evolved CO_2 for the experiments of curves 1, 2, 3, and 4 (of Figure 3B and C), respectively. Accordingly, the surface density of lattice oxygen exchanged atoms (σ_{Os}) were 9.03×10^{11}, 1.20×10^{13}, 3.56×10^{13}, and 0.0 (O_s atoms/cm^2) for those curves, respectively (details of calculation of σ_{Os} are explained in Supporting Information).

In order to check if the O_s are involved in the photooxidation of aromatic compounds different from benzene we carried out similar experiments to those reported in Figure 3 but using phenol and benzaldehyde as organic substrates. Figure 4A and B illustrate the time evolution of the $C^{18}O^{16}O/C^{16}O_2$ ratio for photocatalytic mineralization of phenol and benzaldehyde, respectively. A similar behavior to that of experiments of Figure 3 was observed, namely when $Ti^{18}O_2$ was used as catalyst an ^{18}O enrichment of the evolved CO_2 could be observed. However, in both cases the maximum $C^{18}O^{16}O/C^{16}O_2$ ratio values were lower than those observed in Figure 3B. This is not surprising because both organic substrates have unlabeled oxygen atoms (^{16}O) in their structure. These ^{16}O atoms are incorporated into the evolved CO_2 producing a decrease in the observed

$C^{18}O^{16}O$/ $C^{16}O_2$ ratio values. Again, the time evolution of the rate of CO_2 evolved from the reaction $\left(\gamma_{CO_2} \text{ in } \mu mol/h\right)$ was calculated (Figure 4C).
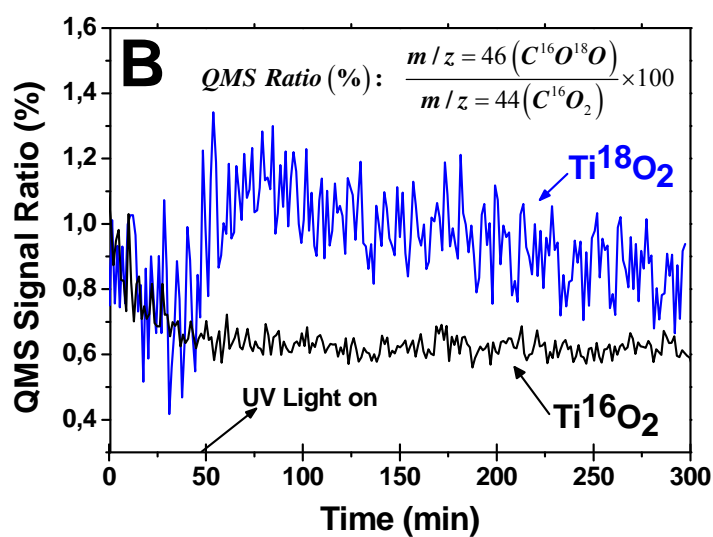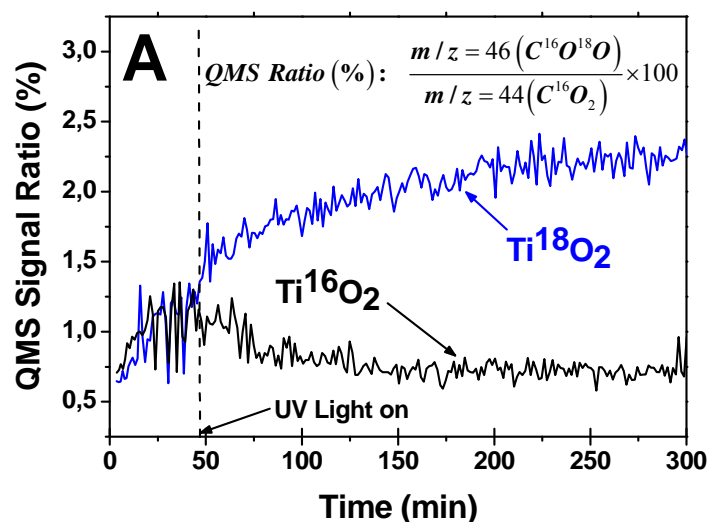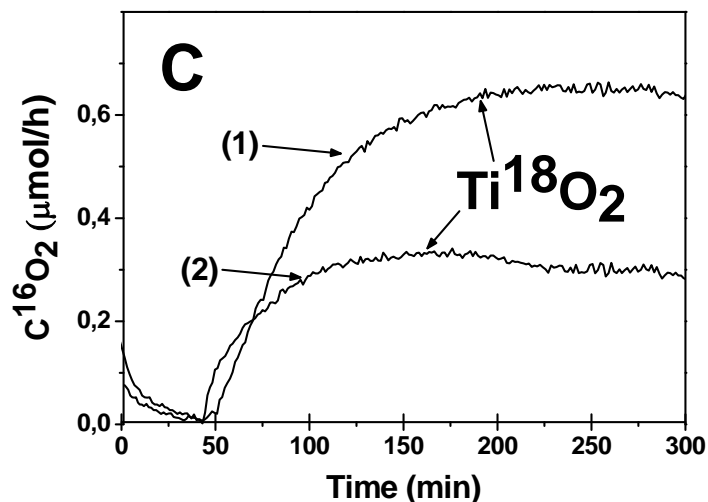
Figure 4. (A) Time evolution of the $C^{16}O^{18}O/C^{16}O_2$ QMS signal ratio from photocatalytic anaerobic mineralization of phenol with $Ti^{18}O_2$ (blue) and $Ti^{16}O_2$ (black). **(B)** Time evolution of the $C^{16}O^{18}O/C^{16}O_2$ QMS signal ratio from photocatalytic anaerobic mineralization of benzaldehyde with $Ti^{18}O_2$ (blue) and $Ti^{16}O_2$ (black). (C) Time evolution of $C^{16}O_2$ production rate $\left(\gamma_{CO_2}\right)$ from PAM of phenol (1) and benzaldehyde (2) with $Ti^{18}O_2$. Experimental conditions for all panels are $V_{ACN} = 50\,\text{mL}$, Concentration of the organic substrate = 10 mM, Catalyst load=50 mg, $\left[AgBF_4\right]_0 = 10\text{mM}$, and $\rho = 9.81\times10^{17}$ photons/s . All experiments were carried out under Ar flow (5 mL/min). Average sampling time interval = 1.04 min. The concentrations of water $\left(\left[H_2O\right] = 24\text{ mM}\right)$ is the same at all experiments.

By using the same calculation methodology that the one used for Figure 3, we calculated the ^{18}O isotopic enrichment, and the amount of $C^{16}O_2$ and $C^{16}O^{18}O$ evolved in a selected time range (35 < t < 280). The calculated values of ^{18}O enrichment were 1.3 and 0.5% for experiments of Figure 4A and B, respectively. The total amount of $C^{16}O_2$ produced were 2.07 and 1.04 µmol, for phenol and benzaldehyde photooxidation, respectively. Combining the above results it was found that the total amount of $C^{16}O^{18}O$ photogenerated were 0.027 and 0.0052 µmol, for phenol and benzaldehyde photooxidation, respectively. Accordingly, σ_{Os} values were $1.01\text{x}10^{12}$ and $1.95\text{x}10^{11}$ (O_s atoms/cm^2) for phenol and benzaldehyde photooxidation, respectively. In both cases the values of σ_{Os} are much lower than those reported for experiments of Figure 3. However, these σ_{Os} values are in a similar order of magnitude than those reported for photoinduced oxygen isotope exchange (POIE) reaction between $^{18}O_2(g)$ and lattice

oxygens (O_s) of TiO_2 P25 $\left(\sigma_{O_s} = 2 \times 10^{11} \text{ atoms/cm}^2\right)$ [67] and those recently reported by us for PBM in water as solvent $\left(\sigma_{O_s} = 5.8 \times 10^{11} \text{ atoms/cm}^2\right)$.[53] In general, the measured values of σ_{Os} can differ by almost two orders of magnitude depending on the solvent (water or acetonitrile) and the organic substrate to be photooxidized. It is remarkable, that the different organic substrates showed not only a very different percentage of ^{18}O enrichment but also a very different rate of production of CO_2 $\left(\gamma_{CO_2} \text{ in } \mu mol/h\right)$, as can be seen comparing Figures 3C and 4C. From these figures it is evident that the γ_{CO_2} values for benzene are higher by more than one order of magnitude to those measured for phenol and benzaldehyde under the same conditions. Hashimoto et al.[26] observed a similar behavior, i.e. a value of γ_{CO_2} higher for benzene than for phenol. Those authors attributed that result to a higher accumulation of reaction products in the liquid phase for phenol photooxidation. In contrast, benzene was readily mineralized and there was a low accumulation of liquid phase products. Recently, Matsumura et. al.[68] demonstrated that, unlike other aromatic compounds, benzene can be mineralized through an efficient route that involves an initial stage of aromatic ring opening, production of muconaldehyde as first intermediate, and followed by a fast degradation of muconaldehyde to CO_2. This explains the high γ_{CO_2} values observed in Figure 3C.

Because our method to measure σ_{Os} values implies the quantification of the concentration and the ^{18}O isotopic composition of CO_2, the values of σ_{Os} measured for benzene photooxidation are more precise than those measured for phenol or benzaldehyde. In the former case, a low concentration of intermediate products remain in solution, thereby thus, an important proportion of the O_s (from $Ti^{18}O_2$) exchanged during the photocatalytic reaction should be accounted for by the calculation of ^{18}O isotopic enrichment of the evolved carbon dioxide, the final reaction product. In the later case, an important proportion of the ^{18}O from the $Ti^{18}O_2$ lattice exchanged during the photocatalytic reaction remain in liquid phase as part of the intermediate products. Thus, the amount of O_s exchanged in the photocatalytic reactions can not be totally accounted for by only tracing the evolved CO_2, being necessary to measure the

concentration and the ^{18}O isotopic composition of the liquid phase intermediate products.

In the case of benzaldehyde photooxidation experiments we were able to identify labeled (^{18}O) and unlabeled (^{16}O) benzoic acid (BA) as reaction intermediate (see Table 1).

Table 1. Photocatalytic oxidation of benzaldehyde [a]
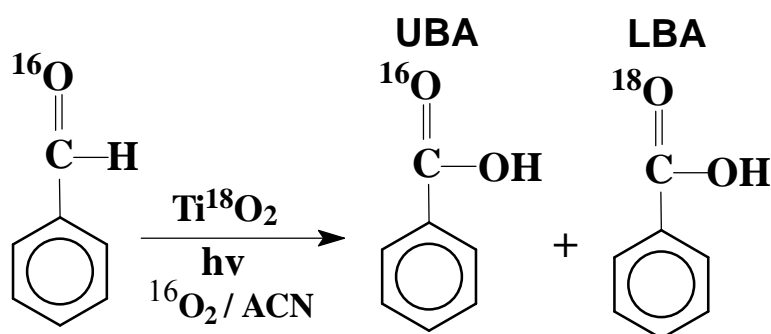
Reaction Parameters	Catalyst	
	$Ti^{18}O_2$	$Ti^{16}O_2$
Time (h)	24	24
Conversion (%)	59.7	65.0
BA Selectivity (%)	78.3	72.0
LBA/UBA ratio (%)	1	0.5
(LBA/UBA) $_{surf}$ ratio (%)	2.2	0.5

[a] Reaction conditions: acetonitrile (ACN) as solvent, $V_{ACN} = 30 \, mL$, Catalyst load=30 mg, Initial benzaldehyde concentration = 8.1 mM, $\rho = 3.89 \times 10^{17}$ photons/s, Reactor Volume = 265 mL, Temperature = 303 K. All experiments were carried out in saturated suspensions of molecular oxygen

$([^{16}O_2(g)] \approx 40$ mM calculated with the ideal gases equation). The product UBA represents unlabeled benzoic acid while LBA is ^{18}O labeled benzoic acid.

Albeit we could detect in all cases several liquid phase reaction intermediates by HPLC and GC-MS, the resolution of the peaks obtained with those techniques was not high enough to allow a precise determination of the ratio between unlabeled and labeled reaction products.

Due to this low sensitivity of the GC-MS and HPLC techniques, and because they have been the main analytical tools used in mechanistic studies of aromatics photooxidation,[25-30,32,34,43-52] the mechanistic pathway that involves the incorporation of O_s from the TiO_2 lattice into the reaction products has been systematically overlooked up to date.

In the case of the photocatalytic oxidation of benzaldehyde the selectivity to benzoic acid was very high (see Table 1). This allowed us to monitor both the BA concentration and the ratio between the ^{18}O labeled BA (LBA in Table 1) and unlabeled BA (UBA in Table 1) in the bulk of the solution (LBA/UBA ratio in Table 1). Additionally, because of the high amount of the photogenerated BA that remained attached to the TiO_2 surface at the end of the reaction (78 μmol BA /gTiO_2) it was also possible to monitor the LBA/UBA ratio at the surface ((LBA/UBA)$_{surf}$ ratio in Table 1).

When the reaction was carried out using $Ti^{16}O_2$ as catalyst, the LBA/UBA ratio after 24 hours of illumination was 0.5% (third column of Table 1). This LBA/UBA ratio value is equivalent to the natural ^{18}O composition of the reaction precursor (benzaldehyde) as it was checked by analyzing the mass spectrum of its GC-MS peak. Thus, in reaction with $Ti^{16}O_2$ there is no ^{18}O isotopic enrichment as it would be expected and the LBA/UBA ratio value of 0.5% for must be taken as a point of reference. When the reaction was carried out using $Ti^{18}O_2$ as catalyst, an ^{18}O isotopic enrichment of the photogenerated BA could be observed both in the bulk of the solution and on the $Ti^{18}O_2$ surface. The former is evidenced by the LBA/UBA ratio value of 1% found in the liquid phase, and the later by the (LBA/UBA)$_{surf}$ ratio value of 2.5% detected on the TiO_2 surface at the end of the reaction. Thus, an ^{18}O enrichment of the photogenerated BA of 0.5% and 2% was observed in the bulk of the solution and at the TiO_2 surface, respectively.

From the data of Table 1, a total amount of 113.6 µmol of benzoic acid produced in the reaction with the $Ti^{18}O_2$ catalyst was calculated. Because the ^{18}O enrichment was 0.5%, the amount of photogenerated LBA was 0.57 µmol which is equivalent to a σ_{O_s} value of 3.6×10^{13} (O_s atoms/cm^2). It is remarkable, that this σ_{O_s} value is as high as the maximum σ_{O_s} value for the experiments reported in Figure 3. Unlike those experiments, benzaldehyde photooxidation experiments of Table 1 were carried out in the presence of $^{16}O_2$ (g). Therefore, the initial $^{16}O/^{18}O$ atomic ratio determined by the ^{16}O and the ^{18}O atoms supplied by molecular oxygen ($^{16}O_2$ (g)) and the $Ti^{18}O_2$ catalyst, respectively, is higher in the benzaldehyde experiments. Despite this higher initial $^{16}O/^{18}O$ ratio value, again we could observe a high σ_{O_s} value for the reaction of Table 1. This makes evident that a reaction route that involves the participation of O_s and therefore the generation of LBA is as important as possible alternatives routes that involve the participation of $^{16}O_2$ (g) and the consequent generation of UBA.

It is worth noting that the σ_{O_s} value for benzaldehyde photooxidation calculated from data of Table 1 $\left(\sigma_{O_s} = 3.6\times10^{13} \ O_s \ atoms/cm^2\right)$ was two orders of magnitude higher to that calculated from data of Figure 4B $\left(\sigma_{O_s} = 1.95\times10^{11} \ O_s \ atoms/cm^2\right)$. This big difference in the σ_{O_s} values corroborate that in the case of benzaldehyde most of the O_s (from the $Ti^{18}O_2$ lattice) exchanged during the photocatalytic reactions can be accounted for by tracing of the ^{18}O labeled products photogenerated in the liquid phase rather than the ^{18}O enrichment of the evolved CO_2.

The relationship between the LBA/UBA ratio values (see Table 1) measured in the bulk of the solution and in the $Ti^{18}O_2$ surface $\left(\left(LBA/UBA\right)_{surf} > \left(LBA/UBA\right)\right)$ is indicative of the location of the different reaction pathways. The higher $\left(LBA/UBA\right)_{surf}$ value suggests that the reaction pathway which involves O_s mainly occur at the $Ti^{18}O_2$ surface while the lower value of $\left(LBA/UBA\right)$ in the bulk of the solution suggest that the reaction pathways that involve $^{16}O_2$ are located into the

solution phase. This is congruent with a recent study of aromatics photooxidation[43] as will be discussed later.

As discussed above, the direct oxidation of water (eq 1) has long been assumed as a source of production of $OH^\bullet$ radicals that further oxidize organic substrates. In consequence, reaction 1 has been considered one of the primary steps of the photocatalytic oxidation reactions. Then, a detailed study of the photocatalytic water oxidation mechanism is of crucial importance because it can help to shed light onto the primary steps of photocatalytic oxidation reactions. With that idea in mind, we carried out IT experiments of water photooxidation in anaerobic conditions, using $Ti^{18}O_2$ or $Ti^{18}O_2$ as catalyst, and with silver ions as electron scavengers. The results of those experiments are reported in Figure 5.
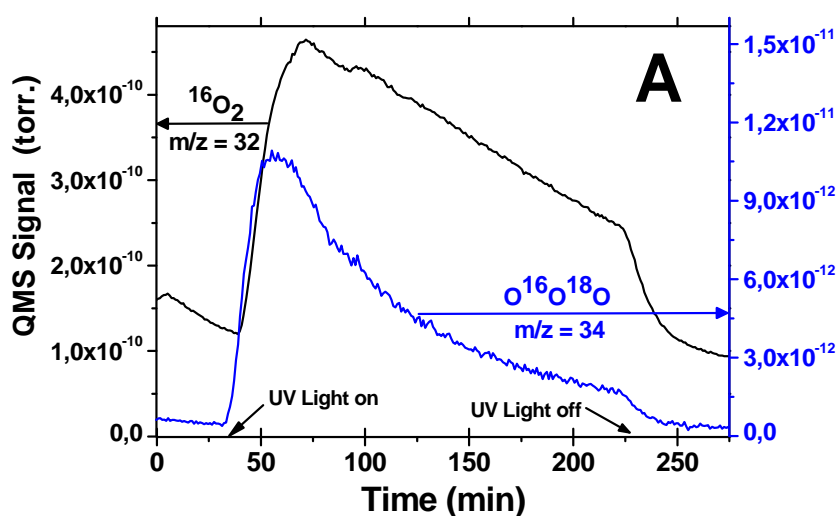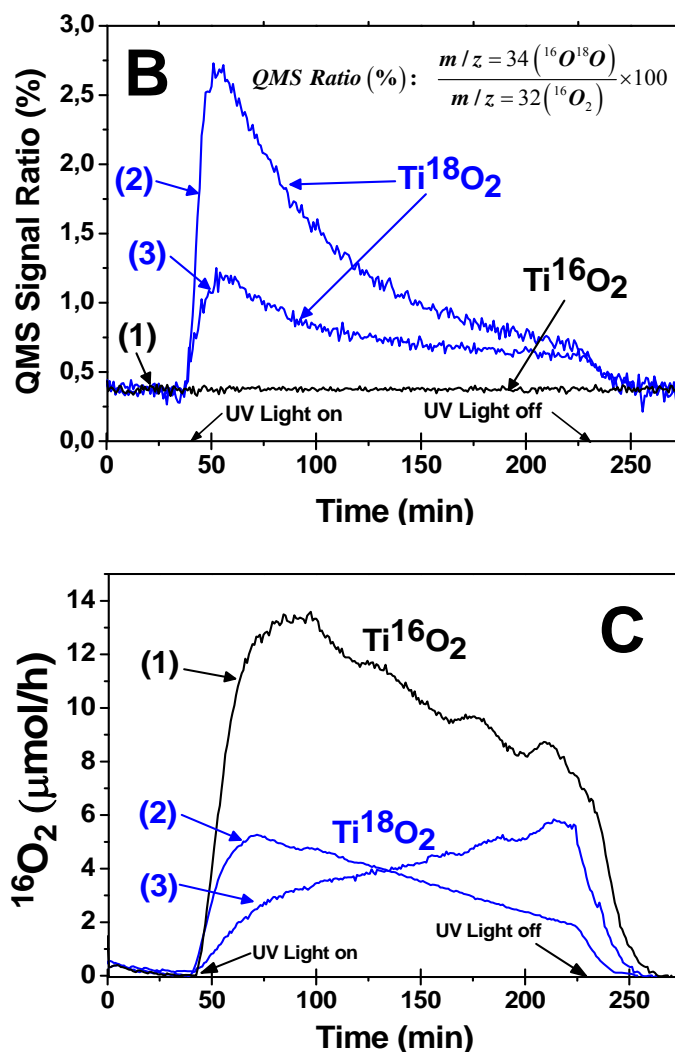
Figure 5. (A) Time evolution of the QMS signal of the $^{16}O^{18}O$ ($m/z = 34$) and $^{16}O_2$ ($m/z = 32$) isotopologues of molecular oxygen (O_2) evolved from water photooxidation with $Ti^{18}O_2$; pH = 4. (B) Time evolution of the $^{16}O^{18}O/^{16}O_2$ QMS signal ratio from water photooxidation experiments with $Ti^{16}O_2$ (curve 1 (black)) and $Ti^{18}O_2$ (curves 2 and 3 (blue)). The initial pH was adjusted to 4 (curves 1 and 2) and 3 (curve 3). (C) Time evolution of $^{16}O_2$ production rate $\left(\gamma_{O_2}\right)$ from water photooxidation experiments reported in panel B. Experimental conditions for all panels are $V_{H_2^{16}O} = 50 \text{ mL}$, Catalyst load=50 mg, $\left[AgBF_4\right]_0 = 10\text{mM}$, $\rho = 9.81 \times 10^{17}$ photons/s. All experiments were carried out under Ar flow (5 mL/min). Average sampling time interval = 1.04 min.

Nishimito et al.[69] studied the water photooxidation reaction under very similar experimental conditions to those reported in Figure 5. Those authors found that the overall photoredox reaction leads to O_2 formation and Ag metal deposition on the TiO_2 surface, according to eq 7.

$$4Ag^+ + 2H_2O \xrightarrow[\text{hv>300nm}]{\text{TiO}_2} 4Ag^0 + O_2 + 4H^+ \qquad\qquad (7)$$
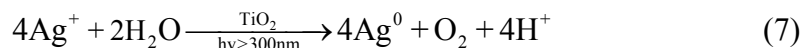
It is well established that the Ag-metal deposition of reaction 7 occurs via reduction of the Ag^+ ions with conduction band electrons[65,69]. It is also generally accepted that O_2 formation occurs via oxidation reactions initiated by holes. However, it is not still clear if holes directly react with water (eq. 1) as has long been assumed[69] or there is a reaction pathway that involves O_s as precursor of the evolved O_2. By tracing the ^{18}O isotopic composition of the evolved O_2 (eq 7) a plausible answer to this question can be elucidated.

Figure 5A illustrates the time evolution of the QMS signal of the $^{18}O^{16}O$ (*m/z = 34*), and $^{16}O_2$ (*m/z = 32*) isotopologues of molecular oxygen (O_2) evolved during a representative water photooxidation experiment. Although the QMS signal of $^{18}O_2$ (*m/z = 36*) was also monitored, it is not reported in Figure 5A because that signal was overlapped with that of ^{36}Ar that was present in the carrier gas. Thus, it was not possible to have a precise quantification of the $^{18}O_2$ (*m/z = 36*) evolved during these experiments.

From Figure 5A it can be seen that the shape of the time profile of the $^{18}O^{16}O$ and the $^{16}O_2$ QMS signals are almost identical. The $^{16}O_2$ QMS signal is almost two orders of magnitude higher than that of the $^{18}O^{16}O$ isotopologue of O_2. Hence, the ^{18}O isotopic enrichment is not as evident as that observed in Figure 3A. This is not surprising because experiments of Figure 5 were carried out in water as solvent and thereby, the initial $^{16}O/^{18}O$ atomic ratio present in the whole system, estimated from the contribution of ^{16}O atoms supplied by the solvent (all the experiments were carried out in unlabeled water ($H_2^{16}O$)) and the ^{18}O atoms supplied by the $Ti^{18}O_2$ catalyst, is around 70000:1 $\left(^{16}O/^{18}O \approx 70000 \right)$[53]. These experimental conditions are similar to those of aqueous PBM experiments reported before[53]. As a consequence, similar features of the QMS signal profile must be observed if a similar mechanism operates for both reactions. By comparing Figure 5 with Figures 2 and 3 of ref. 53 it can be seen that this is the case. Using the same mathematical method explained for Figure 3 we calculated the $^{18}O^{16}O/^{16}O_2$ ratio during the course of several water photooxidation experiments using $Ti^{18}O_2$ and also $Ti^{16}O_2$ as reference. The results are shown in Figure 5B. It can be seen

that in experiments carried out with $Ti^{16}O_2$ a constant value of $0.4 \pm 0.05\%$ for the $^{18}O^{16}O/\,^{16}O_2$ ratio was obtained regardless of the experimental conditions, being that the natural ^{18}O isotopic composition observed for O_2. Thus, 0.4% must be taken as the baseline to calculate the ^{18}O enrichment of the evolved O_2. In experiments carried out with $Ti^{18}O_2$ a very different behavior could be observed. Immediately after the light was turned on (t = 40 min), there is a fast increase of the $^{18}O^{16}O/\,^{16}O_2$ ratio value from its ground level $\left(aprox. 0.4\%\right)$ to a maximum (at t = 55 min) followed by an exponential decay as the reaction proceeds. Finally, when the light was turned off (t = 230 min) it could be observed that the $^{18}O^{16}O/\,^{16}O_2$ ratio reached again its ground level. Noteworthy, the value of the maxima observed in Figure 5B strongly depends on the initial pH, i.e. as the initial pH of a particular experiment increases the value of the maximum increases.

The total amount of $^{16}O_2$ evolved was quantified through the calibration of the $^{16}O_2$ QMS signal with standard O_2 gas. The results are shown in Figure 5C. It can be observed that the production of $^{16}O_2$ is higher with the $Ti^{16}O_2$ catalyst. As explained elsewhere[53] the higher activity of the reference catalyst is related to its higher surface area (S_g = 52 m^2/g) with respect to that of the $Ti^{18}O_2$ catalyst (S_g = 32 m^2/g). On the other hand, in experiments with the $Ti^{18}O_2$ catalyst the rate of production of O_2 $\left(\gamma_{O_2}\right)$ strongly depends on the initial pH. The γ_{O_2} value initially increases faster for the experiment carried out at initial pH 4 than that at pH 3. However, at initial pH 4 a maximum value of γ_{O_2} is reached followed by a decrease in the value of γ_{O_2} while at initial pH 3 the value of γ_{O_2} continually increases until the light is turned off.

The calculated values of ^{18}O enrichment in the time range of 40 < t < 230 min were 0.0, 1.16, and 0.41 % for curves 1, 2, and 3 of Figure 5B, respectively. On the other hand, the total amount of $^{16}O_2$ produced was 34.3, 13.2, and 14 µmol for curves 1, 2, and 3 of Figure 5C, respectively.

By combining the above results, the amount of the $^{16}O^{18}O$ isotopologue photogenerated at each experiment was 0.0, 0.15, and 0.057 µmol, for experiments of curves 1, 2, and 3, respectively. This means that the surface density of lattice oxygen exchanged atoms

(σ_{Os}) were 0.0, 5.63×10^{12}, 2.14×10^{12} (O_s atoms/cm^2) for experiments of curves 1, 2 and 3 (of Figure 5B and C), respectively.

These σ_{Os} values are almost one order of magnitude higher than those measured for aqueous PBM (see ref. 53). Such high values of σ_{Os} for experiments carried out in unlabeled water (H$_2$^{16}O, ^{16}O/^{18}O ≈ 70000)[53] demonstrate the crucial role played by the O_s in the water splitting reaction (eq 7).
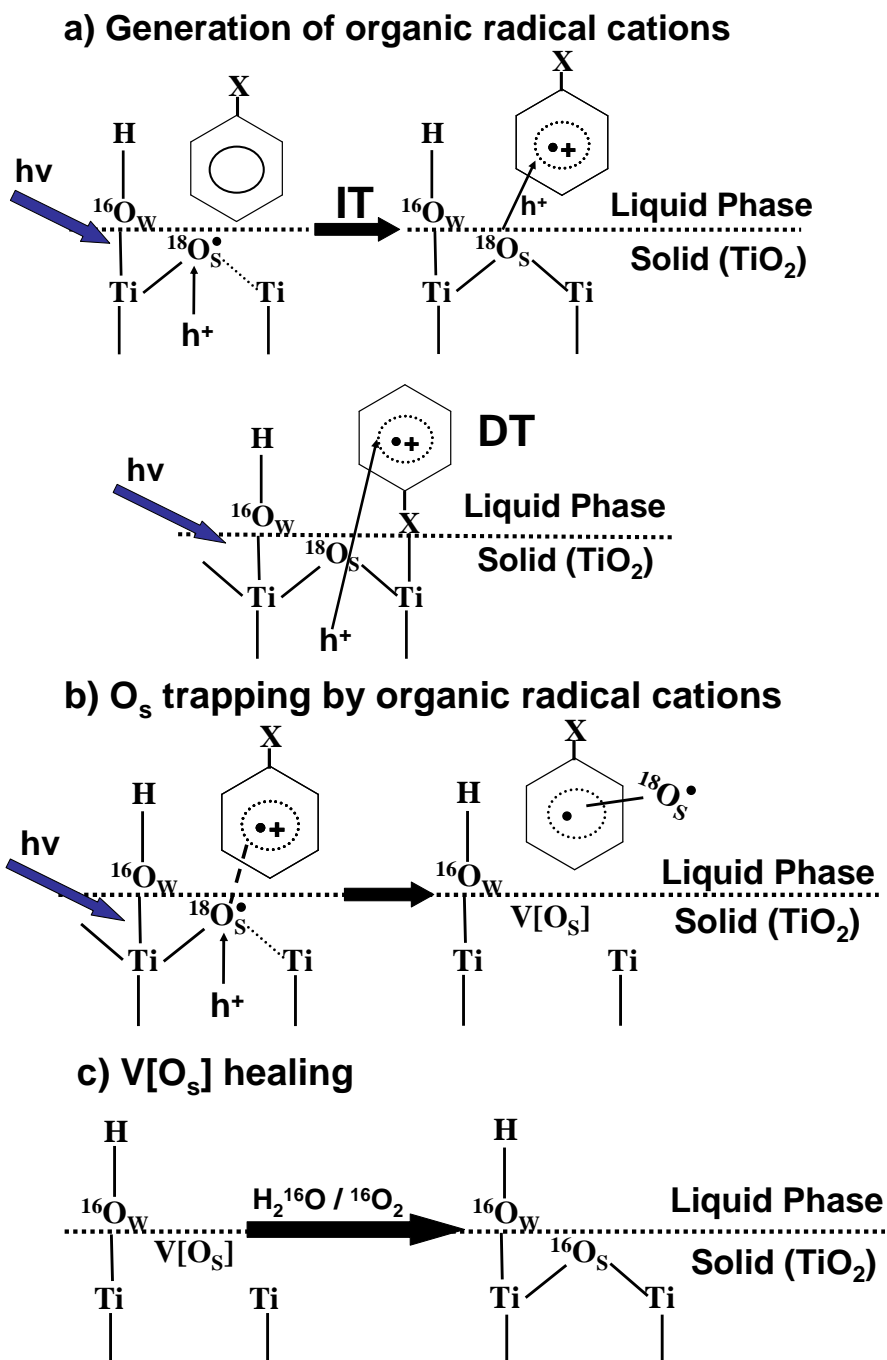
3.5 Implications for mechanistic understanding of TiO$_2$ photocatalysis

The set of results reported sections 3.1 to 3.4 can not be explained in the frame of one of the most traditional mechanistic pathways proposed for TiO$_2$ photocatalysis, namely oxidation of organic substrates through hydroxyl radical chemistry (HRC). [1-3,29] The most important experimental observations that are incongruent with HRC are: (a) When experiments are carried out in the absence of H$_2$O and/or O$_2$ (Figures 1 and 2) the production of $^{\bullet}$**OH** radicals through reactions 1 or 5, respectively, was suppressed. Therefore, if benzene would be oxidized through a HRC pathway, no CO$_2$ production must be observed in those conditions. However, an important production of CO$_2$ was detected, even higher than the stoichiometrically possible if only the oxygen atoms from H$_2$O and/or O$_2$ are taken into account as the oxygen atom sources of the evolved CO$_2$. (b) An intentional increase in the $\left[H_2O \right]$ values (see Fig 1) does not lead to an increase of γ_{CO_2}. This fact is incongruent with $^{\bullet}$**OH** production through reaction 1 because an increase of $\left[H_2O \right]$ must lead to a higher production of $^{\bullet}$**OH** and thereby a higher γ_{CO_2}. (c) For experiments carried out with Ti^{18}O$_2$ (IT experiments reported in Figures 3 to 5 and Table 1) there was always ^{18}O incorporation into the reaction products. No HRC pathway can be invoked to explain this experimental fact. The possible routes for $^{\bullet}$**OH** production (eqs 1 and 5) involve H$_2$O and/or O$_2$. Thus, the only source of the oxygen atoms incorporated into the reaction products would be H$_2$O and/or O$_2$ if the oxidation reactions proceed through the HRC pathways. However, our experiments demonstrated that the TiO$_2$ lattice is another source of oxygen atoms that are incorporated into the products.

The above facts strongly suggest that the TiO_2-assisted photocatalytic oxidation reaction is initiated through single electron transfer (SET) between the organic substrate and the catalyst instead of any HRC pathway. Other research groups have made a similar claim.[70-75] However, former mechanistic proposals that involve SET as initial step did not take into account the possibility of subsequent incorporation of TiO_2 lattice oxygen into the reaction products. Accordingly, a reaction mechanism that invokes SET as initial step with subsequent incorporation of O_s into the reaction products must be formulated in order to give a rational explanation that can account for our experimental results. Scheme 2 illustrates the primary steps of our mechanistic proposal for aromatics photooxidation on the labeled catalyst ($Ti^{18}O_2$) surface.

Scheme 2. Primary steps of photocatalytic oxidation of aromatic compounds on $Ti^{18}O_2$

a

a) Generation of organic radical cations

X

H

X

hν

$^{16}O_W$ **IT**   H   **Liquid Phase**

$^{18}O_S^•$ $^{16}O_W$ h⁺

Ti   Ti $^{18}O_S$ **Solid (TiO$_2$)**

h⁺   Ti   Ti

DT

H

hν

$^{16}O_W$ **Liquid Phase**

X

$^{18}O_S$ **Solid (TiO$_2$)**

Ti   Ti

h⁺

b) O$_s$ trapping by organic radical cations

X   X

H $^{18}O_S^•$

hν   H

$^{16}O_W$ $^{16}O_W$ **Liquid Phase**

$^{18}O_S^•$ V[O$_S$]   **Solid (TiO$_2$)**

Ti   Ti   Ti   Ti

h⁺

c) V[O$_s$] healing

H   H

$^{16}O_W$ **H$_2$^{16}O / ^{16}O$_2$** $^{16}O_W$ **Liquid Phase**

V[O$_S$] $^{16}O_S$ **Solid (TiO$_2$)**

Ti   Ti   Ti   Ti

[a] The Ti^{18}O$_2$ surface is composed of ^{16}O$_w$ atoms which are originated from water chemisorption and ^{18}O$_s$ atoms that belong to the TiO$_2$ lattice.[53] The "X" attached to the aromatic ring represent a functional group (alcohol, aldehyde or a proton for phenol, benzaldehyde or benzene, respectively). Dotted lines represent weakened bonds ready to be broken.

The main steps illustrated in Scheme 2 are: (a) under ultraviolet irradiation $(hv \geq 3.1\,eV)$ the photogenerated holes (h^+) are either trapped by the $^{18}O_s$ species (eqs 2 and 3) or by a chemisorbed aromatic compound (eq 4). An organic radical cation $\left[RH^{\bullet+}\right]$ is directly generated in the later case (direct transfer mechanism (DT)) while in the former an additional step of electron transfer from a dissolved aromatic compound (RH_2) to an oxygen lattice radical $\left(-^{18}O_s^{\bullet}\right)$ is required (indirect transfer mechanism (IT)) to generate the organic radical (see the complete sequence of reaction equations in Table 1 of ref. 53). [53, 76-78] Note that unlike the traditional HRC reaction pathway, hole trapping by adsorbed water species $(^{16}O_w)$ according to eq. 1 is disregarded. (b) Once the organic radical cation has been generated it reacts with another $-^{18}O_s^{\bullet}$ radical at the TiO_2 surface. A subsequent hole trapping breaks the bond of the $^{18}O_s$ with the lattice, being the $^{18}O_s$ captured by the organic radical. This new hole trapping by the surface oxygen radical should be highly favorable because this radical species, being an excited species, should have electrons in energy levels clearly above the energy edge of the valence band of the catalyst, or even above the energy level of the ordinary surface bridging oxygen. This step leaves behind a surface oxygen vacancy $V[O_s]$ at the TiO_2 surface. (c) If the reaction is carried out in the presence of $^{16}O_2$ or $H_2^{16}O$ their ^{16}O atoms fill the $V[O_s]$ sites left behind in step (b) through dissociative adsorption[6,9,10,21,22] regenerating in this way the catalyst surface and closing the catalytic cycle. It is worth noting that this step generates $^{16}O_s$ species at the TiO_2 surface which in subsequent reaction steps can be incorporated into the aromatic reaction intermediate products. Unless previous reaction mechanisms,[1-3,29] the role assigned to $H_2^{16}O$ is just the refilling of the $V[O_s]$ sites and not the direct capture of photogenerated holes (eq 1).

The above mechanism is able to explain the following experimental observations: (1) when $^{16}O_2$ and/or $H_2^{16}O$ are removed from the reaction system (Figures 1 and 2) there is a considerable production of CO_2 that can only be explained considering the incorporation of O_s atoms into the reaction products (steps a and b). However, after long illumination times the production of CO_2 is stopped (Figure 1) as would be expected in the absence of species that can heal the $V[O_s]$ sites generated in step (c). Indeed, a maximum number of 10^{-1} monolayer (ML) of $V[O_s]$ sites can be generated at

the catalyst surface before it collapses.[6,9] (2) The effect of the increase of $[H_2O]$ values (see Figure 1) is to avoid the achievement of an steady state concentration of CO_2. Step c (vacancy healing with water) is congruent with this observation because the introduction of H_2O to the system allows the regeneration of the TiO_2 surface to close the catalytic cycle. (3) The increase in the $[H_2O]$ values (Figure 1) leaded to a decrease of γ_{CO_2}. As discussed above water forms a 3D hydrogen bonding network on the TiO_2 surface. Thus, at higher $[H_2O]$ values the access of the organic substrate to the catalyst surface is hindered by that water network. Because step (a) requires that the organic substrate approaches to the catalyst surface, an increase in the $[H_2O]$ would hinder the step (a) with the consequent γ_{CO_2} depletion, as was actually observed. (4) When the reaction is carried out in the presence of O_2 a higher γ_{CO_2} value than that in the presence of Ag^+ was observed (Figure 2). Step (a) requires hole trapping at the catalyst surface. Ag^+ ions hinder the h^+ trapping at the surface due to electrostatic repulsion. In contrast, there is no such electrostatic repulsion in the presence of O_2 and additionally, the oxygen atoms of O_2 can continuously heal the $V[O_s]$ sites allowing a high concentration of O_s. Therefore, the presence of O_2 promotes steps (a) and (c) which explains the higher γ_{CO_2} values observed in aerobic conditions. (5) IT experiments (Figures 3 and 4 and Table 1) demonstrated that there is always $^{18}O_s$ incorporation into the reaction products. This observation is congruent with step (b). (6) The $C^{16}O^{18}O/C^{16}O_2$ ratio of the reaction products strongly depends on the concentration of H_2O in the solvent (see Figure 3). A higher $[H_2O]$ led to a lower $C^{16}O^{18}O/C^{16}O_2$ ratio in the evolved CO_2. This is in agreement with step (c) because incorporation of water in the surface oxygen vacancies generates $^{16}O_s$ species at the TiO_2 surface that can be subsequently incorporated into the reaction products leading to a decrease of the observed $C^{16}O^{18}O/C^{16}O_2$ ratio. (7) In all the IT experiments (Figures 3 and 4) a fast ^{18}O enrichment after illumination followed by an exponential decay of the $C^{16}O^{18}O/C^{16}O_2$ ratio could be observed. Steps (a) and (b) imply that $^{18}O_s$ are firstly incorporated into the reaction products and, therefore, a high ^{18}O enrichment is expected at the beginning

of the process. As the reaction proceeds, ^{16}O atoms from water generate $^{16}O_s$ species at the TiO_2 surface (step (c)) that can be subsequently incorporated into the reaction products. This must lead to a $C^{16}O^{18}O/C^{16}O_2$ ratio decrease as the reaction proceeds as was actually observed.

In summary, the set of experimental data of Figures 1 to 4 and Table 1 can be accounted for by the reaction mechanism proposed in Scheme 2. A hallmark of this mechanism is the involvement of lattice oxygens in all the reaction steps and the disregarding of $(HO^{\bullet})_{W,ads}$ production from water oxidation (eq 1). This point deserves special attention because it is still a matter of controversy. A reaction mechanism that accounts for the experimental data of water photooxidation shown in Figure 5 can bring a new insight to this debate. Scheme 3 illustrates our mechanistic proposal for water photooxidation reaction on the labeled ($Ti^{18}O_2$) catalyst surface.

Scheme 3. Primary steps of water photooxidation on $Ti^{18}O_2$
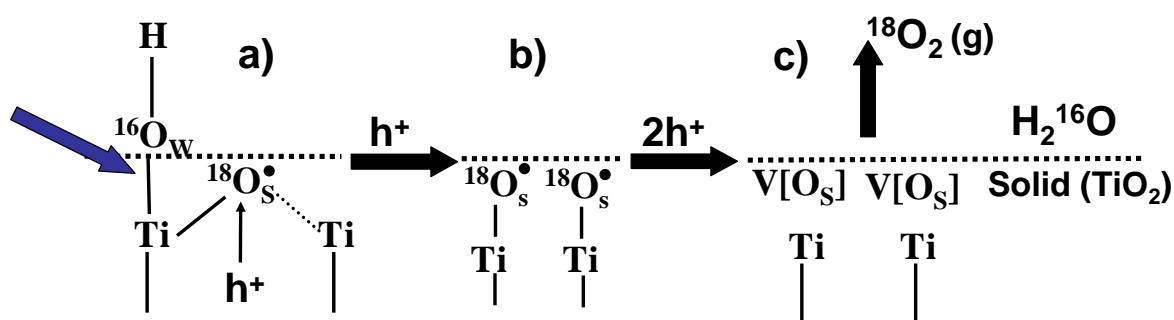
Since one of us[20] recently reported a detailed theoretical formulation of the mechanism depicted in Scheme 3, here we briefly describe the main steps: (a) under ultraviolet irradiation $\left(hv \geq 3.1\,eV\right)$ a photogenerated hole (h^+) is trapped by an $^{18}O_s$ specie (eqs 2 and 3) generating a $-^{18}O_s^{\bullet}$ radical. As stated above, hole trapping by adsorbed water species ($^{16}O_w$) according to eq. 1 is disregarded. (b) Another h^+ traps another $^{18}O_s$ generating two $-^{18}O_s^{\bullet}$ radicals at adjacent surface sites. If the distance between these radicals is short enough (distance ≤ 2.5 A°)[20] they couple each other. (c) Subsequent trapping of two holes breaks the bonds of the $-^{18}O_s^{\bullet}$ species with the TiO_2 lattice and lead to the generation of $^{18}O_2$ (g). This step leaves behind two $V[O_s]$ sites at the TiO_2

surface. As explained before, these V[O_s] sites can be healed by the solvent ($H_2{}^{16}O$) generating $^{16}O_s$ species at the catalyst surface. As the reaction proceeds, the $^{16}O_s$ species can react in the same way explained in steps (a) to (c) of Scheme 3.

The expected outcome of reaction mechanism of scheme 3 is the production of a mixture of the $^{18}O_2$, $^{16}O^{18}O$, and $^{16}O_2$ isotopologues of molecular oxygen. In contrast, the outcome of the traditional mechanism which invokes direct water oxidation (eq 1) is the only production of $^{16}O_2$ (g) if the experiments are carried out in unlabeled water ($H_2{}^{16}O$). It is evident from Figure 5 that $^{16}O^{18}O$ was photogenerated in experiments with $Ti^{18}O_2$, a fact that is in favor of the mechanism of scheme 3. On the other hand, the mechanism of scheme 3 must produce distortion of TiO_2 surface lattice as the reaction proceeds while direct water oxidation (eq 1) does not. Recently reported AFM evidence[18] demonstrated that water photooxidation indeed produce such distortion which supports the mechanism of scheme 3.

Other experimental observations that can be explained in the frame of the reaction mechanism of scheme 3 are: (1) Higher initial pH leaded to a higher initial γ_{O_2} and higher ^{18}O enrichment (see Figure 5). As the pH increases the O_s species become deprotonated and therefore they have a formal negative charge. [18,20] Thus, there is no electrostatic repulsion with h^+ species making easier steps (a) and (b). In contrast, at low pH steps (a) and (b) become hindered due to the electrostatic repulsion between positively charged O_s and h^+.[18] As a consequence, higher pH must lead to higher γ_{O_2} and ^{18}O enrichment as was actually observed (Figure 5). (2) In the experiment of Figure 5 a fast ^{18}O enrichment after illumination followed by an exponential decay of the $^{16}O^{18}O/^{16}O_2$ ratio can be observed. Steps (a) to (c) imply that $^{18}O_s$ are the primary hole traps and their reaction produce $^{18}O_2$ evolution (g), therefore a high ^{18}O enrichment is expected at the beginning of the process. As the reaction proceeds, ^{16}O atoms from water generate $^{16}O_s$ species at the TiO_2 surface leading to the production of $^{16}O^{18}O$ and $^{16}O_2$. This must lead to a $^{16}O^{18}O/^{16}O_2$ ratio decrease as the reaction proceeds as was actually observed (Figure 5B).

In summary, the set of experimental data of Figures 5 can be accounted for by the reaction mechanism proposed in Scheme 3. Again O_s is involved in the primary

reaction steps and the production of $(HO^{\bullet})_{W,ads}$ from water oxidation (eq 1) is disregarded. Thus, the primary steps of water and aromatic compound photooxidation occur at the TiO_2 surface, and imply hole trapping by the O_s and the subsequent incorporation of the O_s into the reaction products.

The highest σ_{O_s} values obtained in this work $\left(\sigma_{O_s} = 3.6 \text{x} 10^{13} \dfrac{O_s \text{ atoms}}{cm^2}, \text{see Figure 3 and Table 1}\right)$ demonstrated that around 10^{-2} ML of O_s atoms are exchanged in the course of the studied photocatalytic reactions if we consider $1ML \approx 1\text{x}10^{15}$ atoms/cm^2 as reported[79] for anatase nanoparticles similar to our $Ti^{18}O_2$ catalyst. Thus, just around 1% of the O_s are actively involved in the photocatalytic reaction. This suggests that only some O_s species located at surface defects of the nanoparticles are reactive. However, this aspect can only be elucidated with further study at well defined TiO_2 crystals with a well-known chemical structure of the surface.

Finally, we would like to stress that we are not totally disregarding the possibility of a HRC reaction pathway in liquid phase photocatalytic oxidation of aromatic compounds. Several researchers have given evidence about the existence of the HRC-pathway in this type of reactions[25-30,32,34,44-49] However, those studies were carried out in the presence of both H_2O and O_2. Such kind of system does not allow distinguishing the origin of the radical species because they could be generated through reaction of H_2O with holes (eq. 1) or via reactions of O_2 with electrons (eq. 5). The results presented here just challenge the commonly assumed hypothesis of production of radicals via reactions initiated by holes (eq. 1). In contrast, the production of several radicals $\left(O_2^{\bullet-}, {}^{\bullet}OOH \text{ and } {}^{\bullet}OH\right)$ via reaction of O_2 with electrons is an experimental fact that can not be disregarded. Actually, the most recent studies on TiO_2 aromatics photooxidation have demonstrated the pivotal role of the oxidation pathway initiated by O_2-derived radicals. [43,50] Those studies demonstrated that such oxidation pathway is initiated by electrons and it is located mainly in the bulk of the solution rather than at the TiO_2 surface. Moreover, this pathway becomes more prominent at long illumination times. [43,50] In contrast, the oxidation pathway of scheme 3 is initiated by holes, located at the TiO_2 surface, and it

is more prominent at the beginning of the photocatalytic process. Thus, we propose that the former studies of aromatics photooxidation[25-30,32,34,44-49] can be explained in the frame of the coexistence of these two oxidation pathways.

4. CONCLUSIONS AND OUTLOOK

The experimental evidence collected in this study allows us formulating a new mechanistic pathway for photocatalytic oxidation reactions. This pathway involves the participation of the TiO_2 surface lattice oxygens (O_s) as hole traps, their subsequent incorporation into the reaction products, the continuous generation of oxygen vacancies at the TiO_2 surface in the course of the photocatalytic process and their healing through dissociative adsorption of O_2 and/or H_2O to close the catalytic cycle. It is worth noting that unless former mechanistic proposals that assume a "static catalyst surface", our mechanism assumes that the catalytic surface itself is changing and being regenerated in the course of the reaction. This view of the photocatalytic process is more congruent with the findings of SCS on TiO_2 surfaces reported in the last decade.

We are convinced that this prominent role assigned to reactive O_s can be systematically used to explain a large body of experimental observations existing in the scientific literature about TiO_2 assisted heterogeneous photocatalysis. For exemple, in a recent and excellent paper by Mao et al[80] the authors report the remarkable photocatalytic performance of what they call "black TiO_2", a catalyst that is obtained by hydrogenation of the TiO_2 surface and the creation of a "disorder engineered" surface layer. The authors claim that the high absorbance of this black TiO_2, a catalyst that contains a large number of mid-gap states, should be the cause of such a good performance. However, based in the findings described here, the presence of a large number of disordered ("loosened") O_s with a reactivity higher than usual could by itself be a valid explanation of the high photocatalytic activity reported by those authors. However, further work is required to get more precise quantitative information about the O_s exchanged in a photocatalytic reaction and about the nature of the O_s that can be exchanged.

ASSOCIATED CONTENT

Supporting Information

ACKNOWLEDGMENTS

References

(1) Fox, M. A.; Dulay, M. T. Heterogeneous photocatalysis. *Chemical Reviews* 1993, *93* (1), 341-357.

(2) Hoffmann, M. R.; Martin, S. T.; Choi, W.; Bahnemann, D. W. Environmental Applications of Semiconductor Photocatalysis. *Chemical Reviews* 1995, *95* (1), 69-96.

(3) Peral, J.; Domenech, X.; Ollis, D. F. Heterogeneous photocatalysis for purification, decontamination and deodorization of air. *Journal of Chemical Technology and Biotechnology* **1997,** *70* (2), 117-140.

(4) Fujishima, A.; Rao, T. N.; Tryk, D. A. Titanium dioxide photocatalysis. *Journal of Photochemistry and Photobiology C: Photochemistry Reviews* 2000, *1* (1), 1-21.

(5) Grätzel, M. Dye-sensitized solar cells. *Journal of Photochemistry and Photobiology C: Photochemistry Reviews* 2003, *4* (2), 145-153.

(6) Thompson, T. L.; Yates, J. T. Surface Science Studies of the Photoactivation of TiO_2 New Photochemical Processes. *Chemical Reviews* 2006, *106* (10), 4428-4453.

(7) Rajeshwar, K. Hydrogen generation at irradiated oxide semiconductor solution interfaces. *Journal of Applied Electrochemistry* **2007,** *37* (7), 765-787.

(8) Fujishima, A.; Zhang, X.; Tryk, D. A. TiO_2 photocatalysis and related surface phenomena. *Surface Science Reports* 2008, *63* (12), 515-582.

(9) Pang, C. L.; Lindsay, R.; Thornton, G. Chemical reactions on rutile $TiO_2(110)$. *Chemical Society Reviews* 2008, *37* (10), 2328-2353.

(10) Henderson, M. A. A surface science perspective on photocatalysis. *Surface Science Reports* 2011, *66* (6-7), 185-297.

(11) Nakata, K.; Fujishima, A. TiO$_2$ photocatalysis: Design and applications. *Journal of Photochemistry and Photobiology C: Photochemistry Reviews* 2012, *13* (3), 169-189.

(12) Ochiai, T.; Fujishima, A. Photoelectrochemical properties of TiO$_2$ photocatalyst and its applications for environmental purification. *Journal of Photochemistry and Photobiology C: Photochemistry Reviews* 2012, *13* (4), 247-262.

(13) Zhang, L.; Mohamed, H. H.; Dillert, R.; Bahnemann, D. Kinetics and mechanisms of charge transfer processes in photocatalytic systems: A review. *Journal of Photochemistry and Photobiology C: Photochemistry Reviews* 2012, *13* (4), 263-276.

(14) O'Regan, B.; Gratzel, M. A low-cost, high-efficiency solar cell based on dye-sensitized colloidal TiO$_2$ films. *Nature* **1991,** *353* (6346), 737-740.

(15) Fujishima, A.; Honda, K. Electrochemical Photolysis of Water at a Semiconductor Electrode. *Nature* **1972,** *238* (5358), 37-38.

(16) Friedmann, D.; Mendive, C.; Bahnemann, D. TiO$_2$ for water treatment: Parameters affecting the kinetics and mechanisms of photocatalysis. *Applied Catalysis B: Environmental* **2010,** *99* (3-4), 398-406.

(17) Nakamura, R.; Nakato, Y. Primary intermediates of oxygen photoevolution reaction on TiO$_2$ (Rutile) particles, revealed by in situ FTIR absorption and photoluminescence measurements. *Journal of the American Chemical Society* **2004,** *126* (4), 1290-1298.

(18) Imanishi, A.; Okamura, T.; Ohashi, N.; Nakamura, R.; Nakato, Y. Mechanism of Water Photooxidation Reaction at Atomically Flat TiO$_2$ (Rutile) (110) and (100) Surfaces: Dependence on Solution pH. *Journal of the American Chemical Society* **2007,** *129* (37), 11569-11578.

(19) Salvador, P. On the Nature of Photogenerated Radical Species Active in the Oxidative Degradation of Dissolved Pollutants with TiO$_2$ Aqueous Suspensions: A Revision in the Light of the Electronic Structure of Adsorbed Water. *J. Phys. Chem. C* **2007,** *111* (45), 17038-17043.

(20) Salvador, P. Mechanisms of water photooxidation at n-TiO$_2$ rutile single crystal oriented electrodes under UV illumination in competition with photocorrosion. *Progress in Surface Science* **2011,** *86* (1-2), 41-58.

(21) Brookes, I. M.; Muryn, C. A.; Thornton, G. Imaging Water Dissociation on TiO$_2$ (110). *Phys. Rev. Lett.* **2001,** *87* (26), 266103.

(22) Schaub, R.; Thostrup, P.; Lopez, N.; Lmgsgaard, E.; Stensgaard, I.; N°rskov, J. K.; Besenbacher, F. Oxygen Vacancies as Active Sites for Water Dissociation on Rutile TiO$_2$(110). *Phys. Rev. Lett.* **2001,** *87* (26), 266104.

(23) Jaeger, C. D.; Bard, A. J. Spin trapping and electron spin resonance detection of radical intermediates in the photodecomposition of water at titanium dioxide particulate systems. *J. Phys. Chem.* **1979,** *83* (24), 3146-3152.

(24) Van Damme, H.; Hall, W. K. Photoassisted decomposition of water at the gas-solid interface on titanium dioxide. *Journal of the American Chemical Society* **1979,** *101* (15), 4373-4374.

(25) Izumi, I.; Dunn, W. W.; Wilbourn, K. O.; Fan, F. R.; Bard, A. J. Heterogeneous photocatalytic oxidation of hydrocarbons on platinized titanium dioxide powders. *J. Phys. Chem.* **1980,** *84* (24), 3207-3210.

(26) Hashimoto, K.; Kawai, T.; Sakata, T. Photocatalytic reactions of hydrocarbons and fossil fuels with water. Hydrogen production and oxidation. *J. Phys. Chem.* **1984,** *88* (18), 4083-4088.

(27) Okamoto, K. i.; Yamamoto, Y.; Tanaka, H.; Tanaka, M.; Itaya, A. Heterogeneous Photocatalytic Decomposition of Phenol over TiO_2 Powder. *Bulletin of the Chemical Society of Japan* **1985,** *58* (7), 2015-2022

(28) Al-Ekabi, H.; Serpone, N.; Pelizzetti, E.; Minero, C.; Fox, M. A.; Draper, R. B. Kinetic studies in heterogeneous photocatalysis. 2. Titania-mediated degradation of 4-chlorophenol alone and in a three-component mixture of 4-chlorophenol, 2,4-dichlorophenol, and 2,4,5-trichlorophenol in air-equilibrated aqueous media. *Langmuir* **1989,** *5* (1), 250-255.

(29) Turchi, C. S.; Ollis, D. F. Photocatalytic degradation of organic water contaminants: Mechanisms involving hydroxyl radical attack. *Journal of Catalysis* **1990,** *122* (1), 178-192.

(30) . Mills, A.; Morris, S.; Davies, R. Photomineralisation of 4-chlorophenol sensitised by titanium dioxide: a study of the intermediates. *Journal of Photochemistry and Photobiology A: Chemistry* **1993,** *70* (2), 183-191.

(31) Sun, L.; Bolton, J. R. Determination of the Quantum Yield for the Photochemical Generation of Hydroxyl Radicals in TiO_2 Suspensions. *J. Phys. Chem.* **1996,** *100* (10), 4127-4134.

(32) Theurich, J.; Lindner, M.; Bahnemann, D. W. Photocatalytic Degradation of 4-Chlorophenol in Aerated Aqueous Titanium Dioxide Suspensions: A Kinetic and Mechanistic Study. *Langmuir* **1996,** *12* (26), 6368-6376.

(33) Schwarz, P. F.; Turro, N. J.; Bossmann, S. H.; Braun, A. M.; Wahab, A. M.; Dürr, H. A New Method To Determine the Generation of Hydroxyl Radicals in Illuminated TiO_2 Suspensions. *The Journal of Physical Chemistry B* **1997,** *101* (36), 7127-7134.

(34) Yang, J.; Dai, J.; Chen, C.; Zhao, J. Effects of hydroxyl radicals and oxygen species on the 4-chlorophenol degradation by photoelectrocatalytic reactions with TiO_2-film electrodes. *Journal of Photochemistry and Photobiology A: Chemistry* **2009,** *208* (1), 66-77.

(35) Howe, R. F.; Gratzel, M. EPR study of hydrated anatase under UV irradiation. *J. Phys. Chem.* **1987,** *91* (14), 3906-3909.

(36) Micic, O. I.; Zhang, Y.; Cromack, K. R.; Trifunac, A. D.; Thurnauer, M. C. Trapped holes on titania colloids studied by electron paramagnetic resonance. *J. Phys. Chem.* **1993,** *97* (28), 7277-7283.

(37) Dimitrijevic, N. M.; Saponjic, Z. V.; Rabatic, B. M.; Poluektov, O. G.; Rajh, T. Effect of Size and Shape of Nanocrystalline TiO_2 on Photogenerated Charges. An EPR Study. *J. Phys. Chem. C* **2007,** *111* (40), 14597-14601.

(38) Nosaka, Y.; Komori, S.; Yawata, K.; Hirakawa, T.; Nosaka, A. Y. Photocatalytic $OH^\bullet$ radical formation in TiO_2 aqueous suspension studied by several detection methods. *Phys. Chem. Chem. Phys.* **2003,** *5* (20), 4731-4735.

(39) Lawless, D.; Serpone, N.; Meisel, D. Role of hydroxyl radicals and trapped holes in photocatalysis. A pulse radiolysis study. *J. Phys. Chem.* **1991,** *95* (13), 5166-5170.

(40) Rajh, T.; Saponjic, Z. V.; Micic, O. I. Reactions of hydrous titanium oxide colloids with strong oxidizing agents. *Langmuir* **1992,** *8* (5), 1265-1270.

(41) Walling, C. Fenton's reagent revisited. *Accounts of Chemical Research* **1975,** *8* (4), 125-131.

(42) Eberhardt, M. K. The effect of metal ions on the hydroxylation of fluorobenzene and toluene by peroxydisulfate. *J. Org. Chem.* **1977,** *42* (5), 832-835.

(43) Li, Y.; Wen, B.; Yu, C.; Chen, C.; Ji, H.; Ma, W.; Zhao, J. Pathway of Oxygen Incorporation from O_2 in TiO_2 Photocatalytic Hydroxylation of Aromatics: Oxygen Isotope Labeling Studies. *Chem. Eur. J.* **2012,** *18* (7), 2030-2039.

(44) Stafford, U.; Gray, K. A.; Kamat, P. V. Radiolytic and TiO_2-Assisted Photocatalytic Degradation of 4-Chlorophenol. A Comparative Study. *J. Phys. Chem.* **1994,** *98* (25), 6343-6351.

(45) Goldstein, S.; Czapski, G.; Rabani, J. Oxidation of Phenol by Radiolytically Generated $^\bullet OH$ and Chemically Generated $SO_4^{\bullet -}$. A Distinction between $^\bullet OH$ Transfer and Hole Oxidation in the Photolysis of TiO_2 Colloid Solution. *J. Phys. Chem.* **1994,** *98* (26), 6586-6591.

(46) Hathway, T.; Jenks, W. S. Effects of sintering of TiO_2 particles on the mechanisms of photocatalytic degradation of organic molecules in water. *Journal of Photochemistry and Photobiology A: Chemistry* **2008,** *200* (2-3), 216-224.

(47) Rockafellow, E. M.; Stewart, L. K.; Jenks, W. S. Is sulfur-doped TiO2 an effective visible light photocatalyst for remediation? *Applied Catalysis B: Environmental* **2009,** *91* (1-2), 554-562.

(48) Rockafellow, E. M.; Haywood, J. M.; Witte, T.; Houk, R. S.; Jenks, W. S. Selenium-Modified TiO2 and Its Impact on Photocatalysis. *Langmuir* **2010,** *26* (24), 19052-19059.

(49) Hathway, T.; Chernyshov, D. L.; Jenks, W. S. Selectivity in the photo-Fenton and photocatalytic hydroxylation of biphenyl-4-carboxylic acid and derivatives (viz. 4-phenylsalicylic acid and 5-phenylsalicylic acid). *J. Phys. Org. Chem.* **2011,** *24* (12), 1151-1156.

(50) Li, Y.; Wen, B.; Ma, W.; Chen, C.; Zhao, J. Photocatalytic Degradation of Aromatic Pollutants: A Pivotal Role of Conduction Band Electron in Distribution of Hydroxylated Intermediates. *Environmental Science & Technology* **2012,** *46* (9), 5093-5099

(51) Bui, T. D.; Kimura, A.; Ikeda, S.; Matsumura, M. Determination of Oxygen Sources for Oxidation of Benzene on TiO_2 Photocatalysts in Aqueous Solutions Containing Molecular Oxygen. *Journal of the American Chemical Society* **2010,** *132* (24), 8453-8458.

(52) Augugliaro, V.; Bellardita, M.; Loddo, V.; Palmisano, G.; Palmisano, L.; Yurdakal, S. Overview on oxidation mechanisms of organic compounds by TiO_2 in heterogeneous photocatalysis. *Journal of Photochemistry and Photobiology C: Photochemistry Reviews* **2012,** *13* (3), 224-245.

(53) Montoya, J. F.; Ivanova, I.; Dillert, R.; Bahnemann, D. W.; Salvador, P.; Peral, J. Catalytic Role of Surface Oxygens in TiO_2 Photooxidation Reactions: Aqueous Benzene Photooxidation with $Ti^{18}O_2$ under Anaerobic Conditions. *J. Phys. Chem. Lett.* **2013,** *4* (9), 1415-1422.

(54) Kavan, L.; Zukalova, M.; Ferus, M.; Kurti, J.; Koltai, J.; Civis, S. Oxygen-isotope labeled titania: $Ti^{18}O_2$. *Phys. Chem. Chem. Phys.* **2011,** *13* (24), 11583-11586.

(55) Frank, O.; Zukalova, M.; Laskova, B.; Kurti, J.; Koltai, J.; Kavan, L. Raman spectra of titanium dioxide (anatase, rutile) with identified oxygen isotopes (16, 17, 18). *Phys. Chem. Chem. Phys.* **2012,** *14* (42), 14567-14572.

(56) Burfield, D. R.; Lee, K. H.; Smithers, R. H. Desiccant efficiency in solvent drying. A reappraisal by application of a novel method for solvent water assay. *J. Org. Chem.* **1977,** *42* (18), 3060-3065.

(57) Finnie, K. S.; Cassidy, D. J.; Bartlett, J. R.; Woolfrey, J. L. IR Spectroscopy of Surface Water and Hydroxyl Species on Nanocrystalline TiO_2 Films. *Langmuir* **2001,** *17* (3), 816-820.

(58) Nosaka, A. Y.; Fujiwara, T.; Yagi, H.; Akutsu, H.; Nosaka, Y. Characteristics of Water Adsorbed on TiO_2 Photocatalytic Systems with Increasing Temperature as Studied by Solid-State 1H NMR Spectroscopy. *The Journal of Physical Chemistry B* **2004,** *108* (26), 9121-9125.

(59) Nosaka, A. Y.; Nishino, J.; Fujiwara, T.; Ikegami, T.; Yagi, H.; Akutsu, H.; Nosaka, Y. Effects of Thermal Treatments on the Recovery of Adsorbed Water and Photocatalytic Activities of TiO_2 Photocatalytic Systems. *The Journal of Physical Chemistry B* **2006,** *110* (16), 8380-8385.

(60) Nováková, J. Isotopic Exchange of Oxygen ^{18}O Between the Gaseous Phase and Oxide Catalysts. *Catalysis Reviews* **1971,** *4* (1), 77-113.

(61) Hatchard, C. G.; Parker, C. A. A New Sensitive Chemical Actinometer. II. Potassium Ferrioxalate as a Standard Chemical Actinometer. *Proceedings of the Royal Society of London. Series A. Mathematical and Physical Sciences* **1956,** *235* (1203), 518-536.

(62) Boehm, H. P. Acidic and basic properties of hydroxylated metal oxide surfaces. *Discuss. Faraday Soc.* **1971,** *52*, 264-275.

(63) Zhao, Z.; Li, Z.; Zou, Z. Structure and Properties of Water on the Anatase TiO_2 (101) Surface: From Single-Molecule Adsorption to Interface Formation. *J. Phys. Chem. C* **2012,** *116* (20), 11054-11061.

(64) Mohamed, H. H.; Bahnemann, D. W. The role of electron transfer in photocatalysis: Fact and fictions. *Applied Catalysis B: Environmental* **2012,** *128*, 91-104.

(65) Mohamed, H. H.; Dillert, R.; Bahnemann, D. W. Growth and Reactivity of Silver Nanoparticles on the Surface of TiO_2: A Stopped-Flow Study. *J. Phys. Chem. C* **2011,** *115* (24), 12163-12172.

(66) Mohamed, H. H.; Dillert, R.; Bahnemann, D. W. Reaction dynamics of the transfer of stored electrons on TiO_2 nanoparticles: A stopped flow study. *Journal of Photochemistry and Photobiology A: Chemistry* **2011,** *217* (1), 271-274.

(67) Mikhaylov, R. V.; Lisachenko, A. A.; Titov, V. V. Investigation of Photostimulated Oxygen Isotope Exchange on TiO_2 Degussa P25 Surface upon UV-Vis Irradiation. *J. Phys. Chem. C* **2012,** *116* (44), 23332-23341.

(68) Bui, T. D.; Kimura, A.; Higashida, S.; Ikeda, S.; Matsumura, M. Two routes for mineralizing benzene by TiO_2-photocatalyzed reaction. *Applied Catalysis B: Environmental* **2011,** *107* (1-2), 119-127.

(69) Nishimoto, S. I.; Ohtani, B.; Kajiwara, H.; Kagiya, T. Photoinduced oxygen formation and silver-metal deposition in aqueous solutions of various silver salts by suspended titanium dioxide powder. *J. Chem. Soc. , Faraday Trans. 1* **1983,** *79* (11), 2685-2694.

(70) Draper, R. B.; Fox, M. A. Titanium dioxide photosensitized reactions studied by diffuse reflectance flash photolysis in aqueous suspensions of TiO_2 powder. *Langmuir* **1990**, *6* (8), 1396-1402.

(71) Grabner, G.; Li, G.; Quint, R. M.; Quint, R.; Getoff, N. Pulsed laser-induced oxidation of phenol in acid aqueous TiO_2 sols. *J. Chem. Soc. Faraday Trans.* **1991**, *87* (8), 1097-1101.

(72) Mao, Y.; Schoeneich, C.; Asmus, K. D. Identification of organic acids and other intermediates in oxidative degradation of chlorinated ethanes on titania surfaces en route to mineralization: a combined photocatalytic and radiation chemical study. *J. Phys. Chem.* **1991**, *95* (24), 10080-10089.

(73) Hoffman, A. J.; Carraway, E. R.; Hoffmann, M. R. Photocatalytic Production of H_2O_2 and Organic Peroxides on Quantum-Sized Semiconductor Colloids. *Environmental Science & Technology* **1994**, *28* (5), 776-785.

(74) Ishibashi, K. i.; Fujishima, A.; Watanabe, T.; Hashimoto, K. Quantum yields of active oxidative species formed on TiO_2 photocatalyst. *Journal of Photochemistry and Photobiology A: Chemistry* **2000**, *134* (1-2), 139-142.

(75) Chen, Y.; Yang, S.; Wang, K.; Lou, L. Role of primary active species and TiO_2 surface characteristic in UV-illuminated photodegradation of Acid Orange 7. *Journal of Photochemistry and Photobiology A: Chemistry* **2005,** *172* (1), 47-54.

(76) Monllor-Satoca, D.; Gomez, R.; Gonzalez-Hidalgo, M.; Salvador, P. The "Direct-Indirect" model: An alternative kinetic approach in heterogeneous photocatalysis based on the degree of interaction of dissolved pollutant species with the semiconductor surface. *Catalysis Today* **2007,** *129* (1-2), 247-255.

(77) Montoya, J. F.; Salvador, P. The influence of surface fluorination in the photocatalytic behaviour of TiO_2 aqueous dispersions: An analysis in the light of the direct-indirect kinetic model. *Applied Catalysis B: Environmental* **2010,** *94* (1-2), 97-107.

(78) Montoya, J. F.; Peral, J.; Salvador, P. Surface Chemistry and Interfacial Charge-Transfer Mechanisms in Photoinduced Oxygen Exchange at O_2-TiO_2 Interfaces. *ChemPhysChem* **2011,** *12* (5), 901-907.

(79) Kobayakawa, K.; Nakazawa, Y.; Ikeda, M.; Sato, Y.; Fujishima, A. Influence of the Density of Surface Hydroxyl-Groups on TiO$_2$ Photocatalytic Activities. *Berbunsenges Phys. Chem. Chem. Phys.* **1990,** *94* (12), 1439-1443.

(80) Chen, X.; Liu, L.; Yu, P. Y.; Mao, S. S. Increasing Solar Absorption for Photocatalysis with Black Hydrogenated Titanium Dioxide Nanocrystals. *Science* **2011,** *331* (6018), 746-750.